

**Transcriptome- and proteome-wide responses to
putrescine depletion in the human malaria parasite,
*Plasmodium falciparum***

by

Katherine Clark

Submitted in partial fulfilment of the requirements for the degree

Philosophiae Doctor Biochemistry

in the Faculty of Natural and Agricultural Sciences
University of Pretoria
Pretoria
South Africa

January 2013

SUBMISSION DECLARATION

I, Katherine Clark, declare that this dissertation, which is herewith submitted for the degree *Philosophiae Doctor* at the University of Pretoria, is my own work and has not previously been submitted by me for a degree at this or any other tertiary institution.

Signature: _____ Date: _____

PLAGIARISM DECLARATION

UNIVERSITY OF PRETORIA
FACULTY OF NATURAL AND AGRICULTURAL SCIENCES
DEPARTMENT OF BIOCHEMISTRY

Full name: Katherine Clark

Student number: 92385062

Title of the work: Transcriptome- and proteome-wide responses to putrescine depletion in the human malaria parasite, *Plasmodium falciparum*

Declaration

1. I understand what plagiarism entails and am aware of the University's policy in this regard.
2. I declare that this thesis is my own, original work. Where someone else's work was used (whether from a printed source, the internet or any other source) due acknowledgement was given and reference was made according to departmental requirements.
3. I did not make use of another student's previous work and submit it as my own.
4. I did not allow and will not allow anyone to copy my work with the intention of presenting it as his or her own work.

Signature _____

Date _____

ACKNOWLEDGEMENTS

I wish to express my sincere gratitude to the following people:

My supervisor, **Prof L Birkholtz** (Department of Biochemistry, University of Pretoria), for her enthusiasm, support, patience, insight and advice;

My co-supervisor, **Prof AI Louw** (Department of Biochemistry, University of Pretoria), for his valuable insight and advice;

My husband, **Dale**, for his unfailing support, encouragement and infinite patience;

Prof J Hyde (Faculty of Life Sciences, University of Manchester) for hosting me in his lab. **Dr P Sims**, the staff and students of their lab, especially Dr N Nirmalan for their help and friendship;

Prof F Joubert (Department of Biochemistry, Bioinformatics Unit, University of Pretoria), and **Mr J de Ridder** (Department of Biochemistry, University of Pretoria) for their help with various computer-related analyses;

Mr D Theron and **Mr N Olivier** (ACGT Microarray Facility, University of Pretoria) for their help with all the various aspects of microarrays;

Everyone in the Molecular Parasitology Lab, University of Pretoria (**Malaria team**), especially Dr S Smit, Ms E Human, Dr T van Brummelen and Dr J Niemand for their friendship, advice and help in the lab;

Mrs S van Wyngaardt (Department of Biochemistry, University of Pretoria) for her unhesitating help with technical matters and her friendship;

Dr C Maritz-Olivier (Department of Genetics, University of Pretoria) for many helpful discussions and advice; and

The **National Research Foundation**, **National Drug Development Programme**, **South African Malaria Initiative** and the **University of Pretoria** for financial support.

SUMMARY

Malaria is a disease afflicting millions of people and prevalent in developing countries that can ill afford the cost of prevention, treatment and the effect of sick workers on their economy. Unfortunately, many of the currently used drugs are failing and an effective vaccine is still unavailable. The identification of novel therapeutic drug targets is thus essential. Polyamines are ubiquitous polycations found in almost all living species and are essential for numerous cellular processes. The polyamine pathway is thus an attractive target for chemotherapeutic drug intervention.

This study focussed on the functional consequences of the inhibition of the ornithine decarboxylase-subunit (ODC) of the bifunctional S-adenosylmethionine-ornithine decarboxylase enzyme, the rate-limiting enzyme of the polyamine metabolic pathway, by the addition of difluoromethylornithine. Inhibition of ODC results both in global transcriptome and proteome changes, with a total of 997 transcripts being differentially expressed. Comparison of the data from this study with other perturbations focussed on enzymes in the polyamine pathway indicated 81 transcripts as common to all four inhibitions, but highlighted 438 transcripts that are unique to ODC-inhibition. This fingerprint profile indicated uniquely affected transcripts compensating for changes to the ODC substrate and from interference with the polyamine pathway. Transcripts that increased in abundance were related to host-parasite interaction, protein modification and signal transduction, while those that decreased were related to primary metabolism and DNA metabolism. Particularly interesting, this work comprehensively established a link between polyamine metabolism and redox metabolism and offers auxiliary targets for drug discovery.

This doctoral study thus proved the validity of the application of a functional genomics approach as a contribution to understanding the functional consequences of novel drug treatments in malaria parasites.

TABLE OF CONTENTS

CHAPTER 1: INTRODUCTION	15
1.1 THE BIOLOGY AND IMPACT OF MALARIA	15
1.2 PATHOGENESIS OF MALARIA.....	17
1.3 CONTROL OF MALARIA.....	18
1.3.1 Vector control	19
1.3.2 Vaccines	20
1.3.3 Drugs	21
1.4 POLYAMINES.....	25
1.4.1 General characteristics of the polyamines.....	25
1.4.1 Polyamines within the mammalian system	27
1.4.2 Inhibition of ornithine decarboxylase (ODC) with α -difluoromethylornithine (DFMO).....	28
1.4.3 Polyamine regulation within eukaryotic cells	30
1.4.4 The polyamines in <i>P. falciparum</i> parasites.....	32
1.5 DRUG DISCOVERY IN THE GENOMIC AND POST-GENOMIC ERA	37
1.5.1 Functional genomics and <i>P. falciparum</i> parasites.....	39
1.5.2 Transcriptomics.....	40
1.5.3 Proteomics	45
1.6 OBJECTIVE AND OUTPUTS	47
1.6.1 Papers	48
1.6.2 Conference proceedings.....	48
CHAPTER 2: Transcriptional response of ODC-inhibited <i>Plasmodium falciparum</i> parasites	50
2.1 INTRODUCTION	50
2.1.1 Transcriptomic profiling and methods of detecting differentially expressed genes.....	50
2.1.1.1 Suppression subtractive hybridisation.....	50
2.1.1.2 Microarrays.....	52
2.1.1.3 The application of transcriptional profiling to <i>P. falciparum</i> parasites	55
2.2 MATERIALS AND METHODS.....	56
2.2.1 <u>PART 1</u> : Transcriptional profile of ODC-inhibited <i>P. falciparum</i> parasites using SSH and cDNA microarray	56
2.2.1.1 <i>In vitro</i> <i>P. falciparum</i> parasite cultivation	56
2.2.1.2 Morphological evaluation of DFMO-treated and untreated parasites	57

2.2.1.3 Parasite culture, treatment and sampling for transcriptional profiling by SSH-cDNA microarray	57
2.2.1.4 RNA Isolation and electrophoresis	57
2.2.1.5 Suppression Subtractive Hybridisation (SSH)	58
2.2.1.6 Agarose gel electrophoresis	60
2.2.1.7 Microarray printing	60
2.2.1.8 Differential screening with cDNA microarray	61
2.2.1.8.1 Target preparation	61
2.2.1.8.2 Microarray hybridisation, washing and scanning	62
2.2.1.8.3 Data analysis	63
2.2.1.9 Sequencing	63
2.2.1.10 Identification of redundant clones of decreased abundance	64
2.2.1.11 Microarray result validation	65
2.2.2 <u>PART 2</u> : Transcriptional profile of ODC-inhibited <i>P. falciparum</i> parasites using whole genome oligo microarray	67
2.2.2.1 Parasite culture, treatment and sampling for transcriptional profiling by oligo DNA microarray	67
2.2.2.2 RNA Isolation	67
2.2.2.3 cDNA synthesis and aminoallyl-dUTP incorporation	67
2.2.2.4 Cy3 and Cy5 coupling	68
2.2.2.5 Microarray hybridisation, washing and scanning	69
2.2.2.6 Data analysis	70
2.2.2.7 Validation of microarray results using semi-quantitative real-time PCR	70
2.3 RESULTS	72
2.3.1 <u>PART 1</u> : Transcriptional profile of ODC-inhibited <i>P. falciparum</i> parasites using SSH and cDNA microarray	72
2.3.1.1 Morphology of DFMO-treated and untreated Fab9 <i>P. falciparum</i> parasites	72
2.3.1.2 Generation of transcripts differentially expressed upon DFMO-treatment	73
2.3.1.3 cDNA microarray screening of differentially expressed libraries	75
2.3.1.4 Effect of DFMO-treatment on <i>P. falciparum</i> parasites	79
2.3.1.5 Validation of microarray data	85
2.3.2 <u>PART 2</u> : Transcriptional profile of ODC-inhibited <i>P. falciparum</i> parasites using whole genome oligo microarray	86
2.3.2.1 Oligo microarray	86
2.3.1.2 Effect of DFMO-treatment on <i>P. falciparum</i> parasites	90

2.3.1.3 Validation of microarray data	99
2.3.1.4 Comparison of the SSH-cDNA and whole genome oligo microarray datasets.	100
2.3.1.5 Comparison between the transcriptomes of the enzymes of the polyamine pathway.....	102
2.3.1.6 Comparison between the ODC-inhibited transcriptomes with other perturbations of <i>P. falciparum</i> parasite culture.....	109
2.4 DISCUSSION	111
2.5 CONCLUSION	119
CHAPTER 3: Translational response of ODC-inhibited <i>Plasmodium falciparum</i> parasites	120
3.1 INTRODUCTION	120
3.2 MATERIALS AND METHODS.....	121
3.2.1 Parasite culture, treatment and sampling	121
3.2.2 Protein isolation and determination of concentration	122
3.2.3 Isoelectric focussing (IEF)	122
3.2.4 Second dimension sodium dodecyl sulphate polyacrylamide gel electrophoresis (SDS-PAGE).....	123
3.2.5 Data analysis and protein identification	123
3.3 RESULTS	125
3.4 DISCUSSION	133
3.5 CONCLUSION	135
CHAPTER 4: The relationship between ornithine metabolism and polyamine metabolism.....	136
4.1 INTRODUCTION	136
4.2 MATERIALS AND METHODS	138
4.2.1 Biochemical investigation of the effect of polyamines on the activity of <i>P. falciparum</i> ornithine aminotransferase	138
4.2.1.1 Cloning of OAT into pGEM T-Easy	138
4.2.1.2 Cloning of OAT into pET15b	142
4.2.1.3 Expression and purification of OAT	142
4.2.1.4 OAT activity assay	144
4.2.2 Effect of exogenously supplemented ornithine on the polyamine pathway related transcripts in <i>P. falciparum</i>	145
4.2.2.1 <i>P. falciparum</i> culture and treatment.....	145
4.2.2.2 Malstat	145

4.2.2.3 Treatment and harvesting of parasites for real-time PCR analyses	146
4.2.2.4 RNA isolation and cDNA synthesis	146
4.2.2.5 Semi-quantitative real-time PCR	147
4.3 RESULTS	148
4.3.1 Biochemical investigation of the effect of polyamines on the activity of <i>P. falciparum</i> ornithine aminotransferase	148
4.3.1.1 Cloning of PfoAT	148
4.3.1.2 Expression of PfoAT	149
4.3.1.3 Assay of PfoAT in the presence of polyamines	150
4.3.2 Effect of exogenously supplemented ornithine on the polyamine pathway related transcripts of <i>P. falciparum</i> parasites	152
4.4 DISCUSSION	155
4.4.1 Biochemical investigation of the effect of polyamines on ornithine aminotransferase	155
4.4.2 Effect of exogenously supplemented ornithine on the polyamine pathway of <i>P. falciparum</i> parasites	157
4.5 CONCLUSION	159
CHAPTER 5: Concluding discussion	160
REFERENCES	165
SUPPLEMENTARY MATERIAL (provided in electronic format on accompanying CD)	

LIST OF FIGURES

Figure 1.1	Life-cycle of the malaria parasite, <i>Plasmodium falciparum</i>	16
Figure 1.2	Global distribution of malaria	17
Figure 1.3	Structures of the commonly used anti-malarial drugs.....	21
Figure 1.4	Conceptual pipeline of drug development employed by the MMV.....	24
Figure 1.5	Potential consequences upon a significant change in cellular polyamine concentration.....	27
Figure 1.6	Polyamine biosynthesis in mammalian cells.....	28
Figure 1.7	Structure of ornithine - the natural substrate for ODC; and DFMO - an irreversible inhibitor of ODC	29
Figure 1.8	Proposed mechanism of DFMO inactivation of mouse ODC.....	30
Figure 1.9	Comparison of polyamine biosynthesis in the protozoan parasites <i>Plasmodium</i> , <i>Trypanosoma</i> , <i>Leishmania</i> and their human host.....	34
Figure 1.10	Representation of the ~170 kDa bifunctional AdoMetDC-ODC polypeptide	35
Figure 1.11	Ribbon diagrams of the homology models of the ODC and AdoMetDC monomers.....	36
Figure 1.12	Diagrammatic representation of the use of functional genomics and systems biology for drug target identification and validation	38
Figure 1.13	Various applications of functional genomic strategies to drug target and therapeutic discovery in the malaria parasite	40
Figure 1.14	The cascade-like 'just-in-time progression' of the <i>P. falciparum</i> parasite transcriptome.....	42
Figure 2.1	Schematic representation of the principle of SSH	52
Figure 2.2	Various microarray experimental designs.....	54
Figure 2.3	Structure of the active components of the coupling reaction	68
Figure 2.4	Morphological monitoring of <i>P. falciparum</i> parasites	73
Figure 2.5	Secondary (nested) amplification of the differentially expressed transcripts	74
Figure 2.6	Stretch-Rig gel of colony screening PCR for the forward and reverse libraries	75
Figure 2.7	Typical microarray slides after scanning (time-point 2, early trophozoites).....	76
Figure 2.8	An example of tightly clustered clones	78
Figure 2.9	Nested PCR to identify potentially unique clones.....	79
Figure 2.10	Functional grouping of transcripts of increased abundance and decreased abundance after DFMO-treatment	83

Figure 2.11	Drug-specific transcriptional feedback responses due to DFMO-treatment in <i>P. falciparum</i> parasites.....	85
Figure 2.12	Microarray slides of untreated and treated time-point 2.....	87
Figure 2.13	Boxplots of arrays pre-normalisation and post robust-spline within slide normalisation	88
Figure 2.14	MA plots of array 1_6 pre-normalisation, post background correction, (post within-array normalisation (robust-spline) and post between array normalisation (Gquantile)	89
Figure 2.15	Density plots of the arrays pre-normalisation, post robust-spline normalisation, followed by Gquantile normalisation.....	90
Figure 2.16	Venn diagrams indicating the number of transcripts unique to and in common between, time-points 1 and 2	91
Figure 2.17	Gene ontology based functional classification of the transcripts of increased and decreased abundance	95
Figure 2.18	Heat map of a cluster (cluster node 12044) enriched in polyamine related transcripts	97
Figure 2.19	Comparison of semi-quantitative real-time PCR and microarray data for transcripts that show increased, decreased and unchanged abundance	100
Figure 2.20	Comparison between SSH-cDNA transcriptome and oligo transcriptome.....	101
Figure 2.21	Number of transcripts shared between the various inhibitors of enzymes of the polyamine pathway	102
Figure 2.22	Number of transcripts shared between the various perturbations of <i>P. falciparum</i> parasite culture	110
Figure 2.23	A representation of antioxidant defence within the <i>Plasmodium</i> infected erythrocyte.....	116
Figure 3.1	Simplistic overview of the PDQuest analysis process	126
Figure 3.2	Spots identified as differentially regulated	127
Figure 3.3	Interactions present between the proteins differentially expressed upon DFMO treatment and their binding partners.....	133
Figure 4.1	The synthesis and metabolism of ornithine.....	137
Figure 4.2	Cloning of PfoAT for heterologous protein expression in <i>E. coli</i>	149
Figure 4.3	Protein expression in PfoAT-pET15b transformed IPTG induced and uninduced BL 21 Star™ <i>E. coli</i> cells	150

Figure 4.4	Typical silver stained 12.5% SDS-PAGE gel of IMAC-purified PfOAT	150
Figure 4.5	Relationship between OAT concentration and enzyme activity as determined by amount of pigment formed per minute	151
Figure 4.6	The effect of polyamines (putrescine, spermine, spermidine, cadaverine), ornithine and lysine on the activity of PfOAT	152
Figure 4.7	Dose-response curve of ornithine supplemented <i>P. falciparum</i> parasites <i>in vitro</i>	153
Figure 4.8	Effect of 50 mM ornithine on the various transcripts in the polyamine pathway, normalised to LDH.....	154
Figure 4.9	Fold change of various transcripts within the polyamine pathway upon addition of varying concentrations (50 mM, 125 mM and 250 mM) of ornithine	155
Figure 5.1	Overview of the polyamine and redox pathways indicating those transcripts, enzymes and proteins affected by ODC inhibition.....	162

LIST OF TABLES

Table 1.1	Characteristics of some of the commonly used anti-malarial drugs	23
Table 1.2	Projects within the research component of the MMV pipeline as at end first quarter 2011	25
Table 1.3	The structure, chemical name and molecular weight of the polyamines	26
Table 1.4	Some inhibitors of ornithine decarboxylase (ODC)	29
Table 1.5	Polyamine concentration in uninfected erythrocytes, parasitised erythrocytes and parasitised erythrocytes treated with DFMO	32
Table 1.6	Polyamine concentration in the various parasite life-cycle stages	33
Table 1.7	Features of the enzymes involved in the polyamine metabolic pathway	37
Table 2.1.	Sequences of the primers and adaptors used in the SSH procedure	59
Table 2.2.	Composition and condition of tester and driver cDNA	59
Table 2.3	Nested primers for redundant clones of decreased abundance	65
Table 2.4	Primers designed for use in semi-quantitative real-time PCR to validate microarray data	66
Table 2.5	Thermocycling conditions for real-time PCR validation of microarray data using the Light-Cycler 1.5	66
Table 2.6	Parameters for automated flagging using GenePix	70
Table 2.7	Information for primer sets employed for real-time PCR	71
Table 2.8	Cycling conditions for amplification using the LightCycler 480	71
Table 2.9	Concentration and specifications of RNA isolated from the harvested samples	74
Table 2.10	Information regarding <i>k</i> -means clusters	77
Table 2.11	Identification of differentially expressed transcripts	80
Table 2.12	Verification of differential expression of a selection of identified differential transcripts	86
Table 2.13	Pearson correlation coefficients between the various samples	91
Table 2.14	Commonalities between the various sets of differentially expressed transcripts	92
Table 2.15	Top 25 transcripts of increased abundance for each of the two time-points, respectively	93
Table 2.16	Top 25 transcripts of decreased abundance for each of the two time-points, respectively	94

Table 2.17	Proteins binding to either thioredoxin, plasmoredoxin or glutaredoxin and those present in the DFMO-treatment transcriptomic profiles.....	98
Table 2.18	Enzymes that are dependent on PLP	99
Table 2.19	Details of the commonalities between the SSH-cDNA and oligo transcriptomes.....	102
Table 2.20	Comparison of ODC-, AdoMetDC-, spermidine synthase and AdoMetDC-ODC inhibited transcriptomes.....	104
Table 2.21	Transcripts indicative of a general stress response in <i>P. falciparum</i> parasites <i>in vitro</i> ...	110
Table 2.22	Comparison of the cDNA and oligo microarray platforms	112
Table 3.1	IEF profile employed for 18 cm IPG strips.....	123
Table 3.2	Statistics of spot count and matching for initial and saturated analyses of gels using PDQuest.....	127
Table 3.3	Proteins identified as differentially expressed in the <i>P. falciparum</i> parasite following DFMO-induced inhibition of ODC	128
Table 3.4	Characteristics of the differentially expressed proteins, obtained from PlasmoDB	129
Table 3.5	Proteins identified as binding to either thioredoxin, plasmoredoxin or glutaredoxin	131
Table 3.6	Number of interacting proteins found for the proteins showing differential expression upon DFMO treatment.....	132
Table 4.1	Primers used for the cloning, sub-cloning and sequencing of OAT.....	139
Table 4.2	Information for primer sets employed for real-time PCR	147
Table 4.3	Cycling conditions for amplification using the LightCycler 480.....	148
Table 4.4	Comparison of differences observed in polyamine related transcripts upon ODC-inhibition.....	157

SUPPLEMENTARY MATERIAL

The Supplementary Material is enclosed on the accompanying CD. It consists of a PDF file entitled 'Supplementary Material' and an Exel file of the transcripts identified as differentially expressed in the oligo microarray study entitled 'Oligo transcriptome DE transcripts'.

The 'Supplementary Material' PDF contains the following:

S1. R SCRIPT USED FOR OLIGO MICROARRAY NORMALISATION AND IDENTIFICATION OF DIFFERENTIALLY EXPRESSED GENES.....	I
S2. TRANSCRIPTS DIFFERENTIALLY EXPRESSED UPON DFMO-TREATMENT AS IDENTIFIED IN OLIGO TRANSCRIPTOME	III
Table S2.1. Transcripts showing decreased abundance upon treatment with DFMO.....	III
Table S2.2. Transcripts showing increased abundance upon treatment with DFMO.....	XXIV
S3. DIFFERENCES BETWEEN ODC-INHIBITED AND ADOMETDC-INHIBITED TRANSCRIPTOMES.....	XXXVI
Table S3.1. Transcripts present in only the ODC-inhibited parasite culture when compared with the AdoMetDC-inhibited parasite culture	XXXVI
Table S3.2. Transcripts present in only the AdoMetDC-inhibited parasite culture when compared with the ODC-inhibited parasite culture	XLIV
Table S3.3. Transcripts common to both ODC- and AdoMetDC-inhibited parasite cultures	XLVII
S4. THE 438 TRANSCRIPTS IDENTIFIED AS UNIQUE TO ODC BETWEEN POLYAMINE PERTURBATIONS	LII
Table S4.1. Transcripts showing differential expression unique to ODC upon ODC-, AdoMetDC-, spermidine synthase- and AdoMetDC-ODC inhibition.....	LII
S5. THE 81 TRANSCRIPTS IDENTIFIED AS COMMON BETWEEN POLYAMINE PERTURBATIONS.....	LX
Table S5.1. Transcripts showing differential expression upon ODC-, AdoMetDC-, spermidine synthase- and AdoMetDC-ODC inhibition.....	LX
S6. COMPARISON BETWEEN DFMO-TREATED TRANSCRIPTOME AND SEVERAL OTHER PERTURBATIONS	LXII
Table S6.1 Transcripts common to both ODC-inhibited <i>P. falciparum</i> parasites and the transcripts identified as the invadome	LXII
Table S6.2. Transcripts common between ODC-inhibited <i>P. falciparum</i> parasites and those identified in chloroquine-treatment, artesunate-treatment, febrile temperature and the anti-folate WR99210, respectively	LXV

S7. MS PROTOCOL AS USED BY CPGR	LXVII
S7.1. In-gel protein digestion	LXVII
S7.2. Sample preparation for mass spectrometry	LXVII
S7.3. Mass spectrometry	LXVIII
S7.4. Data analysis	LXVIII
S8. ALIGNMENT OF OAT FROM HUMAN, <i>P. FALCIPARUM</i> AND THE THREE SPECIES CAPABLE OF INHIBITION BY AMINES (<i>B. SPHAERICUS</i> , <i>P. SATIVUM</i> , <i>R. NORVEGICUS</i>).	LXIX
Figure S8.1. Alignment of OAT from human, <i>P. falciparum</i> and the three proteins capable of inhibition by amines (<i>B. sphaericus</i> , <i>P. sativum</i> , <i>R. norvegicus</i>).	LXIX
REFERENCES.....	LXX

LIST OF ABBREVIATIONS

2D-DIGE	Two-dimensional fluorescence difference gel electrophoresis
2-D PAGE	Two-dimensional polyacrylamide gel electrophoresis
A-value	$A = \frac{1}{2} \log_2 RG$, where R is red and G is green (fluorescent signals)
ACT	Artemisinin combination therapy
AdoMet	S-adenosylmethionine
AdoMetDC	S-adenosylmethionine decarboxylase
AdoMetDC-ODC	Bifunctional S-adenosylmethionine decarboxylase-ornithine decarboxylase
AIDS	Acquired immunodeficiency syndrome
Aminoallyl-dUTP	Aminoallyl deoxyuridine triphosphate
AO	AdoMetDC-ODC
AP2	Apetala 2
APAD	3-acetylpyridine adenine dinucleotide
ARG	Arginase
ATP	Adenosine triphosphate
ATT1	Experiment A, treated time-point 1
ATT2	Experiment A, treated time-point 2
ATT3	Experiment A, treated time-point 3
AUT1	Experiment A, untreated time-point 1
AUT2	Experiment A, untreated time-point 2
AUT3	Experiment A, untreated time-point 3
bp	Base pairs
BSA	Bovine serum albumin
BTT1	Experiment B, treated time-point 1
BTT2	Experiment B, treated time-point 2
BTT3	Experiment B, treated time-point 3
BUT1	Experiment B, untreated time-point 1
BUT2	Experiment B, untreated time-point 2
BUT3	Experiment B, untreated time-point 3
cDNA	Complementary deoxyribonucleic acid
cGMP	Cyclic guanosine monophosphate
CHAPS	3-[(3-Cholamidopropyl)-dimethylammonio]-propane-sulfonate
CHP	<i>Plasmodium falciparum</i> conserved hypothetical protein
Cy3	Cyanine 3
Cy5	Cyanine 5
dATP	Deoxyadenosine triphosphate
dcAdoMet	Decarboxylated S-adenosylmethionine decarboxylase
dCTP	Deoxycytidine triphosphate
DDT	Dichlorodiphenyltrichloroethane
DEPC	Diethylpyrocarbonate
DFMO	DL- α -difluoromethylornithine
dGTP	Deoxyguanosine triphosphate
DHODH	Dihydroorotate dehydrogenase
DMSO	Dimethyl sulphoxide
DNA	Deoxyribonucleic acid

dNTPs	Deoxynucleoside triphosphates
dTTP	Deoxythymidine triphosphate
DTT	Dithiothreitol
dUTP	Deoxyuridine triphosphate
EDTA	Ethylene diamine-tetraacetic acid
ELISA	Enzyme linked immunosorbent assay
GO	Gene Ontology
HGXPRT	Hypoxanthine phosphoribosyltransferase
His-tag	Histidine tag
hpi	Hours post infection
HSP	Heat shock protein
IC ₅₀	Half maximal inhibitory constant
ICAT	Isotope coded affinity tag
IEF	Isoelectric focussing
IFN	Interferon
IL	Interleukin
IMAC	Immobilised metal affinity chromatography
IPG	Immobilised pH gradient
IPTG	Isopropyl-D-galactoside
ITN	Insecticide treated nets
LB-broth	Luria-Bertani broth
LC-MS/MS	Liquid chromatography tandem mass spectrometry
LDC	Lysine decarboxylase
LDH	Lactate dehydrogenase
LD-PCR	Long-distance polymerase chain reaction
LOESS	Locally weighted scatterplot smoothing
M-value	$M = \log_2 \frac{\text{red}}{\text{green}}$ (fluorescent signals)
MADIBA	Micro Array Data Interface for Biological Annotation
MAT	S-adenosylmethionine synthase
MDL73811	5'-{[(Z)-4-amino-2-butenyl]methylamino}-5'-deoxyadenosine
MMV	Medicines for Malaria Venture
MOPS	4-Morpholinepropanesulphonic acid
mRNA	Messenger ribonucleic acid
MS	Mass spectrometry
MS-MS	Tandem mass spectrometry
MudPIT	Multidimensional protein identification technology
N89	1,2,6,7-tetraoxaspiro[7,11]nonadecane
NADP ⁺	Nicotinamide adenine dinucleotide phosphate
NADPH	Reduced nicotinamide adenine dinucleotide phosphate
NBT	Nitroblue tetrazolium
NGO	Non-governmental organisation
NHS	N-hydroxysuccinimidyl-ester
OAT	Ornithine aminotransferase
ODC	Ornithine decarboxylase

ORF	Open reading frame
PBS	Phosphate buffered saline
PCR	Polymerase chain reaction
PES	Phenazine ethosulphate
PfEMP1	<i>Plasmodium falciparum</i> erythrocyte membrane protein-1
pI	Isoelectric point
PLP	Pyridoxal-5-phosphate
PMF	Peptide mass fingerprinting
PXN	<i>Plasmodium falciparum</i> 1-cys peroxiredoxin
R^2	Regression coefficient
RACE	Rapid Amplification of cDNA Ends
RBM	Roll Back Malaria
RNA	Ribonucleic acid
RNase	Ribonucleotidase
ROS	Reactive oxygen species
RT-PCR	Reverse transcriptase polymerase chain reaction
SAGE	Serial analysis of gene expression
SAP	<i>Plasmodium falciparum</i> senescence associated protein
SDS	Sodium dodecyl sulphate
SDS-PAGE	Sodium dodecyl sulphate polyacrylamide gel electrophoresis
SPD	Spermidine synthase
SSH	Suppression subtractive hybridisation
T1	Time-point 1
T2	Time-point 2
TAE	Tris-acetate, EDTA buffer
TBE	Tris-borate, EDTA buffer
T _m	Melting temperature
TNE	10 mM Tris-HCl pH 8, 10 mM NaCl, 0.1 mM EDTA
TNF	Tumour necrosis factor
WHO	World Health Organisation
Y2H	Yeast two hybrid
X-gal	5-bromo-4-chloro-3-indolyl-galactoside

CHAPTER 1

Introduction

1.1 THE BIOLOGY AND IMPACT OF MALARIA

Malaria, an age-old scourge! Thought to be responsible for the controversial death of Francesco I de' Medici (Second Grand Duke of Tuscany) in the 16th century [4], it has also been detected in ancient Egyptian mummies (3200-1304 BC). Descriptions of deadly, intermittent fevers can be found in the writings of Homer (ca 750 BC), Aristophanes (445-385 BC), Sophocles (496-406 BC), Hippocrates (460-370 BC), Plato (428-347 BC), Aristotle (384-322 BC) and in the Chinese classic *Nei Ching* [5]. It was thought that the disease was caused by marshes and in medieval Italy this gave rise to the name, '*mal'aria*' or bad air [6].

In 1897, subsequent to Charles Laveran's 1880 discovery of unicellular parasites as the causative agents of malaria in human blood [5], Ronald Ross discovered that these parasites are transmitted by *Anopheles* mosquitoes [7]. The life-cycle of the parasite was completely elucidated in 1948, when Shortt and Garham observed exo-erythrocytic schizonts in the livers of monkeys and humans [8].

Infection originates through the bite of an infected female *Anopheles* mosquito, whereby sporozoites are injected into the human bloodstream. These invade hepatocytes and form exo-erythrocytic schizonts (which contain up to 30,000 merozoites). Upon release of mature merozoites into the bloodstream, they invade erythrocytes where they progress through the ring, trophozoite and multinucleate schizont stages, with the ultimate formation of new merozoites that re-invade new erythrocytes. This asexual cycle can repeat several times. Gametocytes (sexually differentiated parasites) form from merozoites later in the cycle. Upon ingestion of a blood meal by the female mosquito, these gametocytes undergo further differentiation with the ultimate formation of a diploid ookinete, which matures and forms sporozoites that migrate to the salivary glands and the cycle recommences [8]. The life-cycle of the parasite is shown in Figure 1.1.

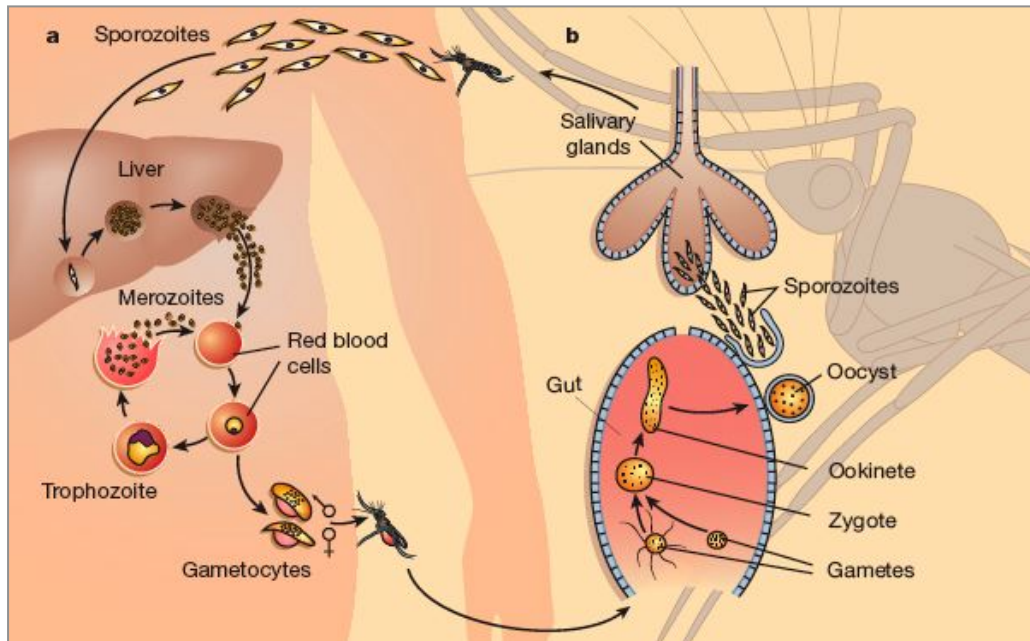


Figure 1.1. Life-cycle of the malaria parasite, *Plasmodium falciparum*. (a) The initial invasion of hepatocytes by sporozoites, followed by the asexual intra-erythrocytic developmental cycle (IDC) and the formation of gametocytes within the human host. (b) The gametocytes are ingested with the bloodmeal and undergo the sexual stage within the mosquito midgut. Sporozoites are subsequently formed, which can then infect a human host. Taken from [9].

The apicomplexan protozoan malaria parasite falls within the domain Eukaryota, superphylum Alveolata, phylum Apicomplexa, class Aconoidasida, order Haemosporida and genus *Plasmodium*. (www.uniprot.org/taxonomy/31272). There are numerous species of *Plasmodium* and their hosts include mammals (e.g. *P. berghei* infects rodents), birds (e.g. *P. gallinaceum* infects chickens) and reptiles (e.g. *P. mexicanum* infects lizards) [10-12]. Until fairly recently, it was accepted that four species of *Plasmodium* cause human malaria (*P. vivax*, *P. ovale*, *P. malariae*, *P. falciparum*) [13]. However, *P. knowlesi*, whose natural host is the monkey *Macaca fascicularis* [14], has been shown to infect humans through zoonotic transfer [15]. Previously misdiagnosed as *P. malariae* infection, *P. knowlesi* infection in humans is potentially life-threatening and *P. knowlesi* is now considered the fifth human malaria parasite [15, 16]. *P. falciparum* parasites account for the most morbidity and mortality amongst malaria infected individuals [13].

Sub-Saharan Africa suffers extensively from the burden of malaria. In 2009, there were an estimated 225 million cases of malaria worldwide, with approximately 781 000 deaths (Figure 1.2 indicates the global distribution of malaria). Of these deaths, approximately 91% were in Africa and 85% were children under five [17]. This results in a huge economic and social burden in countries that are already struggling with poverty.

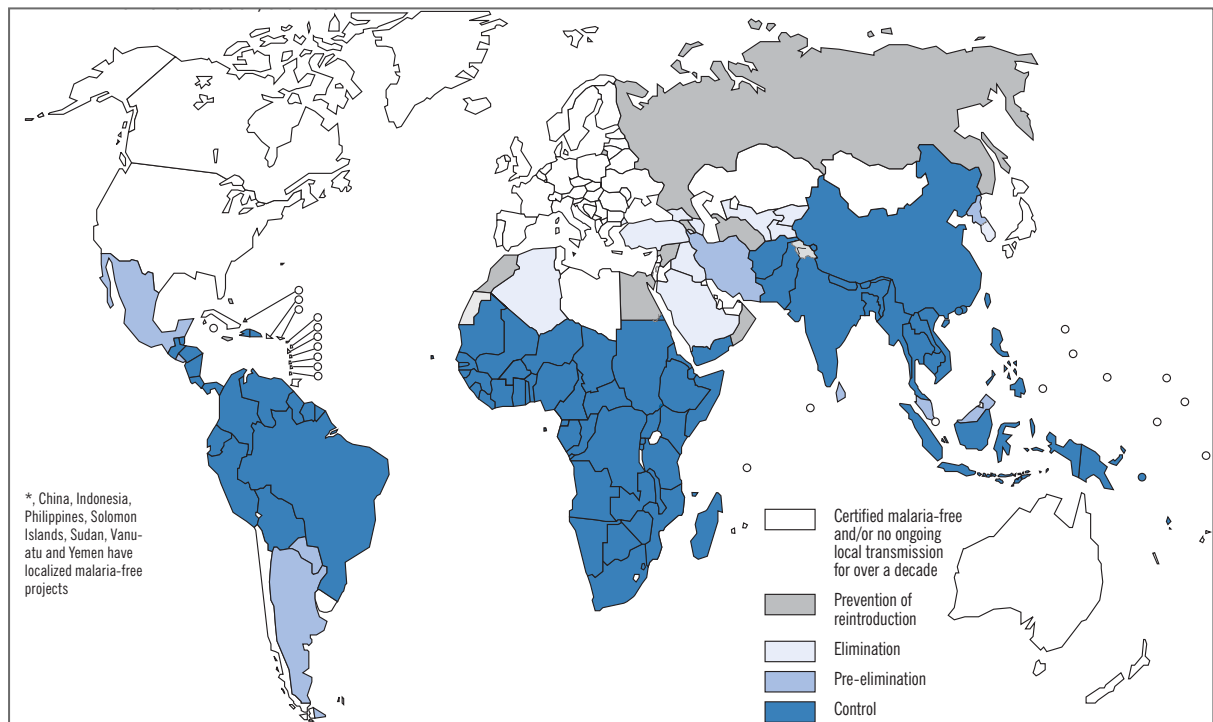


Figure 1.2. Global distribution of malaria, indicating malaria-free countries and malaria-endemic countries, along with the various phases of control (as at the end of 2008). Taken from [18].

Within the African region, South Africa is considered a low-transmission country and malaria is highly seasonal. This situation is however unstable and malaria transmission is tightly controlled within this country through the National Malaria Control Programme (www.doh.gov.za/docs/factsheets/guidelines/malaria/prevention.pdf). Most cases of malaria are caused by *P. falciparum* parasites. Since 2000, a decrease in the incidence of malaria within South Africa has been observed, probably due to the adoption of artemisinin combination therapies (ACT) as first-line malaria treatment in 2001, combined with improved mosquito control (this includes spraying with dichloro-diphenyl-trichloroethane (DDT)) [18].

1.2 PATHOGENESIS OF MALARIA

Initially, malaria presents with non-specific flu-like symptoms, including fever, headaches, malaise, mild jaundice, hyperventilation, hepatosplenomegaly and myalgia [19]. Of the five species infecting humans, *P. falciparum* parasites are the most malignant and can cause the most severe complications, including cerebral malaria and renal failure [20]. Pregnant women are particularly vulnerable to malaria infection and once infected tend to show an increased severity of the disease [19]. Severe malaria is a multi-system disorder and presents with a range of clinical features which may include neurological impairment, severe anaemia, hypoglycaemia, acidosis, hyperlactaemia, circulatory collapse, multi-organ failure and coagulopathies [20, 21]. Two features distinguish *P.*

falciparum parasites from the other malaria species infecting humans, namely the ability to infect erythrocytes of all ages and adherence of *P. falciparum* parasite infected erythrocytes to various tissues (cytoadherence and rosetting) [20]. Much of the cytoadherence is due to a *var* gene encoded protein, *P. falciparum* erythrocyte membrane protein 1 (PfEMP-1), of approximately 240 kDa. The sequence is highly polymorphic and enables antigenic variation, thus facilitating avoidance of and subsequent clearance by the immune system. Parasitised erythrocytes bind several host receptors, amongst others, thrombospondin, CD36, intercellular adhesion molecule 1 (ICAM-1) and vascular cell adhesion molecule [21]. The host inflammatory response to infection also plays a role in disease. The cytokines TNF- α , IFN- γ , IL-1 and IL-6 have all been implicated in disease, while the production of nitric oxide also contributes to pathogenesis [20].

1.3 CONTROL OF MALARIA

Control of malaria is deteriorating due to a variety of reasons. These include climate instability, global warming (albeit only a slight contribution), civil disturbances, travel, HIV, insecticide and drug resistance. Of these, drug resistance is a primary contributor to the decline of effective control [13].

The fight against malaria is driven by a combination of various approaches. Currently, several strategies are aimed at increasing awareness of malaria worldwide, as it is still considered a neglected disease, particularly outside Africa. On one front, Kingsley Holgate and his team use an adventure based approach to save and improve lives. On a recent expedition through Africa they promoted awareness of malaria prevention and distributed bed nets to especially vulnerable individuals (pregnant women and children) (www.kingsleyholgate.co.za/foundation). Another alternative approach to raising funds and raising global malaria awareness is the 'United Against Malaria' Campaign. It consists of a partnership of football teams and sports personalities, celebrities, government agencies, corporations, health organisations and ordinary citizens, united in the fight against malaria. Awareness is raised through various strategies including the worldwide media (billboards, newspapers, television) and garnering global attention by leveraging world events (World Economic Forum in Davos, World Economic Forum meeting in Africa, participation in the 2009 and 2010 Roll Back Malaria board meetings and going global on World Malaria Day where various projects were undertaken). Nando's (a fast food chain) marketed and sold beaded bracelets based on the campaign logo. Both the private sector (financial resources, employee time and brands were contributed) and new stakeholders (relationships were forged between ministry representatives and NGO leaders) were engaged. Football games were used for education, particularly the much publicised and attended/viewed 2010 Football World Cup in South Africa [22].

Beyond these philanthropic ventures, there are formalised concerted efforts to prevent malaria. The World Health Organization (WHO) has long had malaria eradication strategies and programmes in place and first launched a campaign to eradicate malaria in 1957. This was successful in that malaria was eradicated in some countries and disease incidence greatly reduced in several others. However, over the course of the next few decades there was a resurgence of the disease, resulting in a new initiative in 1998, namely the 'Roll Back Malaria Partnership'. The goal of this initiative was to halve deaths from malaria by 2010 and by three quarters by 2015 [8, 18]. In 2008, the 'Global Malaria Action Plan' was launched. This defined the steps required to achieve the 2010 and 2015 targets of the RBM Partnership [18].

The Millenium Declaration in 2000 highlighted eight Development Goals that represent the basic rights and human needs that each individual worldwide should be entitled to. The aim is to fulfil these goals by 2015. Malaria comes to the fore in Goal 6: Combat HIV/AIDS, malaria and other diseases. One of the targets is to have halted and begun to reverse the incidence of malaria and other major diseases by 2015 [23]. Although malaria is primarily a problem for developing nations, the control of malaria and other diseases are also on the agenda of the G8 (eight leading industrialised nations). Significant funding from these countries is provided to programmes like the 'Global Fund to Fight AIDS, Tuberculosis and Malaria' (a public/private partnership that attracts and disburses funds for disease treatment and prevention) [24].

The strategies in place for malaria control, elimination and ultimately eradication include vector control (indoor residual spraying with compounds like DDT and the use of insecticide treated nets - ITN), chemoprophylaxis of travellers and chemotherapy of infected individuals. Although vaccine studies remain ongoing there is no vaccine in current use [13] and widespread usage of one is still several years away [25].

1.3.1 Vector control

Vector control contributes to a reduction in the transmission of malaria. Vector control is currently two-pronged, namely the use of pyrethroid (insecticide) treated nets and indoor residual spraying (IRS) with pyrethroids or DDT. The use of DDT for spraying is effective, but controversial and alternatives are being investigated [26, 27]. Over the last few years, the number of households with an insecticide treated net, as well as the number of children aged under five sleeping under them, has increased [18]. Vector control efforts are however hampered by the development of resistance to insecticides such as DDT and pyrethroids, by mosquitoes. This problem is fairly widespread, particularly in West Africa [28, 29]. This has also been problematic in South Africa, where houses

were sprayed annually with DDT in the malaria endemic region of northern KwaZulu/Natal. However, in 1996 DDT use was banned and the insecticide was changed to deltamethrin (a pyrethroid). Alarmingly, between 1995 and 1999, the incidence of malaria in the area increased more than six-fold. An entomological survey revealed that pyrethroid resistant mosquitoes of the *A. funestus* group were now present in sprayed houses, even though this species had been eliminated from South Africa during the 1950s [30]. This had a large impact on the vector control measures used in the area and the South African government decided to reintroduce DDT spraying within traditional style houses. This has proved highly effective and a dramatic decrease in the number of malaria cases was observed from 64624 (probable and confirmed) in 2000, to the 6072 (confirmed) in 2009 [17, 31].

1.3.2 Vaccines

Vaccine development is hampered by the fact that the parasite is capable of escaping the immune response through antigenic variation. A further complication is that the parasite has different life-cycle stages and a vaccine would thus only be effective against a specific stage [32]. Development currently comprises three focus areas, namely pre-erythrocytic stage vaccines (which would protect against the early stages of infection), erythrocytic stage vaccines (which would reduce the severity of the disease) and sexual stage vaccines (which would interrupt the parasite life-cycle and thus be transmission blocking) [33]. Pre-erythrocytic stage vaccine target approaches include whole cells (irradiation attenuated sporozoites, genetically attenuated sporozoites and concurrent treatment with infectious sporozoites and drugs such as chloroquine or primaquine) and subunit vaccines (targeting sporozoites or liver stage parasites). Subunit vaccines are also under consideration for the erythrocytic stage. Multistage vaccines which combine vaccine targets from different life-cycle stages are also under development [32]. The most advanced of malaria vaccines is RTS,S. The vaccine was designed in the 1980s and Phase II studies in infants and children in endemic areas proved effective in reducing morbidity from clinical malaria, but is only 50% effective [34]. The vaccine is currently in Phase III multi-centre trials in sub-Saharan Africa and appears to yield an efficacy of between 30 and 50% [35, 36]. RTS,S comprises the parasite circumsporozoite (CS) protein construct of 19 NANP repeats of the central region and the entire C-terminal flanking region, which is then combined with the primary surface protein of the hepatitis B virus (HBsAg). Various adjuvants have also been tested. Results from clinical trials indicate that RTS,S elicits an anti-CS humoral response to the B-cell epitopes in the central NANP repeat region. However, the underlying immune mechanisms responsible for protective immunity require further elucidation and will facilitate both the design of second generation vaccines, as well as better comprehension of the disease [34].

1.3.3 Drugs

The armoury of drugs effective against malaria is rapidly diminishing and yet in the period between 1975 and 1996, of the 1223 new drugs that were registered, only 3 were anti-malarials [37].

The current drug arsenal contains the following major categories [38]:

- aminoquinolines (includes chloroquine, primaquine and amodiaquine);
- pyrimidines (includes pyrimethamine);
- sulfonamides and sulfones (includes sulfadoxine and dapsona);
- amidines and guanidines (includes proguanil, chlorproguanil and cycloguanil);
- 9-aminoacridines (mepacrine);
- antibiotics (includes doxycycline and tetracycline); and
- sesquiterpene lactones (includes artemesinin, artemether and artesunate).

The structures of some of these commonly used drugs are given in Figure 1.3.

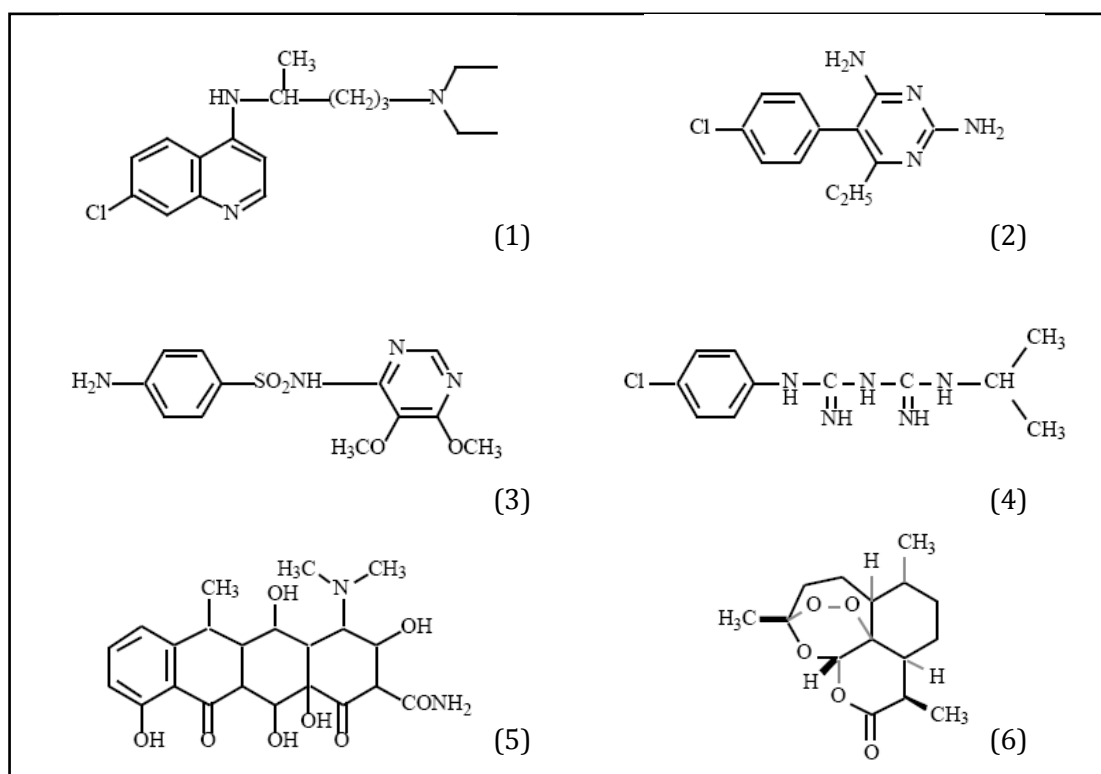


Figure 1.3. Structures of the commonly used anti-malarial drugs. (1) Chloroquine, (2) pyrimethamine, (3) sulfadoxine, (4) proguanil, (5) doxycycline and (6) artemisinin. Modified from [38].

Unfortunately, *Plasmodium* parasites have shown the capacity to develop resistance to many of the commonly used anti-malarials. Resistance in *P. falciparum* parasites to chloroquine was first noted in Southeast Asia and South America during the late 1950s [39]. Resistance can occur via several

mechanisms, but is often the result of a mutation within either the target protein or a transport protein. Table 1.1 provides the characteristics of some of the commonly used anti-malarials, including the proteins, which undergo mutation resulting in resistance.

Chloroquine was the drug of choice for many years and exerts its anti-malarial action by interfering with the polymerisation of the toxic haem (released upon haemoglobin digestion) into less harmful haemozoin in the parasite food vacuole. However, point mutations in the chloroquine resistance transporter gene (*pfcr1*) and an increase in the copy number of the multidrug resistance transporter (*mdr1*), both in the membrane of the food vacuole, result in less accumulation of chloroquine within the food vacuole and consequently a chloroquine resistant phenotype in the parasite [40].

Another successful group of anti-malarial drugs, the anti-folates, inhibit dihydropteroate synthase (DHPS) and dihydrofolate reductase (DHFR). These enzymes are involved in folic acid biosynthesis and provide reduced cofactors for one-carbon transfer reactions and nucleotide provision for DNA synthesis, respectively [40]. A comprehensive study of the anti-folate targets during 1988 – 1997 brought the genetic basis of resistance to the anti-folate drugs to light and proved the existence of point mutations within the *dhfr* and *dhps* genes leading to reduced binding of the drugs to the enzymes [40, 41].

Artemisinin and its derivatives (artemether, artesunate and dihydroartemisinin) are the current treatment of choice, as they produce rapid clearance of parasites and show broad activity against all the asexual stages. However, one of the genes that has been proposed to encode a target for artemisinin, namely *PfATPase6* (an essential calcium adenosine triphosphatase), is highly polymorphic [42, 43]. It has been shown that in French Guiana, a mutation within this gene leads to increased IC_{50} values for artemether [44]. In an attempt to extend the therapeutic life-time of the drug, the WHO mandated that artemisinin and derivatives were only to be used in combination with other drugs (such as lumefantrine, amodiaquine, piperaquine), resulting in artemisinin combination therapies (ACT) [40, 43].

Table 1.1. Characteristics of some of the commonly used anti-malarial drugs. *atp*: ATPase; *crt*: chloroquine resistance transporter; *cytb*: cytochrome b; *dhfr*: dihydrofolate reductase; *dhps*: dihydropteroate synthase; *mdr*: multidrug resistance. Compiled from [33, 40, 41, 43, 45, 46].

Drug	Molecular weight (g/mol)	Target	Location / function	Life-cycle stage	Resistance	Prophylaxis and/or treatment
Antibiotics						
Clindamycin	425.0	Protein translation	Apicoplast	Blood stage and liver stage	apicoplast 23S rRNA	Treatment
Doxycycline	444.4	Protein translation	Apicoplast	Blood stage and liver stage	?	Prophylaxis
Quinolines						
Chloroquine	436.0	Haemozoin formation	Food vacuole	Blood stage	<i>crt / mdr1</i>	Treatment and prophylaxis
Amodiaquine	355.9	Haemozoin formation	Food vacuole	Blood stage	<i>crt / mdr1</i>	Treatment and prophylaxis
Primaquine	259.4	Unknown	Unknown	Liver stage and gametocytes	Some resistance reported	Treatment and limited prophylaxis
Anti-folates						
Sulfadoxine	310.3	DHPS	Parasite cytoplasm	Blood stage	<i>dhps</i>	Treatment and prophylaxis
Pyrimethamine	248.7	DHFR	Parasite cytoplasm	Blood stage	<i>dhfr</i>	Treatment and prophylaxis (in combination)
Chlorproguanil / Proguanil	288.2 / 253.7	DHFR	Parasite cytoplasm	Blood stage	<i>dhfr</i>	Treatment and prophylaxis (in combination)
Sesquiterpene lactones						
Artemisinin [§]	282.3	PfATPase6 / Haemozoin formation ^{&}	Food vacuole	Blood stage and gametocytes	<i>atp6 / mdr1</i>	Treatment only
Aryl aminoalcohols						
Lumefantrine [#]	528.9	Haemozoin formation	Food vacuole	Blood stage	<i>mdr1</i>	Treatment only
Mefloquine	378.3	Haemozoin formation	Food vacuole	Blood stage	<i>mdr1</i>	Treatment and prophylaxis
Quinine	324.4	Haemozoin formation	Food vacuole	Blood stage	(<i>mdr1</i>)	Treatment
Respiratory chain inhibitors						
Atovaquone	366.8	Cytochrome bc ₁ complex	Mitochondria	Blood stage and liver stage	<i>cytb</i>	Treatment and prophylaxis

* No published data to confirm drug action

[§] Exact drug target is not known

[&] Possible drug target

[#] Only available in combination with artemether (ACT)

There is however an urgent requirement for new classes of anti-malarial drugs and concomitantly the identification of new anti-malarial drug targets. The Medicines for Malaria Venture (MMV) focuses on the identification and development of anti-malarial drugs. The MMV provides the gold standard and aims to develop a strong pipeline of molecules that will lead to the new generation of drugs (Figure 1.4) (www.mmv.org/research-development/r-d-process).

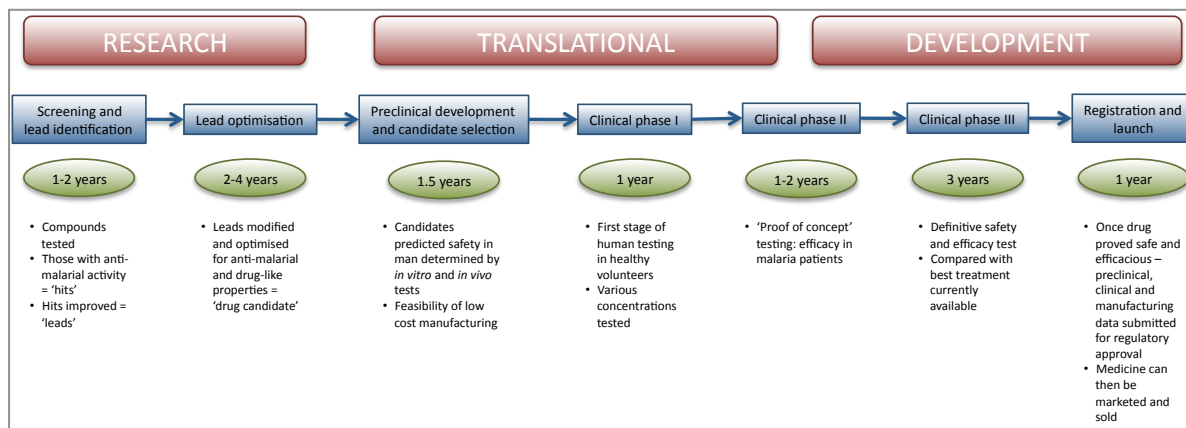


Figure 1.4. Conceptual pipeline of drug development employed by the MMV. Progression of a potential drug candidate through the various developmental and testing phases is indicated. Compiled from www.mmv.org/research-development/r-d-process and [47].

The MMV portfolio currently has numerous projects within the 'Research' component of its pipeline (Table 1.2) and their science portfolio now contains the most diverse group of anti-malarial drug discovery projects ever, with six projects in the translational phase, a further six in the development phase and has even progressed to the approval of new drugs [47]. The MMV works on the principle of public-private partnerships to create a product development partnership. Public and philanthropic funds enable both academic institutions and the pharmaceutical industry to perform research and development on what would normally be neglected diseases (www.mmv.org). One of the philanthropic sources of funding is the Bill and Melinda Gates Foundation, through their Global Health Program, which looks to develop and implement technology based health solutions. Their primary focus areas include enteric and diarrheal diseases, HIV/AIDS, malaria, pneumonia, tuberculosis and other neglected and infectious diseases. For malaria their grants include almost 300 million of dollars to programmes like the 'Medicines for Malaria Venture' and the 'Malaria Control and Evaluation Partnership in Africa' (www.gatesfoundation.org/global-health/Pages/overview.aspx).

Table 1.2. Projects within the research component of the MMV pipeline as at end first quarter 2011. DHODH: dihydroorotate dehydrogenase. Modified from <http://www.mmv.org/research-development/science-portfolio>.

Lead generation		Lead optimisation	
Novartis miniportfolio	Screening activities to identify new targets for the liver stages of <i>P. vivax</i> infection as well as optimization of externally identified compounds for <i>P. falciparum</i>	Novartis 2 projects	Series of imidazolopyrazines and pyrrolidines with potent and selective antimalarial activity
GlaxoSmithKline miniportfolio	Focusing on seeking a back-up pyridone, identifying inhibitors of DHODH, pathway and target-based screening and Hit-to-Lead activities on multiple whole-cell active series	GlaxoSmithKline 2 projects	Two series of heterocycles with potent and selective antimalarial activity
Broad & Genzyme miniportfolio	Three major approaches include: screening compound libraries, target-based screening in search of inhibitors of DHODH and sourcing new chemistry from nature.	Genz Aminoindole	A promising aminoindole preclinical candidate with high potency emerging from a whole cell screen
Pfizer screening	Screening activities to identify new chemical series active against <i>P. falciparum</i>	Aminopyridine	A project to identify novel antimalarial aminopyridines from a whole cell screen of the Biofocus DPI library
sanofi-aventis Orthologue screen	A project that focuses on identifying new molecules via a novel ortholog screening approach as well as refining previously identified molecules	Pyrazoles	A series of novel pyrazole antimalarials identified from virtual and whole cell screening
AstraZeneca Screening	Screening activities to identify new chemical series active against <i>P. falciparum</i>	Quinolines	New technologies being applied to improve the profile of a historical class of antimalarials
Kinases Monash	A novel way of rapidly screening each of the parasite's protein kinases against a compound library	DHODH	This project aims to identify a compound able to inhibit the parasite's DHODH enzyme.
Antimalarials St Jude/Rutgers	Screening of St Jude's library for active compounds		
Other projects 12 projects	MMV currently has 12 other projects underway to identify compounds that meet the MMV early lead criteria		


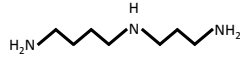
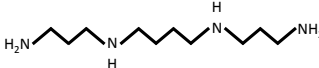

The search for new drug targets has accelerated with increased availability and annotation of genomic, proteomic and metabolomic data. Mining of this data has led to the identification of several possible targets that require further investigation (among others [48-51]). The inverse approach, that is, the search for drugs that show anti-malarial activity is also progressing well. GlaxoSmithKline recently screened their chemical library of over 2 million compounds and identified around 13500 compounds that show anti-malarial activity. The data and chemical structures of these compounds were made publically available [52] and this increases the exposure of these compounds to scientists in the academic, public and private sector, enabling greater and more rapid evaluation of the compounds to occur. The sheer number of compounds showing anti-malarial activity also creates hope as present drugs are failing.

1.4 POLYAMINES

1.4.1 General characteristics of the polyamines

Polyamines were first discovered in human semen by Antonie van Leeuwenhoek in 1678, when he described "three-sided" crystals [53]. They are low molecular weight aliphatic compounds [53] (Table 1.3) and are found in all living species with the exception of two orders of the Archaea [54].

Table 1.3. The structure, chemical name and molecular weight of the polyamines. Compiled from [53] and <http://pubchem.ncbi.nlm.nih.gov>.

Common name	Structure	IUPAC name	Molecular weight (g/mol)
Putrescine		butane-1,4-diamine	88.2
Spermidine		N-(3-aminopropyl)butane-1,4-diamine	145.2
Spermine		N,N'-bis(3-aminopropyl)butane-1,4-diamine	202.3
Cadaverine		pentane-1,5-diamine	102.2

At physiological pH, the polyamines are protonated, resulting in polycationic compounds, which are capable of electrostatic interactions with a variety of polyanionic molecules. Spermine and spermidine are capable of bridging both the major and the minor groove of DNA, with research suggesting that binding with distant fragments of the same DNA molecule being favoured [54]. This is possible due to the unique charge-structure conformation, as the positive charges are present at regularly spaced intervals along the flexible hydrocarbon chain [55]. Polyamines are also capable of covalent bonding to molecules. It has been found that within the cell polyamines bind not only to DNA, but also to RNA and to acidic phospholipids found within the membrane. They have also been implicated in the regulation of several membrane bound proteins (including adenylate cyclase, tissue transglutaminase and various ion channels) [54]. Polyamines are thus involved in numerous and diverse processes. Amongst these are regulation of gene expression, translation, cell proliferation, modulation of cell signalling, membrane stabilisation and modulation of certain ion channel activities. In plants, they are involved in stress responses and diseases [53], while it has also been established that polyamines play a role in cell death through apoptosis [56]. Polyamines thus regulate both cell proliferation and cell death, though which occurs depends on the cell type as well as environmental signals [57]. In *Plasmodium* species, apoptosis has been demonstrated in *P. berghei* [58] and it has been concluded that apoptosis in *P. falciparum* is possible [59]. Since they perform such a variety of functions, polyamine homeostasis is vital, as a major change (be it an increase or a decrease) in polyamine levels has numerous potential consequences on the cell (Figure 1.5) [53, 56].

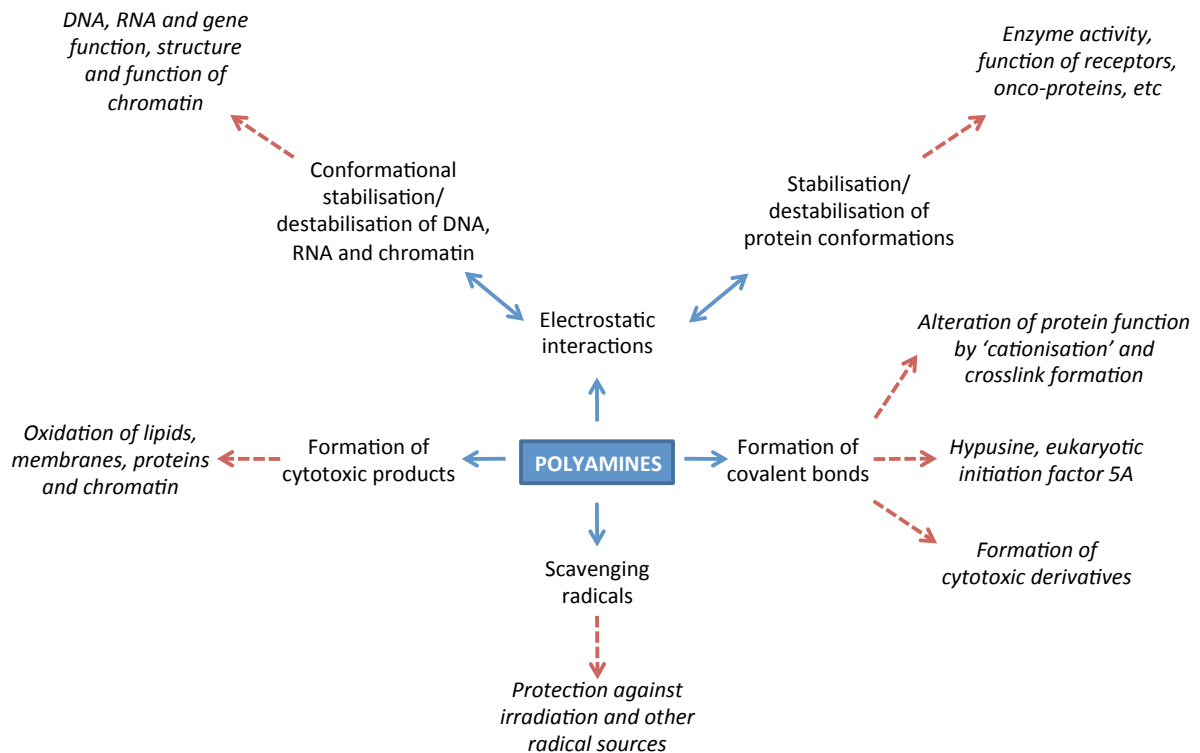


Figure 1.5. Role of polyamines in the cell and potential consequences upon a significant change in cellular polyamine concentration. Modified from [56].

1.4.1 Polyamines within the mammalian system

In mammalian cells, *de novo* synthesis is the major source of polyamines, but transport in the form of both import and export (as well as polyamine internalisation through endocytosis) does occur and contributes to polyamine homeostasis [54, 60]. In eukaryotic cells, L-arginine is converted into polyamines by means of a series of interdependent enzyme reactions. The decarboxylation of ornithine by ODC forms putrescine, which is then converted to spermidine by the incorporation of dcAdoMet (produced by AdoMet decarboxylase), catalysed by spermidine synthase. Another round of dcAdoMet incorporation and the action of spermine synthase yields spermine [54]. The biosynthesis of polyamines in mammalian cells is indicated in Figure 1.6.

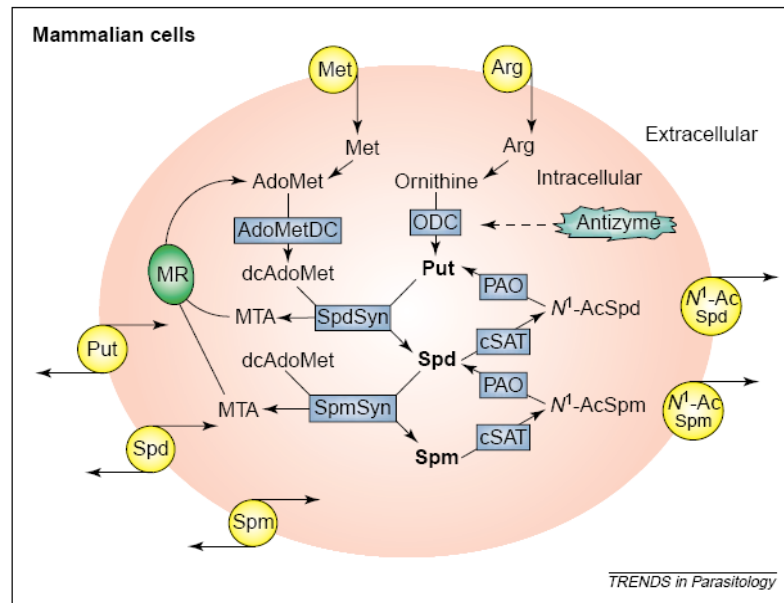


Figure 1.6. Polyamine biosynthesis in mammalian cells. The ‘inter-conversion’ pathway involving cSAT and PAO is capable of back converting the polyamines. A multi-enzyme pathway recycles MTA to methionine. AdoMet: S-adenosylmethionine; AdoMetDC: S-adenosylmethionine decarboxylase; cSAT: cytosolic N1-acetyltransferase specific for spermidine and spermine; dcAdoMet: decarboxylated S-adenosylmethionine; MR: Met recycling pathway; MTA: methylthioadenosine; N¹-AcSpd: N1-acetyl spermidine; N¹-AcSpm: N1-acetyl spermine; ODC: ornithine decarboxylase; PAO: polyamine oxidase; Put: putrescine; Spd: spermidine; SpdSyn: spermidine synthase; Spm: spermine; SpmSyn: spermine synthase. Taken from [61]

The mammalian ODC is a highly inducible cytosolic enzyme with a very short half-life (between 10 minutes and one hour) and a requirement for the cofactor pyridoxal-5'-phosphate. The enzyme forms a homodimer and the active site is localised to the interface between the two subunits. The enzyme is subject to both positive and negative feedback regulation by polyamines [54].

1.4.2 Inhibition of ornithine decarboxylase (ODC) with α -difluoromethylornithine (DFMO)

Ornithine decarboxylase (ODC) is a rate-limiting enzyme in polyamine biosynthesis. Some inhibitors of ODC are listed in Table 1.4 [54].

Table 1.4. Some inhibitors of ornithine decarboxylase (ODC). Modified from [54].

Inhibitors of ornithine decarboxylase (ODC)	
AEO	α -Ethylornithine
AHO	α -Hydrazino-ornithine
APA	1-Amino-oxy-3-aminopropane
AVO	α -Vinylornithine
AHMPA	(\pm)-5-Amino-2-hydrazine-2-methylpentanoic acid
DAB	1,4-Diaminobutane
DAP	1,3-Diaminopropane
DAPOH	1,3-Diaminopropan-2-ol
DFMO	α -Difluoromethylornithine
DL-HAVA	DL- α -Hydrazino- δ -aminovaleric acid
MAP	(2R,5R)-6-Heptyne-2,5-diamine
MFMP	DL- α -Monofluoromethylputrescine
V-MFMO	(E)-2-Fluoromethyldehydro-ornithine
α -MO	α -Methylornithine

DL- α -difluoromethylornithine (DFMO) is a rationally designed suicide (irreversible) enzyme-activated inhibitor of ODC and is analogous to the natural ODC substrate, ornithine [62]. The structure of DFMO, as compared with ornithine, is indicated in Figure 1.7.

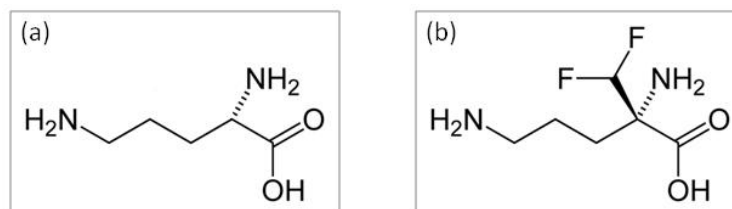


Figure 1.7. Structure of (a) ornithine - the natural substrate for ODC and (b) DFMO - an irreversible inhibitor of ODC.

Treatment with DFMO depletes cells of putrescine and spermidine, but has little influence on the spermine concentration [63]. DFMO uptake is unpredictable and slow as it is taken up by the cell through diffusion. DFMO treatment also appears to halt cell growth in the G1 phase and has proved to have a cytostatic effect. This could be due to the role that transport from the extracellular milieu has on polyamine homeostasis. DFMO has shown some, though limited, efficacy as an anti-tumour agent, but has proved much more useful as a treatment for African sleeping sickness (*Trypanosoma brucei gambiense* infection) [54, 64].

The mechanism of ODC inhibition by DFMO was determined using mouse ODC (Figure 1.8). It was found that Lys69 and Cys360 fall within the active site of the enzyme and upon decarboxylation of

the DFMO they bind the decarboxylated DFMO fragment covalently. The DFMO thus remains bound to the active site, rendering the enzyme inactive [65]. Both stereoisomers of DFMO are capable of inhibiting ODC activity, though L-DFMO is more potent than D-DFMO (kinetics reveal that 20 times less enzyme-inhibitor complexes form for D-DFMO than for L-DFMO, but that the enzyme decarboxylates the two enantiomers at a similar rate) [66].

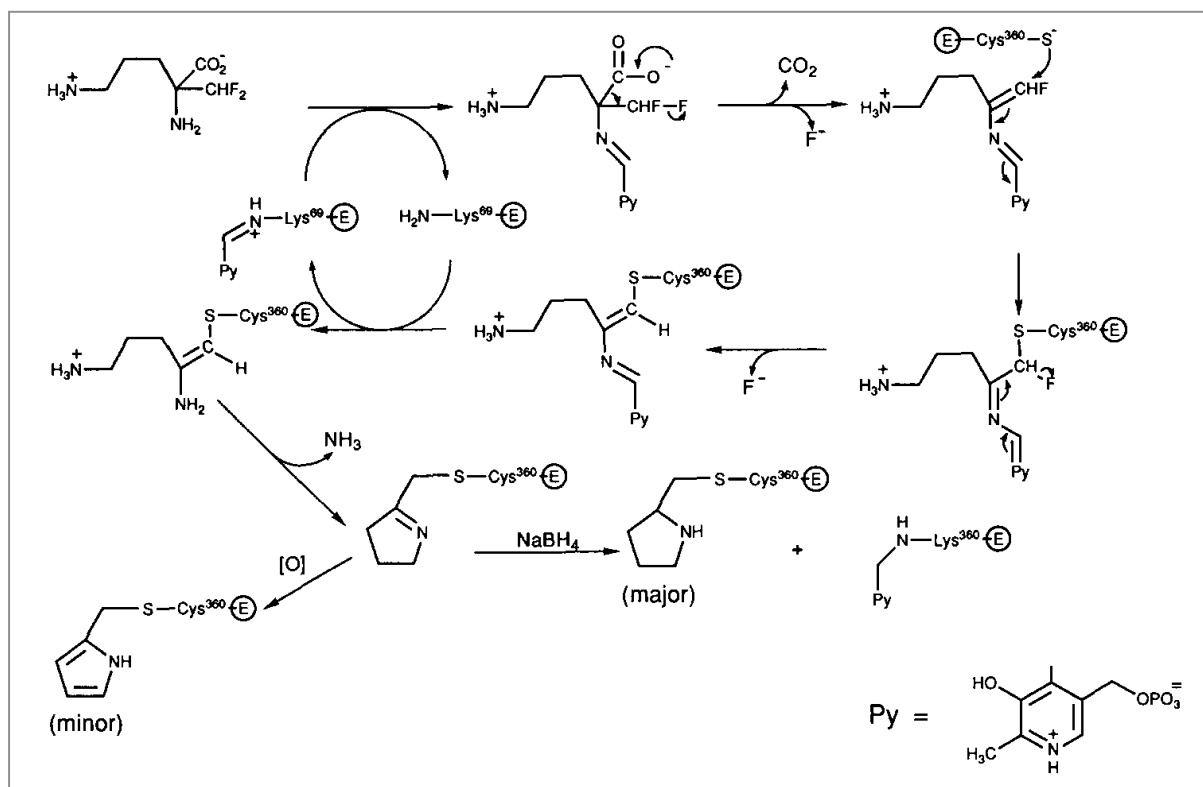


Figure 1.8. Proposed mechanism of DFMO inactivation of mouse ODC. Taken from [65].

1.4.3 Polyamine regulation within eukaryotic cells

Some of the polyamine regulation within mammalian cells is achieved through regulation of the rate-limiting enzymes, ODC and AdoMetDC. Mammalian ODC is regulated at several levels namely, transcriptional, translational and protein turnover/degradation [67, 68]. On the transcriptional level, the promoter region of the *odc* gene has several sequences that allow a response to hormones, growth factors and tumour promoters (cAMP response element, CAAT and LSF motifs, AP-1 and AP-2 sites, the GC-rich Sp1 binding sites and a TATA box). The promoter region is also a target of the oncogene *c-myc*, where an increase in the activity of the Myc/Max transfer complex results in an increase in ODC [67]. Another oncogene, *ras*, also has an effect and activation of the Ras pathway stimulates both ODC mRNA transcription and translation [67].

Translation of ODC can occur in both a cap-dependent and a cap-independent (through an internal ribosome entry site) manner [67]. Translational regulation is mostly controlled through the long 5' UTR of the gene and the intracellular polyamine concentration, where a decrease in cellular polyamine concentration results in increased ODC activity and *vice versa*. This increase is not due to increased mRNA production, but rather is attributed to increased protein synthesis. This effect is not ribosomal, but appears to be a product of a change in the secondary structure of the 5' UTR, which affects the rate of initiation and elongation of translation [69, 70]. Initiation of translation depends on the intracellular amount of active eIF-4E (the cap-binding subunit of the eIF-4F complex) present. The presence of an internal ORF may also play a role in translational regulation. Translational control of mammalian AdoMetDC differs from that of ODC in that although it too has both a long 5' UTR and an internal ORF, regulation does not appear to be dependent on secondary structure, nor concentration of eIF-4E. Like ODC, translation is repressed by increased polyamines. Upon inhibition of AdoMetDC, the enzyme levels increase, though the increase in mRNA does not correlate with the increase in the amount of protein (too little mRNA for the amount of protein) – polyamine depletion again results in an increase in the initiation of AdoMetDC translation [68].

Reduction in the amount of ODC present is facilitated by the rapid turnover rate of the enzyme [69]. Degradation is ubiquitin independent and is effected by the 26S proteasome. It is mediated by antizyme, which binds the C-terminal and enhances interaction with the proteasome, though it does not affect the rate of proteasome activity. Antizyme is a non-competitive inhibitor of ODC, synthesis of which is stimulated by an increase in polyamine concentration. The mRNA transcript for antizyme consists of two overlapping ORFs, the second of which contains no initiation codon. Through a +1 frameshift event upon increased polyamine concentration, both ORFs are translated. Antizyme consists of the product from both these ORFs. Antizyme is released from the ODC-proteasome complex and reused. Degradation of antizyme is ubiquitin dependent, a process that is inhibited in the presence of increased polyamines. An increase in polyamine concentration thus results in an increase in antizyme synthesis and concomitant decrease in antizyme degradation. Of the polyamines, spermidine and spermine are more effective than putrescine at stimulating antizyme synthesis. A further player is antizyme inhibitor that is similar to ODC, though exhibits no ODC activity. It has a higher affinity for antizyme than ODC does, resulting in the release of ODC. Antizyme inhibitor also has a short half-life (less than 30 minutes) and ubiquitin dependent degradation by the 26S proteasome occurs. Ubiquitination is prevented when the antizyme inhibitor is bound to antizyme, thus the inhibitor is stabilised. There are thus many factors that play a role in maintaining polyamines at the appropriate concentration [67]. Down-regulation of AdoMetDC activity is achieved

through an internal ORF (coding for the hexapeptide MAGDIS) that results in ribosomal stalling. The mechanism of AdoMetDC degradation is unknown [68].

1.4.4 The polyamines in *P. falciparum* parasites

In the 1980s, Assaraf and colleagues initiated the investigation of polyamines within the malaria parasite [63, 71-73]. They found that the concentration within infected erythrocytes was greatly increased and that DFMO treatment results in a decrease in putrescine and spermidine concentrations, with no effect on spermine levels (Table 1.5) - similar to treatment in mammalian cells [63].

Table 1.5. Polyamine concentration in uninfected erythrocytes, parasitised erythrocytes and parasitised erythrocytes treated with DFMO [63].

Polyamine	Polyamine concentration (pmol/10 ⁸ cells)		
	Uninfected erythrocytes	Parasitised erythrocytes	Parasitised erythrocytes + DFMO
Putrescine	1.9 ± 0.3	1720 ± 17	27 ± 3
Spermidine	18 ± 2	5090 ± 585	352 ± 27
Spermine	86 ± 10	1270 ± 70	1210 ± 107

Another similarity is that treatment of *P. falciparum* parasites with DFMO halts schizogony in the early trophozoite stage, resembling the late G1 phase in eukaryotic cells [71]. DFMO (5 mM) inhibited ODC activity by greater than 99%. The cytostatic effect of DFMO can be reversed and cell growth restored by the addition of 0.1 mM putrescine or 0.25 mM spermidine, though the addition of spermine does not have the same effect (although it was suggested this may be due to low penetration of the larger spermine molecule into the system) [73].

An investigation of the stage specificity of polyamine production within *P. falciparum* parasites found that the trophozoite and schizont stages contained the greatest concentration [74], which is not surprising as these are the stages at which the most growth and concomitant synthesis of DNA occurs (Table 1.6) [75].

Table 1.6. Polyamine concentration in the various parasite life-cycle stages. uRBC: uninfected erythrocytes [74].

Cell type	Polyamine concentration (nmol 10 ¹⁰ cells ⁻¹)		
	Putrescine	Spermidine	Spermine
Rings	35.9 ± 24.2	93.4 ± 62.9	5.1 ± 3.3
Trophozoites	454.5 ± 195.8	1079 ± 185	39.8 ± 17.2
Schizonts	624 ± 227.7	1295.4 ± 398.9	112.5 ± 53.2
uRBC	23.1 ± 10.3	43.5 ± 19.6	11.9 ± 8

The potential value of the polyamine pathway as a drug target is highlighted by the fact that the bis(benzyl)polyamine analogue MDL27695 (*N,N'*-bis{3-[(phenylmethyl)amino]propyl}-1,7-diaminoheptane), in combination with DFMO, proves 100% curative of murine (*P. berghei*) malaria and treated mice proved immune to re-infection. Various bis(benzyl)polyamine analogues also show strong anti-malarial activity against *P. falciparum* (both drug resistant and drug sensitive) *in vitro*, with potency increasing with an increase in length of the central methylene chain. The most potent of these analogues was approximately as potent as quinine [76]. The effect of MDL27695 was studied in rat hepatoma cells and is responsible for the down-regulation of polyamine biosynthesis (by inhibiting ODC and to a lesser degree AdoMetDC), with resultant polyamine depletion and growth inhibition [77].

The biosynthesis of polyamines in *Plasmodium* and several other protozoan parasites is compared with their human host in Figure 1.9. Within *P. falciparum* parasites the process is initiated by the action of arginase, which produces ornithine and urea from arginine [78]. An alternative pathway common in plants and bacteria that uses arginine decarboxylase to produce putrescine from arginine via agmatine has been excluded in *Plasmodium* [79]. ODC then catalyses the decarboxylation of ornithine to produce putrescine. In another branch of the pathway, AdoMet is generated from methionine and ATP by AdoMet synthetase. AdoMet is then decarboxylated by AdoMetDC and the decarboxylated AdoMet provides an aminopropyl moiety for the production of spermidine from putrescine via the action of spermidine synthase (with the release of methylthioadenosine (MTA)) [79, 80]. Spermidine synthase also shows some capacity for spermine synthesis [81]. MTA is recycled back into the purine pool through the action of adenosine deaminase (ADA) and purine nucleoside phosphorylase (PNP).

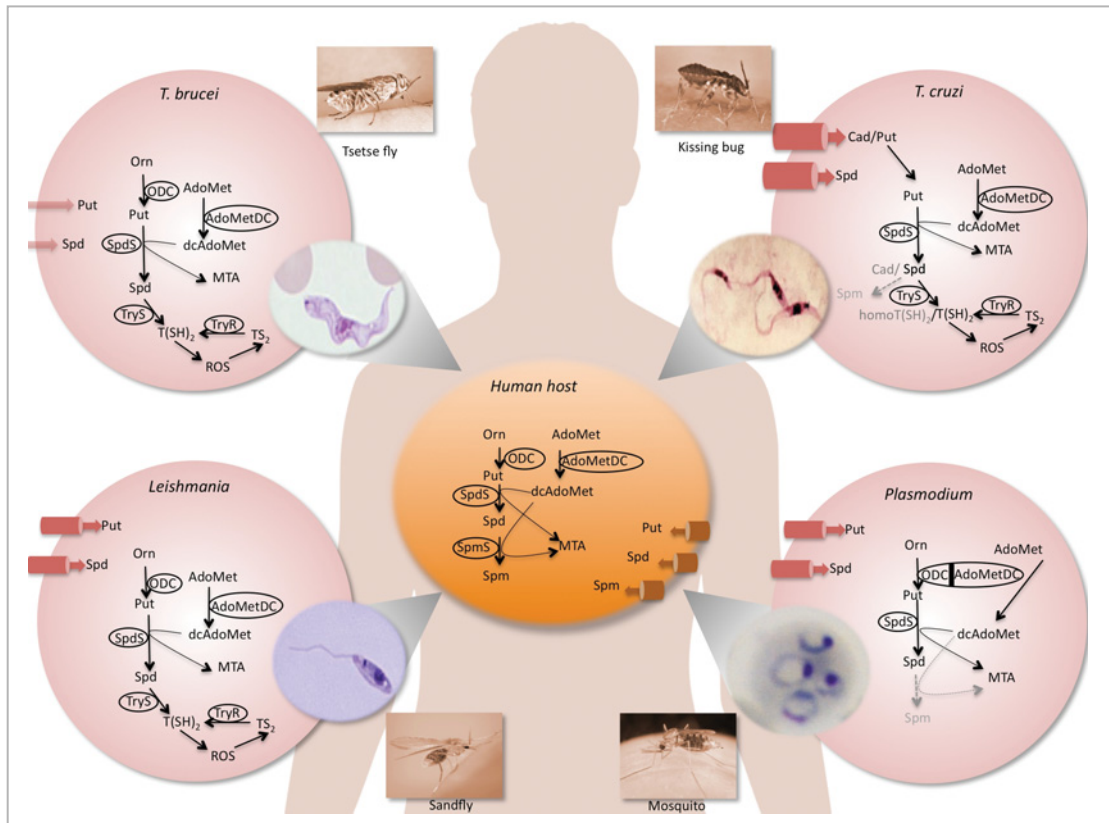


Figure 1.9. Comparison of polyamine biosynthesis in the protozoan parasites *Plasmodium*, *Trypanosoma*, *Leishmania* and their human host. The parasites and their insect vectors are also shown. Cell membrane transporters (cylinders) are sized approximately in proportion to their efficiencies. Cad: cadaverine; homoT(SH)₂: homotrypanothione; MTA: methylthioadenosine; Put: putrescine; ROS: reactive oxygen species; Spd: spermidine; Spm: spermine; TryR: trypanothione reductase; TryS: trypanothione synthetase; TS₂: trypanothione disulphide; T(SH)₂: dihydrotrypanothione. Taken from [82].

Within *P. falciparum* parasites, arginase is produced from a single gene and shows specificity for arginine ($K_m = 13$ mM). While the enzyme has a K_i for ornithine of 19 mM, the intracellular ornithine concentration is so low (29 μ M) that feedback inhibition by ornithine is unlikely. The functional enzyme is a homotrimer of around 160 kDa and is dependent on manganese to maintain this quaternary structure [78]. The crystal structure of arginase in the presence of a boronic acid inhibitor was recently determined and clarified the role of two of the polypeptide insertions that are unique to the malarial enzyme [83].

Unique to *Plasmodium*, the rate limiting enzymes ODC and AdoMetDC are found on a single polypeptide. Transcription of the gene occurs at 24–30 hours post-invasion in the late trophozoite stage of *P. falciparum* parasites. Translation results in a polypeptide of \sim 170 kDa, while both native and recombinant enzymes occur as a bifunctional heterotetramer of 330 kDa. Autocatalytic post-translational processing of the AdoMetDC domain contributes to the formation of the

heterotetramer [75]. Regions of sequence homology of both ODC and AdoMetDC are interrupted by large, parasite-specific insertions. Figure 1.10 indicates the layout of the bifunctional polypeptide, along with the size and position of the parasite specific inserts.

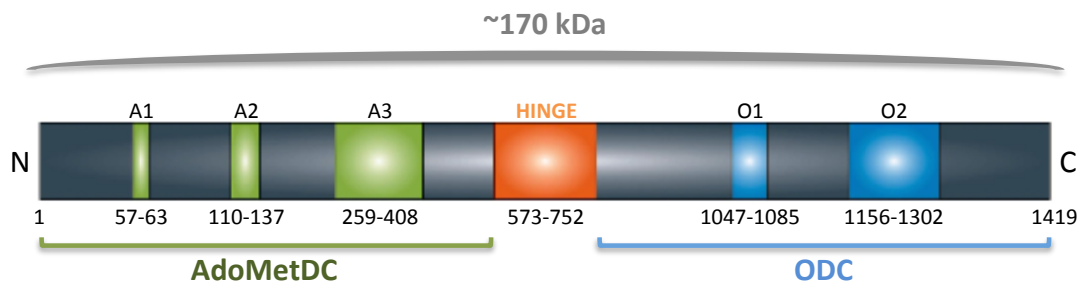


Figure 1.10. Representation of the ~ 170 kDa bifunctional AdoMetDC-ODC polypeptide. Two of these polypeptides associate to form the functional ~330 kDa complex. The N- and C-termini are indicated, along with the position the hinge and the positions of the parasite specific inserts in each component (A and O respectively). Modified from [82, 84].

Wrenger *et al.* speculated that the bifunctional nature of *Plasmodium* AdoMetDC-ODC may lead to balanced production of putrescine and decarboxylated AdoMet, as specific activities of two subunits are similar [85]. This is supported by a study of the PfAdoMetDC monomer, where the enzyme efficiency is better (k_{cat} of 5.3 min^{-1}) and the K_m is lower (250 mM) than that of the bifunctional protein (k_{cat} of 3.3 min^{-1} ; K_m of 58 mM), leading to the proposal that within the bifunctional protein AdoMetDC activity is modulated by the presence of the hinge/ODC such that metabolically important AdoMetDC is not pre-emptively removed from the system for decarboxylation to form spermidine in the absence of putrescine [86]. Bifunctional expression also allows co-ordinated regulation, which could prove important, as no antizyme is present for regulation [87].

The active sites of AdoMetDC-ODC operate independently of one another and the hinge is required for bifunctional complex formation [85, 87]. However, the parasite-specific inserts mediate both intra- and interdomain interactions, providing stability to the bifunctional complex and improving decarboxylase activities. These modulations are relevant to ODC in particular, where these interdomain regions appear more important for activity of the bifunctional complex than the presence of the hinge, as ODC is almost 10 times less active when recombinantly expressed in monofunctional form [87, 88].

A biochemical investigation of several aspects of the bifunctional protein revealed that the K_m of ODC for L-ornithine is $42.4 \pm 8.9 \mu\text{M}$, while that of AdoMetDC for AdoMet is $33.5 \pm 14.6 \mu\text{M}$ [75]. ODC is inhibited by putrescine, with a K_i of $68 \mu\text{M}$, which enables feedback regulation, as the intracellular putrescine concentration is $81 \mu\text{M}$. This differs from mammalian cells where ODC inhibition by putrescine hardly occurs [85].

Structural modelling has revealed several properties of the *P. falciparum* parasite's bifunctional protein [89, 90]. An homology model of ODC (Figure 1.11) reveals a doughnut shaped obligate homodimer, in which the N- and C-termini associate in a head-to-tail manner. Each ODC monomer has two distinct structural domains, namely an N-terminal α/β TIM barrel and a modified Greek-key β -barrel in the C-terminus. The two active sites are present at the domain interface and differences between human and *P. falciparum* ODC were observed in both the active site and the dimerisation interface. It also appears that one of the parasite specific insertions may play a role in stabilising the bifunctional protein complex [90].

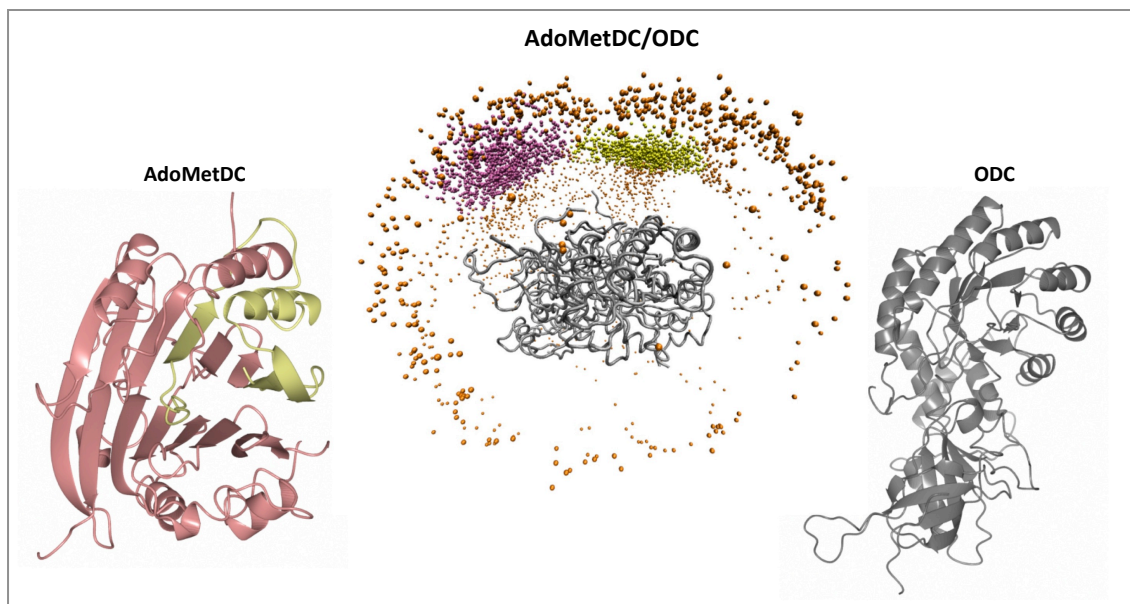


Figure 1.11. Ribbon diagrams of the homology models of the ODC and AdoMetDC monomers. The predicted bifunctional arrangement is shown in the middle. Modified from [82].

An homology model of AdoMetDC identified the presence of three parasite specific inserts and identified that the topology adopted is an $\alpha\beta\beta\alpha$ fold, the same as that of the human and potato AdoMetDC. The model also explained the lack of putrescine stimulation on activity and/or proteolytic processing of PfAdoMetDC that had been observed in mammalian cells [89]. This lack of putrescine stimulation indicates that the parasite enzyme lacks the regulatory mechanism proposed for mammalian cells, which relates putrescine abundance to spermidine synthesis [85].

Spermidine synthase is a 321 amino acid enzyme of 36.6 kDa and catalyses the formation of spermidine by transferring an aminopropyl group from dcAdoMet ($K_m = 35.3 \pm 4.1 \mu\text{M}$) to the terminal amino group of putrescine ($K_m = 52 \pm 0.6 \mu\text{M}$). It also shows some spermidine aminopropyltransferase activity, thus possibly accounting for the presence of spermine in the parasite in which spermine synthase is absent. Concentrations of up to $150 \mu\text{M}$ of dcAdoMet were

tested and showed no feedback inhibition [81]. The three dimensional crystal structure of spermidine synthase in the presence of dcAdoMet and two inhibitors showed that the flexibility of the gatekeeper loop allows binding of longer chain polyamines and may be what allows the enzyme to show limited spermine synthase activity [91]. One of the key features of spermidine synthase inhibition is the depletion of hypusine (produced from spermidine), which results in a decrease in the amount of eukaryotic elongation factor eIF5A present [92, 93]. Although the function of eIF5A remains to be definitively proven, it has been suggested that it functions in post-transcriptional processing of a subset of mRNAs, which encode factors responsible for cell viability and proliferation [94, 95].

When considering the specific activity of the enzymes involved in polyamine biosynthesis (Table 1.7), it is apparent that arginase produces ornithine in vast quantities. The remaining specific activities are all similar with the exception of spermidine synthase, which is at least 10 times greater (Table 1.7). This indicates that putrescine is rapidly removed from the system to form spermidine.

Table 1.7. Features of the enzymes involved in the polyamine metabolic pathway. All the values are for recombinant enzymes (the values of native AdoMetDC-ODC are given in parentheses) Compiled from [75, 78, 81, 85, 96] and <http://malaria.ucsf.edu/comparison/index.php>.

Enzyme	Arginase	AdoMetDC*	ODC*	Spermidine synthase	OAT
Specific activity	31 ± 6 umol/min/mg	20 ± 7 nmol/min/mg (native: 14.8 ± 5.6 pmol/min/mg)	38 ± 2nmol/min/mg (native: 93.2 ± 26.5 pmol/min/mg)	500 nmol/min/mg	56.12 ± 7.43 nmol/min/mg
K _m	13 ± 2 mM	58 ± 8 uM (native: 33.5 ± 14.6 uM)	41 ± 9 uM (native: 42.4 ± 8.9 uM)	52 ± 0.6 uM (putrescine) 35.3 ± 4.1 uM (dcAdoMet)	3.95 ± 1.04 mM
k _{cat}	96 / s	3.3 / min	NG	0.48 ± 0.05 / s	NG
Optimum pH	8.5 - 9.0	7.0 - 8.5	7.0 - 8.5	NG	NG
Assay pH	8.0	7.5	7.5	7.0	7.4
Feedback inhibition	Unlikely as intracellular ornithine concentration too low	NG	Putrescine	5'-methylthioadenosine	NG
K _i	Ornithine: 19 mM	NA	Putrescine: 68 uM	MTA - IC ₅₀ : 159 ± 27 uM	NA
IDC transcript expression profile					
Maximum :: minimum expression (hpi)	53 :: 31	24 :: 53	24 :: 53	18 :: 53	18 :: 53

NG: not given; NA: not applicable.

AdoMetDC* and ODC* are tabulated separately, but are part of a single bifunctional protein.

1.5 DRUG DISCOVERY IN THE GENOMIC AND POST-GENOMIC ERA

The genomes of all participants within the malaria life-cycle (*P. falciparum*, *Anopheles gambiae* and *Homo sapiens*) have been sequenced [8]. The genome of the 3D7 strain of *P. falciparum* parasites was published in 2002, following a whole chromosome shotgun sequencing strategy. The 23 megabase genome consists of 14 chromosomes and codes for approximately 5300 genes. It has an overall A+T nucleotide-composition of 80.6%. Some characteristics of the genome are that genes encoding for antigenic variation are located in the subtelomeric regions of the chromosomes and that the proportion of genes devoted to antigenic variation and host-parasite interactions is larger than that commonly found in free-living eukaryotes. It is predicted that 54% of the genes contain

introns. The predictive *P. falciparum* parasite proteome contains 5268 proteins, of which almost 60% are hypothetical and show insufficient similarity in function to any other known proteins. Of the predicted proteins, 31% have predicted transmembrane domains, 17% have putative signal peptides or anchors and ~14% of the proteins are predicted to be enzymes. With regard to energy metabolism, genes for glycolysis (but not gluconeogenesis), the pentose phosphate pathway (with the exception of one gene) and the tricarboxylic acid pathway were found [97].

Although a genome sequence is an invaluable tool, the genome alone will not provide a comprehensive understanding of parasite biology [98]. It does however provide the opportunity for detailed investigations of parasite biology, host-parasite interactions, vaccine and drug candidates and mechanisms of drug resistance and action [99]. Dissemination of information among all members of the malaria research community is also key in the post-genomic era [100] and this is greatly facilitated by the creation and continued improvement of the PlasmoDB database (www.plasmodb.org) [101-104].

Functional genomics is the application of high-throughput mRNA (transcriptomics), protein (proteomic) and metabolite (metabolomic) analysis techniques, which have been facilitated by the availability of a genome sequence, to investigate the spatial and temporal accumulation patterns of these molecules [105]. The subsequent step is a systems biology approach where the data obtained through functional genomics experiments is consolidated to discover unique data within the datasets [106]. The application of functional genomics and systems biology to the identification and validation of potential drug targets is indicated in Figure 1.12.

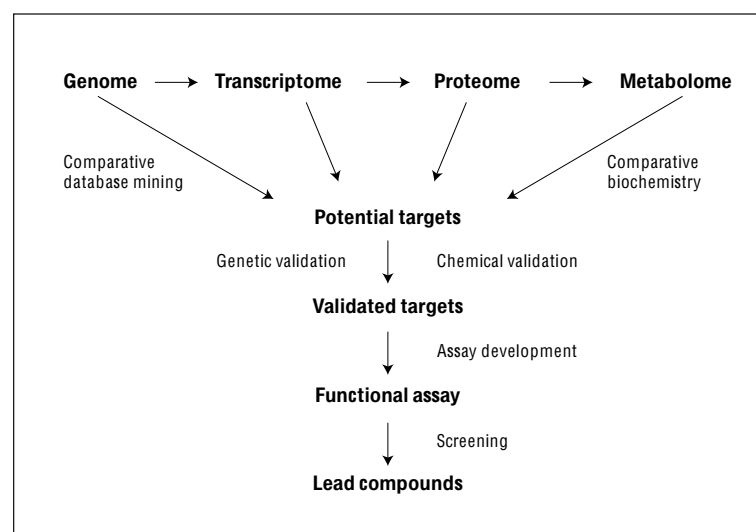


Figure 1.12. Diagrammatic representation of the use of functional genomics and systems biology for drug target identification and validation. Taken from [107].

Validation of a drug target requires verification that inhibition of the target is responsible for the therapeutic action of a proven drug, or demonstration that the putative target is essential for growth/survival of the organism. The target must also be capable of being selectively inhibited *in vivo*. In parasites, target validation is complicated by their complex life-cycles. Selectivity can be achieved through exploiting divergent biology between the parasite and the host, the simplified metabolism of parasites (they often have a strict dependency on certain metabolic pathways), differential binding of an inhibitor to the target (as a result of evolutionary sequence or structural target proteins) or the different metabolic fate of the target enzyme, a metabolite or the drug [108].

The essential and singular nature of a target can be demonstrated by genetic (knock-out of the target gene or knock-down of the target mRNA) or chemical means (drug inhibition), followed by rescue of the parasite through addition of the missing metabolite [108].

1.5.1 Functional genomics and *P. falciparum* parasites

The data generated from functional genomics approaches provides comprehensive information to understand numerous aspects of parasite biology. These include mechanisms of drug resistance, mechanism of drug action, gene regulation and annotation of hypothetical proteins (Figure 1.13).

Genome-wide questions	Transcriptome-specific questions
Life-cycle development (stage-specific expression)	Transcriptional machinery
Reproduction genes (strategy-specific expression)	Regulation of transcription
Drug resistance mechanisms	Transcriptional inheritance
Mechanism of drug action	
Responses to environmental stressors	Proteome-specific questions
Drug target specification	Post-transcriptional regulation
Host-specific adaptation and expression	Post-translational regulation
Identification of vaccine targets	
Virulence determinants	Interactome-specific questions
Severe disease progression <i>in vivo</i>	Protein function
	Relationships
	Regulatory mechanisms
Biological and mechanistic insights	
Metabolic pathways	
Identity determination of hypothetical proteins	
Cell cycle regulators	
Sex determinants	
Chemical validation of drug targets	
Mode of action of inhibitory compounds	
Improved drug target action	
Gene expression regulators (transcription & translation)	
Virulence factors	
Specialised organelle function and metabolism	
Damage compensation	

Figure 1.13. Various applications of functional genomic strategies to drug target and therapeutic discovery in the malaria parasite. Taken from [109].

1.5.2 Transcriptomics

It appears that protein abundance is tightly regulated in *Plasmodium*, despite the fact that the early analyses of the genome predicted that relatively few proteins for gene transcription are encoded. There are also few transcriptional regulatory elements present in the genome [9, 110].

Within the parasite, initiation of transcription is the same as in all eukaryotes. It is monocistronic, performed by RNA polymerase II, is dependent on a specific interaction with nuclear *trans* acting factors and binding activity of these factors is correlated with promoter activity [111].

With regard to transcriptional regulation within the Apicomplexa, there is no evidence that polycistronic transcription, trans-splicing or extensive posttranslational regulation of gene expression occurs [112]. The case can currently be made for control of gene expression at transcriptional, post-transcriptional and translational control (repression) [111, 113]. Nuclear run-on experiments indicate that there are three groups of genes, namely those that showed a high correlation between changes in transcriptional activity and steady state mRNA levels (transcriptional regulation), those that had major discrepancies between the two (post-transcriptional regulation) and those that had a low level of transcriptional activity. A significant level of antisense transcriptional activity was also observed indicating that antisense regulation may also contribute to gene regulation [114]. Many non-protein

coding RNAs (npcRNAs) have been identified and include some from repetitive regions of the telomeres and sub-telomeres, indicating that they may be involved in maintaining telomeric integrity and sub-telomeric gene silencing. Others are *cis*-encoded antisense npcRNAs, which are complementary to protein coding genes from various biochemical pathways [115].

An important development in understanding gene regulation in *P. falciparum* parasites was the identification of members of a *trans* acting transcription factor family, the apicomplexan AP2 (ApiAP2) [110, 116-119]. The ApiAP2 family contains 26 members, all of which contain at least a single copy of a small (~ 60 amino acids) domain that is highly conserved across *Plasmodium* [110]. The AP2 domains have been characterised and outside of this AP2 domain, there is low homology between the proteins (which can range in size from 200 to 4000 amino acids) [116, 120]. With the ability of the ApiAP2 proteins to bind both distinct primary and secondary motifs the complexity of the transcriptional regulatory network is increased. Using these motifs, potential target genes of the ApiAP2 family of transcription factors in *P. falciparum* parasites were identified. Since the transcription factors are expressed at distinct points during the 48 hour intra-erythrocytic developmental cycle (IDC) and bind a diversity of sequences, they can account for the regulation of the full cascade of gene expression. Furthermore, an interaction network between themselves suggests that they are also capable of regulating their own expression [121].

Genes cluster according to function in *Plasmodium* with the *var* genes of *P. falciparum* [122] and the *vir* genes of *P. vivax* [123] localising to the highly recombinogenic, subtelomeric regions of the chromosomes. Chromosomal clusters encoding co-expressed proteins are prevalent in the *P.falciparum* genome [124]. However, data mining of the transcriptome by examination of pathways that are metabolically linked has shown that transcription of genes coding for enzymes of intra- and inter-metabolic pathways is not necessarily always coordinated, with the transcription of certain genes limiting the full deployment of the pathway's activity [125].

Two separate studies initially investigated the transcriptional changes induced by life-cycle progression within *P. falciparum* parasites [126, 127]. Le Roch *et al.* investigated nine different stages of development namely sporozoites, merozoites, six time-points within the IDC and gametocytes [126], while Bozdech *et al.* delineated the 48 hour IDC into hourly intervals [127]. One of the major findings from these studies was the spectacular regulation of gene expression in the parasite, such that the timing of mRNA expression of a particular gene correlates extremely well with the functional requirement of the protein coded for and that this only occurs in a particular life-cycle stage of the parasite. Therefore a 'just-in-time' mechanism of gene expression is present in *P. falciparum*

parasites resulting in a cascade of mRNA production throughout the IDC where transcripts are produced when needed at a particular time-point within the life-cycle stage (Figure 1.14) [127] and subsequently efficiently removed through mRNA decay mechanisms [128]. This implies a significant contribution by post-transcriptional gene regulation [128]. The *P. falciparum* transcriptome is highly conserved, with little variation observed between geographically distinct strains like Dd2, HB3 and 3D7 [129].

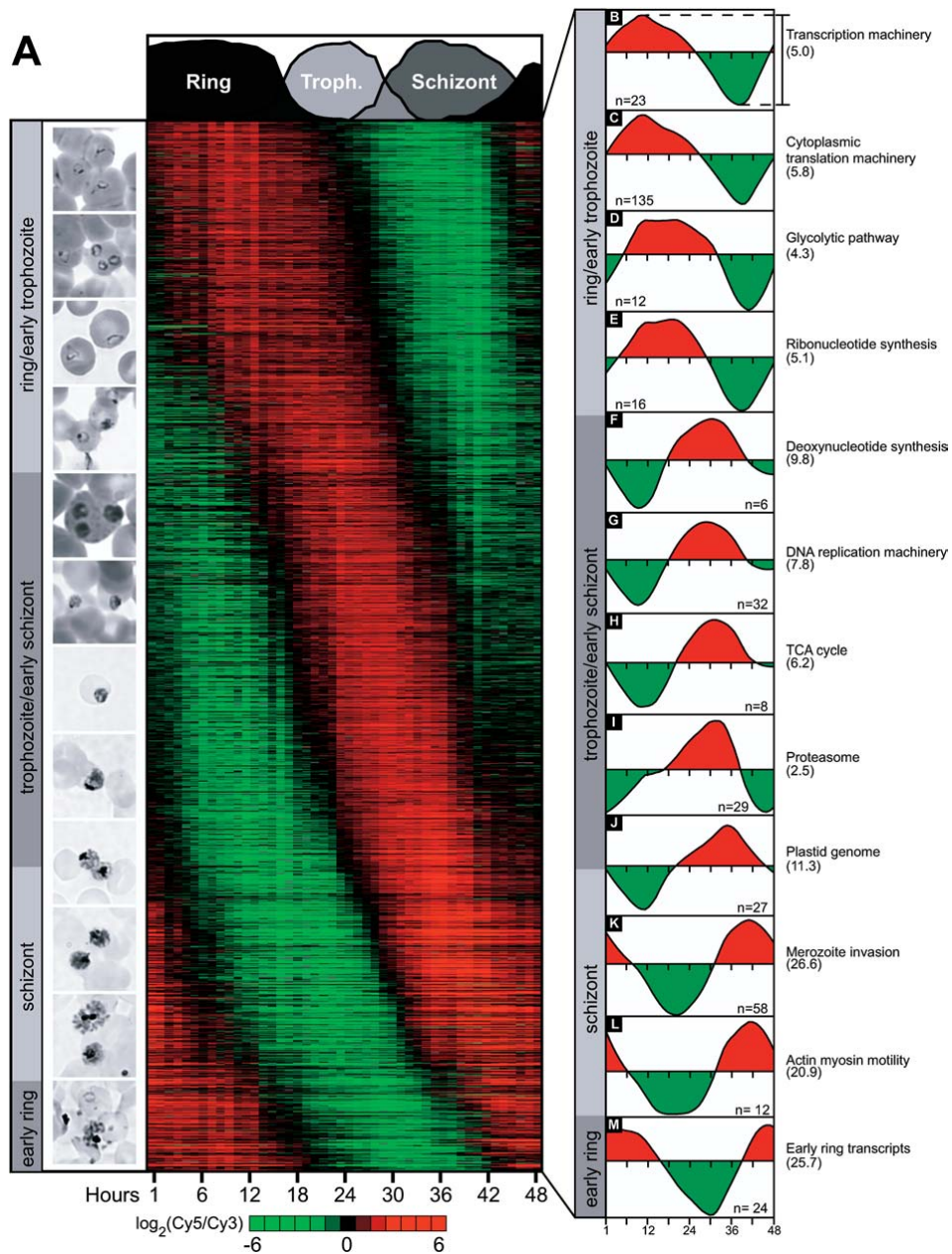


Figure 1.14. The cascade-like ‘just-in-time progression’ of the *P. falciparum* parasite transcriptome (A) Ordered transcriptional profiles of transcriptome. (B-M) Temporal ordering of biochemical processes. Taken from [127].

Other microarray studies continued investigations into the life-cycle and stage specific variation of various *Plasmodium* species [130, 131], pathogenicity factors [132, 133] and invasion preferences [134, 135]. Additionally, a global view of the non-protein coding transcriptome, indicated particular involvement thereof in gene regulatory mechanisms [115]. Although the *in vitro* transcriptome of *P. falciparum* parasites corresponds well to that of *in vivo* parasites, with differences limited to sexual stage antigens and surface proteins, it contributes to an understanding of parasite biology within the host environment where factors like the host immune system present challenges that are not encountered *in vitro* [136, 137].

Beyond the tight basal control of the transcriptome of *P. falciparum* parasites throughout the IDC, clear evidence now exists for the fact that the parasite is able to respond to external perturbations (e.g. drug treatments) on a transcriptional level. Even though the fold change of differentially expressed genes in the *P. falciparum* parasite transcriptome are atypically low compared with those usually observed in other systems, it is still useful in analyses of the functional consequences of drug treatment of the parasites. However, although differentially regulated gene expression was observed, this strategy was unable to shed light on a specific signature response for the classic anti-malarial drug chloroquine, supporting the notion that this drug has an intricate mechanism of action [138, 139].

The antifolate WR99210 inhibits dihydrofolate reductase-thymidylate synthase (DHFR-TS, a validated drug target) and differentially regulated genes were identified in the *P. falciparum* transcriptome that were anti-folate death-related, although transcripts for DHFR-TS and 14 other enzymes of the folate and pyrimidine biosynthesis pathways were not affected [139]. Microarrays were also used to show that the known anti-malarial doxycycline prevented the expression of apicoplast genes, resulting in aberrant apicoplasts, which eventually leads to parasite death [140]. Interestingly, a transcriptomic investigation of the addition of the bithiazolium choline analogue T4, which prevents the biosynthesis of phosphatidylcholine, showed no effect on the transcripts for enzymes of the phosphatidylcholine biosynthetic pathway [141]. The dynamic changes in RNA profiles after exposure to artesunate revealed no change in mRNA expression levels of *PfATPase6* (the SERCA-type *PfATPase6* is the putative target for artesunate). In fact no single specific metabolic pathway was identified, though differentially regulated genes included chaperones, transporters, cell cycle related proteins, kinases, zinc finger proteins, transcription activating proteins and proteins involved in proteasomal degradation [142].

Several biological processes of *P. falciparum* parasites have been investigated on the whole transcriptome level, including sporozoite penetration of skin cells [143] and febrile temperature changes [144]. The latter mimicked the temperature changes that the parasite would be subjected to in infected hosts and showed that this affected the expression of 6.3% of the genome, provided an indication of apoptosis-like death and allowed the assignment of biological function to more than 100 genes previously classified as 'hypothetical' [144]. This predictive value of whole transcriptome analysis, especially pertaining to the hypothetical proteins of unknown function, also indicated a previously annotated hypothetical protein to be required for tubovesicular network maintenance and hence parasite growth, in parasites treated with a sphingomyelin synthase inhibitor [145].

Epigenetic control of gene regulation has received a fair amount of attention over the last few years, especially with application to the virulence factor encoding *var* gene family. Chromatin modification plays a role in gene regulation and a full complement of chromatin remodelling proteins is present in *Plasmodium*. Histone modification (which includes amongst others, acetylation and methylation) can activate or silence genes [110, 111, 146, 147]. In an attempt to evaluate epigenetic control in the 'just-in-time' regulatory mechanism of the *P. falciparum* IDC transcriptome, parasites were treated with apicidin, an histone deacetylase inhibitor. This induced profound transcriptional changes in all parasite life-cycle stages, with a dramatic deregulation of the transcriptional cascade due to a disruption in histone modifications [148]. Evaluation of the parasite transcriptome after treatment with anacardic acid (an histone acetyltransferase inhibitor) revealed that approximately 5% of the parasite genes in the late trophozoite stage were affected, with the majority down-regulated due to reduced acetylation near the putative regions [149].

Transcriptome profiling has also progressed beyond the ability to determine if genes are just differentially expressed, to an evaluation of the entire genome, including intergenic regions, allowing the evaluation of genetic variation within defined phenotypes. This allows the identification of copy number variations as gene amplification events and demonstrated the presence of 90% of the single nucleotide polymorphisms (SNPs) between *P. falciparum* Dd2 and 3D7 parasite strains. The gene amplification of *pfgch1* and *pfdmr1* could be mapped and the mechanism of fosmidomycin resistance was also elucidated. The putative target protein 1-deoxy-D-xylulose 5-phosphate reductoisomerase (*pfdxr*) involved in isoprenoid biosynthesis, was shown to be amplified in fosmidomycin resistant parasites. Such amplification events may be an easy way for the parasite to increase transcription of important genes without resorting to modifying transcription rates [150]. This has recently also been extended to investigate compounds that interfere with the utilisation of the essential amino acid

isoleucine (that the parasite needs to obtain exogenously) to determine possible mechanisms of the development of resistance and thus whether isoleucine utilisation is a potential drug target [151].

Transcriptional profiles of parasites that were respectively challenged with 20 compounds showed that the data generated, along with a guilt-by-association prediction of protein function can be used to create an interaction network that reflects the functional relationship between genes. It was demonstrated that functionally related genes share a similar transcription profile to the diverse chemical challenges and thus may share a regulatory mechanism that responds to external stimuli [152].

A study with particular reference to this investigation (the effect of DFMO-induced ODC inhibition), as it forms part of a focused evaluation on the effect of inhibition of the bifunctional AdoMetDC-ODC, was the co-inhibition of the enzyme using DFMO and MDL73811. Transcriptional arrest in the trophozoite stage was observed and three compensatory transcripts, along with several genes within the polyamine pathway were identified as differentially regulated [1]. Another polyamine-related study was the inhibition of spermidine synthase with cyclohexylamine. As with AdoMetDC-ODC, transcriptional arrest in the trophozoite stage was noted. Transcripts and proteins involved in the polyamine biosynthetic pathway and also associated pathways were differentially regulated and this effect was also observable on metabolite level [3].

It has been established that the parasite is capable of altering its global pattern of gene expression when subjected to an external challenge, thus indicating that transcriptional gene regulation occurs. There is thus sufficient evidence that high throughput transcriptomic studies can be used to investigate amongst numerous others, the effect of drug perturbation within the malaria parasite.

1.5.3 Proteomics

Since there are fundamental differences between the processes of transcription and translation, transcriptomics alone does not provide sufficient information for a comprehensive understanding of parasite biology [153]. Additional information that may be highlighted during a proteomic approach include the presence of post-translational modification, the occurrence of isoforms of a particular protein, proteolytic processing events and consequently evidence for different levels of regulation may be obtained [153, 154]. Indeed, the presence of protein isoforms in *P. falciparum* has been observed using 2-dimensional gel electrophoresis [154].

As technology has advanced over the last several years, the amount of proteomic information has increased tremendously. Initially, multi-dimensional protein identification technology (MudPIT) analyses of four stages of the parasite life-cycle (sporozoites, merozoites, trophozoites and gametocytes) identified 2415 proteins including hypothetical proteins, confirming that these hypothetical ORFs are indeed coding regions. Additionally many surface proteins (particularly from the *var* and *rif* genes) were shown to be more widely expressed through the life-cycle than initially thought [124]. Individual high accuracy mass spectrometry analyses of asexual blood stages (714 proteins), gametocytes (931 proteins) and gametes (645 proteins) shed light on the *P. falciparum* parasite sexual stage protein expression [155]. Quantification of differential protein expression progressed with the establishment of a metabolic labelling approach, exploiting the absolute requirement of *P. falciparum* parasites for exogenous isoleucine. This allowed description of post-translational modification of parasite proteins after treatment of *P. falciparum* parasites with the anti-folate, pyrimethamine [156].

Proteome profiling has also focussed on specific aspects of parasite biology. A detailed time-course study of both transcript and protein levels during the IDC revealed that, like the transcripts, the proteins of *P. falciparum* parasites also showed cyclic abundance profiles. Protein abundance however peaks significantly later than the respective transcript, perhaps due to the dynamics of translation and protein degradation. Most proteins also had more than one isoform, probably as a result of post-translational modifications [157]. A comparison of the erythrocyte membrane and the parasites Maurer's clefts shed light on the biological function of the Maurer's clefts and established that the Maurer's clefts function as a secretory compartment, directing parasite proteins to the erythrocyte membrane. A degree of clustering of genes whose products are destined for/through the Maurer's clefts was also observed [158]. The rhoptries of three different *Plasmodium* species were also investigated using proteomics with 36 proteins identified as potentially being localised to the rhoptries, including homologues of the rhoptry proteins, proteases and enzymes involved in lipid metabolism [159]. Further localised proteomics analyses included studies of the parasitophorous vacuole [160], while one of the male and female gametocyte revealed sex-specific proteins and consequently sex-specific regulatory pathways [161].

As with transcriptomics, investigations into the effect of drug perturbation on the proteome are advancing rapidly. Particularly, treatment of *P. falciparum* parasites with CoArtem (i.e. lumefantrine and artemether) revealed the opposing effects of these drugs on key glycolytic enzymes [162]. Drug-specific effects were also described for treatment of *P. falciparum* parasites with chloroquine and artemisinin [163]. The effect of novel, potential anti-malarials have been also been investigated on

the proteome level. Bisthiazolium T4, an inhibitor of phosphatidylcholine biosynthesis, reduced the amount of choline/ethanolamine-phosphotransferase protein (a key enzyme in the final step of PC synthesis) [141]. Treatment of *P. falciparum* schizonts with the antibiotic doxycycline confirmed that the apicoplast and mitochondria are the likely targets of doxycycline [164]. The effect of a new anti-malarial endoperoxide, N-89 (1,2,6,7-tetraoxaspiro[7,11]nonadecane) was determined using comparative proteomics between an N-89 sensitive and an N-89 resistant strain of *P. falciparum* and revealed that proteins in the glycolytic pathway and the metabolism of proteins and lipids were affected [165].

Proteomics is also useful for investigating only selected proteins. As the mechanism of chloroquine action results in an increase in radical oxygen species and consequently oxidative damage, redox proteomics highlighted which proteins were specifically affected. Oxidation results in the formation of carbonyl groups in susceptible amino acids. These can be derivatised using 2,4-dinitrophenylhydrazine (DNPH) and the proteins separated with 2-dimensional gel electrophoresis. The derivatised proteins can then be detected using anti-dinitrophenyl antibodies. This revealed that the number and extent of functional proteins in protein folding, proteolysis, energy metabolism, signal transduction and pathogenesis were mostly affected by chloroquine treatment [166].

1.6 OBJECTIVE AND OUTPUTS

The primary objective was to investigate the transcriptomic and proteomic consequences of inhibition of ODC (induced by DFMO-treatment) on *P. falciparum* parasites, in order to contribute to the chemical validation of bifunctional AdoMetDC-ODC as a therapeutic drug target.

Chapter 2 presents a comprehensive transcriptome analysis of *P. falciparum* parasites treated with DFMO. Firstly, a profile of transcripts affected by DFMO induced inhibition of ODC within the parasite as determined by SSH-microarray, along with a more complete view of the effect of ODC inhibition on the global transcriptome as determined with an oligo-based DNA microarray. Chapter 3 investigates the effect of DFMO-treatment in a limited proteomics study, while Chapter 4 describes the relationship between ornithine metabolism and polyamine metabolism. Chapter 5 is a concluding discussion describing the highlights of the study, as well as the scientific contribution and future perspectives in this field.

Results from this study have been published and also presented at several local and international conferences as listed below.

1.6.1 Papers

Clark K, Dhoogra M, Louw AI, Birkholtz, L. (2008) Transcriptional responses of *Plasmodium falciparum* to α -difluoromethylornithine-induced polyamine depletion. *Biol Chem.* 389, 111-125

Birkholtz L, van Brummelen AC, Clark K, Niemand J, Maréchal E, Llinás M, Louw AI (2008) Exploring functional genomics for drug target and therapeutics discovery in Plasmodia. *Acta Trop.* 105, 113-123

Clark K, Niemand J, Reeksting S, Smit S, van Brummelen AC, Williams M, Louw AI, Birkholtz, L. (2010) Functional consequences of perturbing polyamine metabolism in the malaria parasite, *Plasmodium falciparum*. *Amino Acids* 38, 633-644

1.6.2 Conference proceedings

Clark K, Louw AI and Birkholtz L. (2005) Gene expression profiling of polyamine depleted malaria parasites using SSH and DNA microarray (poster). XIXth SASBMB, Conference, Stellenbosch, South Africa

Clark K, Claudel-Renard C, Joubert F, Louw AI and Birkholtz L. (2006) The effect of polyamine depletion on the transcriptome of the malaria parasite *Plasmodium falciparum* (poster). XXth SASBMB Conference, Pietermaritzburg, South Africa

Birkholtz L, Claudel-Renard C, Clark K and Louw AI. (2006) Differential transcriptome profiling indicates the physiological significance of polyamines in the human malaria parasite, *Plasmodium falciparum* (poster). Keystone Symposia on Malaria: Functional Genomics to Biology to Medicine, Taos, New Mexico, USA

Birkholtz L, van Brummelen AC, Clark K and Louw A. (2008) Functional genomics investigations of polyamine depleted *Plasmodium falciparum* reveal compensatory responses and novel metabolic activities (poster). Polyamines: Forty years of mammalian ornithine decarboxylase, Kuopio, Finland

Birkholtz L, van Brummelen AC, Clark K, Smit S and Louw A. (2009) Functional consequences of polyamine depletion in malaria parasites. Gordon Conference Expert Meeting on Polyamines (invited talk – L Birkholtz). New Hampshire, USA

Birkholtz L, van Brummelen AC, Clark K, Smit S and Louw A. (2011) Functional consequences of treatment of malaria parasites with polyamine analogues and biosynthesis inhibitors. Gordon Research Conference on Polyamines (invited talk – L Birkholtz). New Hampshire, USA

CHAPTER 2

Transcriptional response of ODC-inhibited *Plasmodium falciparum* parasites

2.1 INTRODUCTION

2.1.1 Transcriptomic profiling and methods of detecting differentially expressed genes

In the post-genomic era, global gene expression profiling has gained prominence as part of a functional genomics approach to answering various biological questions. Just over a decade ago three main techniques encompassed the tools for the study of transcriptional differences. These were hybridisation based (including Northern blotting, subtraction cloning, DNA microarrays, differential plaque hybridisation, and S1 mapping/RNase protection), PCR based (including differential display and Representational Difference Analysis, RDA) and sequence based (including Serial Analysis of Gene Expression, SAGE; Expressed Sequence Tags, ESTs; DNA sequencing chips; and mass spectrometry sequencing) techniques. Each of these techniques had its own advantages and disadvantages [167].

2.1.1.1 Suppression subtractive hybridisation

Suppression subtractive hybridisation (SSH) is a technique that preferentially selects for gene transcripts that are differentially expressed between two RNA samples, usually originating from two cell populations. These populations may be different types of cells, diseased versus healthy cells, or treated (with for example drugs or anti-metabolites) versus untreated cells from the same organism. Due to normalisation and subtraction steps, SSH allows the successful identification of transcripts of varying degrees of abundance (including those of low abundance) and differential expression, with a wider coverage of the total transcriptome *in situ*. A focussed library of differentially expressed transcripts of interest is thus created [168]. A further advantage of using SSH is that, similar to SAGE, the open platform profiling technology contributes to the annotation of previously uncharacterised open reading frames [169].

A diagram illustrating the SSH procedure is given in Figure 2.1. Firstly, cDNA is synthesised from RNA obtained from the two populations of interest. After digestion of both tester and driver cDNA with *Rsa1*, the tester cDNA is sub-divided into two and each portion ligated to a different adaptor. Both adaptors contain a stretch of identical sequence, allowing amplification using the PCR primer. Subsequently, two hybridisations are performed. The first commences with the addition of excess

driver to each tester sample and following heat denaturation and annealing, generates molecule types 'a', 'b', 'c' and 'd'. Due to the second-order kinetics of hybridisation, the reannealing of more abundant molecules is faster and the concentration of high and low abundance sequences (among type 'a' molecules) is thus equalised. Concomitantly type 'a' molecules are also enriched for differentially expressed sequences, while type 'c' molecules are formed (with the driver) by those that are not differentially expressed. A second hybridisation of the two initial hybridisations (without denaturing) allows only the single stranded tester cDNA (now equalised and subtracted) to reassociate and form type 'e' molecules. These are again enriched for differentially expressed sequences by the addition of fresh denatured driver cDNA. These type 'e' molecules are double stranded and contain different adaptors on either end, which can be used as annealing sites for nested PCR primers. Following PCR and nested PCR (to reduce background) the exponential amplification of the differentially expressed type 'e' sequences is achieved [170].

The application of SSH to answer wide-ranging biological questions in a variety of organisms is still relevant. Recent diverse studies include (amongst numerous others) the investigation of phosphorus accumulation and tolerance in sunflower plants (a commercial oilseed crop) for potential phytoremediation of phosphorus contaminated soil [171]; the identification of genes present in dormant (due to mechanical/harvesting stress) buds of tea plants to enable identification of genotypes with favourable phenotypes and thus improve yield and quality of the tea crop [172]; the identification of a gene involved in human breast cancer that can potentially be used as an expression marker for early identification [173]; as well as the identification of a 16S rRNA marker for a PCR based assay to detect human faecal contamination of water [174]. SSH has also successfully been applied to the malaria parasite to identify mosquito midgut stage-specific antigens [175]; to investigate the induction of novel genes in infected mosquitoes [176]; to identify ring stage transcripts [177]; and genes differentially expressed in the merozoite stage of *P. falciparum* [178]. Kappe and colleagues have applied SSH to both *P. yoelii* [179] and *P. berghei* [180] in order to identify sporozoite specific transcripts. More recently, some of the genes expressed during ookinete development and mosquito midgut invasion were identified [181] and the SSH library constructed to evaluate merozoite morphogenesis [178] was exploited to evaluate schizont specific gene polymorphism and structure [182].

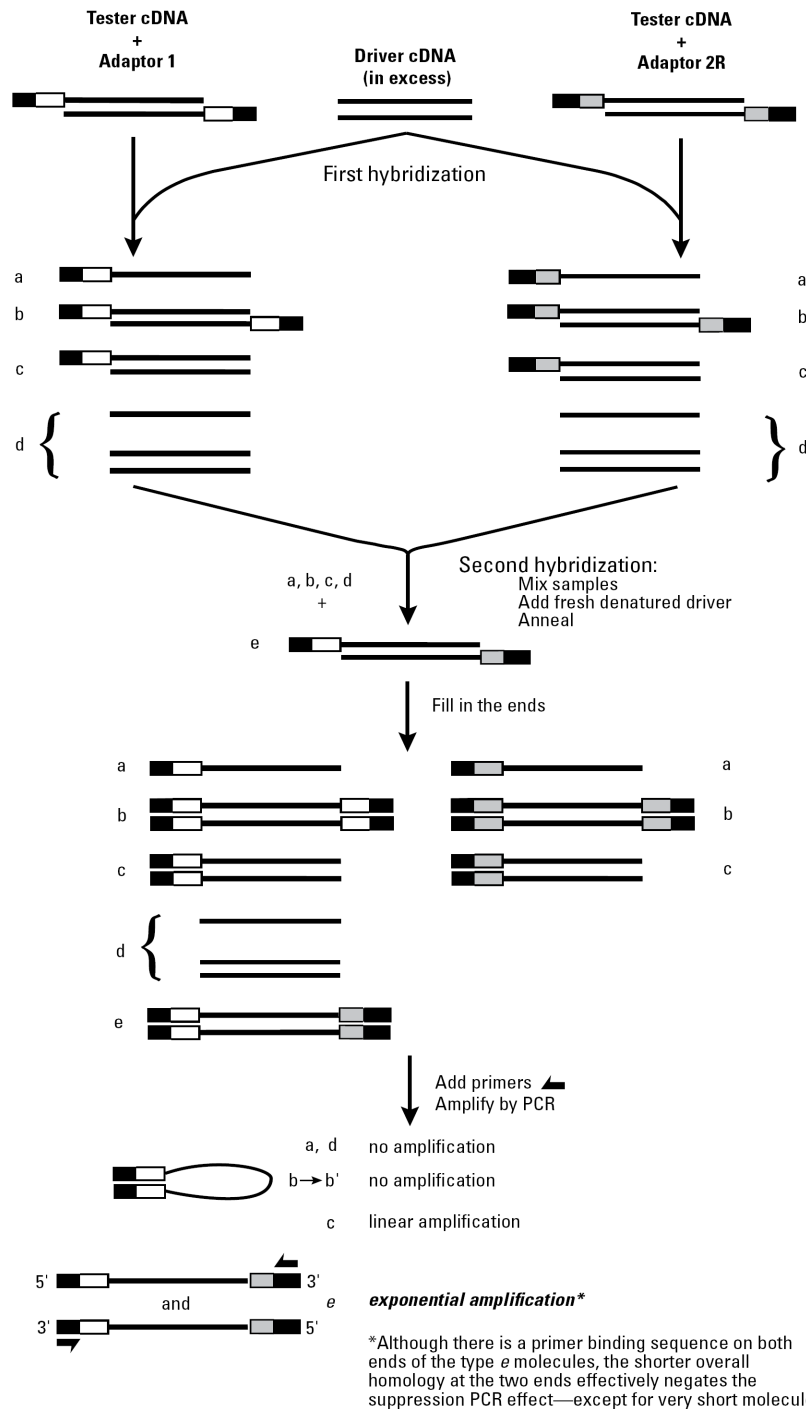


Figure 2.1. Schematic representation of the principle of SSH [170]. The equalisation of abundance and enrichment of differentially expressed sequences is achieved through two hybridisation steps. The differentially expressed sequences (type 'e' molecules) are then amplified using PCR and the background reduced with nested PCR. The solid lines are *Rsa1* digested tester or driver cDNA. The solid boxes represent the adaptors containing identical stretches of sequence corresponding to the PCR primer, while the clear and shaded boxes represent adaptors containing sequences for the nested PCR primers, respectively.

2.1.1.2 Microarrays

Microarrays are another method of investigating differential gene expression and several microarray technologies for the measurement of gene expression have emerged. These are primarily

characterised by probe type (cDNA and oligo – either presynthesised or generated *in situ*) and target labelling (one vs two colour) [183].

Spotted cDNA microarrays allow great scope for customisation, as only genes of interest are present on the slide resulting in ‘boutique’ arrays. Spotted microarrays include both cDNA microarrays and oligonucleotide arrays. cDNA microarrays are particularly useful if little genome sequence information is available, as a library of amplified cDNA can simply be printed onto a microarray slide and the sequence of the regulated transcripts determined after the analysis [184]. Either an inkjet dispensing system or a pin based robotic arrayer is used to print the prepared cDNA onto slides. The length of the probes is variable and a two-colour target labelling approach, with competitive hybridisation between two samples, is used [183].

An advantage of predesigned oligos over cDNA is that they are designed *in silico*, thus reducing the likelihood of misidentification of a probe through experimental error. Affymetrix and Agilent Technologies are two of the companies that offer slides with the probes generated *in situ*. Affymetrix uses a combination of photolithography and solid phase DNA synthesis to generate 25-mer oligo probes. They also employ a one-colour target labelling experimental methodology, where only one sample is hybridised per slide. Agilent, on the other hand, uses a non-contact inkjet delivery system utilising phosphoramidite chemistry (SurePrint technology, www.chem.agilent.com) to synthesise 60-mer oligos. The additional length offers advantages in hybridisation through increased specificity, as well as a steric effect, where some elevation from the slide enables better hybridisation. Sequence mismatches are also better tolerated with the longer oligos. As with the spotted cDNA microarrays, a two-colour target labelling approach is employed [183].

The planning of a microarray experiment is crucial to the outcome. While there are many factors to consider, the initial planning should focus on the type of comparison and the degree of replication required. Comparison may be direct, that is two samples are compared directly with each other; or indirect, where two samples are compared with each other, but via an intermediate. Direct comparisons are often performed within the slide (utilising two colour hybridisations where each sample is labelled with a different dye), while indirect comparisons utilise several slides [185]. For example Figure 2.2 (a) could have sample A labelled with Cy3 and sample B with Cy5. These are hybridised within a single array enabling a direct comparison between A and B. Figure 2.2 (b) represents an indirect comparison, where for example the Reference is labelled with Cy3 and each of the independent samples A-C with Cy5. Each individual sample is then hybridised with the Reference on an array. This obviously necessitates the use of several arrays (three in this case, one each for

samples A, B and C). Samples A and B can then be indirectly compared with each other (via the intermediary Reference). A loop design (Figure 2.2 (c)) is suitable for up to eight samples. In this design the reference sample is excluded in favour of comparing each sample with a subsequent one and the last sample with the first. The number of samples and the information desired should be considered when choosing an experimental design. The various designs can also be extrapolated to time-course sampling from a single experiment (Figure 2.2 (d)-(g)).

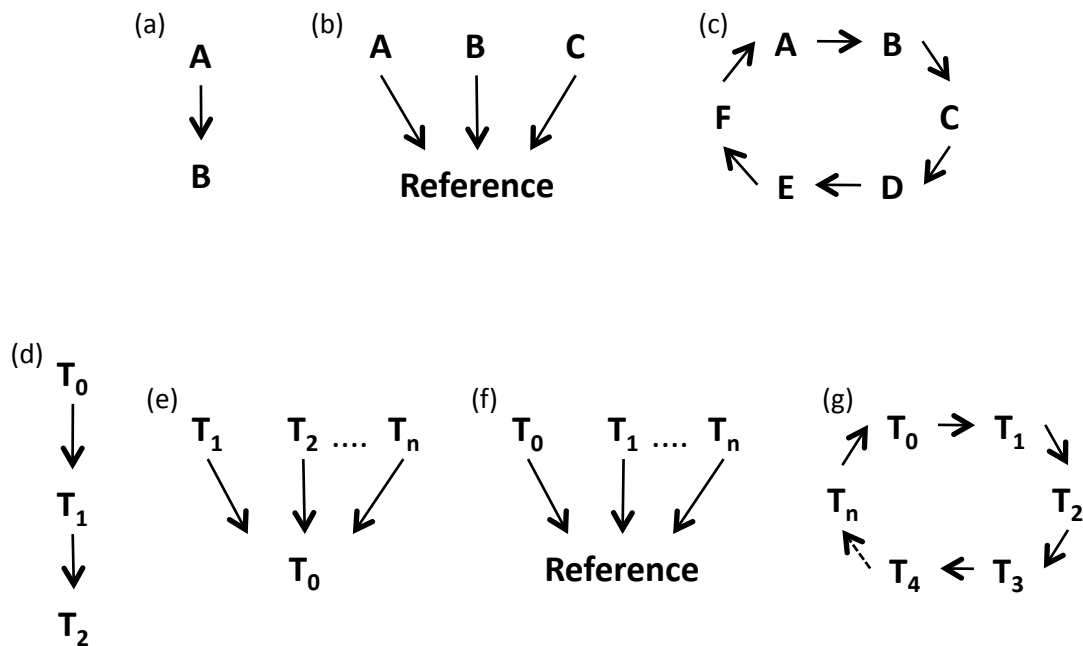


Figure 2.2. Various microarray experimental designs. (a) A direct comparison between two independent samples, (b) hybridisation against a common reference, (c) a basic loop design. (d-g) Extrapolation of design models to a time-course: (d) a sequential comparison, (e) hybridisation against a single time-point, (f) hybridisation against a common reference sample, and (g) a loop. Adapted from [185].

The second factor to consider is the degree of replication required. Replication is necessary to ensure statistical confidence in the data. There are two types of replication to minimise the two sources of variation, namely biological replication (for biological variation inherent to all living organisms) and technical replication (for variation introduced in the lab i.e. RNA isolation, labelling, etc). Biological replication is inherently at a level of completely independent replication of the entire experiment. Technical replication can occur at various levels, from labelling of the RNA, through to duplication of the target spots on the array. Generally, there is greater variation between biological replicates than between technical replicates [185-187].

2.1.1.3 The application of transcriptional profiling to *P. falciparum* parasites

The beginning of the century brought about a new age in malaria research, sparked by the publication of the *Plasmodium* genome in 2002. The genome sequence along with microarray technology has allowed for the global evaluation of the parasites response to, amongst several others, perturbations on a transcript level (see Chapter 1).

In this study, a combination of various techniques was used to study the transcriptome wide response of *P. falciparum* parasites to inhibition of ODC by DFMO. In order to investigate the complete genome response of the parasite to this treatment, the open nature of SSH was employed. The transcriptomic response of DFMO-induced polyamine depletion on late trophozoite stage of malaria parasites has been investigated using classical SSH [188]. However, this was expanded in order to provide additive data and allow stage specificity comparisons, by including sampling at several time-points (ring, early, mid and late trophozoite stages). This was combined with cDNA based (SSH libraries) DNA microarray to facilitate the evaluation of the differentially expressed genes. Therefore, SSH was used to generate libraries of genes that were differentially expressed and subsequently analysed using the high-throughput nature of DNA microarray to screen the libraries (results published in [189]).

However, upon more complete annotation of the *P. falciparum* genome, a more recent version of PlasmoDB (version 5.4) was available to be used to generate oligo-based DNA microarray slides spanning the complete predicted transcriptome of the parasite. Of late, technology to increase the density of spots on a microarray slide has increased in leaps and bounds. Agilent currently offers up to 8 arrays (capable of individual, though simultaneous hybridisation) on a single slide. Practically, these multi-array slides result in a massive cost and labour reduction for the researcher. The advantages of several whole genome microarrays on one slide are obvious especially that, due to the reduced feature size, significantly less volumes of parasite culture are required to obtain sufficient quantities of RNA. Therefore, in a follow-up experiment and due to technological developments, complete global oligo-based DNA microarray was performed on DFMO-treated parasites.

This chapter will therefore be structured in two parts, part 1 focussing on SSH-based technology and part 2 on classical oligo-based DNA microarray analysis of ODC-inhibited *P. falciparum* parasites.

2.2 MATERIALS AND METHODS

2.2.1 PART 1:

Transcriptional profile of ODC-inhibited *P. falciparum* parasites using SSH and cDNA microarray

2.2.1.1 *In vitro* *P. falciparum* parasite cultivation

A continuous *in vitro* culture of *P. falciparum* parasites (isolate Fab9) was maintained under conditions that support intracellular development of the parasites [190], with the replacement of 5% (w/v) Albumax II (Gibco) for human serum in the culture medium [191]. Culture medium consisting of 1.04% (w/v) RPMI 1640, with L-glutamine and without bicarbonate (Sigma) was supplemented with 22.2 mM glucose (Sigma), 25.2 mM HEPES (Sigma), 48 mg/l gentamycin (Sigma) and 21.4 mM sodium bicarbonate (Merck). In the SSH-cDNA microarray the culture medium was supplemented with 88 mg/l hypoxanthine, while in all other experiments, the hypoxanthine concentration was adjusted to 50 mg/l to conform to the most commonly used concentration in the literature.

Human blood (A⁺ or O⁺) was collected in vacuum collection tubes containing ethylene diamine-tetraacetic acid (EDTA) as an anti-coagulant. The blood was aseptically transferred to 10 ml centrifuge tubes and the cells pelleted by centrifugation at 1500g (Hermle Z320) for 5 minutes. The supernatant and leucocyte containing Buffy coat were aspirated, an equal volume of culture medium (excluding Albumax II) added to the erythrocytes and mixed by pipetting. The cells were pelleted by centrifugation at 1500g for 5 minutes. This wash step was repeated a further 3 times. The washed erythrocytes were resuspended in an equal volume of Albumax II free culture medium.

Cryopreserved *P. falciparum* was placed in culture by thawing the culture in the cryovial at 37°C and transferring the contents (approximately 1 ml) to a 10 ml centrifuge tube. NaCl (0.2 ml of 12%) was added and carefully mixed in, followed by the careful addition and mixing of 1.8 ml of 1.6% NaCl. The cells were pelleted by centrifugation at 1500g for 5 minutes, the supernatant aspirated and 10 ml culture medium (containing Albumax II) added. The suspension was transferred to a 75 cm² tissue culture flask and the haematocrit adjusted to 5% with washed erythrocytes. The atmosphere in the culture flask was replaced with 5% O₂, 5% CO₂ and 90% N₂ (Afrox) and the culture incubated at 37°C.

An erythrocyte haematocrit of 5% and a parasitaemia of 10% were maintained during culture growth. The health of the cultures was monitored by means of a thin smear, fixed with methanol and stained with Giemsa's azur eosin methylene blue stain (Merck) in phosphate buffered saline (1x PBS:

137 mM NaCl, 2.7 mM KCl, 1.8 mM KH_2PO_4 , 10 mM $\text{Na}_2\text{HPO}_4 \cdot 7\text{H}_2\text{O}$, pH 7.4). The smear was examined using a light microscope (Nikon Labophot), under a 1000x magnification.

2.2.1.2 Morphological evaluation of DFMO-treated and untreated parasites

The morphological monitoring of drug treated parasites was conducted with two flasks (75 cm²) each containing 10 ml of parasite culture. The parasites were synchronised twice using sorbitol [192], pelleted by centrifugation at 1500g (Hermle Z320) for 5 minutes, followed by aspiration of the supernatant. The pellet was resuspended in 5 pellet volumes of 5% sorbitol (Sigma) and again pelleted by centrifugation. The cells were washed with 5 pellet volumes of complete medium, which was subsequently removed by centrifugation and aspiration and the cells resuspended in an appropriate volume of complete culture medium to re-establish a 5% haematocrit. Smears of the parasite culture were prepared every 6 hours and examined microscopically to determine the proportion of parasites present in each asexual blood stage.

2.2.1.3 Parasite culture, treatment and sampling for transcriptional profiling by SSH-cDNA microarray

Parasites (strain Fab9; synchronised twice using sorbitol [192]; 50 ml culture in 175 cm² flasks) were treated with 10 mM DFMO (10x IC₅₀ [1]) at approximately 2-3 hours post-merozoite invasion. Untreated parasite culture was maintained in parallel. A biological replicate of each culture was also maintained. Samples of culture (10-15 ml) were removed at 4 (ring), 18 (early trophozoite), 21 (mid-trophozoite) and 27 (late-trophozoite) hours post-treatment and smears for microscopic evaluation were prepared at these time-points. The parasites were pelleted by centrifugation at 1500g (Hermle Z320) for 5 minutes, then washed three times with 1x PBS and the pellets were subsequently stored at -70°C.

2.2.1.4 RNA Isolation and electrophoresis

RNase-free water was generated by incubating a 0.1% (v/v) diethylpyrocarbonate (DEPC, Sigma) solution at 37°C for several hours, followed by a minimum of two rounds of autoclaving (121°C for 20 minutes) to inactivate the DEPC.

Total RNA was isolated using a combined TRI-Reagent (Sigma-Aldrich Inc.) and RNeasy® Protect Mini Kit (Qiagen) method, with the inclusion of on-column DNase digestion. Briefly, lysis buffer from the RNeasy Kit was added to the thawed parasite pellet. This was passed through a QIAshredder™ (Qiagen) column. TRI-Reagent was added and the manufacturer's protocols followed for TRI-Reagent

up to transfer of the aqueous phase after chloroform extraction. An equal volume of 70% ethanol was added, after which the manufacturer's protocols for the RNeasy kit were followed.

The integrity of the isolated RNA was determined by gel electrophoresis on a 1% denaturing agarose gel (1% (w/v) agarose (Promega), 1x MOPS (contains 20 mM 4-morpholinepropanesulphonic acid (MOPS, Sigma), 5 mM sodium acetate and 0.5 mM EDTA) and 5.5% (v/v) 37% formaldehyde). RNA (3 µg) was suspended in a 1x MOPS solution containing 12% (v/v) formaldehyde and 40% (v/v) deionised formamide. The samples were denatured at 55°C for 15 minutes before adding loading/tracking dye (0.025% (w/v) bromophenol blue, 30% (v/v) glycerol) and 3 µg of ethidium bromide. The RNA was electrophoresed using a MiniCell® EC 370M Electrophoretic Gel System (E-C Apparatus Corporation) at 78 V (5.2 V/cm) and visualised using a transilluminator (Spectroline® TC-312A, 312 nm, Spectronics Corporation).

2.2.1.5 Suppression Subtractive Hybridisation (SSH)

Two kits were used for the SSH. Firstly, double stranded cDNA was synthesised, purified and digested with *Rsa*I using the BD SMART™ PCR cDNA Synthesis Kit (BD Biosciences). The suppression subtractive hybridisation and related steps were performed using the PCR-Select™ cDNA Subtraction Kit (BD Biosciences).

RNA from the four time-points (from both biological replicates) was quantitatively pooled into a 'Treated' and 'Untreated' pool respectively. Both forward and reverse subtracted libraries were generated with SSH. For the forward subtracted library, the tester originated from treated RNA and the driver from untreated RNA, while in the reverse subtracted library, tester originated from untreated RNA and driver from treated RNA. To facilitate the explanation of the methodology, the primers used in the SSH procedure are given in Table 2.1.

First strand cDNA was synthesised using the BD SMART™ PCR cDNA Synthesis Kit as per the manufacturer's instructions (BD Biosciences Clontech), followed by amplification by means of long distance PCR (LD PCR), without disturbing mRNA ratios (20 cycles of amplification proved optimal for achieving this). The LD-PCR samples were cleaned by column chromatography. cDNA was also synthesised from skeletal muscle poly A⁺ RNA (supplied in PCR-Select™ cDNA Subtraction kit) for use as control C2, as per the manufacturer's instructions.

Table 2.1. Sequences of the primers and adaptors used in the SSH procedure. The kit from which the oligonucleotides originated is listed. The bold, underlined nucleotides indicate the *Rsa1* site (or half site – double underlined).

Primer/Adaptor name	Sequence	Source
cDNA synthesis primer	5'-TTTT <u>GTAC</u> AAGCTT ₍₃₀₎ NN-3'	PCR-Select cDNA Subtraction Kit
BD SMART II™ A oligonucleotide	5'-AAGCAGTGGTATCAACGCAGAG <u>GTAC</u> GCGGG-3'	BD SMART™ PCR cDNA Synthesis Kit
3' BD SMART™ CDS primer II A	5'-AAGCAGTGGTATCAACGCAGAG <u>GTACT</u> ₍₃₀₎ V N-3'	BD SMART™ PCR cDNA Synthesis Kit
5' PCR primer II A	5'-AAGCAGTGGTATCAACGCAGAGT-3'	BD SMART™ PCR cDNA Synthesis Kit
Adaptor 1	5'-CTAATACGACTCACTATAGGGCTCGAGCGGCCGCCGGG <u>CAGGT</u> -3' 3'-GGCCCGTCCA-5'	PCR-Select cDNA Subtraction Kit
PCR primer 1	5'-CTAATACGACTCACTATAGGGC-3'	PCR-Select cDNA Subtraction Kit
Nested primer 1	5'-TCGAGCGGCCGCCGGG <u>CAGGT</u> -3'	PCR-Select cDNA Subtraction Kit
Adaptor 2R	5'-CTAATACGACTCACTATAGGGCAGCGTGGT <u>CGCGCCGAGGT</u> -3' 3'-CGGCTCCA-5'	PCR-Select cDNA Subtraction Kit
G3PDH 5'-primer	5'-ACCACAGTCCATGCCATCAC-3'	PCR-Select cDNA Subtraction Kit
G3PDH 3'-primer	5'-TCCACCACCCTGTTGCTGTA-3'	PCR-Select cDNA Subtraction Kit
Nested primer 2R	5'-AGCGTGGT <u>CGCGCCGAGGT</u> -3'	PCR-Select cDNA Subtraction Kit

The samples at this point consisted of double stranded cDNA for treated, untreated and control samples, generated using the SMART kit and cleaned using column chromatography and double stranded cDNA of control C2, generated using the PCR Select kit. All the samples were digested with *Rsa1* and the *Rsa1* digested products cleaned using the PCR clean-up protocol of the Nucleospin Extract kit (Machery Nagel) as per the manufacturer's instructions.

At this point, the suppression subtractive hybridisation reactions commenced using the PCR-Select™ cDNA Subtraction Kit (BD Biosciences). Adaptors were ligated and ligation efficiency tested. This was followed by the primary and secondary hybridisations to select for the differentially expressed transcripts. These differentially expressed transcripts were then amplified and the background reduced using PCR, followed by nested PCR. In all cases, the manufacturer's instructions were followed, with one notable exception, namely the hybridisation temperature of 68°C recommended for the first and second hybridisations was lowered to 64°C [177, 178]. Table 2.2 indicates the composition and condition of the tester and driver cDNA used for the forward and reverse subtractions respectively.

Table 2.2. Composition and condition of tester and driver cDNA.

Forward subtraction			Reverse subtraction		
Name	Type	Condition	Name	Type	Condition
cDNA1	Tester	Treated	cDNA1	Driver	Treated
cDNA2	Driver	Untreated	cDNA2	Tester	Untreated

At this point, the SSH procedure was complete and a forward subtracted library and a reverse subtracted library of gene transcripts affected by DFMO-treatment had been generated. The

subtracted libraries were sub-cloned using the pGEM[®]-T Easy Vector System (Promega) and transformed into XL2-Blue ultracompetent and SURE competent *E. coli* cells (Stratagene) by heat shock [193].

Colony PCR was used to screen the transformants for positive clones using nested PCR primer 1 and nested PCR primer 2R (from the PCR Select[™] cDNA subtraction kit; Table 2.1). PCRs (100 µl reaction volume) were conducted in 96-well format and contained 30 pmol of each primer (nested primer 1 and nested primer 2R), 20 nmol of dNTPs, 1 µl of template (*E. coli* culture) and 1.25 U TaKaRa ExTaq[™] DNA polymerase in 1x ExTaq PCR buffer containing 2 mM MgCl₂. The cycling conditions were 94°C for 5 minutes (to lyse the bacterial cells), followed by 25 cycles of 94°C for 30 seconds, 68°C for 30 seconds and 72°C for 2 minutes (Applied Biosystems thermal cycler). The PCR ended with 7 minutes at 72°C to extend any incomplete products. The products (5 µl) were analysed using 1.5% agarose and using the Applied Biosystems Stretch Rig, which enables the loading of two 96-well plates onto a single gel using a multichannel pipette. The Stretch Rig system was run at ~3 V/cm.

2.2.1.6 Agarose gel electrophoresis

DNA (both single stranded and double stranded) was separated on agarose gels. The percentage gel ($^w/v$) was dependent on the type and size of the DNA under investigation. Gels were prepared and run in 1x TAE (40 mM Tris-acetate, 1 mM EDTA). Loading/tracking dye was added to the samples (1:5; dye:sample) prior to electrophoresis. Large quantities of samples were generally run on a Maxicell[™] EC 360M Electrophoretic Gel System (E-C Apparatus Corporation) at 109 V (3.5 V/cm), while smaller sample quantities were run on a Minnie Submarine Agarose Gel Unit, Model HE33 (Hoefer Scientific Instruments) at 4-10 V/cm. Ethidium bromide (0.5 ng/ml) was usually included in the gel and visualisation was by means of the Spectroline[®] TC-312A transilluminator.

2.2.1.7 Microarray printing

The remainder of the PCR products were purified using Montage PCR₉₆ Plates (Millipore). Samples were transferred from the PCR tube to the plate under a vacuum manifold at 24 mm Hg for 10 minutes. The plate was removed from the vacuum manifold and 50 µl of water added. The plate was shaken vigorously for 15 minutes and the clean PCR products transferred to a 96-well plate. The water was evaporated using a Savant Speedy Vac with a refrigerated vapour trap (Thermo Electron Corporation), resuspended in 15 µl of water and subsequently shaken at 37°C for 2 hours. Any wells that contained multiple or no bands (as evaluated from the agarose gels) had their contents removed, the well thoroughly washed with water and replaced with an appropriate PCR product. This process was repeated until 856 products from the forward subtracted library and 864 products

from the reverse subtracted library were available. The concentration of several of the cleaned, resuspended products was determined using a NanoDrop® ND-1000 spectrophotometer. The products chosen for quantification included bands of high, low and intermediate intensity.

The purified, resuspended PCR products were transferred to 384-well microwell plates, appropriate for use by the microarray spotter. Microarray printing was performed on the GenIII Spotter (Molecular Dynamics, GE Healthcare) at the ACGT Microarray Facility of the University of Pretoria (www.acgt.co.za). The products were dried and subsequently resuspended in the microarray spotting solution of 50% dimethylsulphoxide (DMSO). The products were arrayed in duplicate on GAPS II slides (Corning). The average concentration of the products used for spotting was 235 ng/μl.

2.2.1.8 Differential screening with cDNA microarray

2.2.1.8.1 Target preparation

For the microarray, only samples from time-points 4, 18 and 27 were used for each individual biological replicate. A reference design was employed for the microarray hybridisations, whereby each time-point (treated and untreated) was hybridised with the reference pool, which contained all RNA of both treated and untreated samples for each biological replicate. In all cases the individual time-point was labelled with Cy5-dUTP, while the reference pool was labelled with Cy3-dUTP.

cDNA was synthesised using a SMART™ PCR cDNA Synthesis Kit (BD Biosciences Clontech). RNA (500 ng of either reference or sample) was combined with 84 pmol of 3' SMART CDS Primer and 84 pmol of SMART IIA Oligo and incubated at 72°C for 5 minutes. The temperature was reduced to 42°C, whereafter first strand buffer (Invitrogen), 200 nmol of DTT, 25 nmol of dNTPs (*TaKaRa*), 100 U of RNasin ribonuclease inhibitor (Promega), and 500 U of Superscript II Reverse Transcriptase (Invitrogen) were added, incubated at 42°C for 1 hour and terminated by the addition of 2 μl of 0.5 M EDTA. The synthesised cDNA was purified using the QIA-Quick PCR Purification Kit (QIAGEN) as per the manufacturer's instructions, with the exception that Wash Buffer PE step was performed three times (instead of the once in the manufacturer's protocol) and the DNA was eluted in 85 μl of water.

The cDNA was diluted by adding 5 μl of cDNA to 74 μl of water and used as template for linear amplification using the adaptor sequences present on either end for priming in a 100 μl reaction containing, 1x ExTaq buffer, 20 nmol dNTPs, 24 pmol 5' PCR Primer IIA and 5 U of ExTaq Hot Start DNA Polymerase (*TaKaRa*). Reactions were denatured at 95°C for 1 minute, followed by 24 cycles of 95°C for 5 seconds, 65°C for 5 seconds and 68°C for 3 minutes, with a final extension of 5 minutes at 68°C. Products (5 μl) were examined electrophoretically (1.5% agarose). The adaptors were removed

by digestion with 15 U *Rsa*1 (Fermentas) in 1x *Rsa*1 buffer for 3 hours at 37°C and digested products were purified using the QIAquick PCR Purification Kit (QIAGEN) with DNA elution in 50 µl of water. The concentration was determined using the GeneQuant Pro (Amersham Biosciences)

The resulting product was labelled using Klenow Exo⁻ DNA polymerase with Cy3-dUTP and Cy5-dUTP respectively. Approximately 500 ng of purified, amplified, digested cDNA was used in a labelling reaction, along with 2 µl of random hexanucleotides (Fermentas, 100 µM), a dNTP mix (5 nmol each of dATP, dCTP, dGTP and 2.5 nmol of dTTP), 1x Klenow buffer (Fermentas), 2.5 nmol of either Cy3-dUTP or Cy5 dUTP (Amersham Biosciences) and 5 U of Klenow Exo⁻ DNA polymerase (Fermentas). The reaction was incubated at 37°C, overnight and terminated by the addition of 2 µl of 0.5 M EDTA. Unincorporated label was removed by purification using the QIAquick PCR Purification Kit (QIAGEN) as above (600 µl washes with Buffer PE) and the labelled cDNA eluted in 40 µl of water. The concentration was determined using the NanoDrop[®] ND-1000 spectrophotometer. The efficiency of the dye labelling and coupling is calculated using equation 1 and corresponds to the number of labelled nucleotides per 1000 nucleotides.

Equation 1: Efficiency = $\frac{\text{pmol dye} \times 324.5 \text{ pg/mol}}{\text{ng DNA}}$

where: 324.5 is the average mass of a nucleotide

For a labelling reaction to be considered successful and used further, an efficiency of at least 10 labelled nucleotides per 1000 nucleotides is required.

The Cy3-labelled reference and Cy5-labelled sample (40 pmol of each) were used for hybridisation to the microarray slide. The appropriate volumes were combined and dried in a vacuum concentrator (Bachofen). Samples were dissolved in 50 µl of a hybridisation solution (50% formamide (Roche Diagnostics), 25% microarray hybridisation buffer (Amersham Biosciences), 25% water) denatured by heating at 95°C for 2 minutes in a PE2400 Thermal Cycler, followed by snap-cooling on ice.

2.2.1.8.2 Microarray hybridisation, washing and scanning

The slides were pre-treated in a 3.5x SSC (Invitrogen), 0.2% SDS (Invitrogen), 1% BSA (Roche Diagnostics) solution at 60°C for 20 minutes and rinsed three times with water. Excess water was removed by centrifugation at 1000g (Beckman J6) for 2 minutes. The pre-treated slides were placed in a hybridisation chamber (HYB-UP) and 40 µl of the denatured target was placed on the slide and

tightly covered. The hybridisation chamber was incubated in a water-bath at 42°C overnight. The slides were subsequently washed in 1x SSC, 0.2% SDS for 4 minutes at 42°C, followed by two washes of 0.1x SSC, 0.2% SDS (4 minutes at 42°C), three washes in 0.1x SSC at room temperature and finally three water rinses. The excess water was subsequently removed by centrifugation at 1000g for 2 minutes. The slides were scanned using a GenePix™ 4000B (Axon Instruments).

2.2.1.8.3 Data analysis

The scanned slides were analysed with GenePix Pro 5.1.0.0 (Axon Instruments). After a combination of automated spot-finding and manual flagging of bad spots, the expression ratios obtained were further analysed using LimmaGUI [194, 195], an application running in R (www.r-project.org) [196]. Within-slide normalisation was by means of global LOESS and there was no between-slide normalisation. The linear model fit was least squares (with a resulting duplicate correlation of 0.74935). Top-tables were generated using a False Discovery Rate (FDR) adjustment method [197]. The initial comparisons were the treated or untreated sample versus the reference, while the contrasts were the treated versus untreated results of each time-point. Clones that fulfilled the minimum requirements of 2-fold increase or decrease in abundance at $P < 0.05$ were considered differentially expressed.

2.2.1.9 Sequencing

A selection of the clones identified as differentially expressed by LimmaGUI were sequenced. The identified clones were inoculated into LB-Broth containing 50 µg/ml ampicillin and incubated overnight at 30°C, with shaking.

Plasmid DNA was isolated from the overnight culture using the Roche High Pure Plasmid Isolation Kit (Roche Diagnostics) according to the manufacturer's instructions. Plasmid DNA was eluted in 100 µl of elution buffer and quantified using the Gene Quant Pro (Amersham Biosciences). The presence of an insert was confirmed by *Rsa*I (Fermentas) digestion (10 U of enzyme was added to ~1000 ng of plasmid DNA and digested at 37°C for 3 hours in 1x *Rsa*I buffer). The samples were electrophoresed (1.5% agarose) to visualise the digestion.

Sequencing was performed using Big Dye V3.1 (Applied Biosystems) as per the manufacturer's instructions. Approximately 360 ng of plasmid DNA was used in reactions containing 5 pmol of T7 promoter primer (5' GTAATACGACTCACTATAGGGC 3'), 4 µl of Big Dye Ready reaction and 2 µl of the sequencing buffer. The cycling conditions were 25 cycles of 96°C for 10 seconds, 50°C for 5 seconds and 60°C for 4 minutes. The reactions were subsequently precipitated by the addition of 2 µl of 3 M

sodium acetate (pH 4.6) and 50 μ l of ice-cold 95% ethanol and centrifuged at 16100g (Eppendorf 5415R) for 30 minutes. The pellets were washed with 175 μ l of ice-cold 70% ethanol and centrifuged at 16100g for 15 minutes. The pellets were dried in a vacuum concentrator and were subsequently run on an ABI Prism 3100 Capillary Sequencer (Perkin Elmer) by the DNA Sequencing Facility of the University of Pretoria (<http://www.bi.up.ac.za/seqlab/>). The sequences were identified using MADIBA (<http://www.bi.up.ac.za/MADIBA/>) [198], a web interface for the functional analysis of gene clusters showing similar expression profiles (with particular application to *Plasmodium* and plants).

2.2.1.10 Identification of redundant clones of decreased abundance

As sequencing showed that many of the decreased abundance clones were redundant (they contained inserts derived from the same three genes), two approaches were used to identify which clones were redundant and thus identify additional unique clones.

Firstly, a clustering approach entailed sorting data from the list of differentially regulated clones for rings, early and late trophozoites, as analysed with limmaGUI, in Excel to obtain only those with M-values of ≥ 1 and ≤ -1 ($P \leq 0.05$). The rings only had 1 gene and were thus excluded from any further analyses. The resultant list was used in TIGR-MEV [199] for *k*-means (12 clusters, maximum of 50 iterations) and hierarchical clustering (genes only) and the data evaluated and compared with clones already sequenced. Based on similarities and differences in the expression profiles and position in the cluster, several additional clones were selected for sequencing.

A second approach using nested PCR to identify clones as one of the three over-represented clones in the decreased abundance population (MAL8P1.310: putative senescence associated protein; MAL13P1.460: conserved hypothetical protein; or PF08_0131: 1-cys peroxiredoxin). The nucleotide sequences of these genes was obtained from PlasmoDB (www.PlasmoDB.org) and aligned using Clustal W in BioEdit [200] with the sequences obtained from the clones already sequenced, to confirm that there were no sequence differences between the database sequence and the clones. Primers for the genes were designed using Oligo v6.71 (Table 2.3)

Table 2.3. Nested primers for redundant clones of decreased abundance.

Primer name	Primer sequence (5' - 3')	Product length (bp)	Primer length (bp)	Most stable dimer (kcal/mol)	ΔG 3' (kcal/mol)	%GC	T _m (°C) ¹
PXNNf	AGGACTTCCATTAACCTGTAG	199	21	-4.8	-5.8	38.1	54
PXNNr	GGTAAGATACAGCATTGTCTC		22		-6.1	40.91	57
CHPf	ACGCAGAAGTCTCAAAGTGTC	167	21	-4.9	-6.1	47.62	58
CHPr	TAATCCTCTCGTACCAAGTTG		21		-6.7	42.86	56
SAPf	ATCCCTGTGGTAACTTTTCAG	128	21	-3.5	-7	42.86	56
SAPr	TTGTTTGATTCTATTTTCAG		21		-7	23.81	48

¹T_m is calculated by $69.3 + (0.41 \times \%GC) - (650/L)$ where L is the primer length [201].

PXN: 1-cys peroxiredoxin; CHP: Conserved hypothetical protein; SAP: Senescence associated protein

Inserts were amplified from all the remaining decreased abundance clones (104) using primers NP1 (nested primer 1) and NP2R (nested primer 2R, see Table 2.1). PCR reactions (25 μ l) contained 0.5 μ l of overnight bacterial culture of each clone (diluted 1/4 with LB-broth), 2mM MgCl₂, 2 μ l dNTPs (2.5 mM), 50 pmol of the primers and 0.625 U of Taq DNA polymerase (Promega) and were incubated at 94°C for 5 minutes to lyse the bacteria and ensure complete denaturation of the plasmid DNA. This was followed by 25 cycles of 94°C for 30 seconds, 68°C for 30 seconds and 72°C for 2 minutes. The reaction was terminated with a final extension at 72°C for 7 minutes (PE9700, Applied Biosystems). Positive controls for MAL8P1.310, MAL13P1.460 and PF08_0131 were included. Amplification was confirmed using agarose gel electrophoresis (1.5% gel). The amplicons thus generated were subsequently used as template for the nested PCR. Any clones that did not amplify in the initial PCR were omitted from the nested reaction. The nested PCR included 1 μ l of template from the first amplification, 2 mM MgCl₂, 2 μ l dNTPs (2.5 mM), 5 pmol of nested primers (all complexed in a single reaction) and 0.625 U of Taq DNA polymerase. The reactions were incubated at 94°C for 5 minutes, followed by 25 cycles of 94°C for 30 seconds, 48°C for 30 seconds and 72°C for 1 minute on a PE9700. The reactions were terminated with a final extension at 72°C for 5 minutes. The reactions were electrophoresed on a 2% agarose gel and clones that showed no amplicon were selected for sequencing as before.

2.2.1.11 Microarray result validation

The microarray data were validated by semi-quantitative real-time PCR using a LightCycler™ FastStart DNA Master^{PLUS} SYBR Green 1 kit (Roche Diagnostics) on the LightCycler 1.5 (Roche Diagnostics). Four genes were chosen for validation, namely exported protein 2 (EXP2), ornithine aminotransferase (OAT), L27 ribosomal protein (L27) and 1-cys peroxiredoxin (PXN). Lactate dehydrogenase (LDH) was chosen as a constitutively expressed control gene. Primers for these genes were designed using Oligo v6.71 (Table 2.4). Primers were designed to produce amplicons of a similar length (~100 bp), and the annealing temperature was similar so that all primers could be tested in a single LightCycler run.

Table 2.4. Primers designed for use in semi-quantitative real-time PCR to validate microarray data.

Primer name	Position	Primer sequence (5' - 3')	Product length (bp)	Primer length (bp)	Most stable dimer (kcal/mol)	$\Delta G 3'$ (kcal/mol)	%GC	T _m (°C) ¹
EXP2f	114	CACCGTTATTAAAGATCCAATTAG	168	24	-5.3	-6	33.3	56
EXP2r	257	CCAACAATTTCTCTACTAACAATA		25		-6.3	28	55
OATf	495	CAACTTTGGTCCATTCGTACC	165	21	-5	-6.7	47.6	58
OATr	637	GCTACACCTGGGAAATAACTATC		23		-5.7	43.5	59
L27f	2	TGGGAAAATTATTGAAACCAGGA	141	23	-6.3	-8.2	34.8	55
L27r	120	TTTCTATACCAGCTACTAAGCAG		23		-8.2	39.1	57
PXNf	129	TACTCCCGTTTGTACCCTGA	162	21	-4.4	-6.4	47.6	58
PXNr	269	ATATCCCACTTATCTAGGTTTC		22		-6.7	36.4	55
LDHf	205	GATTTGGCTGGAGCAGATGTA	169	21	-4.7	-5.7	47.6	58
LDHr	348	CAACAATAATAAAGCATTGGACAA		26		-6.7	26.9	55

¹T_m is calculated by $69.3 + (0.41 \times \%GC) - (650/L)$ where L is the primer length [201].

A standard curve was generated for LDH using a dilution series of untreated cDNA (13 ng/μl). The series contained undiluted cDNA and the following dilutions: $1/_{10}$, $1/_{20}$, $1/_{50}$ and $1/_{100}$. The reaction contained 5 μl of the appropriate cDNA, 10 pmol each of the respective primer pair, 4 μl of prepared FastStart DNA Master^{PLUS} SYBR Green reaction mix (in a total reaction volume of 20 μl). The reaction components were placed in a LightCycler capillary and the cycled according to the conditions in Table 2.5.

Table 2.5. Thermocycling conditions for real-time PCR validation of microarray data using the Light-Cycler 1.5.

Name	Analysis mode	Cycles	Target temperature	Hold time	Acquisition mode	Slope (°C/sec)
Pre-incubation	None	1	95°C	10 min	None	20
Amplification	Quantification	45	95°C	10 sec	None	20
			55°C	5 sec	None	20
			72°C	7 sec	Single	20
Melting curves	Melting curves	1	95°C	0 sec	None	20
			65°C	15 sec	None	20
			95°C	0 sec	Continuous	0.1
Cooling	None	1	40°C	30 sec	None	20

The cDNA used for the validation was the treated and untreated cDNA from time-point 4 and was used in the reactions at 3.25 ng. The reactions were run in triplicate and were set-up and run as for the LDH standard curve.

2.2.2 PART 2:

Transcriptional profile of ODC-inhibited *P. falciparum* parasites using whole genome oligo microarray

2.2.2.1 Parasite culture, treatment and sampling for transcriptional profiling by oligo DNA microarray

P. falciparum parasites were grown in continuous *in vitro* culture as described in Part 1. The parasite culture (strain 3D7) was synchronised at least twice using 5% sorbitol [192] (15 ml of culture in a 75 cm² culture flask (Greiner Bio One)) whereafter the parasites were treated with 10 mM DFMO at approximately 2 hours post-merozoite invasion. Untreated parasite culture was maintained in parallel. A biological replicate of each culture was also maintained. Samples of parasite culture (15 ml) were removed at 23 and 31 hours post-invasion and smears for microscopic evaluation were prepared. The samples were pelleted by centrifugation at 1500g (Hermle Z320) for 5 minutes, the supernatant aspirated and the pellet washed once with 25 ml of 1x PBS. The erythrocytes were pelleted by centrifugation at 1500g (Hermle Z320) for 5 minutes, the supernatant aspirated and the pellet was subsequently stored at -70°C.

2.2.2.2 RNA Isolation

Total RNA was extracted from the samples using a combined TRI-Reagent (Fluka) and RNeasy® Protect Mini Kit (QIAGEN) method as described in Part 1 (Section 2.2.1.4).

2.2.2.3 cDNA synthesis and aminoallyl-dUTP incorporation

cDNA was synthesised from the isolated RNA and aminoallyl-dUTP (5-(3-aminoallyl)-2'-deoxyuridine-5' triphosphate, Ambion) was simultaneously incorporated using Superscript® III (a modified version of M-MLV reverse transcriptase, Invitrogen). Firstly, RNA (from the replicate A and the replicate B samples) was quantitatively pooled (4 µg of each sample) to create a reference sample. The reference was split into 8 reactions each for cDNA synthesis and aminoallyl-dUTP incorporation. Individual reactions of each sample (4 µg of RNA) were also performed. The reactions contained 250 pmol of poly-T (T₂₃VN), 775 pmol of random nonamer and 4 µg of RNA (reaction volume of 16.6 µl) and heated at 70°C for 10 minutes, followed by cooling at 4°C for 10 minutes in a thermal cycler (PE 2720, Applied Biosystems). Subsequently First Strand Buffer (Invitrogen), dNTP mix (0.57 mM dATP (Promega) and 0.28 mM each of dCTP (Promega), dGTP (Promega), dTTP (Promega) and aminoallyl-dUTP (Ambion)), 40 U RNasin® RNase inhibitor (Promega), 340 U Superscript®III Reverse Transcriptase (Invitrogen) and 10 mM DTT (Invitrogen) were added, to a total reaction volume of 30 µl. The reaction was incubated at 42°C for 16 hours, the enzyme inactivated and the RNA hydrolysed

by the addition of 3 μmol of EDTA (6 μl of 0.5M) and 6 μmol NaOH (6 μl of 1M), followed by incubation at 65°C for 10 minutes (reaction volume of 42 μl). The samples were cleaned using the Nucleospin® Extract II kit (PCR clean up and gel extraction) (Machery Nagel), as per the manufacturer's instructions. The DNA was eluted in 30 μl of DNA-grade water (prewarmed to 37°C) and quantified using the NanoDrop®ND-1000 spectrophotometer.

2.2.2.4 Cy3 and Cy5 coupling

Coupling occurs by nucleophilic attack of the N-hydroxyl succinimidyl-ester (NHS) dye by the terminal amino group of the aminoallyl-dUTP (at a pH between 8.5 and 9) (Figure 2.3). This results in a covalent bond formation between the dye and the dUTP (<http://cmgm.stanford.edu/pbrown/protocols/RTaminoAllylCoupling.html>). The reference sample was always labelled with Cy3, while the individual time-point samples were labelled with Cy5.

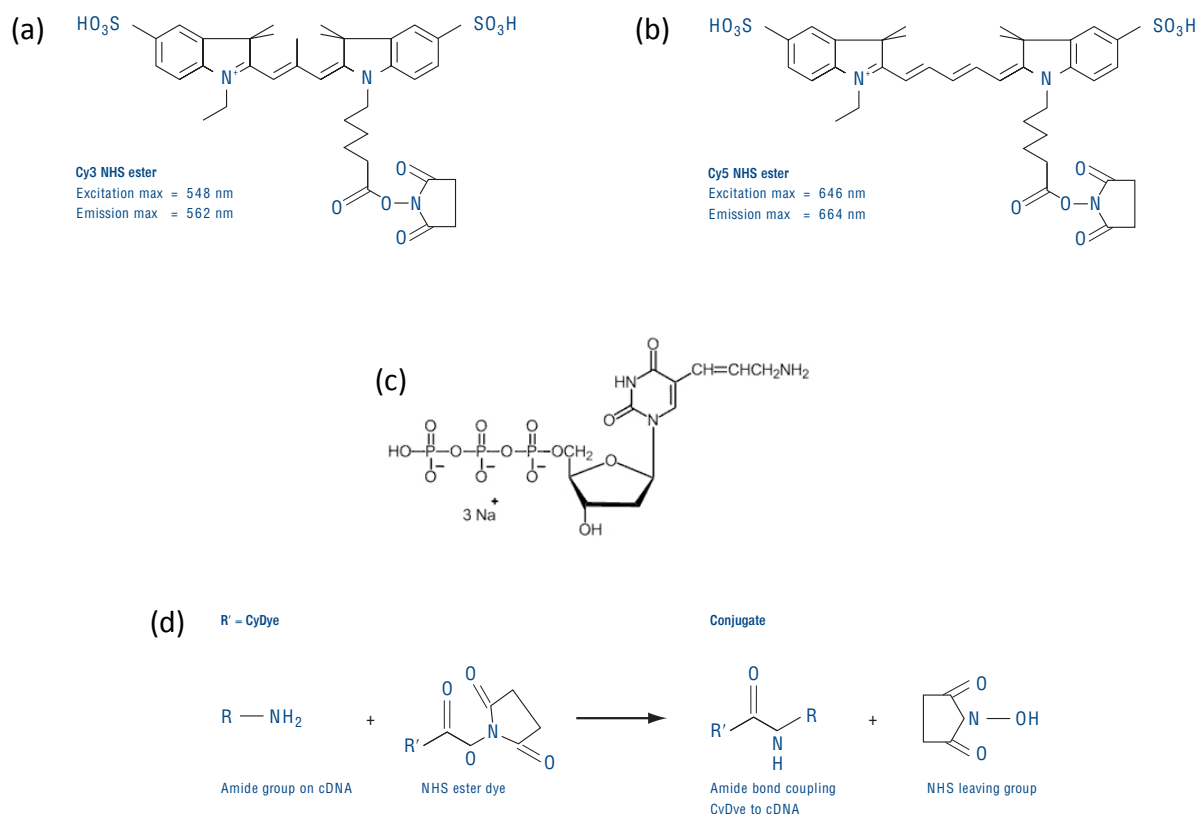


Figure 2.3. Structure of the active components of the coupling reaction (a) NHS-Cy3 [202], (b) NHS-Cy5 [202], (c) aminoallyl-dUTP (<http://probes.invitrogen.com/media/structure/17246.jpg>) and (d) nucleophilic reaction between the aminoallyl-dUTP and the CyDye [202].

A volume of sample (one reference and one individual time-point per microarray array) containing 1.5 μg of cDNA was reduced to a total volume of 2.5 μl . Carbonate buffer (5 μl of 0.2M, pH 9) and 2.5 μl of either Cy3 or Cy5 monofunctional reactive dye (2308 pmol/ μl , GE Healthcare) was added and

incubated in a desiccator at room temperature for 2 hours (in the dark). The samples were cleaned using the QIAQuick PCR Product Purification Kit (QIAGEN). The manufacturer's protocols were followed with two modifications: 1) the volume of binding buffer used was 10x the sample volume (as opposed to 5x); and 2) three wash steps of 500 µl Buffer PE (as opposed to one wash of 750 µl) were included.

2.2.2.5 Microarray hybridisation, washing and scanning

Custom microarray slides, containing 60-mer oligos of the *P. falciparum* genome, were obtained from Agilent Technologies. The design of the oligos was performed by Jeff Verlinden, Jaco de Ridder and Lyn-Marié Birkholtz (University of Pretoria)[2].

The slides required no preparation prior to hybridisation. Based on the concentration of dye present, equimolar amounts (20 pmol) of dye for the sample (Cy5) and the reference (Cy3) were combined. Target cDNA was prepared by the addition of 5 µl of 10x blocking buffer (Agilent Technologies), 1 µl of 25x fragmentation buffer (Agilent Technologies) and water to a final volume of 25 µl to the labelled cDNA. The target was incubated at 60°C for 30 minutes (in a PE2400 thermal cycler, Applied Biosystems), then placed on ice. GE-Hybridisation buffer (2x, HI-RPM, 25 µl) was added and the prepared target kept on ice until use.

The 8-array gasket slide (Agilent Technologies) was placed into the hybridisation chamber (Agilent Technologies) and 40 µl of the prepared and appropriate target was placed in each of the 8 spaces. The custom microarray slide was carefully positioned over the gasket slide, the chamber was closed, fastened and placed into the Agilent Hybridisation Oven (G2545A, Agilent Technologies). Hybridisation was at 65°C overnight (approximately 17 hours), with the rotation set at 10.

Following hybridisation, the slides were removed from the chamber and placed in Wash Buffer 1 (Agilent Technologies). The gasket slide was carefully slipped off the microarray slide in this wash buffer and the microarray slide transferred to a second tube of Wash Buffer 1 and incubated with slight rotation for 1 minute. The slide was then transferred to a tube containing Wash Buffer 2 (which had been incubated at 37°C, overnight) and rotated for 1 minute. The slide was transferred to a Slide Spinner centrifuge (C1303, Labnet International Inc) and spun for 1 minute to dry the slide. The slides were scanned using a GenePix™ 4000B (Axon Instruments) scanner.

2.2.2.6 Data analysis

Initial data processing, including spot-finding, was performed using GenePix Pro 5.1 (Acuity). Normalisation and the identification of differentially regulated genes was accomplished using R (www.r-project.org) [196], Bioconductor [203] with the limma [194] and marray [204] packages (see Supplementary Material S1 for the R-script used). Poor quality spots (such as those that were saturated, showed little signal over background, or too much colour variance within the spot) were automatically flagged by GenePix, using the parameters given in Table 2.6.

Table 2.6. Parameters for automated flagging using GenePix.

Type	Parameters	Flag
Spot saturation	F532%sat>20 OR F635%sat>20	Bad
Colour variance	F532CV>400 OR F635CV>400	Bad
Green background	F532mean<150	Absent
Signal to noise ratio	SNR532<3 AND SNR635<3	Absent

More specifically, data analyses included robust-spline within-slide normalisation, Gquantile between-slide normalisation and the fit of a linear model. Pearson correlations between the various samples were also computed using R. The correlations indicated which the most appropriate untreated sample to use as a comparison point was. The *P*-values were adjusted to control the false discovery rate [197]. A log₂ fold change of -0.75 (decreased abundance) and +0.75 (increased abundance) for a fold change of 1.7 was considered to be the cut-off point for significance and an adjusted *P*-value cut-off of 0.05 was used. Once the list of differentially expressed genes was obtained, the given IDs were used to obtain the gene annotation from PlasmoDB (www.plasmoDB.org).

Further analysis of the differentially expressed gene transcripts involved grouping them into several categories based on similar biological process terms from the GO Consortium. Hierarchical clustering was also employed to identify relationships between gene transcripts using Cluster 3.0 for Mac OS X (C Clustering Library 1.47). The data used for clustering were normalised both within- and between-slides. The similarity metric used was an uncentred correlation, with an average linkage clustering method.

2.2.2.7 Validation of microarray results using semi-quantitative real-time PCR

The primers that were designed for the real-time PCR validation of the SSH-microarray were employed for these experiments, along with several primer sets designed by Tharina van Brummelen

(University of Pretoria) [205] and a primer set for spermidine synthase designed by John Becker (CSIR) [3] (Table 2.7).

Table 2.7. Information for primer sets employed for real-time PCR.

Primer name	Position	Primer sequence (5' - 3')	Product length (bp)	Primer length (bp)	Most stable dimer (kcal/mol)	ΔG 3' (kcal/mol)	%GC	Tm1	Design
OATf	495	CAA CTT TGG TCC ATT CGT ACC	165	21	-5	-6.7	47.6	58	KC
OATr	637	GCT ACA CCT GGG AAA TAA CTA TC		23		-5.7	43.5	59	
PXNf	129	TAC TCC CGT TTG TAC CAC TGA	162	21	-4.4	-6.4	47.6	58	KC
PXNr	269	ATA TCC CAC TTA TCT AGG TTT C		22		-6.7	36.4	55	
SAMDC/ODCF	694	AAT CAA TTC CAT GAC GCT TAT CTG	165	24	-5.3	-6.6	37.5	58	KC
SAMDC/ODCr	835	ACA ATT CAC CAT TCC TGT ATC TTC		24		-6.7	37.5	58	
LDCf	2778	AGA GGG ATA TGG ATT GGT AGA	161	21	-5.7	-5.5	42.9	56	TvB
LDCr	2916	TTC TCT TCA TGT ATG ATA CAG TA		23		-5.8	30.4	54	
CYCLOf	1997	AAT TCT TTG ACC ATC TTA ATC ATT C	167	25	-5.7	-6.9	28.0	55	TvB
CYCLOr	2138	CAA AAC AAT TTT ACT TCC TTG GGT TA		26		-7.3	30.8	57	
ARGf	69	CGT TTC CAT TAT TGG TTC TC	164	20	-5	-6.7	40.0	53	TvB
ARGr	208	GTT TCA TTT CAT TAT CCC CAT TAT C		25		-6	32.0	56	
MATf	273	TTT AGA TTA CAA AAC GGC AGA GAT AA	160	26	-5.3	-6	30.8	57	TvB
MATr	407	AGG CAT ATA ATT CTC AGT TTC ATC AG		26		-6.6	34.6	58	
SPDf	650	ACA ACG CCC TAA AGC CTA AC	70	20	-10	-5.8	50	57	JB
SPDr	718	ATT GTT CCC ACG TGT ATC CAG		21		-8.2	47.6	58	

KC: Katherine Clark (this study), TvB; Tharina van Brummelen [205], JB: John Becker [3]

The template used for real-time PCR was the cDNA with the incorporated amino-allyl dUTP, generated as probes for microarray hybridisation. A standard curve for cyclophilin was produced using cDNA from time-point BUT1. Samples were named using a 3 letter, 1 number convention. 'A' or 'B' indicated the biological replicate; 'U' or 'T' whether the sample was treated or untreated; and 'T1' or 'T2', the harvesting time-point, i.e. BUT1: biological replicate B, untreated, time-point 1. A dilution series of the cDNA was prepared (13 ng, 3.25 ng, 1.625 ng, 0.65 ng and 0.325 ng). Primer (in this case 5 pmol each of CYCLOf and CYCLOr) was used, along with the KAPA™ SYBR® FAST qPCR kit (Mastermix (2x) LightCycler® 480) from KAPA Biosystems (South Africa). Duplicate 10 µl reactions were set up for each of the cDNA dilutions, along with a negative control. The cycling conditions on the LightCycler 480 (Roche) are given in Table 2.8.

Table 2.8. Cycling conditions for amplification using the LightCycler 480.

Name	Analysis mode	Cycles	Target temperature	Hold time	Acquisition mode	Ramp rate (°C/s)
Pre-incubation	None	1	95°C	10 min	None	4.8
Amplification	Quantification	40	95°C	10 sec	None	4.8
			55°C	5 sec	None	2.5
			72°C	7 sec	Single	4.8
Melting curves	Melting curves	1	95°C	5 sec	None	4.8
			65°C	5 sec	None	2.5
			95°C		Continuous (5 per °C)	0.11
Cooling	None	1	40°C	30 sec	None	2.5

At the same time, reactions (in triplicate) of treated (BTT1) and untreated (BUT1) samples were run to determine the effect of treatment on cyclophilin. cDNA (1.625 ng) was used as template, with 5

pmol of the cyclophilin primers and the KAPA™ SYBR® FAST qPCR kit. The cycling conditions are given in Table 2.8.

Real-time PCR was performed for both time-points of the microarray (i.e. treated samples: TT1 and TT2; untreated samples: UT1 and UT2) using the primers indicated in Table 2.7. In each case 5 pmol of the appropriate primer was used, with 1.625 ng of template cDNA and the KAPA™ SYBR® FAST qPCR kit. Cycling on the LightCycler 480 was as in Table 2.8.

2.3 RESULTS

2.3.1 PART 1:

Transcriptional profile of ODC-inhibited *P. falciparum* parasites using SSH and cDNA microarray

2.3.1.2 Morphology of DFMO-treated and untreated Fab9 *P. falciparum* parasites

Morphological monitoring of DFMO-treated *P. falciparum* parasites aimed to 1) monitor parasite growth through one life-cycle under current culture conditions, to determine if growth approximated that of the HB3 strain used by Bozdech *et al.* [127] for their elucidation of the transcriptome of the IDC of *P. falciparum*; and 2) determine time-points for sample extraction for transcriptome analysis of DFMO-treated *P. falciparum* parasites. As anticipated, the progression of the untreated South African Fab9 strain of *P. falciparum* through its IDC shows similar timing to that of the HB3 strain used by Bozdech *et al.* (untreated parasites, Figure 2.4).

In contrast, treatment of *P. falciparum* parasites with DFMO resulted in an arrest of the IDC at the early trophozoite stage (Figure 2.4). The trophozoites of DFMO-treated parasites at 21 and 27 hours post-treatment appear pyknotic (smaller), while their nuclei stained darker than their untreated counterparts, possibly indicating stress-induced chromatin condensation [59] (Figure 2.4).

Based on these results, the time-points for harvesting of material for SSH and microarray could be identified and a focus was placed on sampling in the trophozoite stage at 4, 18, 21 and 27 hours post-treatment.


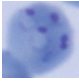



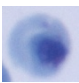



Time-point	Untreated	Treated	Hours post-treatment	Hours post-invasion
T0			0	2
T1			4	6
T2			18	20
T3			21	23
T4			27	29

Figure 2.4. Morphological monitoring of *P. falciparum* parasites. Parasite cultures were treated with 10 mM DFMO at invasion, or remained untreated. Both treated and untreated cultures were monitored for a complete parasite life-cycle of 48 hours.

2.3.1.2 Generation of transcripts differentially expressed upon DFMO-treatment

Forward and reverse libraries of transcripts affected by DFMO-treatment were generated by SSH and screened using cDNA microarray. The concentration of the RNA obtained from the respective samples is given in Table 2.9. As expected, less RNA was obtained from the *P. falciparum* ring stage parasites, than from the trophozoites. Additionally, less RNA was also obtained from the DFMO-treated *P. falciparum* parasites compared with the untreated parasites, as reflected by the ratio of average treated to average untreated RNA concentration (Table 2.9). The A_{260}/A_{280} ratio is an indication of the quality of the RNA and should ideally be greater than 1.8 [193]. The RNA isolated conformed to this requirement indicating an isolation of suitable integrity, a conclusion confirmed by electrophoretic evaluation of the RNA (results not shown).

Table 2.9. Concentration and specifications of RNA isolated from the harvested samples.

Sample	Concentration (ng/ml)	A ₂₆₀ / A ₂₈₀	Total RNA isolated (µg)	Average RNA isolated (µg)	Average treated / average untreated
ATT1	176.4	2.239	5.292	5.184	0.728
BTT1	169.2	2.192	5.076		
AUT1	248.8	2.198	7.464		
BUT1	225.6	2.178	6.768		
ATT2	475.2	2.141	14.256	13.53	0.866
BTT2	426.8	2.305	12.804		
AUT2	625.6	2.293	18.768		
BUT2	416	2.266	12.48		
ATT3	418.4	2.188	12.552	13.38	0.701
BTT3	473.6	2.197	14.208		
AUT3	637.6	1.909	19.128		
BUT3	635.2	2.249	19.056		
ATT4	495.6	2.294	14.868	16.2	0.867
BTT4	584.4	2.224	17.532		
AUT4	688	2.231	20.64		
BUT4	557.2	2.291	16.716		

The RNA was subsequently converted to cDNA, amplified using LD-PCR and digested with *Rsa*1. The resultant cDNA populations were used for SSH, to create differentially expressed transcript libraries. Nested PCR was employed to amplify differentially expressed transcripts after subtractive hybridisation. Significant differential amplification was achieved during the nested PCR (Figure 2.5) with clear differences observed between the forward and reverse subtracted libraries, compared with the unsubtracted population.

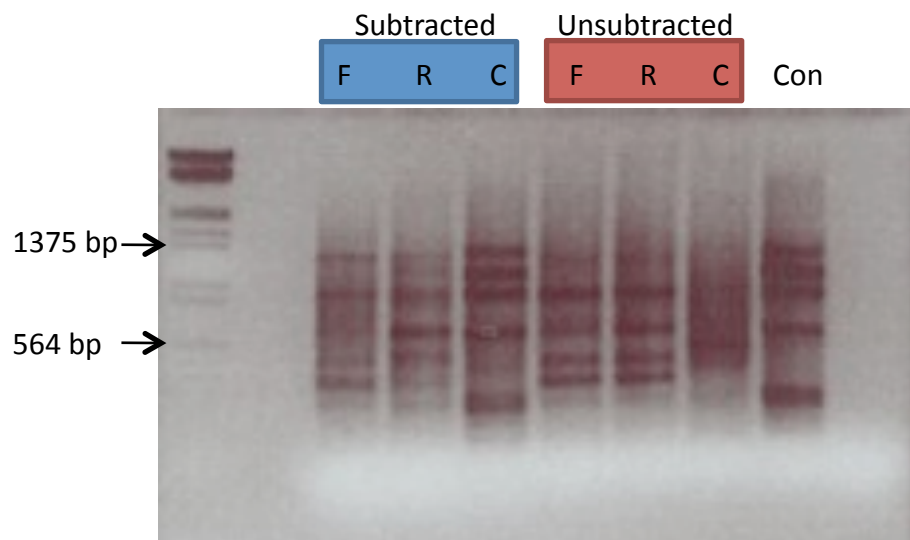


Figure 2.5. Secondary (nested) amplification of the differentially expressed transcripts. The forward (F), reverse (R) and control (C) subtracted and unsubtracted products are compared. The PCR subtracted control (Con) is also included.

The SSH procedure was thus successfully executed for the generation of pre-selected libraries of differentially expressed genes upon DFMO-treatment. Following AT-cloning into pGEM® T-Easy and

transformation into *E. coli* (XL2-Blue and SURE), positive clones were identified by PCR colony screening of the differentially expressed libraries. An example is shown in Figure 2.6.

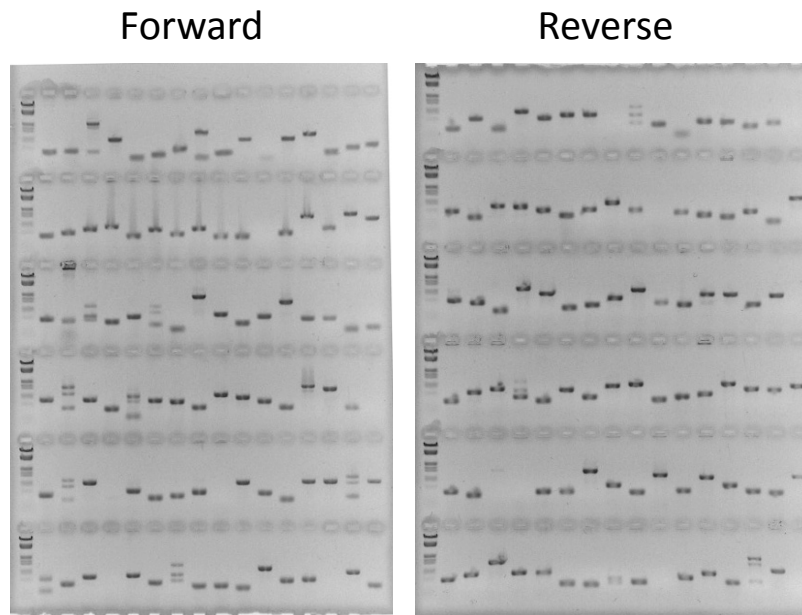


Figure 2.6. Stretch-Rig gel of colony screening PCR for the forward and reverse libraries. The gel had been a single unit, which was split in half to facilitate visualisation on the transilluminator.

2.3.1.3 cDNA microarray screening of differentially expressed libraries

Many of the screened clones contained inserts and these were amplified for printing onto microarray slides as probes. Targets to be used for hybridisation against the probes on the slides were generated by cDNA synthesis from the original RNA samples and labelled with CyDye labelled dUTP. An average labelling efficiency of 26 was achieved (calculated using Equation 1, Section 2.2.1.8.1), the maximum was 35 and at worst 14, well above the minimum efficiency requirement of 10.

Following generation of targets, the microarray hybridisations were performed. In total, 24 hybridisations were performed consisting of each of the samples from the three treated and the three untreated time-points (6), hybridised in duplicate (a further 6). The inclusion of the same for the biological replicate added the last 12. Duplication of the spots on the slide added a further dimension of technical replication. Figure 2.7 shows an example of typical scanned slides of the SSH-based cDNA microarray. The intensity of the spots was generally good, enhanced by the absence of significant background fluorescence.

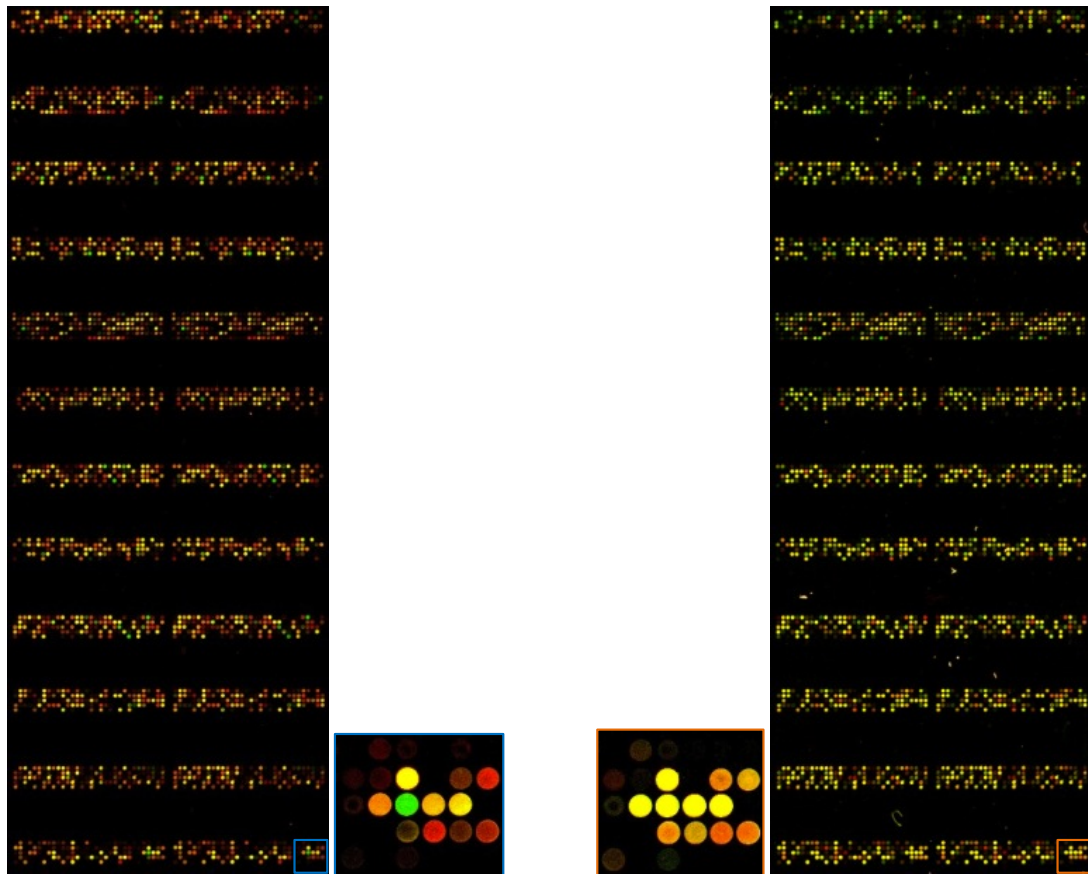


Figure 2.7. Typical microarray slides after scanning (time-point 2, early trophozoites). The coloured framed inset is magnified in the middle of the figure to enable a more detailed view. The slide with the blue-framed inset (left) is the untreated sample, while that with the orange inset (right) is the treated sample.

After extensive data analysis, clones that were significantly differentially expressed (with a fold-change of 2, $P < 0.05$) were identified and some sequenced. However, redundancy prohibited sequencing of all the clones obtained and necessitated applying various strategies to minimise this. Clustering of the clones (using the M-value) was based on the presumption that clones clustering together with the same expression profiles could potentially be identical. Twelve *k*-means clusters were generated and compared with hierarchical clusters. It was found that the *k*-means clusters fell into defined groups within the hierarchical cluster. Six *k*-means clusters of transcripts of decreased abundance, five of increased abundance and one containing mixed (of decreased abundance for one time-point and increased abundance for the second) were obtained with varying numbers of transcripts in each cluster (Table 2.10). The clusters were evaluated using the sequences already obtained.

Table 2.10. Information regarding *k*-means clusters. Blue highlighted clusters contain many previously sequenced clones that proved to be identical and cluster together tightly.

Cluster	Number of genes in cluster	% of genes in cluster	Direction of change
1	28	8	Up
2	14	4	Down
3	34	10	Up
4	34	10	Up
5	59	17	Down
6	29	8	Up
7	57	16	Down
8	47	13	Up
9	25	7	Up
10	14	4	Down
11	9	3	Down
12	5	1	Mixed

Cluster 10 (decreased abundance) contained only controls, while 33% of the clones fell into clusters 5 and 7 (also both of decreased abundance). Of the redundant clones, several could be allocated to clusters, thus validating the methodology. Several clones were selected for sequencing based on their relative position within a cluster in an attempt to annotate the clusters. Clusters 1, 5 and 7 are given in Figure 2.8, to illustrate the predominance of similar genes grouping together.

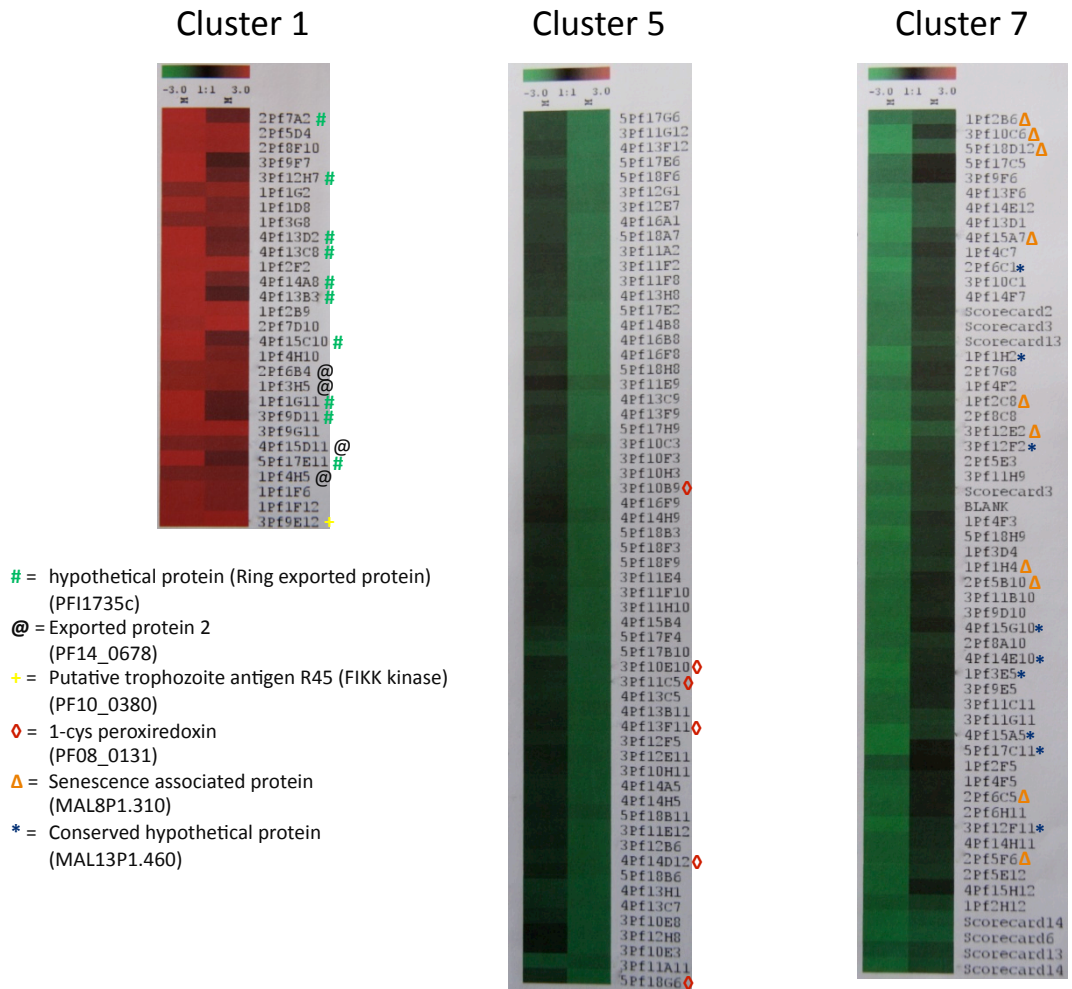


Figure 2.8. An example of tightly clustered clones. With the exception of one clone (1Pf3B10 – should be in cluster 1 as it is ring exported protein, but is present in cluster 6), these transcripts do not appear in any other clusters.

In addition to clustering the clones, a second strategy was employed to identify identical clones of decreased abundance. Nested PCR with primers for commonly occurring transcripts (conserved hypothetical protein, senescence associated protein and 1-cys peroxidoredoxin) identified only 20 clones out of the remaining 104 decreased abundance clones as being unique (Figure 2.9 shows an example of these results).

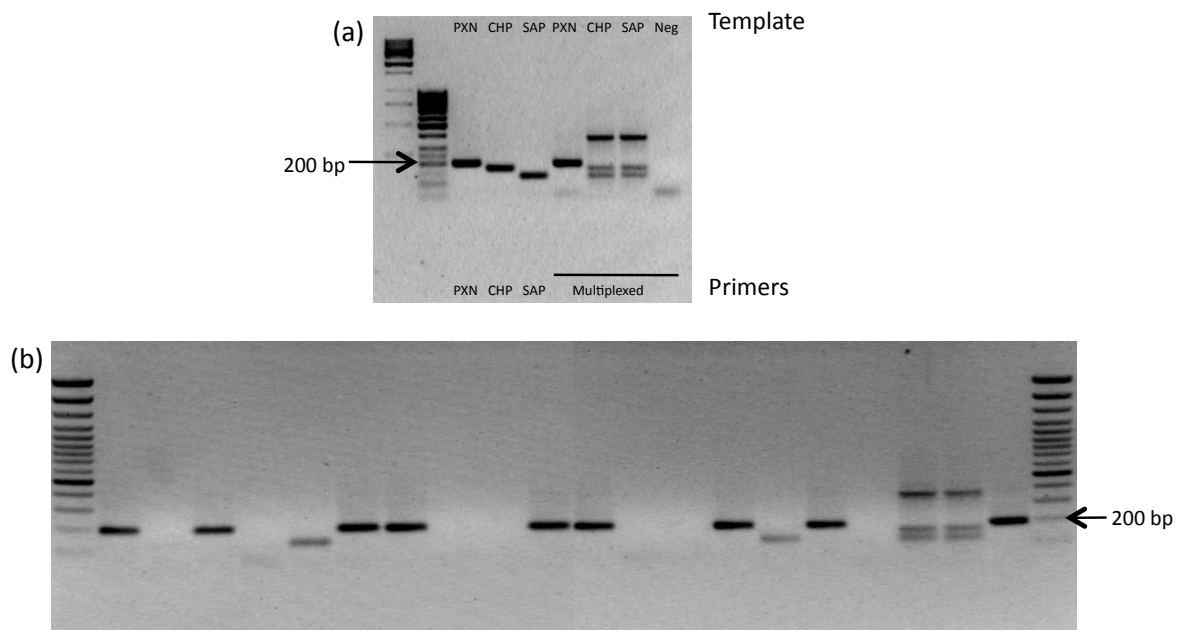


Figure 2.9. Nested PCR to identify potentially unique clones (a) Products obtained using the CHP (conserved hypothetical protein), SAP (senescence associated protein) and PXN (1-cys peroxiredoxin) primers on the appropriate template, both as individual primer pairs and multiplexed. (b) An example of the application of the nested PCR approach to the unsequenced clones of decreased abundance. The lanes with no amplicon contain template DNA from clones that are not CHP, SAP or PXN and can thus be sequenced in order to obtain additional unique clones.

DNA sequencing allowed identification of 19 clones. Two were identified as senescence associated protein, one as conserved hypothetical protein and one as 1-cys peroxiredoxin. These should have been identified by PCR screening, but it is possible that the bands were of a very low intensity and thus overlooked. Of the remaining 15 clones, four were unique clones, two were identified as PFB0435c, three as PFI1445w and six as PF13_0338.

2.3.1.4 Effect of DFMO-treatment on *P. falciparum* parasites

The complete list of clones identified, of both increased and decreased abundance, is given in Table 2.11. The genes previously identified with a SSH study alone [188] are also included, as further analyses of the data was performed in combination with that obtained from this study.

Table 2.11. Identification of differentially expressed transcripts. (A) Transcripts of increased abundance and (B) transcripts of decreased abundance upon DFMO-treatment.

A								
Number of clones	PlasmoDB ID	PlasmoDB annotation (additional annotation)	Early trophozoites: fold upregulated	Late trophozoites: fold upregulated	Normal IDC transcript expression profile Maximum :: minimum expression (hpi)	Noteworthy characteristics	GO term: Function	GO term: Process
1	PFF0435w	Ornithine aminotransferase	ND	1.5	18 :: 53	PLP	Ornithine-oxo-acid transaminase activity	Ornithine metabolism
1	PF07_0029	Heat shock protein 86	ND	1.5	18 :: 53	LCR; HSP90; ATPase; MC	No GO terms	Response to unfolded protein / response to heat
2	MAL7P1.228	Heat shock 70 kDa protein	ND	2	No results	SP; LCR; HSP70; AL	No GO terms	None
1	PF08_0054	Heat shock 70 kDa protein	ND	5	19/16 :: 47/53	LCR; HSP70; AL; MC	No GO terms	Response to unfolded protein / response to heat
1	PF11_0351	Heat shock protein hsp70 homologue	ND	3	19 :: 49	LCR; HSP70; AL; CPDNaK; MC	No GO terms	Response to unfolded protein / response to heat
1	PF11_0111	Asparagine-rich antigen	ND	2	16/14/23 :: 53/53/16	LCR; GETHR; RNABr; EF	No GO terms	No GO terms
1	PF13_0011	<i>P. falciparum</i> gamete antigen 27/25	ND	1.5	49 :: 17	Pfg27	Molecular function unknown	Biological process unknown
1	PF13_0065	Vacuolar ATP synthase catalytic subunit a	ND	2	42 :: 53	VATPase; AS	No GO terms	Vacuolar acidification / ATP hydrolysis coupled proton transport
1	PF13_0218	Putative ABC transporter	ND	1.5	32 :: 12	4 TM; LCR; PEXEL; ABC	ATPase activity, coupled to transmembrane movement of substances	Transport
1	PF13_0350	Putative signal recognition particle receptor alpha subunit	ND	2	No results	LCR; SRP	Signal recognition particle binding / GTP binding	No GO terms
1	PF14_0425	Fructose-bisphosphate aldolase	ND	3	53 :: 43	LCR; FA; MC	Fructose-bisphosphate aldolase activity	Glycolysis/ gluconeogenesis
1	PFL1125w	Putative phospholipid-transporting ATPase	ND	1.5	11 :: 53	10 TM; LCR; PATPase	Phospholipid-translocating ATPase activity / ATP binding	Aminophospholipid transport
1	PF11_0174	Dipeptidyl aminopeptidase 1	ND	2	17 :: 44	SP; 1 TM; LCR; CP	No GO terms	No GO terms
1	MAL13P1.295	Hypothetical <i>P. falciparum</i> protein	ND	2	27 :: 53	LCR	No GO terms	No GO terms
1	MAL8P1.139	Hypothetical <i>P. falciparum</i> protein	ND	2	37/42/35/46/42/45 :: 53/53/10/53/53/53	8 TM; LCR; WD; RGD; DAG	No GO terms	No GO terms
1	PF10_0204	Hypothetical <i>P. falciparum</i> protein	ND	2	47 :: 16	NZP	No GO terms	No GO terms
1	PFA0255c	Hypothetical <i>P. falciparum</i> protein	ND	7	27 :: 7	LCR	No GO terms	No GO terms
1	MAL13P1.249	Hypothetical <i>P. falciparum</i> protein	ND	2	32/47 :: 53/53	2 TM; LCR	No GO terms	No GO terms
1	MAL8P1.141	Hypothetical <i>P. falciparum</i> protein	ND	1.5	8/13 :: 37/32	LCR	No GO terms	No GO terms
1	PF11_0347	Hypothetical <i>P. falciparum</i> protein	ND	15	15/11 :: 31/32	LCR; FHA; RNABr; GETHR	No GO terms	No GO terms
1	MAL7P1.170	Ring stage expressed protein	4	2	53 :: 36	LCR; PEXEL; ARM	No GO terms	No GO terms
1	MAL7P1.228	Heat Shock 70 KDa Protein	NS	3	No results	SP; LCR; HSP70; AL	No GO terms	No GO terms
1	PF08_0019	Putative guanine nucleotide-binding protein (RACK receptor)	3	NS	16 :: 47	WD; MC	Protein kinase C binding	G-protein coupled receptor protein signaling pathway
1	PF10_0380	Putative trophozoite antigen R45 (FIKK - kinase)	6	7	14 :: 51	LCR; PEXEL; PKL	Protein kinase activity	Protein amino acid phosphorylation
3	PF11_0224	Circumsporozoite-related antigen (Exp-1 / antigen 5.1)	6	5	53 :: 42	SP; 1 TM; LCR; CRA; MC	Molecular function unknown	Biological process unknown
1	PF14_0078	HAP protein	2	NS	18 :: 46	1 TM; ASP	Aspartic-type endopeptidase activity	Biological process unknown
2	PF14_0231	Putative ribosomal protein L7a	4	3	21 :: 47	LCR; RL7	Structural constituent of ribosome	Protein biosynthesis
1	PF14_0579	Putative ribosomal protein L27	6	5	14 :: 47	LCR; RL27	Structural constituent of ribosome	Protein biosynthesis
1	PFE0350c	Putative 60S ribosomal subunit protein L4/L1	3	NS	16 :: 53	LCR; RL4	RNA binding / structural constituent of ribosome	Protein biosynthesis
4	PF14_0678	Exported protein 2	5	5	18/18 :: 46/45	SP; LCR; MC	Molecular function unknown	Biological process unknown
5	PFE1590w	Early transcribed membrane protein (ETRAMP 5)	2	4	16 :: 53	SP; 1 TM; LCR; ETRAMP; MC	No GO terms	No GO terms
2	PFF0435w	Ornithine aminotransferase	3	4	18 :: 53	PLP	Ornithine-oxo-acid transaminase activity	Ornithine metabolism
1	PF10_0121	Hypoxanthine phosphoribosyltransferase	4	4	18 :: 49	PRT; MC	Hypoxanthine phosphoribosyltransferase activity	Purine ribonucleoside salvage
1	PFF1095w	Putative leucyl-tRNA synthetase cytoplasmic	2	NS	14/20/24 :: 53/53/53	LCR; ABD; ATS	Leucine-tRNA ligase activity	Leucyl-tRNA aminoacylation
1	MAL13P1.283	Putative TCP-1/cpn60 chaperonin family	2	NS	17 :: 47	TCP	ATPase activity, coupled / unfolded protein binding	Protein folding
1	MAL8P1.40	Putative RNA-binding protein	4	3	17/17 :: 44/47	LCR; RNABr; WW	RNA binding	Regulation of translation
11	PF11735c	Hypothetical <i>P. falciparum</i> protein (ring exported protein - REX)	9	4	11 :: 36	1 TM; LCR; MC	No GO terms	No GO terms
1	PF14_0016	Hypothetical <i>P. falciparum</i> protein (ETRAMP 14.1 / Sep14)	3	2	53 :: 34	SP; 2 TM; LCR; MC	Molecular function unknown	Biological process unknown
1	PFL0050c	Hypothetical <i>P. falciparum</i> protein	4	4	18 :: 48	LCR; PEXEL; MC	No GO terms	No GO terms
1	PFF0090w	Hypothetical <i>P. falciparum</i> protein	4	3	No oligos	1 TM; LCR	No GO terms	No GO terms
1	PF14_0344	Hypothetical <i>P. falciparum</i> protein	4	NS	53 :: 33	SP; LCR; EF	No GO terms	No GO terms
1	PF14_0045	Hypothetical <i>P. falciparum</i> protein	NS	4	53 :: 34	SP; 1 TM; LCR	Molecular function unknown	Biological process unknown
1	PFB0194w	Conserved hypothetical <i>P. falciparum</i> protein	3	2	53/53/53 :: 30/31/27	SP; 1 TM; LCR; AP	Molecular function unknown	Biological process unknown

B

Number of clones	PlasmoDB ID	PlasmoDB annotation (additional annotation)	Early trophozoites: fold downregulated	Late trophozoites: fold downregulated	Normal IDC transcript expression profile Maximum :: minimum expression (hpi)	Noteworthy characteristics	GO term: Function	GO term: Process
1	MAL13P1.60	Erythrocyte binding antigen 140	ND	7	49/50 :: 26/25	SP; 1 TM; LCR; DBL	Molecular function unknown	Biological process unknown
1	PF10_0203	ADP ribosylation factor	ND	9	43 :: 14	SAR; Arf; Ras	GTP binding	Protein amino acid ADP-ribosylation / intracellular protein transport
1	PF14_0102	Rhoptry-associated protein 1	ND	10	47/47 :: 21/20	SP; LCR; RAP	Molecular function unknown	Biological process unknown
2	PFB0340c	Putative cysteine protease (SERA 4)	ND	26	44 :: 17	LCR; CP; MC	Cysteine-type peptidase activity	Proteolysis
1	PFB0935w	Cytoadherence linked asexual protein 2	ND	5	47/47 :: 19/16	SP; LCR; CLAG	Cell adhesion molecule binding	Cytoadherence to microvasculature
1	PF0020c	Erythrocyte membrane protein 1	ND	16	47/7 :: 53/53	LCR; DBL	Cell adhesion molecule binding	Cell-cell adhesion / rosetting / antigenic variation / cytoadherence to microvasculature
1	PF0255w	ag-1 blood stage membrane protein homologue	ND	8	47/47/47/47 :: 16/18/17/16	LCR; C2	No GO terms	No GO terms
2	PF10265c	Putative rhoptry protein (RhopH3)	ND	22	47/47/47 :: 19/19/20	SP; LCR; MC	No GO terms	No GO terms
1	PF11475w	Merozoite surface protein 1 precursor	ND	8	48/47/47/47 :: 20/19/19/19	SP; 1 TM; LCR; EGF	No GO terms	No GO terms
1	MAL8P1.310	Putative senescence-associated protein	ND	12	No results	None	No GO terms	No GO terms
2	PF11445w	Hypothetical <i>P.falciparum</i> protein (RhopH2)	ND	9	47/46/47 :: 18/18/18	SP; LCR	No GO terms	No GO terms
1	PF11_0278	Hypothetical <i>P.falciparum</i> protein	ND	2	48 :: 26	2 TM; LCR; AP	Molecular function unknown	Biological process unknown
1	PF11145c	Hypothetical <i>P.falciparum</i> protein (Rhoptry neck protein, Rh5)	ND	6	52/52 :: 24/25	LCR	No GO terms	No GO terms
1	PFB0475c	Hypothetical <i>P.falciparum</i> protein	ND	5	50/50 :: 26/25	SP; LCR; C2	No GO terms	No GO terms
1	PF11_0513	Hypothetical <i>P.falciparum</i> protein	ND	18	53 :: 30	LCR; HSP	No GO terms	No GO terms
1	PF14_0260	Hypothetical <i>P.falciparum</i> protein (Drug:H+ Antipporter-1 family (metabolite / drug transporter))	ND	10	12 :: 27	12 TM; LCR; MFS	Molecular function unknown	Biological process unknown
1	MAL13P1.308	Hypothetical <i>P.falciparum</i> protein	ND	7	48 :: 19	LCR; ARM; EF	No GO terms	No GO terms
1	PF10_0351	Hypothetical <i>P.falciparum</i> protein (Peripherial surface or parasitophorous vacuole (H103))	ND	22	49 :: 23	SP; LCR; PR	No GO terms	No GO terms
1	MAL13P1.435	Conserved hypothetical <i>P.falciparum</i> protein	ND	32	No results	None	No GO terms	No GO terms
10	MAL8P1.310	Putative senescence-associated protein	4	NS	No results	None	No GO terms	No GO terms
6	PF08_0131	1-cys peroxiredoxin	2	3	34 :: 53	AhpC/TSA; TL	Peroxidase activity / antioxidant activity	Response to oxidative stress
4	PFB0345c	Putative cysteine protease (SERA 5)	3	5	3 :: 16	SP; LCR; CP	Cysteine-type peptidase activity	Proteolysis
1	PFB0340c	Putative cysteine protease (SERA 4)	2	2	44 :: 17	LCR; CP; MC	Cysteine-type peptidase activity	Proteolysis
1	PF0780w	Putative glutamyl-tRNA (Gln) amidotransferase subunit A	NS	3	7/35 :: 53/12	SP; LCR; AP; AM	Glutamyl-tRNA(Gln) amidotransferase activity	No GO terms
7	PF13_0338	Hypothetical <i>P.falciparum</i> protein (PF92)	2	4	42 :: 15	SP; 1 TM; LCR; SSA	No GO terms	No GO terms
5	PF11445w	Hypothetical <i>P.falciparum</i> protein (RhopH2)	NS	4	47/46/47 :: 18/18/18	SP; LCR	No GO terms	No GO terms
1	PF0400w	Hypothetical <i>P.falciparum</i> protein	NS	2	47/47 :: 16/14	LCR; Ank	No GO terms	No GO terms
8	MAL13P1.460	Conserved hypothetical <i>P.falciparum</i> protein	6	NS	No results	None	No GO terms	No GO terms
1	MAL13P1.455	Conserved hypothetical <i>P.falciparum</i> protein	2	NS	No results	None	No GO terms	No GO terms

In both A and B the top half of the table indicates the SSH dataset [188], while the bottom half originates from the SSH-microarray dataset. Fold change for SSH was calculated by dividing spot intensities of forward subtracted libraries by reverse subtracted libraries for the increased abundance transcripts and vice versa for the decreased abundance transcripts. For multiple clones, the value given is the average of the values. Fold change for SSH-microarray was calculated by 2^M , where $M = \log_2 \frac{Red}{Green}$ (i.e. the \log_2 expression level for the gene). For redundant clones, the value given is that with the best *P*-value. ND = not determined; NS= not significant (*P*>0.05). The normal transcript expression profile is data obtained from the Malaria IDC Strain Comparison Database (<http://malaria.ucsf.edu/comparison/index.php>). The data given is for the 3D7 strain and the values are the time (hours post invasion) of minimum and maximum transcript expression. Multiple values indicate multiple oligos for the respective transcript. Noteworthy protein characteristics include: ABC: ATP binding cassette transporter motif; ABD: anticodon binding domain; AhpC/TSA: alkyl hydroperoxide reductase and thiol specific antioxidant families; AL: actin-like ATPase domain; AM: amidase signature; Ank: Ankyrin repeat domain; AP: targeted to apicoplast; Arf: ADP-ribosylation factor family; ARM: ARM repeat; AS: ATP synthase domain; ASP: aspartic protease; ATPase: ATPase domain of HSP90, DNA topoisomerase II and histidine kinase; ATS: aminoacyl tRNA synthetase class 1 signature; C2: C2 calcium lipid binding domain; CLAG: cytoadherence linked asexual protein; CP: cysteine protease family; CPDnak: chaperone protein Dnak; CRA: circumsporozoite related antigen; DAG: diacylglycerol binding domain; DB: Duffy binding domain; EF: EF-hand calcium binding domain; EGF: epidermal growth factor-like domain; ETRAMP: early transcribed membrane protein; FA: glycolytic fructose biphosphate aldolase class I; FHA: Forkhead associated domain; GETHR: GETHR pentapeptide repeat; HSP: heat shock protein DnaJ domain; HSP70: 70kDa heat shock protein signature; HSP90: 90kDa heat shock protein signature; LCR: low complexity region; MC: Maurer's clefts associated; MFS: major facilitator superfamily; NZP: Clostridium neurotoxin zinc protease; PATPase: P-type ATPase; PEXEL: Plasmodium export element; Pfg27: gametocyte protein Pfg27 superfamily; PKL: protein kinase-like domain; PLP: PLP dependent transferase superfamily; PR: Pumilio RNA-binding repeat profile; PRT: phosphoribosyltransferase domain; RAP: rhoptry associated protein; Ras: Ras GTPase; RGD: RGD signal sequence; RNAbr: RNA binding and recognition motifs; RL4: ribosomal family L4/L1 signature; RL7: ribosomal family L7a signature; RL27: ribosomal family R27e signature; SAR: GTP binding SAR1 protein signature; SP: signal peptide; SRP: SRP54-type protein GTPase domain; SSA: sexual stage antigen s48/45 domain; TCP: TCP-1/Cpn60 chaperonin family; TL: thioredoxin like fold; TM: transmembrane domain; VATPase: V-type ATPase; WD: WD domain; WW: WW (trp/trp) domain.

In the initial SSH study (late trophozoite stage) [188], 20 and 19 unique, differentially expressed transcripts were identified in each of the increased and decreased abundance libraries, respectively (Table 2.11). Fold changes for the transcripts of increased abundance ranged from 1.5- to 15-fold, whereas the transcripts of decreased abundance were more dramatically affected with the level of repression ranging from 2- to 32-fold. In the SSH-cDNA microarray study, an additional 23 transcripts of increased abundance and 10 of decreased abundance were identified with a fold change ($P < 0.05$) ranging from 2- to 9-fold (increased abundance) and 2- to 6-fold (decreased abundance). Surprisingly, only two of increased abundance (PFF0435w and MAL7P1.228) and three of decreased abundance (MAL8P1.310, PFB0340c and PFI1445w) transcripts were observed to be in common between the two studies. Interestingly, 35% of the increased abundance and 60% of the decreased abundance transcripts showed significant ($P < 0.05$) stage-dependent differential expression between the early and the late trophozoites (Table 2.11). A considerable level of redundancy was observed amongst the transcripts of decreased abundance.

GO classification indicated that the transcripts of increased abundance encoded various general processes including haemoglobin digestion, protein targeting, signalling, transport mechanisms and general metabolism (Figure 2.10). To mediate enhanced haemoglobin degradation, an increase in abundance of transcripts for a lysosomal exopeptidase (cathepsin C) homolog: dipeptidyl aminopeptidase 1 (DPAP1) (PF11_0174, Table 2.11 A) and a histo-aspartic protease (HAP) (PF14_0078, previously known as Plasmepsin III, Table 2.11 A) was observed. Transcripts that may be involved with signalling include a putative trophozoite antigen R45 (PF10_0380) which is included in the FIKK family of kinases identified by Ward *et al.* [206] and guanine binding protein (PF08_0019, Table 2.11 A) which is a receptor for activated C kinase (RACK) [207]. Two surface antigens (Asp-rich antigen, PF11_0111 and gamete antigen 27/25, PF13_0011) also showed increased abundance. Finally, an increase in abundance of the transcripts for fructose-bisphosphate aldolase (PF14_0425), a putative ABC transporter (PF13_0218), as well as several proteins normally transcribed during the ring stage (e.g. PFI1735c, MAL7P1.170, PF14_0678, PFE1590w and PF14_0016) was noted.

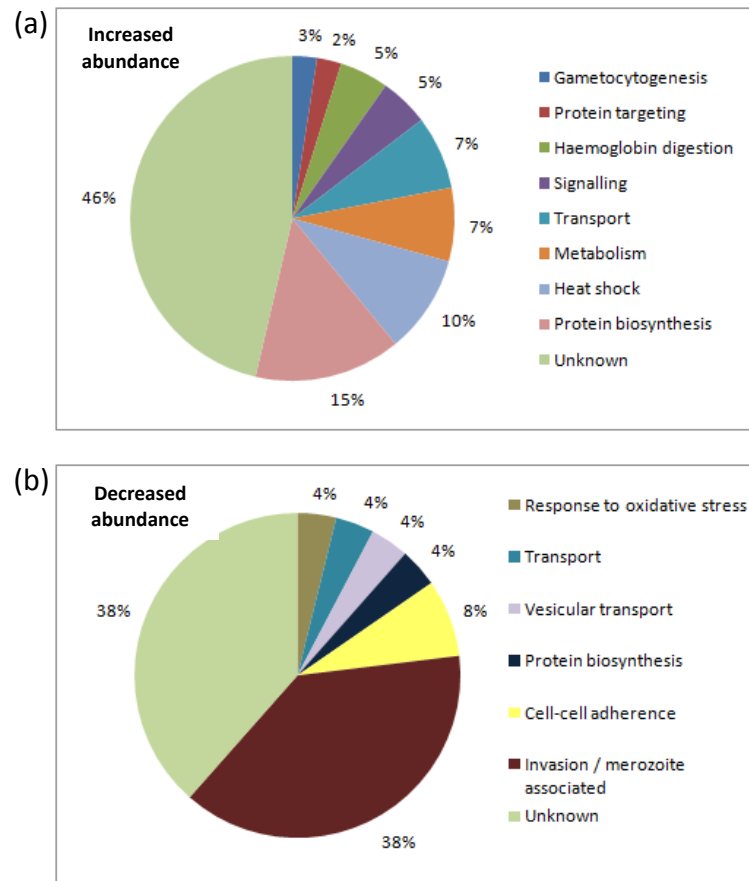


Figure 2.10. Functional grouping of (a) transcripts of increased abundance and (b) decreased abundance after DFMO-treatment. The transcripts were assigned to the various groups based on GO terms (biological process) and annotation.

The decrease in abundance of several transcripts that encode proteins involved in cell-cell adhesion (cytoadherence and sequestration), as well as erythrocyte invasion (Table 2.11 B) was observed upon DFMO-treatment. These include several transcripts for surface proteins (PF13_0338, PF10_0351, PFB0345c, PFB0340c, PFI1475w); several rhoptry-proteins (PF14_0102, PFI1445w, PFI0265c, PFB0935w); and a microneme-associated protein (MAL13P1.60) [208]. The decrease in abundance of transcripts for an ADP-ribosylation factor (PF10_0203) and 1-cys peroxiredoxin (PF08_0131) was also observed.

Just after completion and annotation of the genome in 2002, over 60% of the genome consisted of hypothetical proteins, predicted open reading frames that had, as yet, no functional annotation due to low homology with known proteins [97, 124, 209]. Since then, the genome has undergone additional annotation and consideration; though it is unknown how many of the hypothetical proteins have now been functionally annotated. In this investigation, 34% of the transcripts of increased abundance encode hypothetical proteins of which two (5%) could be tentatively annotated by additional literature and database investigations. Half (50%) of the transcripts of decreased

abundance encode hypothetical proteins of which four (15%) could be additionally annotated (Table 2.11). Analyses of predicted protein features of these differentially regulated hypothetical proteins indicated a high prevalence of low complexity regions in the majority of the proteins, thus conforming to the observation that almost 90% of *P. falciparum* proteins contain at least one low-complexity region [210]. Furthermore, 30% of the hypothetical proteins contained signal peptides compared to the 17% of total *P. falciparum* proteins [97]. Up to 37% of the hypothetical proteins contained one or more transmembrane segments, an amount similar to that of the proteome predicted to contain such areas [97]. PF11_0347 showed a 15-fold increase in abundance, indicating a potentially important role of this transcript in overcoming the effects of DFMO-treatment and warrants its further investigation. Pfam analysis of its predicted protein features indicates a conserved FHA domain (phosphopeptide binding domain found in many regulatory proteins) and a RNA recognition motif. Furthermore, PF11_0513 and PF10_0351 transcripts were of decreased abundance (18 and 22 fold, respectively). Interestingly, PF14_0260, showed a 10-fold decrease in abundance and has been identified as a novel *P. falciparum* putative transport protein and predicted to fall in the drug:H⁺ antiporter family [211].

A significant number of the differentially expressed transcripts identified were associated with the Maurer's clefts [158, 212]. Of the transcripts with an increase in abundance, PF07_0029, PF08_0054, PF11_0351, PF14_0425, PF08_0019, PF11_0224, PF14_0678, PFE1590w, PF10_0121, PFI1735c, PF14_0016 and PFL0050c all are known or proposed to be associated with the Maurer's clefts (Table 2.11). Less of the decreased abundance transcripts show this association, namely only PFI0265c, PFI1445w and PFB0340c.

Drug-specific effects induced by DFMO-treatment on the transcriptome of *P. falciparum* were observed in the increase in abundance of ornithine aminotransferase (OAT) and hypoxanthine phosphoribosyltransferase (HGXPRT) (Figure 2.11). The initial SSH study indicated a 1.5-fold increase in abundance of OAT transcripts, while data from the SSH-microarray indicated a 3 to 4-fold increase in abundance in the early and late trophozoite stages of *P. falciparum*. The difference in the values observed most likely stems from the different technologies used to calculate values for differential expression in the two studies (densitometric measurements of blots versus scanned fluorescence of microarrays). A maximum 4-fold increase in abundance of HGXPRT transcripts were observed in both trophozoite stages (Figure 2.11), but was not observed in the initial study, possibly due to non-exhaustive clone selection. The malaria parasite is incapable of forming purines *de novo* and thus is reliant on hypoxanthine and purine salvage [213]. Putrescine depletion would result in a decrease in MTA, which acts as a precursor for the production of hypoxanthine. A compensatory increase in

HGXPRT transcripts (4-fold increase in abundance) would allow the improved utilisation of hypoxanthine in order to meet the demand for IMP production. None of these transcripts show significant differential regulation in the earlier ring stages, prior to DFMO-induced putrescine depletion.

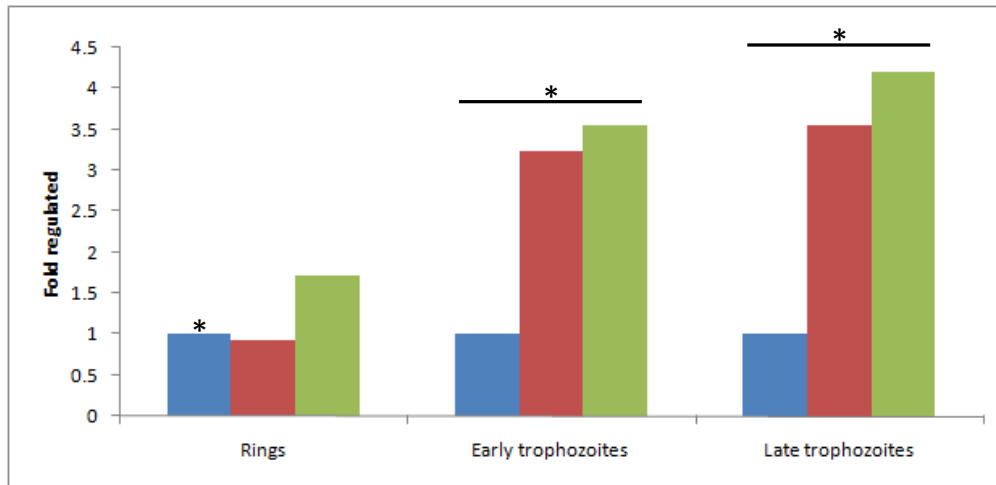


Figure 2.11. Drug-specific transcriptional feedback responses due to DFMO-treatment in *P. falciparum* parasites. Fold increase in abundance of ornithine aminotransferase (pink bars) and hypoxanthine phosphoribosyltransferase (green bars) for the various life-cycle stages are indicated normalised to the untreated control at a value of 1 (blue bars). *Indicates significant differential expression ($P < 0.05$).

2.3.1.5 Validation of microarray data

The primers designed for the four genes used for validation, namely exported protein 2 (EXP2), ornithine aminotransferase (OAT), L27 ribosomal protein (L27) and 1-cys peroxidoxin (PXN) are tabulated in Table 2.4, along with lactate dehydrogenase (LDH), the constitutively expressed control gene. As LDH had been chosen as a household gene, a standard curve was prepared using serial dilutions of cDNA and a regression coefficient (R^2) of 0.998 was obtained. It was confirmed that the gene was unaffected by treatment, as the ratio of LDH treated to untreated was 1.0986 and was transformed to a value of 1 for use in normalisation. In all cases, the microarray data and the semi-quantitative real-time PCR data correlated in terms of increase or decrease in abundance of the transcripts (Table 2.12).

Table 2.12. Verification of differential expression of a selection of identified differential transcripts. All the primers for semi-quantitative real-time PCR produced small amplicons of a similar length (between 141 and 169 bp) and had similar annealing temperatures (55-59°C), such that a common annealing temperature of 55°C could be used and all primers could be tested in the same thermocycling run.

Gene	Fold change ^a	Confirmation fold change ^b	Direction of change
Exported protein 2	4.91	2.28	Up
Ornithine aminotransferase	2.99	3.38	Up
L27 ribosomal protein	5.13	2.25	Up
1-cys peroxiredoxin	-2.6	0.42 *	Down
Lactate dehydrogenase	ND	1	-

ND=not determined.

^aFold change for microarray (late trophozoite sample) was calculated by 2^M , where $M = \log_2 \frac{Red}{Green}$ (i.e., the \log_2 expression level for the gene).

^bThe validity of the microarray data was verified by semi-quantitative real-time PCR (late trophozoite sample). The data represent the fold change difference between DFMO-treated and untreated parasites and are from one experiment, performed in triplicate, relative to lactate dehydrogenase, a gene unaffected by treatment.

*Decreased abundance transcripts fold change is equivalent to 3.

2.3.2 PART 2:

Transcriptional profile of ODC-inhibited *P. falciparum* parasites using whole genome oligo microarray

2.3.2.1 Oligo microarray

As observed previously for the SSH-cDNA microarray, the *P. falciparum* parasite culture exhibited morphologically observable cytotaxis in the trophozoite stage as a result of DFMO-treatment. The parasites were harvested at 21 and 29 hours post-treatment (corresponding to approximately 23 and 31 hours post-invasion). At time-point 1, approximately 30% of the untreated culture still contained rings, while around 70% of the treated culture was rings. RNA of sufficient concentration, total quantity and purity (as evidenced by the A_{260}/A_{280} ratio) was obtained for DNA microarray. Figure 2.12 shows representative examples (treated and untreated) of a scanned array after hybridisation of the samples to the *P. falciparum* DNA microarray (composed of in-house designed oligos).

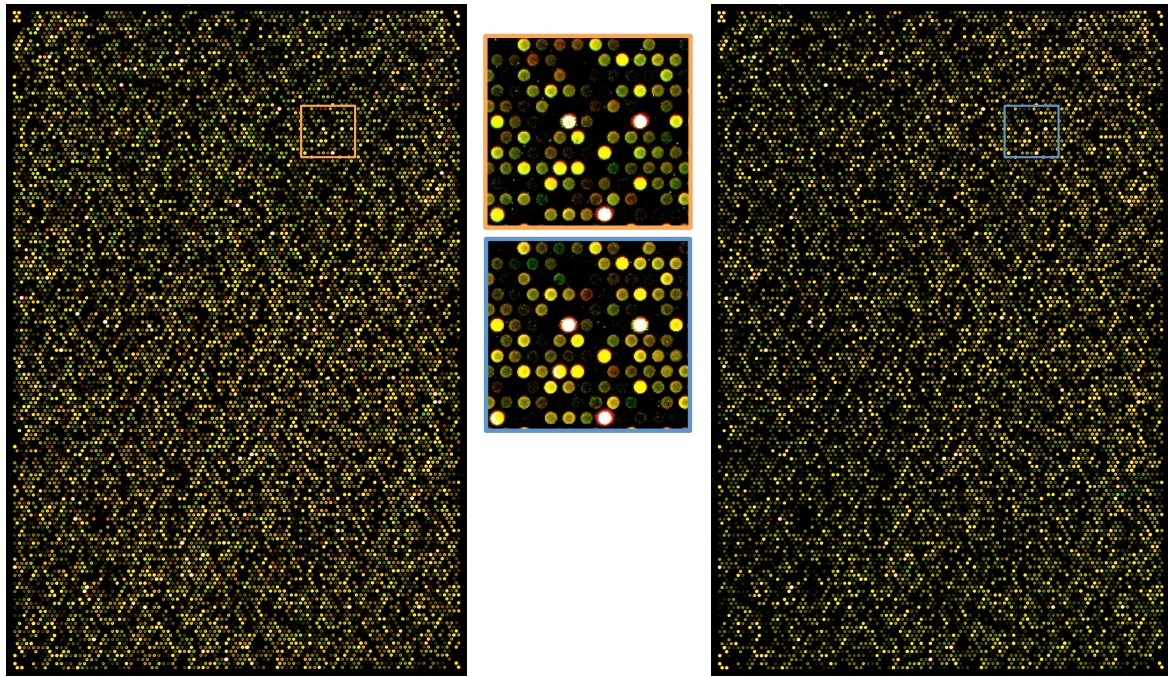


Figure 2.12. Microarray slides of untreated (left - orange border) and treated (right - blue border) time-point 2. These are only two of eight arrays present on one slide

After automatic spot finding and flagging of those spots that were unsuitable for further data analysis (due to excessive green background or an unacceptable signal to noise ratio), preliminary processing (pre-processing) of the data could be performed. This entailed data evaluation, cleaning and analytical methods, which are employed to obtain reliable estimates of the relative abundance of each gene [214]. There was a slight elevation of the background for the second time-point (last eight arrays), although it was not a significant amount, the background on all the arrays was subsequently removed during processing. The data was subsequently normalised to remove systematic variation by adjusting the individual hybridisation intensities to balance them, so that meaningful biological comparisons can be made. This compensates for potential differences between the arrays, such as the amount of RNA, labelling differences or dye detection efficiency [215, 216]. Normalisation can be within an array or between various arrays. In this case, robust-spline normalisation within the arrays proved the most appropriate. Robust-spline normalisation is an empirical Bayes compromise between print-tip and global loess normalisation, with 5-parameter regression splines used in place of the loess curves [217].

Figure 2.13 shows the effect of applying robust-spline normalisation within the arrays. In Figure 2.13 (a) the log differential expression values (M-values, $M = \log_2^{\text{Red}} / \text{Green}$) differ between the various arrays and are not entirely centred around zero. An M-value of zero indicates that the gene is unchanged – an assumption for normalisation is that the majority of the genes remain unaffected by treatment. After normalisation (Figure 2.13 (b)), the arrays have shifted to centre around zero.

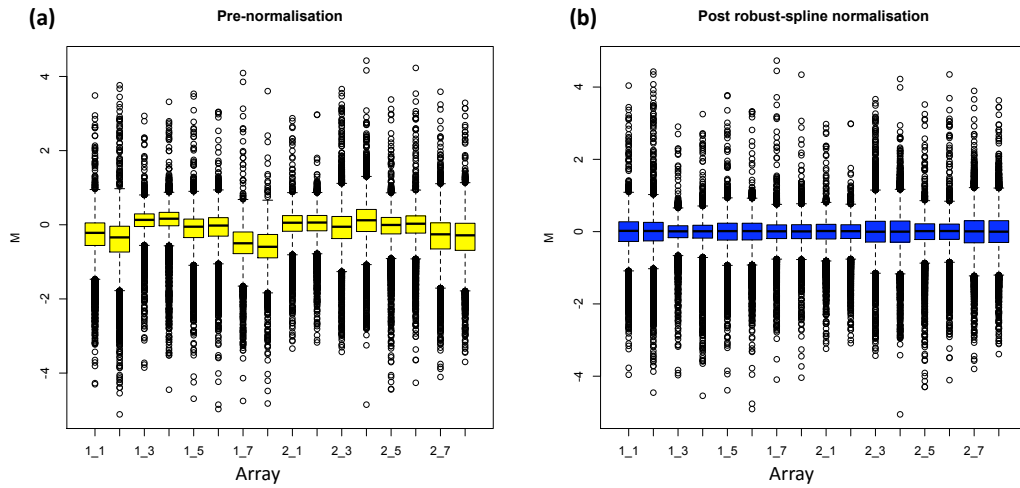


Figure 2.13. Boxplots of arrays (a) pre-normalisation and (b) post robust-spline within-slide normalisation.

The effects of both within and between array normalisation can be further explored using MA plots (plots of the log differential expression ratio, M versus the log intensity of the spot, A). Figure 2.14 gives MA plots of the data for the various stages of pre-processing. It is noticeable that the background subtraction and robust-spline within array normalisation affect the data rather dramatically, while the G-quantile between array normalisation has less effect.

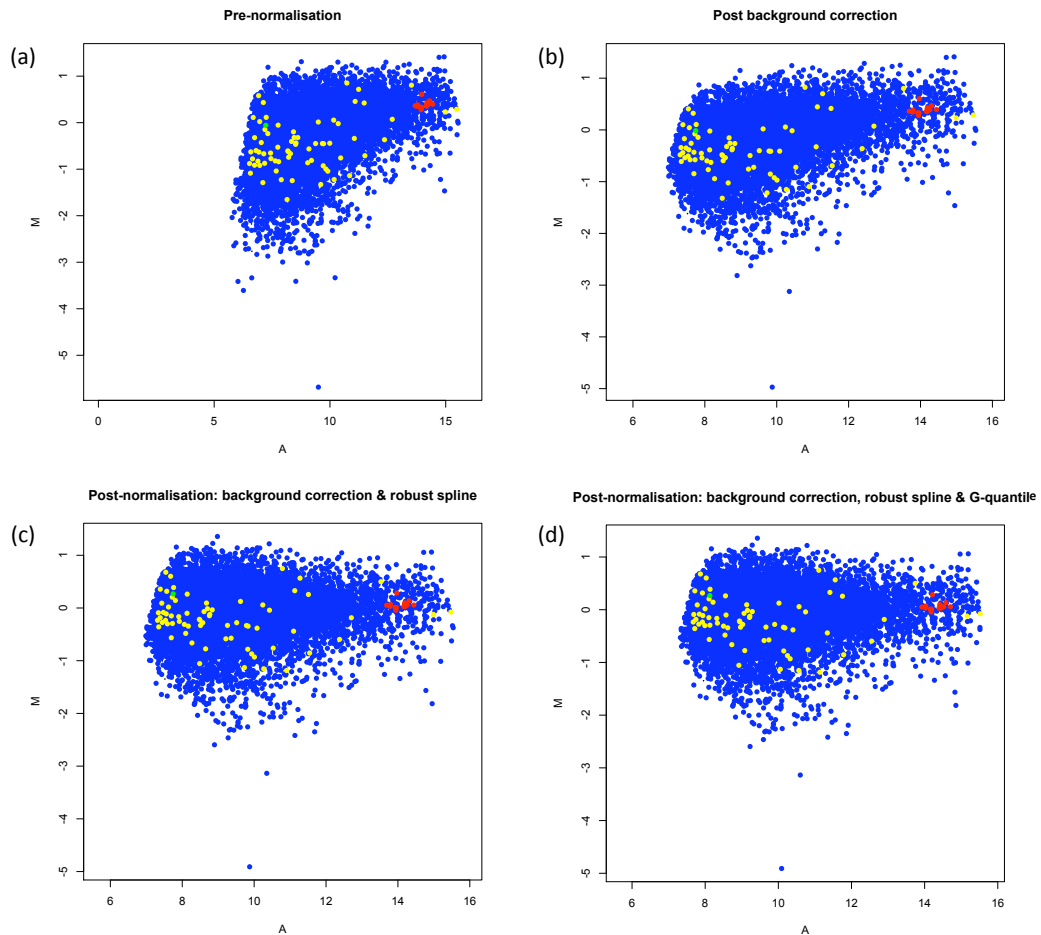


Figure 2.14. MA plots of array 1_6 (a) pre-normalisation, (b) post background correction, (c) post within-array normalisation (robust-spline) and (d) post between-array normalisation (G-quantile). Blue: oligo; yellow: malaria controls, red: control - bright corner; green: control – dark corner.

Quantile normalization was proposed by Yang and Thorne for two-color cDNA arrays [216]. Quantile normalisation ensures that the intensities have the same empirical distribution across arrays and across channels, while G-quantile normalisation specifically ensures that the green channel has the same empirical distribution across the arrays, leaving the M-values unchanged [194]. This is appropriate for the situation as the green channel (Cy3) was the reference channel in this experimental design. Figure 2.15 plots density versus intensity and shows the effect of the two normalisation steps on the data. Following G-quantile normalisation, only a single curve is visible for the green channel.

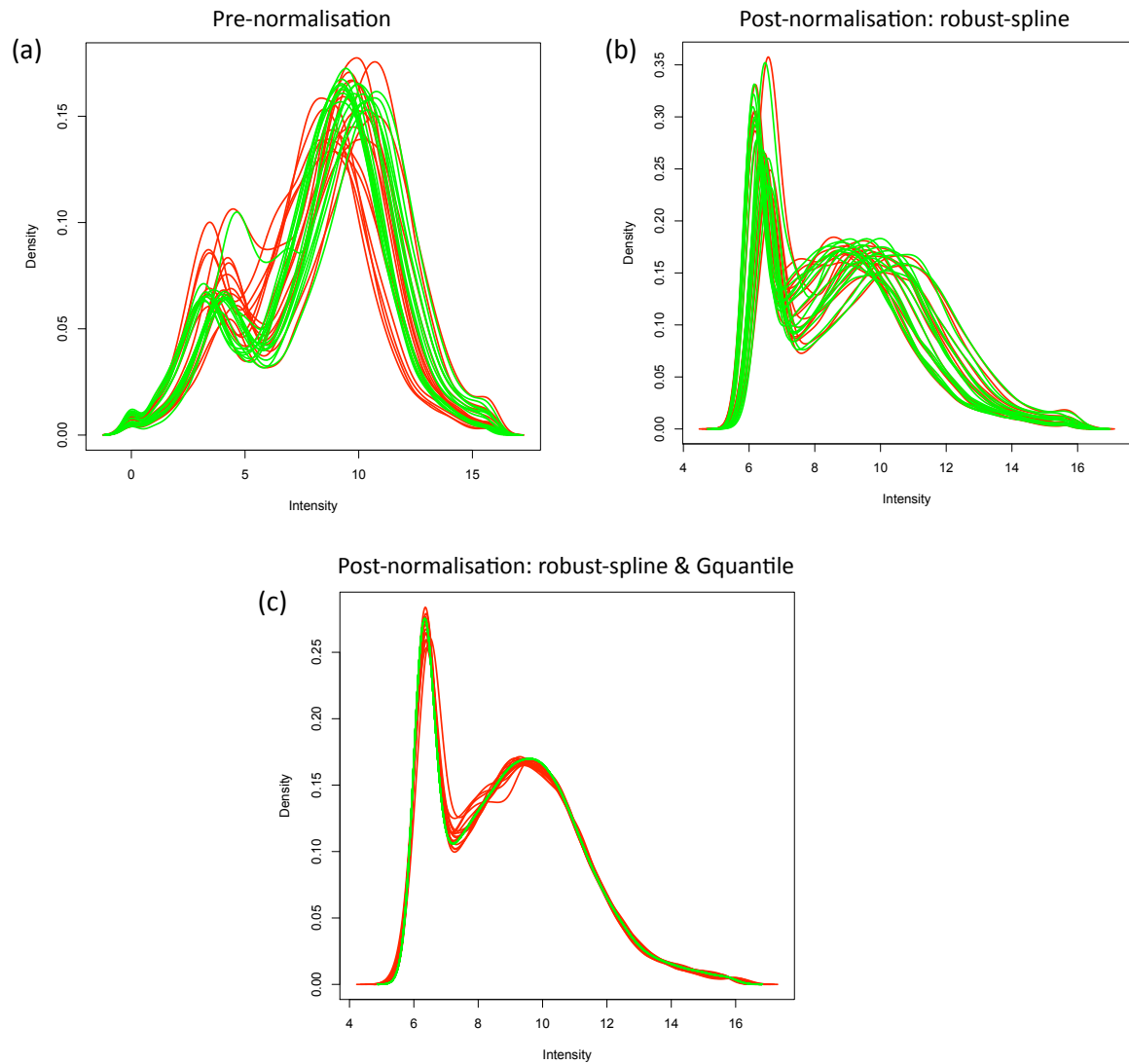


Figure 2.15. Density plots of the arrays (a) pre-normalisation, (b) post robust-spline normalisation, followed by (c) G-quantile normalisation

2.3.1.2 Effect of DFMO-treatment on *P. falciparum* parasites

Since van Brummelen *et al.* showed that the cytostatic effect of inhibiting AdoMetDC-ODC causes generalised transcriptional arrest [1], it is necessary to compare the various samples with each other in order to determine which should be used as a comparison point, in order to eliminate life-cycle specific variations during the parasite's IDC. This was achieved by obtaining the Pearson correlation coefficients of each sample relative to the others (Table 2.13). As observed by van Brummelen *et al.* the later untreated time-point cannot be used for comparison due to the poor (negative) correlation with the treated sample at the same time-point [205]. This is a result of the cytostatic nature of DFMO. The first untreated sample was thus used for comparison. Interestingly, the correlation between the two treated samples and U1 is very similar, and when T1 is compared with T2, the correlation is good, thus the treated samples correlate with each other well. As expected, the

correlation between U1 and U2 is not good, due to the transcriptome differences resulting from life-cycle progression.

Table 2.13. Pearson correlation coefficients between the various samples.

	TT1	TT2	UT1
TT1			
TT2	0.657		
UT1	0.203	0.217	
UT2	-0.506	-0.416	0.112

Using BioConductor and limma, a linear model was fitted to the processed (background subtracted and normalised) data to determine which transcripts were differentially expressed. Following analysis for time-point 1, a total of 638 transcripts of decreased abundance (of which 8 IDs were not found in PlasmDB) and 252 transcripts of increased abundance (6 not found) were identified (see Supplementary Material S2, Table S2.1 and S2.2). This approximately two-fold excess of transcripts with decreased abundance was mirrored in time-point 2, where 334 of decreased abundance (5 not found) and 145 of increased abundance (2 not found) were identified. Approximately twice as many transcripts were differentially expressed in time-point 1, as compared with time-point 2. The number of transcripts identified in more than one of the samples is indicated in Figure 2.16 and Table 2.14. Within the decreased abundance transcripts, 43% of the time-point 1 transcripts are common to both time-points, while this rises to 83% of the time-point 2 transcripts. The percentages are somewhat lower within the increased abundance transcripts with 26% of time-point 1 and 45% of time-point 2.

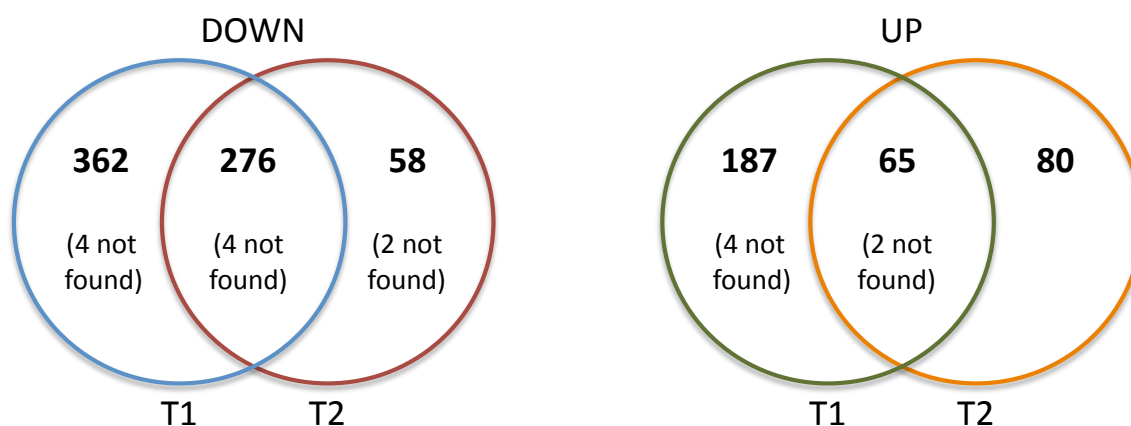


Figure 2.16. Venn diagrams indicating the number of transcripts unique to and in common between, time-points 1 (T1) and 2 (T2).

Obviously, most of the overlapping transcripts were shared amongst either the 'down' (decreased abundance), or the 'up' groups (increased abundance). There were however, a few transcripts in common between 'down' and 'up'. These are given in Table 2.14.

Table 2.14. Commonalities between the various sets of differentially expressed transcripts.

	TT1 DOWN	TT2 DOWN	TT1 UP
TT1 DOWN			
TT2 DOWN	276 (figure 2.16)		
TT1 UP	PF10_0034	MAL7P1.61	
TT2 UP	PF10_0034 PF10_0224 PF10_0212 PF11_0483	PF11_0483	65 (figure 2.16)

The identity of the transcripts (PF10_0034: conserved *Plasmodium* protein of unknown function; PF10_0224: dynein heavy chain; PF10_0212: conserved *Plasmodium* protein of unknown function; PF11_0483: farnesyltransferase β -subunit; MAL7P1.61: not found) reveals little about why these transcripts would show both increased and decreased abundance.

Table 2.15 contains the transcripts with the highest degree of increase in abundance for each of the two time-points. The transcripts showing the greatest increase in abundance in each of the time-points were for a PHISTa like exported protein, although the gene for this differed between the two time-points (MAL7P1.255 versus PF11_0514). The maximum fold change in each case was similar (3.49 for T1 versus 3.61 for T2).

Amino peptidase appears in both time-points and also shows a slight increase between T1 and T2 (2.69 to 2.99 fold). This protein is involved in haemoglobin digestion and thus supports the observations in the SSH-cDNA microarray that haemoglobin digestion is increased. LDC occurs in both time-points, supporting the observation by van Brummelen *et al.* (2.8 fold change, [1]) and shows a marginal increase from T1 (2.2 fold) to T2 (2.6 fold). Unfortunately, many of these most differentially expressed transcripts (such as conserved *Plasmodium* protein, *Plasmodium* exported protein) are functionally unannotated.

Table 2.15. Top 25 transcripts of increased abundance for each of the two time-points, respectively.

PlasmoDB ID	Product description	Log fold change	Fold change	Adjusted p-value
Time-point 1				
MAL7P1.225	<i>Plasmodium</i> exported protein (PHISTA-like), unknown function	1.80	3.49	3.08255E-09
PF11_0514	<i>Plasmodium</i> exported protein (PHISTa), unknown function	1.67	3.18	4.93367E-08
PF14_0015	Aminopeptidase, putative	1.43	2.69	4.04792E-09
MAL7P1.141	Conserved <i>Plasmodium</i> protein, unknown function	1.39	2.63	2.28543E-08
MAL8P1.2	<i>Plasmodium</i> exported protein (PHISTb), unknown function	1.39	2.62	8.2277E-08
PFA0130c	Serine/Threonine protein kinase, FIKK family, putative	1.39	2.62	3.57124E-09
PFIO540w	Conserved <i>Plasmodium</i> protein, unknown function	1.38	2.59	1.23928E-08
PFL1885c	Calcium/calmodulin-dependent protein kinase 2	1.35	2.56	4.2026E-09
PF11780w	<i>Plasmodium</i> exported protein (PHISTc), unknown function	1.35	2.55	1.586E-08
PFB0923c	<i>Plasmodium</i> exported protein, unknown function	1.31	2.49	6.15247E-10
PFD1140w	<i>Plasmodium</i> exported protein (PHISTc), unknown function	1.30	2.47	1.19146E-08
PFL2520w	Reticulocyte-binding protein 3 homologue	1.29	2.45	0.00115918
PFD1135c	Probable protein, unknown function	1.28	2.42	1.4976E-08
PFIO120c	Serine/Threonine protein kinase, FIKK family	1.26	2.40	8.1055E-09
MAL7P1.144	Serine/Threonine protein kinase, FIKK family	1.26	2.39	3.35894E-07
PF13_0058	RNA binding protein, putative	1.23	2.35	2.39186E-06
PF11_0513	DNAJ protein, putative	1.23	2.35	2.08564E-08
PFD0700c	RNA binding protein, putative	1.20	2.30	0.002546948
PF08_0001	<i>Plasmodium</i> exported protein, unknown function	1.19	2.29	1.14902E-08
PF08_0119	Conserved <i>Plasmodium</i> protein, unknown function	1.19	2.28	4.01499E-06
MAL8P1.204	DNAJ protein, putative	1.18	2.26	6.2943E-07
MAL8P1.81	Phosphopantothenoylcysteine decarboxylase, putative	1.15	2.22	2.32944E-08
PFD0285c	Lysine decarboxylase, putative	1.14	2.20	5.31237E-09
PF11720w	Gametocyte-implicated protein (Fragment)	1.14	2.20	6.64888E-07
PF08_0035	Conserved <i>Plasmodium</i> protein, unknown function	1.14	2.20	1.57502E-05
Time-point 2				
PF11_0514	<i>Plasmodium</i> exported protein (PHISTa), unknown function	1.85	3.61	2.79333E-08
PFL1885c	Calcium/calmodulin-dependent protein kinase 2	1.61	3.06	8.91035E-10
PF14_0015	Aminopeptidase, putative	1.58	2.99	3.47541E-08
MAL7P1.225	<i>Plasmodium</i> exported protein (PHISTA-like), unknown function	1.55	2.92	1.96986E-07
PF10_0374	Pf11-1 protein	1.40	2.64	3.58356E-08
PFF0855c	Rifin	1.37	2.58	3.42504E-05
PFIO175w	Conserved <i>Plasmodium</i> protein, unknown function	1.30	2.46	6.17599E-06
PFB0115w	Conserved <i>Plasmodium</i> protein, unknown function	1.28	2.42	4.10329E-06
PFF0075c	<i>Plasmodium</i> exported protein (PHISTb), unknown function	1.22	2.32	7.59239E-08
PF08_0060	Asparagine-rich antigen	1.21	2.31	1.78029E-05
PFB0923c	<i>Plasmodium</i> exported protein, unknown function	1.21	2.31	7.12392E-08
PF13_0029	Conserved <i>Plasmodium</i> protein, unknown function	1.19	2.29	7.56859E-08
PF14_0703	Conserved <i>Plasmodium</i> protein, unknown function	1.19	2.28	1.32607E-06
PF08_0001	<i>Plasmodium</i> exported protein, unknown function	1.19	2.28	2.14839E-08
PFD0285c	Lysine decarboxylase, putative	1.18	2.26	9.09844E-09
PF14_0662	Nucleoside transporter, putative	1.17	2.25	3.08241E-07
PFC0245c	Conserved <i>Plasmodium</i> protein, unknown function	1.11	2.16	1.46752E-06
PF14_0402	Conserved <i>Plasmodium</i> protein, unknown function	1.11	2.16	1.28701E-08
PFE1615c	<i>Plasmodium</i> exported protein, unknown function	1.10	2.15	7.56859E-08
PFC0180c	Membrane skeletal protein, putative	1.10	2.15	0.000308278
PF10_0036	N-acetyltransferase, putative	1.10	2.14	1.79215E-08
PFB0946c	Conserved <i>Plasmodium falciparum</i> protein family	1.10	2.14	0.010630365
PF14_0346	cGMP-dependent protein kinase	1.09	2.13	7.68433E-06
PF11_0483	Farnesyltransferase beta subunit, putative	1.09	2.12	4.55983E-06
PF10_0307	Conserved <i>Plasmodium</i> protein, unknown function	1.08	2.12	1.11818E-07

The transcripts of decreased abundance (Table 2.16) show a generalised greater fold change than observed in the transcripts of increased abundance, with PF11_0282 (deoxyuridine 5'-triphosphate nucleotidohydrolase, dUTPase) showing the greatest decrease of 7.05 fold in time-point 1. This dUTPase also shows the greatest decrease in abundance in time-point 2, though the fold change is reduced to 5.34, although this is still quite a change considering that the greatest fold change for the transcripts of increased abundance was 3.61.

Table 2.16. Top 25 transcripts of decreased abundance for each of the two time-points, respectively.

PlasmoDB ID	Product description	log fold change	Fold change	Adjusted p-value
Time-point 1				
PF11_0282	Deoxyuridine 5'-triphosphate nucleotidohydrolase, putative	-2.82	7.05	5.3046E-12
PF13_0328	Proliferating cell nuclear antigen	-2.53	5.78	3.91033E-14
PF10_0020	Alpha/beta hydrolase, putative	-2.53	5.78	1.097E-12
PFL1670c	Conserved <i>Plasmodium</i> protein, unknown function	-2.48	5.59	7.4293E-12
PFA0115w	<i>Plasmodium</i> exported protein, unknown function	-2.46	5.51	7.7577E-10
PFI0180w	Alpha tubulin	-2.37	5.19	1.69262E-12
PFI0905w	Probable protein, unknown function	-2.37	5.16	1.43928E-11
PFI0135c	Serine repeat antigen 9 (SERA-9)	-2.30	4.94	6.25361E-12
PF07_0065	Zinc transporter, putative	-2.22	4.67	1.4365E-11
PF14_0526	Conserved <i>Plasmodium</i> protein, unknown function	-2.22	4.66	3.30622E-12
PFF0630c	Conserved <i>Plasmodium</i> protein, unknown function	-2.21	4.62	3.5127E-13
PFA0520c	Chromatin assembly factor 1 protein WD40 domain, putative	-2.20	4.59	6.2934E-13
PFL1720w	Serine hydroxymethyltransferase	-2.20	4.58	3.5127E-13
PF14_0289	Mitochondrial ribosomal protein L17-2 precursor, putative	-2.19	4.57	3.81023E-10
PF10_0188	Conserved <i>Plasmodium</i> membrane protein, unknown function	-2.17	4.49	7.89273E-11
PF10_0154	Ribonucleotide reductase small subunit, putative	-2.16	4.47	3.5127E-13
chr8.rRNA-2-28s-pseudo		-2.14	4.42	9.88484E-12
PFI0530c	DNA primase large subunit, putative	-2.09	4.27	6.2934E-13
MAL13P1.307	Conserved <i>Plasmodium</i> protein, unknown function	-2.08	4.23	1.21238E-11
PFE0270c	DNA repair protein, putative	-2.08	4.23	2.7248E-11
PF10_0253	Conserved <i>Plasmodium</i> protein, unknown function	-2.08	4.22	6.7743E-11
PF14_0443	Centrin-2	-2.08	4.22	4.98234E-13
chr8.rRNA-1-5.8s-pseudo		-2.07	4.21	5.3046E-12
PFD0470c	Replication factor a protein, putative	-2.04	4.12	6.40373E-11
PF11_0248	Mitochondrial ribosomal protein L37, putative	-2.04	4.12	3.94783E-12
Time-point 2				
PF11_0282	Deoxyuridine 5'-triphosphate nucleotidohydrolase, putative	-2.42	5.34	1.68855E-10
PFA0115w	<i>Plasmodium</i> exported protein, unknown function	-2.40	5.27	1.07852E-09
PF10_0020	Alpha/beta hydrolase, putative	-2.33	5.02	3.67263E-11
PFD0225w	Conserved <i>Plasmodium</i> membrane protein, unknown function	-2.17	4.50	1.06075E-10
PFD0470c	Replication factor a protein, putative	-2.12	4.34	1.24883E-10
PF10_0289	Adenosine deaminase, putative	-1.96	3.90	3.7815E-10
PFD0465c	Conserved <i>Plasmodium</i> protein, unknown function	-1.91	3.77	6.82062E-11
PFI0135c	Serine repeat antigen 9 (SERA-9)	-1.91	3.75	7.4568E-10
PF14_0696	Conserved <i>Plasmodium</i> protein, unknown function	-1.89	3.70	9.41074E-10
PFL1670c	Conserved <i>Plasmodium</i> protein, unknown function	-1.86	3.64	4.44236E-10
PFI0905w	Probable protein, unknown function	-1.83	3.56	2.08872E-09
PFL0680c	Conserved <i>Plasmodium</i> protein, unknown function	-1.82	3.52	4.20501E-09
PFF1180w	Anaphase-promoting complex subunit, putative	-1.72	3.30	4.85539E-10
MAL13P1.307	Conserved <i>Plasmodium</i> protein, unknown function	-1.69	3.22	2.64466E-10
PFI0530c	DNA primase large subunit, putative	-1.68	3.21	5.88632E-11
MAL7P1.107	Conserved <i>Plasmodium</i> protein, unknown function	-1.68	3.20	3.25495E-09
PF14_0443	Centrin-2	-1.68	3.19	5.88632E-11
PF11_0425	Conserved <i>Plasmodium</i> protein, unknown function	-1.66	3.17	1.06075E-10
PF10_0154	Ribonucleotide reductase small subunit, putative	-1.66	3.16	5.88632E-11
PFL1330c	Cyclin-related protein, Pfcyc-2	-1.65	3.13	5.88632E-11
PF10_0188	Conserved <i>Plasmodium</i> membrane protein, unknown function	-1.60	3.03	2.00583E-08
PF10_0253	Conserved <i>Plasmodium</i> protein, unknown function	-1.59	3.01	9.85292E-09
PFL1720w	Serine hydroxymethyltransferase	-1.59	3.01	6.82062E-11
PFF0630c	Conserved <i>Plasmodium</i> protein, unknown function	-1.55	2.92	1.31481E-10

Using PlasmoDB and grouping similar GO biological process terms together, the differentially expressed gene transcripts were placed in one of several categories (Figure 2.17).

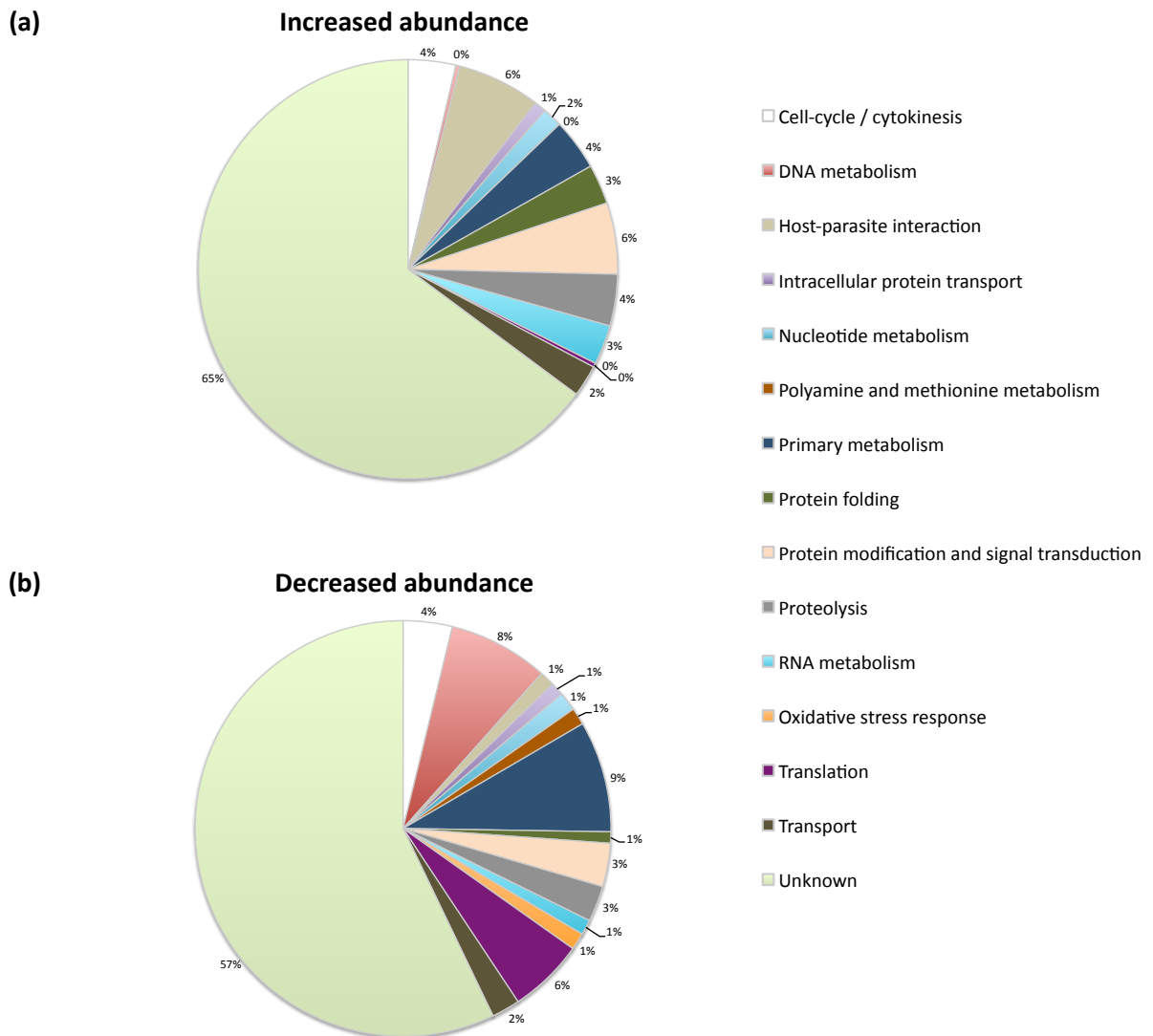


Figure 2.17. Gene ontology based functional classification of the (a) transcripts of increased abundance and (b) decreased abundance, combined from both time-points and given as a percentage of the total of the respective group. The classifications include sub-categories for e.g. host-parasite interaction includes antigenic variation; DNA metabolism includes repair, replication, recombination and integration; while primary metabolism includes energy, fatty acid, amino acid and vitamin metabolism.

As in Part 1, the majority (more than half) of the transcripts are those of unknown function. The transcripts of increased abundance include more of unknown function (65%) than the transcripts of decreased abundance (57%).

Within the increased abundance group, the next highest categories are host-parasite interaction and protein modification and signal transduction, with 6% each. The majority of the transcripts within the host-parasite group are PfEMP1 and related proteins, while in the protein modification and signal transduction category, most are kinases (many are serine/threonine kinases of the FIKK family, but the calcium dependent protein kinases are also well represented). These are followed by cell-

cycle/cytokinesis, primary metabolism and proteolysis, all with 4% each. The remainder consist of nucleotide metabolism (2%), intracellular protein transport (1%), nucleotide metabolism (2%), protein folding (3%), RNA metabolism (3%) and transport (2%). Those that show no, or exceedingly little representation amongst the increased abundance group are DNA metabolism, polyamine and methionine metabolism, oxidative stress response and translation.

The primary group (9%) of decreased abundance transcripts are those involved in primary metabolism (these include various transcripts for carbohydrate, amino acid, vitamin, lipid and fatty acid metabolism), indicating that the cell is starting to 'shut down'. This is closely followed by DNA metabolism (8%), which contains many transcripts for DNA repair, recombination, replication and repair. Next in line is translation (6%), which again conforms with the cytostatic arrest and concomitant reduction of the requirement for additional proteins. The remainder consist of host-parasite interaction (1% and considering the number of genes available, this is indeed very little), intracellular protein transport (1%), nucleotide metabolism (1%), polyamine and methionine metabolism (1%), protein folding (1%), protein modification and signal transduction (3%), proteolysis (3%), RNA metabolism (1%), oxidative stress response (1%) and transport (2%). Of these, polyamine metabolism and the oxidative stress response groups are significant, if one considers the relatively few genes involved in these processes within the parasite, the fact that a significant number of them showed decreased abundance is important. Interestingly, primary metabolism, DNA metabolism, translation, oxidative stress response and polyamine metabolism have many transcripts occurring in both the time-points investigated.

Data clustering provides a means of organising and classifying a large quantity of data [218]. Both array and gene clustering is possible. Array clustering reveals observations made previously with the Pearson correlations (Table 2.13), namely that TT1 and TT2 are the most similar and that their node is then most closely related to UT1, with UT2 being the most different of all. Following hierarchical clustering of all the gene expression data, numerous nodes/clusters are obtained. One particularly interesting node (12044X, which has a correlation coefficient of 0.995708) is given in Figure 2.18.

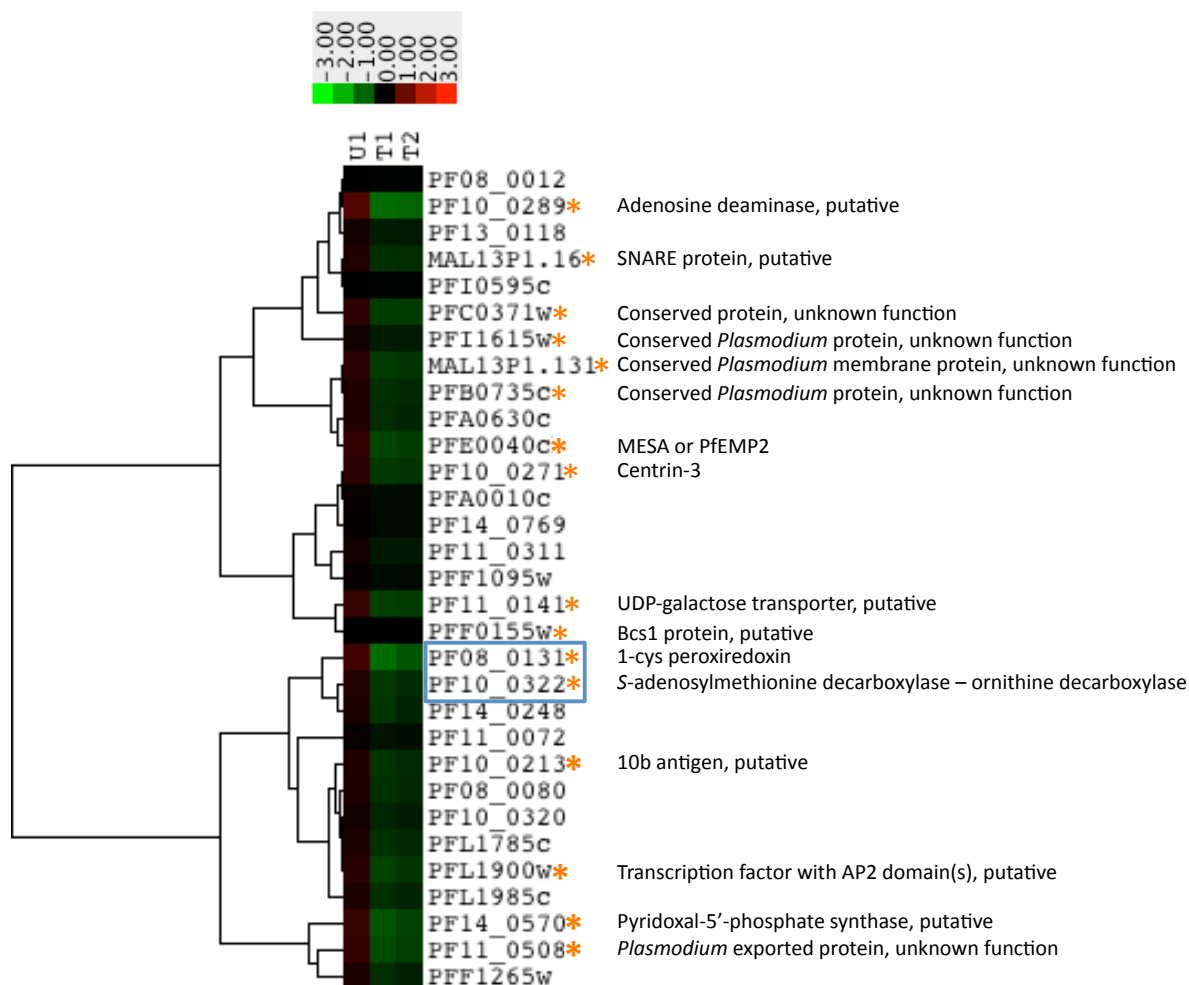


Figure 2.18. Heat map of a cluster (cluster node 12044) enriched in polyamine related transcripts. The transcripts marked with an orange asterisk are those that met the cut-off parameters for selection (i.e. P -value < 0.05 and a fold change that exceeds 1.7 – increased or decreased abundance).

Both 1-cys peroxiredoxin and AdoMetDC-ODC are reflected in this cluster and in close proximity, indicating that their relative levels of expression in the various time-points are exceptionally similar. What is also of particular importance is that both adenosine deaminase and pyridoxal-5'-phosphate synthase (transcripts involved in polyamine metabolism) also cluster within this group.

A redox-polyamine link was suggested by Sturm *et al.* and is supported by the data obtained from the clustering, as well as the number of oxidative stress response and polyamine metabolism transcripts that are differentially expressed (Figure 2.18, Table 2.20). Table 2.17 is modified from [219], to include the DFMO-treatment transcriptomics data. Interestingly, in the context of the polyamines, thioredoxin stimulates OAT activity and OAT is redox regulated [219]. Sturm *et al.* propose that regulation of OAT, S-adenosylmethionine synthase and S-adenosylhomocysteine hydrolase are required to balance the metabolic fluxes of AdoMet between polyamine synthesis and reactions for the transfer of methyl groups [219].

Table 2.17. Proteins binding to either thioredoxin (Trx), plasmoredoxin (Plrx) or glutaredoxin (Grx) and those differentially expressed in the DFMO-treatment transcriptomic profiles. Modified from [219].

Bait			PlasmoDB ID	Gene annotation	Transcriptome (SSH-cDNA array)	Transcriptome (oligo array)
Anti-Oxidative Stress System						
Trx			PF14_0368	2-Cys peroxiredoxin (2-Cys-Prx, cytosolic)		
Trx			PF08_0131	1-Cys peroxiredoxin (1-Cys-Prx, cytosolic)	Down	Down
Trx	Grx		PFC0166w	Plasmoredoxin (Thioredoxin-like redox-active protein)		
Transcription/Translation						
Trx			PF13_0042	Fork head domain protein, putative		
	Grx	Plrx	PF14_0486	Elongation factor 2		
	Grx	Plrx	PFC0295c	40S ribosomal protein S12		
	Grx		PFD1055w	Ribosomal protein S19s, putative		
Protein Folding						
Trx	Grx	Plrx	PFI0875w	Heat shock protein		
Trx	Grx	Plrx	PF08_0054	Heat shock 70 kDa protein	Up	
Trx	Grx	Plrx	PF07_0029	Heat shock protein 86	Up	
		Plrx	PF11_0258	Co-chaperone GrpE, putative		
		Plrx	MAL8P1.17	Disulfide isomerase, putative		
Carbohydrate Metabolism						
Trx	Grx	Plrx	PFF1155w	Hexokinase		
Trx	Grx	Plrx	PFF1300w	Pyruvate kinase, putative		Down
	Grx	Plrx	PF14_0598	Glyceraldehyde-3-phosphate dehydrogenase		
	Grx		PF13_0141	L-lactate dehydrogenase		Down
SAM Metabolism						
Trx	Grx	Plrx	PFF0435w	Ornithine aminotransferase	Up	Saturated
Trx	Grx	Plrx	PFI1090w	S-adenosylmethionine synthetase		Down
Trx	Grx		PFE1050w	S-adenosyl-L-homocysteine hydrolase		Down
Lipid Metabolism						
	Grx		MAL13P1.214	Phosphoethanolamine N-methyltransferase, putative		
		Plrx	PFB0385w	Acyl carrier protein, putative		Down
Hemoglobin Catabolism						
Trx		Plrx	PF14_0078	HAP protein/Plasmeprin III	Up	
DNA Synthesis and Repair						
		Plrx	PFF0715c	Endonuclease iii homologue, putative		
		Plrx	PF14_0053	Ribonucleotide reductase small subunit (R2)		Down
Signal Transduction						
Trx	Grx	Plrx	MAL8P1.69	14-3-3 protein homologue, putative		
		Plrx	MAL13P1.309	14-3-3 protein, putative		
Trx			MAL13P1.241	GTPase, putative		
	Grx		PF08_0019	Guanine nucleotide-binding protein, putative/receptor for activated C kinase homolog, PFRACK	Up	
		Plrx	MAL7P1.122	Conserved GTP-binding protein, putative		
Others						
Trx			PF14_0036	Acid phosphatase, putative		
		Plrx	PF10_0065	Hypothetical protein		
		Plrx	PF14_0190	Hypothetical protein		

The presence of a gene transcript (PF14_0570) annotated as pyridoxal-5'-phosphate synthase in the cluster is significant. PF14_0570 is found on chromosome 14 and encodes a protein with a predicted mass of 32.9 kDa (www.plasmodb.org). It appears that PF14_0570 catalyses the formation of PLP from the vitamers pyridoxine phosphate and pyridoxamine phosphate (<http://sites.huji.ac.il/malaria/maps/vitaminB6metpath.html>). Pyridoxal-5'-phosphate (PLP) is the active form of cofactor vitamin B6 and participates in more than 140 enzymatic reactions where it mediates amino group transfer [220]. A significant number of enzymes (Table 2.18) are dependent on this cofactor, including LDC, OAT and MAL7P1.150, which curiously show increased abundance in the face of putrescine depletion. Of the remaining enzymes represented in Table 2.18, PFL1720w, PFI110w and PF10_0322 were of decreased abundance.

Table 2.18. Enzymes that are dependent on PLP. Transcripts for proteins related to PLP-binding that show differential expression upon DFMO-treatment are indicated (the red arrow indicates increased abundance, while the green arrow indicates decreased abundance). Modified from [220].

EC-Number	EC-Name	PlasmoDB	Annotated in PlasmoDB as	Pathway
2.1.2.1	Glycine hydroxymethyltransferase	PFL1720w PF14_0534 ↓	Serine hydroxymethyltransferase Serine hydroxymethyltransferase (mitochondrial), putative	Folate metabolism; amino acid metabolism
2.3.1.37	5-Aminolevulinate synthase	PFL2210w	Delta-aminolevulinic acid synthetase	Porphyrin metabolism, amino acid metabolism
2.3.1.50	Serine C-palmitoyltransferase	PF14_0155	Serine C-palmitoyltransferase, putative	Sphingolipid metabolism
2.6.1.1	Aspartate aminotransferase	PFB0200c	Aspartate aminotransferase	Amino acid metabolism
2.6.1.13	Ornithine aminotransferase	PFF0435w ↑	Ornithine aminotransferase	Arginine and proline metabolism
2.6.1.42	Branched-chain amino acid aminotransferase	PF14_0557	Conserved Plasmodium protein, unknown function	Pantothenate and CoA biosynthesis; amino acid metabolism
2.6.1.57	Aromatic amino-acid transaminase	PFB0200c	Aspartate aminotransferase	Amino acid metabolism
2.8.1.7	Cysteine desulfurase	PF07_0068 MAL7P1.150 ↑	Cysteine desulfurase, putative Cysteine desulfurase, putative	Iron-sulfur cluster synthesis
4.1.1.17	Ornithine decarboxylase	PF10_0322 ↓	S-Adenosylmethionine decarboxylase/ornithine decarboxylase (bifunctional)	Polyamine biosynthesis
4.1.1.18	Lysine decarboxylase	PFD0285c PFD0670c ↑	Lysine decarboxylase, putative Lysine decarboxylase, putative	Polyamine metabolism
4.1.1.65	Phosphatidylserine decarboxylase	PFI1370c	Phosphatidylserine decarboxylase	Glycerophospholipid metabolism
4.1.3.38	p-Aminobenzoic acid synthetase	PFI1100w ↓	p-Aminobenzoic acid synthetase, putative	Folate biosynthesis

2.3.1.3 Validation of microarray data

The DNA microarray data was validated with semi-quantitative real-time PCR. Cyclophilin was shown to be unaffected by combined DFMO, MDL73811 treatment [205] and was confirmed to be unaffected by DFMO-treatment in the oligo microarray data. It was thus used as the ‘house-keeping’ gene for normalisation of the data. A regression coefficient of 0.9985 was obtained for the cyclophilin standard curve. The ratio of treated to untreated samples was 1.11 for time-point 1 and 1.18 for time-point 2, thus confirming that cyclophilin was indeed unaffected by DFMO-treatment. Figure 2.19 contains the comparison of the microarray and semi-quantitative real-time PCR validation data for both time-points.

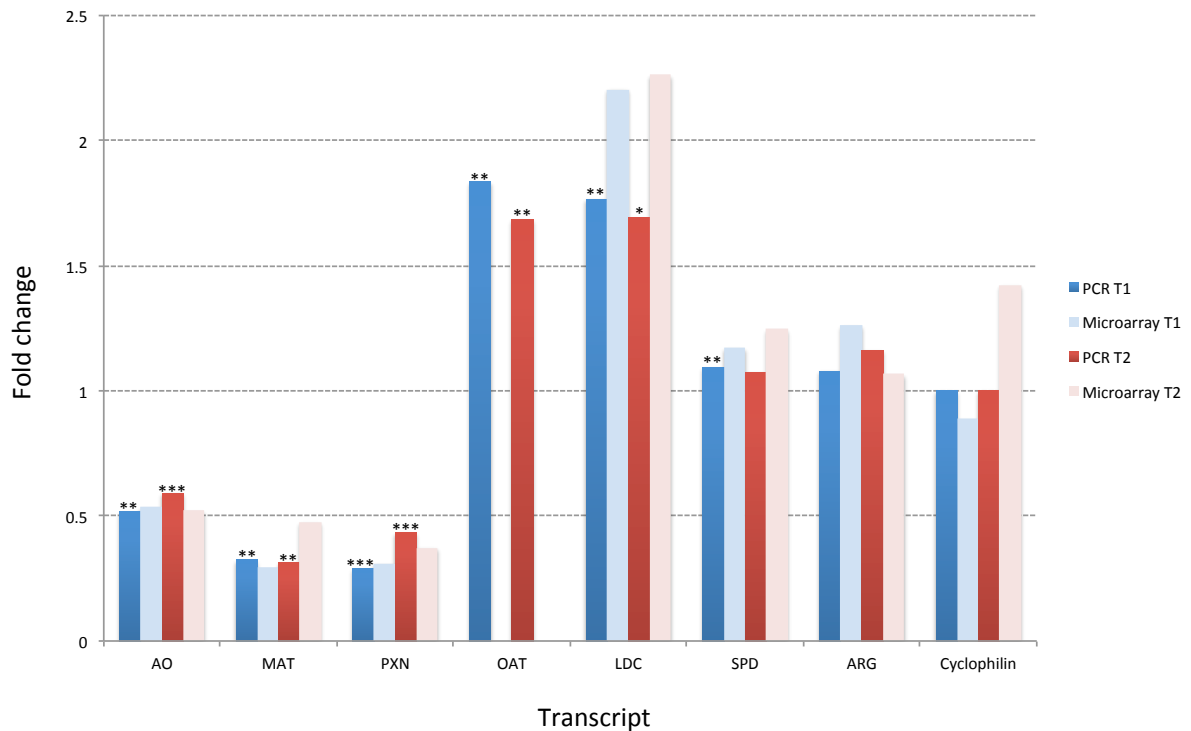


Figure 2.19. Comparison of semi-quantitative real-time PCR and microarray data for transcripts that show increased, decreased, or unchanged abundance. AO: AdoMetDC-ODC, MAT: S-adenosylmethione transferase, PXN: 1-cys peroxiredoxin, OAT: ornithine aminotransferase, LDC: lysine decarboxylase, SPD: spermidine synthase, ARG: arginase. For the microarray data, significance was defined as a fold change of 1.7 up or 0.6 down, with an adjusted P -value of $P < 0.05$ (as calculated by GenePix and regarding data reliability). Of the microarray data, SPD T1, ARG T2 and Cyclophilin T1 had $P \geq 0.05$ for and these values are thus statistically unreliable. OAT microarray data is not present as the spots were saturated on the slide. Cyclophilin was used for normalisation of the semi-quantitative real-time PCR data and the data represent one experiment, performed in triplicate. * $P < 0.05$, ** $P < 0.01$ and *** $P < 0.001$ for the two-tailed paired t -test, as calculated using the raw PCR data (normalised to the average value for cyclophilin) and comparing treated with untreated values for each transcript, respectively.

It is apparent that the trend observed in the microarray data is mirrored by the real-time PCR data, i.e. transcripts that are of decreased abundance (AO, MAT and PXN) in the microarray are of decreased abundance in the PCR. This also holds true for the increased abundance (LDC) and the unchanged abundance transcripts (SPD, ARG, cyclophilin). The fold change observed is also in a similar range between the two data sets. The semi-quantitative real-time PCR again provides validation that OAT shows increased abundance, as no microarray data is available for this transcript (all the OAT transcript spots were saturated).

2.3.1.4 Comparison of the SSH-cDNA and whole genome oligo microarray datasets.

The Venn diagrams in Figure 2.20 illustrate the transcripts identified to be common between the two platforms. While they appear to be very few, it should be borne in mind that the number of

transcripts identified in the SSH-cDNA microarray was very limited. Also, clone sampling in the SSH-cDNA microarray was random and non-exhaustive [221].

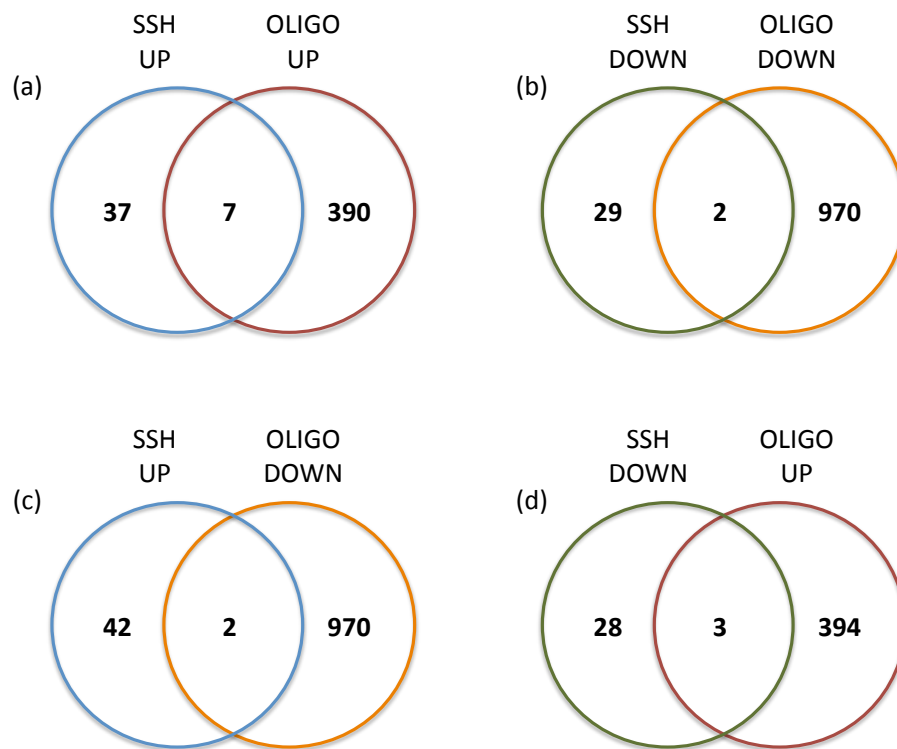


Figure 2.20. Comparison between SSH-cDNA transcriptome and oligo transcriptome.

As observed within the oligo microarray, both the increased and decreased abundance groups contain transcripts in common (Figure 2.20 (a), Figure 2.20 (b) and Table 2.19), but the opposing groups also had transcripts in common (Figure 2.20 (c), Figure 2.20 (d) and Table 2.19). Unfortunately no conclusions can be drawn from the identity of these transcripts, many of which are of unknown function (Table 2.19).

Table 2.19 Details of the commonalities between the SSH-cDNA and oligo transcriptomes.

	SSH UP		SSH DOWN	
OLIGO UP	PF11_0174	Cathepsin C homolog (DPAP1)	PFI0265c	RhopH3
	PF11_0347	Conserved <i>Plasmodium</i> protein, unknown function	PF11_0513	DNAJ protein, putative
	MAL7P1.170	<i>Plasmodium</i> exported protein, unknown function	MAL13P1.308	Conserved <i>Plasmodium</i> protein, unknown function
	PF11_0224	Circumsporozoite related antigen		
	PF14_0016	etramp 14.1		
	PF14_0344	Conserved <i>Plasmodium</i> protein, unknown function		
	PF14_0045	Conserved <i>Plasmodium</i> protein, unknown function		
OLIGO DOWN	PF10_0204	Conserved <i>Plasmodium</i> protein, unknown function	PF08_0131	1-cys peroxiredoxin
	PF10_0121	Hypoxanthine phosphoribosyltransferase	PFD_0780w	Glutamyl-tRNA (Gln) amidotransferase subunit A, putative

2.3.1.5 Comparison between the transcriptomes of the enzymes of the polyamine pathway

The inhibition of all the enzymes within the polyamine pathway (ODC (this study), AdoMetDC [2], AdoMetDC-ODC co-inhibition [1, 205] and spermidine synthase [3]) has been performed. Figure 2.21 shows the number of transcripts in common between the various inhibitions.

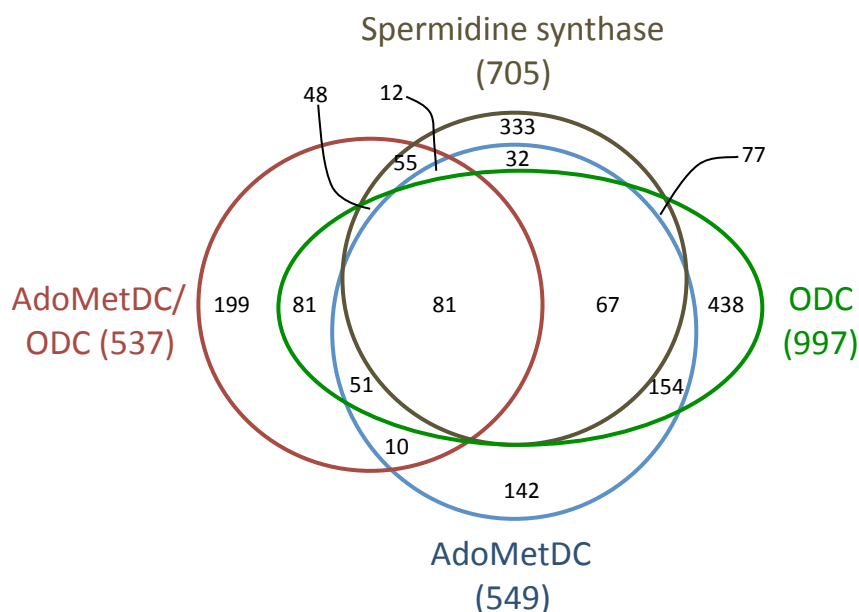


Figure 2.21. Number of transcripts shared between the various inhibitions of enzymes of the polyamine pathway. The number of differentially expressed transcripts present in each transcriptome is indicated in parentheses after the enzyme name.

Of the four inhibitions (ODC, AdoMetDC, ODC-AdoMetDC and spermidine synthase), ODC has the greatest total number of differentially expressed transcripts (997), followed by spermidine synthase (705), while AdoMetDC and ODC-AdoMetDC are similar (549 and 537, respectively). The greatest number of shared transcripts exists between ODC and AdoMetDC (253) (see Supplementary Material S3, Tables S3.1, S3.2 and S3.3 for transcripts in common and unique), although this may be due to the fact that the same microarray platform was used for the analysis of these two inhibitions. Of the differentially expressed transcripts for each inhibition, ODC has 438 (see Supplementary Material S4, Table S4.1) that are unique, spermidine synthase has 333, AdoMetDC has 142 and AdoMetDC-ODC has 199. There are 81 transcripts that are common to all the inhibitions (see Supplementary Material S5, Table S5.1)

The data for selected transcripts are compared in Table 2.20. The allocation of certain transcripts to the various functional divisions is primarily as per van Brummelen *et al.* [1].

Table 2.20. Comparison of ODC-, AdoMetDC-, spermidine synthase and AdoMetDC-ODC inhibited transcriptomes. Green highlights indicate transcripts of decreased abundance, while peach highlights indicate transcripts of increased abundance. Compiled from this study and [1-3].

PlasmoDB ID	Annotation	AdoMetDC-ODC Fold change ^a	ODC Time-point 1 Fold change	ODC Time-point 2 Fold change	AdoMetDC Fold change	Spermidine synthase
Polyamine and methionine metabolism						
PF10_0289	Adenosine deaminase, putative	-2.6	-3.8	-3.9	-3.1	Down (T1, T2, T3)
PF10_0322	S-adenosylmethionine decarboxylase-ornithine decarboxylase	-1.9	-1.9	-1.9	-	-
PF10_0340	Methionine-tRNA ligase	-1.7	-2.0	-1.8	-	-
PFD0285c	Lysine decarboxylase	2.8	2.2	2.3	2.5	Up (T2)
PFE0660c	Uridine phosphorylase, putative	-3.2	-2.8	-2.6	-3.0	Down (T1, T2, T3)
PFE1050w	Adenosylhomocysteinase (S-adenosyl-L-homocysteine hydrolase)	-1.9	-2.4	-2.0	-2.1	-
PFF0435w	Ornithine aminotransferase	1.9	Saturated ^b	Saturated ^b	Saturated ^c	-
PF11090w	S-adenosylmethionine synthetase	-2.4	-3.4	-2.1	-2.3	-
<i>Methyltransferases</i>						
MAL13P1.214	Phosphoethanolamine N-methyltransferase, putative	-2.8	-	-	-5.1	Down (T2, T3)
MAL13P1.31	SAM dependent methyltransferase, putative	-	-2.0	-	-	-
PF13_0016	Methyl transferase-like protein, putative	-	-2.1	-1.7	-1.9	-
PF14_0309	Protein-L-isoaspartate O-methyl transferase, putative	-1.9	-3.8	-2.1	-3.9	-
PF14_0526	Generic methyltransferase (conserved Plasmodium protein, unknown function)	-2.9	-4.7	-2.6	-3.1	Down (T1, T2)
PFB0220w	ubiE/COQ5 methyltransferase family, putative	-	-2.0	-	-2.3	-
PFL1720w	Serine hydroxymethyltransferase	-	-4.6	-3.0	-4.8	-
PFL1780w	Protein-S-isoprenylcysteine O-methyltransferase, putative	-	-1.8	-1.9	-	-
Potential polyamine associated effects						
PF07_0065	Zinc transporter, putative	-2.4	-4.7	-2.5	-4.8	Down (T1, T2)
PF14_0316	DNA topoisomerase II	-1.7	-	-1.8	-	-
PF14_0570	Pyridoxal 5'-phosphate synthase, putative	-	-2.5	-2.2	-2.3	Down (T2)
PFL1885c	Calcium/calmodulin-dependent protein kinase 2, putative	2.4	2.6	3.1	2.2	Up (T1, T2, T3)
Oxidative stress defense						
PF08_0131	1-Cys-peroxidoxin	-3.2	-3.2	-2.7	-2.7	Down (T1, T2, T3)
PF10_0066	Thioredoxin, putative	-	-1.7	-	-	-
PF11_0352	Protein disulfide isomerase	-	-2.3	-2.5	-1.8	-
PF13_0272	Thioredoxin-related protein, putative	-	-1.8	-	-	Down (T1, T2)
PF14_0187	Glutathione S-transferase	-1.8	-	-	-1.8	Down (T1, T2, T3)
PF14_0192	Glutathione reductase	-1.7	-	-	-2.2	Down (T1, T2)
PF14_0545	Thioredoxin, putative	-	-2.4	-2.8	-3.1	-
PFI0790w	Thioredoxin reductase 3	-	-	-1.7	-	-
PFI1170c	Thioredoxin reductase	-	-2.0	-	-1.9	Down (T1, T2, T3)
PFL0595c	Glutathione peroxidase	-	-2.3	-2.0	-2.2	-
PFL1550w	Lipoamide dehydrogenase	-	-2.3	-	-2.3	-

Energy metabolism*Oxidative phosphorylation*

Col	Cytochrome oxidase I, putative	-2	-2.7	-2.1		Down (T1, T2, T3)
CoxI	Cytochrome oxidase I, putative	-1.7	-2.9	-2.2		Down (T1, T2, T3)
CoxIII_2	Mitochondrial encoded cytochrome oxidase subunit 3	-2	-2.6	-1.9		Down (T1, T2, T3)
MAL7P1.75	Mitochondrial ATP synthase F1, epsilon subunit, putative	-1.8	-2.2	-	-	-
PF10_0120	Ubiquinol-cytochrome c reductase complex subunit, putative	-3.2	-2.1	-1.8	-	Down (T1, T2, T3)
PF11_0412	Vacuolar ATP synthase subunit F, putative	-1.8	-	-	-	-
PF13_0121	Dihydroliipoamide succinyltransferase	-1.7	-2.6	-	-2.6	Down (T1, T2)
PF13_0327	Cytochrome c oxidase subunit 2, putative	-	-2.2	-	-	Down (T1, T2)
PF13_0353	NADH-cytochrome B5 reductase, putative	-	-2.1	-	-2.1	Down (T2, T3)
PF14_0331	Cytochrome c oxidase assembly protein, putative	-	-2.9	-1.9	-	Down (T1, T2)
PF14_0597	Cytochrome c1 precursor, putative	-	-2.9	-	-3.2	-
PFE0970w	Cytochrome c oxidase assembly, putative	-1.7	-1.8	-	-	Down (T1, T2, T3)

Glycolysis and pyruvate metabolism

PF08_0045	2-oxoglutarate dehydrogenase E1 component	-	-2.3	-	-	-
PF10_0155	Enolase	-2	-1.8	-	-2.7	-
PF10_0334	Flavoprotein subunit of succinate dehydrogenase	-	-2.0	-	-1.8	Down (T1, T3)
PF11_0097	Succinyl-CoA synthetase alpha subunit, putative	-	-2.0	-	-	-
PF13_0141	L-lactate dehydrogenase	-1.8	-2.0	-2.0	-1.9	Down (T1, T2, T3)
PF13_0269	Glycerol kinase, putative	-	-	1.7	-	-
PF14_0378	Triose-phosphate isomerase	-1.8	-	-	-1.7	-
PF14_0484	Acetyl-CoA acetyltransferase, putative	-	-1.8	-	-	Down (T2)
PF14_0598	Glyceraldehyde-3-phosphate dehydrogenase	-2.1	-	-	-	-
PFF0895w	Malate dehydrogenase	-	-	-1.9	-2.3	-
PFF1300w	Pyruvate kinase	-1.9	-1.7	-	-1.7	Down (T2)

DNA replication

MAL13P1.134	DEAD box helicase, putative	-	-2.3	-1.7	-	Down (T1)
MAL13P1.22	DNA ligase I	-	-2.0	-	-	-
MAL13P1.311	Exonuclease, putative	-	-1.9	-	-	-
MAL13P1.346	DNA repair endonuclease, putative	-	-2.6	-	-2.1	-
MAL13P1.42	Recombinase, putative	-	-2.2	-	-2.1	-
PF07_0023	DNA replication licensing factor mcm7 homologue, putative	-	-2.8	-	-2.4	-
PF08_0126	DNA repair protein rad54, putative	-	-2.1	-	-1.8	-
PF10_0080	Endonuclease, putative	-	-1.7	-	-	-
PF10_0154	Ribonucleotide reductase small subunit, putative	-	-4.5	-3.2	-5.4	Down (T1, T2, T3)
PF10_0165	DNA polymerase delta catalytic subunit	-	-2.1	-1.7	-2.0	-
PF11_0087	Rad51 homolog, putative	-2	-3.9	-2.5	-1.7	Down (T1, T2, T3)
PF11_0117	Replication factor C subunit 5, putative	-2.1	-2.2	-	-1.8	Down (T1, T2, T3)
PF13_0095	DNA replication licensing factor mcm4-related	-2.2	-3.6	-1.9	-3.1	-
PF13_0176	Apurinic/apyrimidinic endonuclease Apn1	-	-2.1	-	-1.8	-
PF13_0251	DNA topoisomerase III, putative	-	-1.9	-	-	-

PF13_0291	Replication licensing factor, putative	-1.8	-2.2	-	-2.5	Down (T1, T2, T3)
PF13_0330	ATP-dependent DNA helicase, putative	-	-	2.0	-	-
PF14_0053	Ribonucleotide reductase small subunit	-	-2.8	-	-3.9	Down (T1, T2, T3)
PF14_0081	DNA repair helicase, putative	-1.7	-1.8	-2.8	-	-
PF14_0112	Pfprex	-2	-2.7	-2.1	-	-
PF14_0148	Uracil-DNA glycosylase, putative	-	-3.5	-2.1	-1.7	-
PF14_0177	DNA replication licensing factor MCM2	-	-2.7	-	-2.0	-
PF14_0254	DNA mismatch repair protein Msh2p, putative	-1.8	-2.1	-	-1.9	Down (T1)
PF14_0314	Chromatin assembly factor 1 p55 subunit, putative	2.4	2.2	1.7	2.0	-
PF14_0316	DNA topoisomerase II, putative	-	-	-1.8	-	-
PF14_0352	Ribonucleoside-diphosphate reductase, large subunit	-	-2.3	-2.5	-2.1	-
PF14_0366	Small subunit DNA primase	-	-2.4	-1.8	-1.7	Down (T2)
PF14_0601	Replication factor C3	-2	-2.5	-1.8	-	Down (T1, T2, T3)
PF14_0602	DNA polymerase alpha subunit, putative	-	-2.4	-1.7	-2.3	-
PFA0290w	DNA binding protein, putative	-	-2.6	-1.8	-	-
PFA0545c	Replication factor c protein, putative	-	-1.8	-	-	-
PFB0180w	5'-3' exonuclease, N-terminal resolvase-like domain, putative	-1.9	-1.9	-	-	-
PFB0720c	Origin recognition complex subunit 5	-	-1.7	-	-	-
PFB0840w	Replication factor C, subunit 2	-	-3.2	-2.3	-3.4	Down (T1, T2)
PFB0895c	Replication factor C subunit 1, putative	-2	-2.3	-	-1.9	Down (T1, T2, T3)
PFC0250c	AP endonuclease (DNA-[apurinic or apyrimidinic site] lyase), putative	-	-2.0	-1.7	-1.7	-
PFD0420c	Flap endonuclease 1	-	-1.7	-	-	-
PFD0470c	Replication factor A protein, putative	-2.5	-4.1	-4.3	-	Down (T1, T2, T3)
PFD0590c	DNA polymerase alpha	-	-3.4	-2.5	-2.0	-
PFD0685c	Chromosome associated protein, putative	-2	-2.7	-	-2.0	Down (T1)
PFD0830w	Dihydrofolate reductase-thymidylate synthase	-2	-3.5	-1.8	-4.9	Down (T1)
PFD0950w	Ran binding protein 1	2	-	-	-	-
PFE0215w	ATP-dependent helicase, putative	-	-1.9	-	-1.7	Down (T1, T2)
PFE0270c	DNA repair protein, putative	-	-4.2	-2.1	-3.5	-
PFE0675c	Deoxyribodipyrimidine photolyase (photoreactivating enzyme, DNA photolyase), putative	-2.2	-2.8	-1.9	-2.8	Down (T2, T3)
PFE0705c	Helicase, belonging to UvrD family, putative	-	-2.1	-	-	-
PFE1345c	Minichromosome maintenance protein 3, putative	-	-2.5	-	-2.3	Down (T1)
PFF0225w	DNA helicase, putative	-	-1.7	-	-	-
PFF1225c	DNA polymerase 1, putative	-	-2.2	-	-2.0	-
PFF1470c	DNA polymerase epsilon, catalytic subunit A, putative	-1.7	-3.1	-2.4	-1.8	-
PFI0235w	Replication factor A-related protein, putative	-1.8	-1.9	-	-2.2	Down (T1, T2, T3)
PFI0530c	DNA primase, large subunit, putative	-1.8	-4.3	-3.2	-3.8	-
PFL0150w	Origin recognition complex 1 protein	-	-2.4	-2.0	-2.6	-
PFL0560c	Minichromosome maintenance protein, putative	-	-2.3	-1.9	-	-
PFL0580w	DNA replication licensing factor MCM5, putative	-	-3.3	-	-3.7	Down (T1, T2, T3)
PFL1655c	DNA polymerase epsilon subunit B, putative	-	-3.0	-	-2.1	Down (T1, T2)
PFL2005w	Replication factor C subunit 4	-	-3.4	-2.0	-4.0	Down (T1, T2, T3)

Translation						
MAL13P1.164	Elongation factor Tu, putative	-	-1.9	-	-	-
MAL13P1.327	Ribosomal protein S17 homologue, putative	1.7	-	-	-	-
PF07_0080	40S ribosomal protein S10, putative	1.9	-	-	-	-
PF08_0009	Translation initiation factor EIF-2b alpha subunit, putative	-	-1.9	-	-	-
PF08_0014	Apicoplast ribosomal protein L21 precursor, putative	-	-1.8	-	-	-
PF10_0038	Ribosomal protein S20e, putative	2.3	-	-	-	-
PF10_0191	tRNA methyltransferase, putative	-	-1.8	-	-	-
PF10_0313	Mitochondrial preribosomal assembly protein rimM precursor, putative	-	-1.9	-	-1.9	-
PF11_0113	Mitochondrial ribosomal protein L11 precursor, putative	-	-2.7	-1.8	-2.0	Down (T1)
PF11_0181	Tyrosine-tRNA ligase, putative	-	-2.1	-1.9	-1.9	-
PF11_0182	Conserved Plasmodium protein, unknown function	-	-2.4	-	-1.9	-
PF11_0386	Apicoplast ribosomal protein S14p/S29e precursor, putative	-	-2.8	-1.7	-2.0	Down (T1)
PF11_0454	Ribosomal protein, 40S subunit, putative	2	-	-	-	-
PF13_0014	40S ribosomal protein S7 homologue, putative	1.8	-	-	-	-
PF13_0126	Translation initiation factor EIF-2B subunit related	-	-2.4	-1.7	-1.8	-
PF13_0171	60S ribosomal protein L23, putative	2	-	-	-	-
PF13_0228	40S ribosomal subunit protein S6	1.8	-	-	-	-
PF14_0041	Mitochondrial ribosomal protein L16 precursor, putative	-	-1.9	-	-	-
PF14_0132	40S ribosomal protein S9A, putative	-	-1.7	-	-	-
PF14_0205	Ribosomal protein S25	2.4	-	-	-	-
PF14_0212	Mitochondrial ribosomal protein L21 precursor, putative	-	-2.0	-	-	-
PF14_0231	Ribosomal protein L7a, putative	1.8	-	-	-	-
PF14_0265	Peptide chain release factor 1, putative	-	-1.8	-	-	-
PF14_0289	Mitochondrial ribosomal protein L17-2 precursor, putative	-	-4.6	-2.7	-3.6	-
PF14_0451	Mitochondrial ribosomal protein S14 precursor, putative	-	-1.8	-1.8	-	Down (T2, T3)
PF14_0579	Ribosomal protein L27, putative	2.1	-	-	-	-
PF14_0606	Mitochondrial ribosomal protein S6-2 precursor, putative	-	-2.0	-	-2.2	-
PF14_0709	Ribosomal protein L20, putative	-2.6	-2.7	-2.0	-2.1	Down (T1, T2)
PFB0390w	Apicoplast ribosomal releasing factor precursor, putative	-	-2.2	-1.7	-1.9	-
PFB0455w	Ribosomal L37ae protein, putative	1.7	-	-	-	-
PFB0645c	Mitochondrial large ribosomal subunit, putative	-	-3.2	-2.7	-2.3	-
PFC0535w	60S ribosomal protein L26, putative	2	-	-	-	-
PFC0701w	Mitochondrial ribosomal protein L27 precursor, putative	-	-3.6	-2.9	-2.5	-
PFC1020c	40S ribosomal protein S3A, putative	1.7	-	-	-	-
PFD0335c	Conserved Plasmodium protein, unknown function	-	-2.6	-	-	-
PFD0675w	Apicoplast ribosomal protein L10 precursor, putative	-	-1.7	-	-2.9	-
PFD0780w	Glutamyl-tRNA(Gln) amidotransferase subunit A, putative	-	-2.2	-2.0	-2.0	Down (T1, T2, T3)
PFD0825c	RNA-binding protein of pumilio/mpt5 family, putative	-	-	2.0	-	-
PFE0145w	Organelle ribosomal protein L28 precursor, putative	-	-1.7	-	-	-
PFE0185c	60S ribosomal subunit protein L31, putative	1.8	-	-	-	-

PFE0960w	Mitochondrial ribosomal protein L14 precursor, putative	-	-2.0	-2.0	-1.9	-
PFE1125w	Mitochondrial ribosomal protein L17 precursor, putative	-	-3.2	-2.4	-	-
PFF0180w	Phenylalanyl-tRNA synthetase subunit	-	-1.8	-	-	-
PFF0495w	Mitochondrial ribosomal protein L19 precursor, putative	-	-3.2	-2.1	-2.0	Down (T1)
PFF0650w	Apicoplast ribosomal protein L18 precursor, putative	-	-2.1	-	-1.9	Down (T1, T2)
PFI0380c	Formylmethionine deformylase, putative	-	-1.9	-	-1.8	Down (T1)
PFI0890c	Organelle ribosomal protein L3 precursor, putative	-	-2.2	-	-2.2	Down (T1, T2, T3)
PFI1240c	Prolyl-t-RNA synthase, putative	-	-2.3	-	-2.8	-
PFI1575c	Peptide release factor, putative	-	-2.8	-1.9	-2.7	-
PFI1585c	Mitochondrial ribosomal protein S6 precursor, putative	1.8	-1.9	-	-1.8	-
PFL1150c	Mitochondrial ribosomal protein L24-2 precursor, putative	-	-1.7	-	-1.7	-
PFL1590c	Elongation factor G, putative	-	-1.8	-	-1.7	-
PFL1895w	Mitochondrial ribosomal protein L23 precursor, putative	-	-2.8	-2.6	-1.7	Down (T1, T2, T3)
PFL2115c	Glucose inhibited division protein A homologue, putative	-	-2.4	-	-2.9	-
Transcription factors						
PF11_0241	Hypothetical protein with Myb-like domains	1.8	-	-	1.7	Up (T1, T2)
PF11_0163	Transcription factor with AP2 domain(s), putative	-	2.0	2.0	-	-
PFI13_0097	Transcription factor with AP2 domain(s), putative	-	1.8	-	1.7	Up (T1, T2, T3)
PFA0525w	Transcription initiation factor TFIIB, putative	-	-	1.7	-	-
PFB0290c	Transcription factor, putative	-	1.7	-	-	-
PFD0560w	Hypothetical protein with a TATA-box -like domain	1.7	-	-	-	-
PFE0305w	Transcription initiation factor TFIid, TATA-binding protein	-	-	1.9	-	-
PFE0415w	Transcription factor IIB, putative	-1.8	-	-1.9	-	Down (T2)
PFE1245w	CCCH-type zinc-finger protein	1.7	-	-	-	-
PFF0550w	Transcription factor with AP2 domain(s), putative	-	-2.4	-	-1.8	-
PFF0670w	Transcription factor with AP2 domain(s), putative	1.9	-	-1.7	-	-
PFI1665w	Transcription factor with AP2 domain(s), putative	-	-1.7	-	-1.9	-
PFL0465c	C2H2-type zinc-finger transcription factor, krox1	2	1.7	1.9	1.8	-
PFL1900w	Transcription factor with AP2 domain(s), putative	-1.4	-2.9	-2.3	-2.7	Down (T2, T3)
Cell cycle mediators						
PF13_0328	Proliferating cell nuclear antigen	-3.3	-5.8	-2.2	-5.7	Down (T1, T2, T3)
PF14_0604	Hypothetical protein with cyclin homology	-1.7	-	-	-	-
PFL1285c	Proliferating cell nuclear antigen 2	-	-2.2	-	-2.7	Down (T1)
PFL1330c	Hypothetical protein with cyclin homology	1.8	-3.0	-3.1	-2.7	-

- a. Average fold-change calculated at the time point of maximum change
b. Real-time PCR shows increased transcript abundance
c. Real-time PCR shows no change in transcript abundance

Generally, the direction of regulation observed is the same for all the perturbations, with the exception of PFL1330c, which shows increased abundance upon co-inhibition of AdoMetDC-ODC and a decrease in abundance in the singular ODC and AdoMetDC inhibitions.

2.3.1.6 Comparison between the ODC-inhibited transcriptomes with other perturbations of *P. falciparum* parasite culture.

The effect of several perturbations on *P. falciparum* parasite culture has been determined. Hu *et al.* conducted an experiment in which 20 compounds that inhibit growth of the schizont stage were tested [152]. When the ODC-inhibited transcriptome is compared with their dataset of differentially expressed transcripts (3706 transcripts), 753 transcripts were found to be present in both datasets (Supplementary Material S6, Table S6.1). However, 244 of the ODC-inhibition differentially expressed transcripts were unique, indicating a specific fingerprint profile for these transcripts only observed with ODC-inhibition in the parasite. The ODC dataset was also compared with that obtained when parasite culture was treated with a lethal anti-folate (WR99210) [139]. Of their 71 differentially expressed transcripts, 15 were present in the ODC dataset (see Supplementary Material S6, Table S6.2).

Figure 2.22 compares the ODC-inhibited transcriptome with parasite cultures subjected to temperatures of 41°C (approximating fever) [144], artesunate-treatment [142] and chloroquine-treatment [138]. Numerous transcripts are found to be common between the perturbations, though only eight are common to all four perturbations, implying general stress responses.

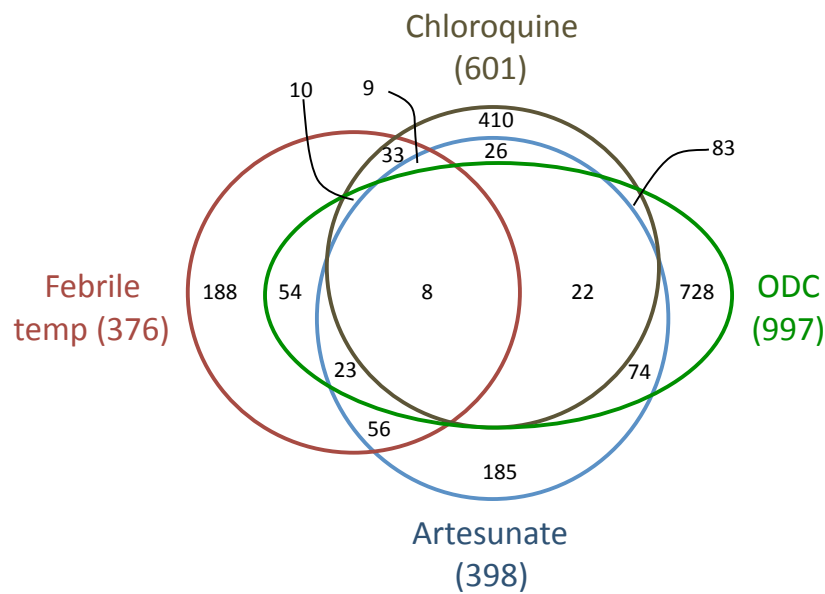


Figure 2.22. Number of transcripts shared between the various perturbations of *P. falciparum* parasite culture [138, 142, 144]. The number of differentially expressed transcripts present in each transcriptome is indicated in parentheses after the enzyme name.

When the eight transcripts common to the ODC, febrile temperature, chloroquine and artesunate perturbations are compared with the anti-folate and 20 compound datasets, five genes are common to all perturbations. These five genes (Table 2.21) were originally identified by Smit and attributed to a general stress response [2]. PFA0660w is also present in all the perturbations, excluding the anti-folate dataset. When these six transcripts were compared with the ODC, AdoMetDC, AdoMetDC-ODC and spermidine synthase datasets, PFA0660w, is present only in the ODC dataset, while PF11_0352 was absent from AdoMetDC-ODC and spermidine synthase, PF14_0531 was absent from AdoMetDC-ODC and PF14_0758 was absent from the spermidine synthase datasets.

Table 2.21. Transcripts indicative of a general stress response in *P. falciparum* parasites *in vitro*. The presence of the five stress response genes was compared in the ODC, AdoMetDC, AdoMetDC-ODC and spermidine synthase datasets.

PlasmoDB ID	Product description	ODC	AdoMetDC	AdoMetDC-ODC	Spermidine synthase
PF08_0060	Asparagine-rich antigen	✓	✓	✓	✓
PF11_0352	Protein disulphide isomerase	✓	✓	✗	✗
PF14_0531	Conserved Plasmodium protein, unknown function	✓	✓	✗	✓
PF14_0758	Plasmodium exported protein (hyp17), unknown function	✓	✓	✓	✗
PFC0085c	Plasmodium exported protein, unknown function	✓	✓	✓	✓
PFA0660w*	Heat shock protein 40, type II	✓	✗	✗	✗

* PFA0660w was present in the ODC, 20 compounds, artesunate, chloroquine and febrile temperature datasets, but not the anti-folate dataset.

2.4 DISCUSSION

In the post-genomic era, gene expression profiling is becoming increasingly important for the assessment of the global effects of chemical inhibition of drug targets on the metabolism of targeted tissues or organisms, especially so in *P. falciparum* [209, 222].

SSH was employed here to create pre-selected libraries of differentially expressed transcripts for subsequent screening using high-throughput microarray hybridisations. This approach was used to investigate the transcriptional response of the parasite to DFMO (a suicide inhibitor of ODC) treatment, which effects putrescine depletion [63]. This combined SSH-microarray approach is commonly used and was recently applied by Datu *et al.* to investigate the transcriptional changes that the hookworm *Ancylostoma caninum* undergoes during life-cycle stage transitions [223] and also by Geng *et al.* in their investigation of female specific transcripts in *Anopheles anthropophagus* [224]. Open platforms like SSH and SAGE can contribute to the annotation of previously uncharacterised open reading frames. In 2001, a SAGE study of the transcriptional profile of *P. falciparum* had 30% of the tags originate from previously uncharacterised ORFs [169]. A further advantage of SSH is the creation of libraries that contain cDNA enriched for differentially expressed genes of both low and high abundance, thanks to the normalisation step [221].

The SSH-cDNA and oligo microarray platforms differ quite significantly and the primary differences and similarities between them are highlighted in Table 2.22. Of the differences, the most dramatic are the probe length and the hybridisation temperature. It should also be remembered that the SSH-cDNA slides contained a selected group of probes, specifically pertaining to DFMO-treatment, while the oligo slides contained the entire genome. Therefore, the coverage advantage of the oligo microarray platform does provide additional data, even though it can be considered a closed system. The combination of SSH-cDNA and oligo microarray data thus provides greater transcriptome coverage with both open and closed systems, as applied here.

Since *P. falciparum* produces gene transcripts 'just-in-time', the different life-cycle stages show differential expression of the transcripts in a cascade [127]. This creates a problem when attempting to study the effect of drug treatment on the parasite. The simple answer to this would be to use an unsynchronised culture for the experiment; however, DFMO is a known synchronising agent for malaria cultures and results in a halt in the life-cycle in the trophozoite stage [225]. For this reason, the *P. falciparum* parasite culture was synchronised prior to treatment and the RNA extracted from the various time-points pooled in equal concentrations for use in the SSH. This will manually

'unsynchronise' the culture thus overcoming the transcriptome difficulties arising from stage-specific transcripts.

Table 2.22. Comparison of the cDNA and oligo microarray platforms.

	cDNA microarray	Oligo microarray
Probe length	Average ~ 570 bp	60-mer oligo
Labelling method	Post-synthesis	Direct
Hybridisation temperature	42°C	65°C
Hybridisation duration	~17 hours	~17 hours
Rotation during hybridisation	No	Yes

An evaluation of the *P. falciparum* expression profile obtained after DFMO-treatment indicated that differential expression was seen only in the trophozoite stage (Table 2.11), which is expected as polyamine levels peak in the trophozoite/schizont stages of *P. falciparum* (maximum 22-fold increase over uninfected erythrocytes) [74]. The absence of these cations results in decreased macromolecular synthesis of DNA/RNA and proteins required during the trophozoite stage in the parasites [63, 71]. DFMO-treatment therefore causes an arrest of schizogony at the mature trophozoite stage [71, 74]. The bifunctional AdoMetDC-ODC transcript is only produced in the early trophozoite stage, peaking between 13 and 25 hours post invasion (<http://malaria.ucsf.edu/>) and the protein will therefore only be subject to inhibition thereafter.

DFMO-treatment resulted in transcripts of both increased and decreased abundance, indicating that the changes were not solely due to a generally decreased rate of transcription during growth arrest (Figure 2.11). A considerable amount of redundancy was observed amongst the transcripts of decreased abundance. This observation was also noted in a differential display investigation of polyamine depleted murine cells [226] and a SAGE investigation of malaria parasite treatment with chloroquine [227]. Of the transcripts showing an increase in abundance in the SSH-cDNA microarray, several are involved in protein synthesis and stabilisation procedures (Table 2.12 A), but this increase in the machinery may simply be a general transcriptional response to perturbation. Several other indicators of general stress responses were obtained, including increased abundance of antigens usually indicating early commitment to forming sexual stages of the parasite (asn rich antigen (PF11_0111) and a gamete antigen 27/25 (PF13_011)), as has been seen for chloroquine-treatment

of the parasite [227]. Additionally, comparison of the oligo microarray data with various other microarray data available from various perturbations of malaria parasites, revealed several shared processes, indicative of general stress responses, even taking technical platform differences into account. Specifically, five transcripts were present in several perturbations of *P. falciparum* parasites (Table 2.21) [2]. Additionally PFA0660w (HSP40, type II – an HSP with a DNAj domain and involved in protein folding) was also present in many of the perturbations, bar anti-folate treatment. Interestingly, this transcript was not present in any of the other polyamine pathway enzyme inhibitions (Table 2.21)

The increase in abundance of the abovementioned 'stress response' transcripts may not necessarily indicate a direct effect due to the absence of the polyamines, but may implicate indirect regulation of these transcripts by the altered level or activity of certain transcription factors. This has been seen in the case of *E. coli* where a 'polyamine modulon' was postulated to describe a group of genes whose expression abundance is increased by polyamines at the level of translation due to enhanced levels of various transcription factors [228]. Although no such differential expression of transcription factors was observed in the SSH-cDNA transcriptome, the differential expression of transcription factors was observed in the oligo microarray (Table 2.20).

However, beyond these general stress responses seen, there is a specific fingerprint profile of differentially expressed transcripts that are only observed after perturbing polyamine metabolism in the parasite. In support of a drug-specific effect induced by DFMO-treatment on the transcriptome of *P. falciparum* parasites, the differential increase in abundance of two distinct transcripts observed in the SSH-cDNA microarray dataset (OAT and HGXPRT) could be directly linked to the resultant ornithine accumulation and putrescine depletion (Figure 2.11). Polyamines are derivatives of ornithine and a defined homeostasis exists between production and degradation of ornithine via the action of OAT. This enzyme catalyses the reversible conversion of ornithine to glutamate-5-semialdehyde, which is subsequently converted to glutamate and proline [96]. Inhibition of polyamine biosynthesis would result in an increase in ornithine levels. The results indicate that this causes an up to 4-fold increase in abundance of OAT transcripts in *P. falciparum* parasites (Figure 2.12) to equalise ornithine levels in the parasite. This therefore indicates the existence of a transcriptional feedback mechanism in the parasite upon drug challenge, specific to DFMO inhibition of ODC activity, as this effect was not observed in the *P. falciparum* parasite transcriptome after other perturbations [138, 139, 142, 144, 227]. An increase in the abundance of the transcript for OAT was observed only in the ODC and AdoMetDC-ODC inhibitions, confirming that this is indeed due to the increase in ornithine concentration upon inhibition of ODC and is not as a consequence of

dcAdoMet, spermidine or spermine depletion. The transcript for LDC was also observed to be increased in the transcriptome of ODC-inhibited (this study), AdoMetDC inhibited [2], spermidine synthase inhibited [3] and the co-inhibited [1] parasites. These results indicate that this is a result of spermine/spermidine depletion and is thus observed in the ODC-inhibited transcriptomes due to the 'knock-on' effect of spermine/spermidine depletion due to putrescine depletion. LDC catalyses the synthesis of the polyamine cadaverine from lysine and is generally an inducible gene [229].

Analysis of the transcripts showing an increase in abundance in the oligo microarray (Table 2.15), revealed that several specific biological processes are affected. Firstly, transcripts of proteins involved in the *P. falciparum* 'exportome' and gametocytogenesis were identified; secondly, cell-cycle associated processes; thirdly, (but most significantly), processes involved in redox-status regulation; and lastly, PLP-dependent proteins were affected. Each of these processes is discussed below.

The PHIST (*Plasmodium* helical interspersed subtelomeric) family of exported proteins feature prominently in both time-points. Unfortunately, very little is known about these proteins even though the PHIST family was first described in 2006 in a study of the 'exportome' of *P. falciparum* parasites. When compared with the 'exportome' 12.4% (59 of the 476 genes) were present in the increased abundance gene transcript list of DFMO-treated parasites. Of these, the majority (40 genes) formed part of the 'unknown function' GO classification, while the remainder were from 'host-parasite interaction' specifically antigenic variation (4 genes), 'signalling' (7 genes), and 'protein folding' (8 genes). Strangely, the greater part of the exportome genes localise to sub-telomeric regions of most of the *P. falciparum* chromosomes and have a two exon structure with the signal sequence in the first exon and the PEXEL sequence at the beginning of the second [230]. As some of the PHIST family appear to be related to gametocytogenesis, data from a study of genes involved with gametocytogenesis were compared with the increased abundance gene transcripts. Pfs16 (PFD0310w) and Pfg27 (PF13_0011) are considered to be early gametocyte markers [131] and neither of these genes are present in the increased abundance data. However, four genes were found to be in common between the two datasets, namely PFI0265c, PFC0120w, PFB0120w and PF11_0224. Silvestrini *et al.* also generated a list of genes that showed a similar expression profile to the two gametocyte markers (*pfg27/pfs16*) [131]. Of these, 25% (29 of a total 177 genes) were present in the increased abundance data and of these, 18% (21 genes) clustered to the same *k*-means cluster that the two gametocyte markers did. Interestingly, a comparison with genes known to be expressed in the gametocytes [231], showed none were present in the increased abundance data.

In general, DNA metabolism (replication, repair, recombination etc) is of decreased abundance upon polyamine depletion (Figure 2.18, Table 2.20), with many of the transcripts showing the most significant decrease being involved in either DNA metabolism or some version of cell cycle control (Table 2.20). It is also apparent that more transcripts of decreased abundance are present in time-point 1 than in time-point 2, where if the transcript is differentially expressed it is to a lesser degree than in time-point 1. This may reflect the cytostatic process in action, that is, at time-point 1 the cell is in the process of shutting down, while in time-point 2 this process of arrest is approaching completion. dUTPase (PF11_0282) plays an important role in nucleotide metabolism and DNA replication, as it catalyses the hydrolysis of dUTP to dUMP, through increasing the dTTP/dUTP ratio and preventing the incorrect incorporation of uracil into DNA [232]. The observed decrease in abundance of this transcript (7.05 fold, Table 2.16) was similar to that observed in the AdoMetDC inhibition (6.32 fold) [2], though significantly greater than that seen in the co-inhibition of AdoMetDC-ODC, where a maximum decrease of 3.23 fold was noted [205] or spermidine synthase (2.81 fold). Another transcript of highly decreased abundance in both ODC (5.8 fold, T1) and AdoMetDC (5.7 fold), though present in all the inhibitions, is that of proliferating cell nuclear antigen (PCNA, PF13_0328). PCNA expression in *Plasmodium* is cell-cycle regulated and occurs in the nuclei of mature trophozoites. It is involved in DNA replication and cell cycle progression [233].

The intra-erythrocytic environment that is home to the intra-erythrocytic stage of the malaria parasite is pro-oxidative due to the presence of large quantities of iron and oxygen, which can lead to the formation of ROS via the Fenton reaction (Figure 2.23). These ROS lead to macromolecular damage [234]. Furthermore, the digestion of haemoglobin in the acidic food vacuole, especially during the trophozoite stage, results in the eventual formation of hydrogen peroxide and superoxide radicals from the initial spontaneous oxidation of Fe^{3+} from Fe^{2+} and formation of superoxide anions. Both of these are highly reactive and toxic [234]. Haemoglobin digestion is also accompanied by the release of toxic haeme (ferriprotoporphylin IX, which is capable of membrane damage, much of this however is mineralised into non-toxic haemozoin [234, 235]. The remainder is processed in the cytosol by glutathione and the $\text{OH}\cdot$ radical that is produced after several interim steps is dealt with by the parasites redox system (with particular involvement of 1-cys-peroxiredoxin) [236]. The parasite is also well known for not having catalase or glutathione peroxidase, thus is particularly susceptible to oxidative stress [235], but has overcome this through its thioredoxin system [237] (Figure 2.23). In addition to its own array of antioxidant proteins and molecules, the parasite also imports human peroxiredoxin 2 into its cytosol in significant amounts, where it is functionally active, uses the parasite thioredoxin-1 as reducing substrate and is responsible for approximately 50% of the total thioredoxin peroxidase activity within the parasite [238].

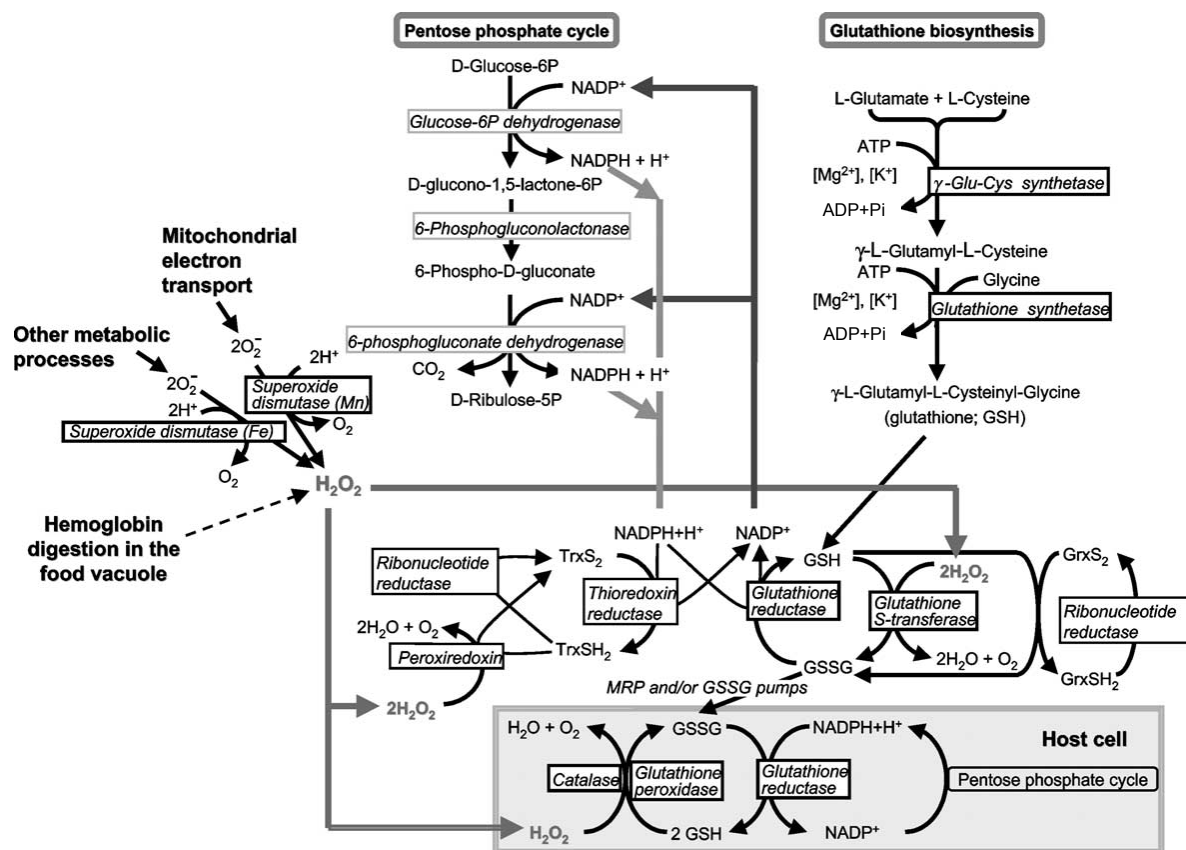


Figure 2.23. A representation of antioxidant defence within the *Plasmodium* infected erythrocyte. Modified from [239].

1-cys peroxiredoxin showed decreased abundance in both SSH-cDNA and oligo microarray studies, appears to be involved in antioxidant defence of the parasite and may play a role in protecting cells from iron-derived radical oxygen species resulting from haemoglobin digestion [236]. A decrease in this transcript (observed in all polyamine pathway inhibitions) in the face of apparent increased haemoglobin digestion upon polyamine depletion is thus inexplicable, other than this transcript is truly polyamine dependant for continued stabilisation or expression. The dependence on polyamines for expression and activation of genes or proteins in various systems is well known and has been reviewed by Childs *et al.* [240]. A link between redox metabolism within the parasite and the polyamine pathway was recently highlighted. Sturm *et al.* investigated the binding partners of three proteins within the thioredoxin superfamily (thioredoxin, glutaredoxin and plasmoredoxin) and revealed that several proteins involved in AdoMet metabolism were binding partners of these proteins [219]. The proteins identified as thioredoxin family binding partners (Table 2.19) are involved in protein biosynthesis, carbohydrate metabolism, haemoglobin catabolism, signal transduction and unsurprisingly, redox metabolism. Of the 32 proteins identified by Sturm *et al.*, 6 (19%) were present in the SSH-cDNA microarray data, while 7 (22%) were present in the oligo microarray data (this would be 25% if OAT was included). Only one transcript (1-cys peroxiredoxin) is

common between the two studies. A relationship between the polyamines and redox homeostasis in parasites is not uncommon, as evidenced by the trypanothione system, which is unique to the Kinetoplastida. Trypanothione (bis(glutathionyl)spermidine) is effectively two glutathione molecules linked by spermidine and its thiol groups are kept reduced by trypanothione reductase. As the Kinetoplastida contain no glutathione reductases or thioredoxin reductases, this trypanothione–trypanothione reductase relationship is the only connection between NADPH and thiol based redox metabolism. This is crucial to act as a redox buffer to balance any perturbation of the cellular redox state that may occur due to the presence of excess reactive oxygen species (ROS) originating from the environment or growth [241].

Interestingly, cadaverine synthesis has been shown to be induced by the transcriptional activator SoxR in *Vibrio vulnificus* in reaction to and to protect the bacterium from superoxide stress, as cadaverine is capable of scavenging superoxide radicals [242, 243]. One of the multiple functions of the polyamines within the cell is the scavenging of oxygen radicals [244, 245], so bearing the putrescine (polyamine) depletion and concomitant decrease in abundance of many of the transcripts for proteins involved in redox metabolism in mind, increased cadaverine production through the action of LDC may be one way in which the parasite compensates for and tries to mediate oxidative stress.

Upon clustering of the oligo microarray data, one cluster (Figure 2.18) proved particularly interesting as it contained 1-cys peroxiredoxin, AdoMetDC-ODC and pyridoxal-5'-phosphate synthase (all transcripts of decreased abundance). Several enzymes are dependent on PLP (Table 2.18) and have proved to be essential as inhibition of them often results in eventual parasite death [246]. Of these PLP-dependent enzymes, several show differential expression upon DFMO-treatment. It is however possible that sufficient PLP is obtained from exogenous sources. Pyridoxine-HCl is available in the RPMI based culture medium at 0.001 g/l, while human erythrocytes contain both pyridoxal/pyridoxine kinase and pyridoxine/pyridoxamine oxidase and are proposed to be the main carrier of vitamin B6 (though PLP is bound primarily to proteins) [246]. It has been established that in *Plasmodium*, *de novo* PLP synthesis is initiated via the action of 2 enzymes, Pdx1 and Pdx2. These constitute a multimeric enzyme complex composed of a core of 12 Pdx1 molecules surrounded by 12 Pdx2 subunits [220]. *pdx1* occurs on chromosome 6, appears to be a single copy gene and codes for a protein with a predicted mass of 33 kDa, while *pdx2* is found on chromosome 11, also appears to have no homologues and the predicted mass of the protein encoded is 24 kDa [247].

As ODC is part of the unique AdoMetDC-ODC bifunctional complex in the parasite, the data from the ODC-inhibition (as evaluated with oligo microarray) was compared with that from the AdoMetDC-, AdoMetDC-ODC and spermidine synthase inhibitions (Figure 2.22 and Table 2.20). In a comparison of all the differentially expressed transcripts between the ODC and the AdoMetDC inhibited samples, 354 transcripts are common between the two. There are however transcripts that are unique to either the ODC (642 transcripts), or the AdoMetDC (196 transcripts) inhibitions. Of the unique ODC transcripts, 322 (50%) are functionally unannotated, compared with 88 (45%) of the AdoMetDC group. Of the remaining transcripts unique to each of the two enzymes there are still common groups that are represented between the two (e.g. mitochondrial ribosomal protein), even though the specific transcripts differ.

With the exception of a two transcripts (PFI1585c and PFL1330c) that show opposing directions, many of the transcripts present in the AdoMetDC-ODC co-inhibition are also found in the ODC and AdoMetDC inhibitions; and the scale of change is similar. The main difference observed is in the transcripts involved in translation. The majority of the transcripts identified in the co-inhibition show increased abundance. The ODC and AdoMetDC inhibitions however, contain a different subset of transcripts and these are almost all of decreased abundance (only PFD0825c, present in time-point 2, shows increased abundance). Several of this subset observed in the ODC and AdoMetDC inhibitions are also present in the spermidine synthase inhibition and are also of decreased abundance (Table 2.20). Though all inhibitions show decrease in abundance of transcripts involved in DNA replication, significantly more were observed in the ODC and AdoMetDC inhibitions (Table 2.20). As mentioned previously, within the ODC inhibition dataset, the first time-point also contained more transcripts than the second time-point and of those present in both time-points, the amount of decrease in abundance decreased in the second time-point. Perhaps the initial decrease in abundance contributes to the progression towards transcriptional arrest and cytoostasis, which is the mostly established by the second time-point, thus reflecting the cytoostatic arrest that is starting to occur. Also, since the polyamines play a role in DNA stabilisation [54], this may also be linked in some sort of negative feedback mechanism. The presence of those that are still of decreased abundance may indicate that they play a more important role during DNA replication. An interesting transcript is an ATP-dependent DNA helicase (PF13_0330) present in the DNA replication group, that is only present in the second time-point of the ODC inhibition and is of increased abundance. Although generally few transcription factors were identified, they are primarily of increased abundance in both inhibitions. The exception is a putative transcription factor IIB (PFE0415w), which is of decreased abundance in the AdoMetDC-ODC, ODC (T2) and spermidine synthase (T2) transcriptomes. The transcripts for *S*-adenosylmethionine synthetase (PFI1090w) and *S*-adenosylhomocysteinase (PFE1050w) are only

present in the AdoMetDC, ODC and AdoMetDC transcriptomes indicating that this is possibly a consequence of dcAdoMet depletion. The presence of these in the ODC transcriptome may be the result of the decrease observed in the transcript for AdoMetDC-ODC (also not observed in the spermidine synthase transcriptome).

2.5 CONCLUSION

The effect of DFMO-induced inhibition of ODC and the resultant putrescine depletion was studied by investigating the global transcriptome response thereof in *P. falciparum* parasites. This study revealed the emergence of a signature transcriptome fingerprint profile of perturbing the parasites with drugs affecting polyamine metabolism. Additionally, unique processes were identified resultant of only DFMO-induced ODC-inhibition.

Many processes that were seemingly enhanced fall within the host-parasite interaction, protein modification and signal transduction groups, with some in cell-cycle/cytokinesis, primary metabolism and proteolysis. The primary group represented by the transcripts of decreased abundance is primary metabolism, followed by DNA metabolism and translation. ODC-specific signatures are evident in the existence of a transcriptional feedback mechanism in the parasite shown by an increase in OAT transcripts upon DFMO inhibition of ODC activity. The abundance of OAT transcripts increases in order to equilibrate the increase in ornithine concentration due to the inhibition of ODC and thus the failure of ornithine to be converted to putrescine. A link between polyamines and the redox status has been suggested [219] and data emerging from the transcriptomic studies of putrescine depletion support this as many of the transcripts for proteins involved in maintaining the redox status are of decreased abundance upon ODC-inhibition. Uniquely, LDC has been shown to be of increased abundance in the absence of polyamines (in ODC, AdoMetDC, AdoMetDC-ODC and spermidine synthase inhibitions) and this may be an attempt by the parasite to compensate for an increasingly hostile oxidative environment through cadaverine production as a superoxide radical scavenger.

CHAPTER 3

Translational response of ODC-inhibited *Plasmodium falciparum* parasites

3.1 INTRODUCTION

Transcription and translation are fundamentally different processes, thus transcriptomic analysis alone does not provide sufficient information for a comprehensive understanding of parasite biology [153]. Consequently several additional aspects of DFMO-induced inhibition of ODC on *P. falciparum* parasites were investigated in this study. These included the differences in actual protein expression of the parasite under inhibitory stress of ODC.

A proteomics approach can highlight aspects such as sub-cellular localisation, post-translational modification and protein-protein interactions [248] and can be divided into expression proteomics and functional proteomics. Expression proteomics looks at the expression of the protein complement of a cell under a specific condition, while functional proteomics focuses on the interaction of a protein with other ligands (and also other proteins) [249]. Proteomics has been greatly facilitated by technological developments in the reproducibility of 2D electrophoresis (2DE), particularly by the advent of immobilised pH gradient (IPG) strips; mass spectrometry; and the accessibility to and expansion of protein databases [249, 250].

There are two main strategies for protein expression profiling. Firstly, electrophoretic separation of proteins (eg. 2D PAGE), followed by identification using mass spectroscopy; secondly, chromatographic separation of proteins (peptides) directly coupled to protein identification by LC-MS/MS [251]. Both approaches allow direct labelling of the proteins for quantification and determination of differential protein expression between samples. There are four major classes of MS-based quantitation, based on the type of labelling and the level at which the labelling is performed. These classes are metabolic labelling (eg. SILAC – stable isotope labelling in culture, ^{15}N or ^{13}C); chemical labelling of either proteins (eg. iTRAQ – isobaric tags for relative and absolute quantitation, or iCAT – isotope coded affinity tag) or peptides (eg. iTRAQ or TMT – tandem mass tags); synthetic spiking using standards of known concentration; and label free quantitation [252]. Nirmalan *et al.* developed a quantitative methodology employing 2DE and the metabolic incorporation of heavy-isotope containing isoleucine, particularly for application to the *P. falciparum* proteome [156]. The advantage of 2DE is that the samples can be quantified [156], while the

disadvantage is that generally only soluble proteins of mid to low molecular weight can be evaluated [99]. LC-MS/MS has the advantage that the insoluble protein fraction can be treated with cyanogen bromide to allow hydrophilic loops to be cleaved from integral membrane proteins and subsequently analysed [99].

As with transcriptomics, proteomics of *Plasmodium* has already been established. Both electrophoretic and chromatographic methods of proteomic investigation are currently in use as several groups have employed the 2D PAGE followed by MS strategy [156, 162, 165, 166], while several others have used variations of the LC-MS/MS strategy [99, 124, 155, 163, 251]. Some of the most recent work includes the large-scale proteome of drug treated parasites as determined by LC-MS/MS [163], an investigation of post-transcriptional regulation and modification in schizonts by 2D-DIGE [253] and a detailed time-course study of the protein levels during the intraerythrocytic developmental cycle using 2D-DIGE [157].

3.2 MATERIALS AND METHODS

3.2.1 Parasite culture, treatment and sampling

Continuous 3D7 *P. falciparum* parasite culture was maintained *in vitro* as per the method of Trager and Jensen [190], with the replacement of 5% Albumax II (Gibco) for serum [191], as described in Chapter 2 (Section 2.2.1.1). However, a different approach to blood collection was followed, due to the amount of culture required. Human blood (A⁺) was collected in a Fenwall blood collection bag (containing citrate-phosphate-glucose-adenine anti-coagulant, Adcock Ingram Critical Care), stored in the bag at 4°C overnight, whereafter it was transferred to tissue culture flasks and washed as required. For washing, the required amount of blood was removed from the flask and transferred to a 50 ml tube. The cells were pelleted (5 minutes at 1500g, Hermle Z320), the supernatant aspirated and the pellet washed (4 times in total) with an equal volume of 1x PBS. The washed erythrocytes were resuspended in an equal volume of complete culture medium (i.e. containing Albumax II) resulting in a 50% haematocrit.

The culture was synchronised thrice using 5% sorbitol [192]. Eight 75 cm² flasks containing 30 ml of culture were treated with 10 mM DFMO at approximately two hours post-merozoite invasion. A further eight flasks containing 30 ml of culture were kept as untreated control. Samples of culture were removed at 16 hours post-treatment and smears for microscopic evaluation were prepared at this time-point. The erythrocytes were lysed by the addition of saponin to a final concentration of 0.01%, followed by incubation on ice for 5 minutes. The released parasites were pelleted by

centrifugation at 1500g for 10 minutes. The supernatant was aspirated and discarded. PBS (750 µl of 1x) was added to the parasite pellet and the samples transferred to microfuge tubes. The parasites were washed a total of four times with 750 µl 1x PBS and the parasite pellets subsequently stored at -70°C for no more than one month.

3.2.2 Protein isolation and determination of concentration

Rehydration buffer (1 ml of 8 M urea, 2 M thiourea, 2% CHAPS, 5 mg DTT and 7 µl IPG buffer, pH 3–10 linear) was added to each of the thawed protein pellets from the treated and untreated samples, respectively. The samples were subsequently subjected to four rounds of pulsed sonification (Virsonic microtip) of 20 seconds (1 second on and 1 second off). Each sample was incubated on ice for 1 minute between sonification rounds. Insoluble protein was pelleted by centrifugation at 16000g for 1 hour at 4°C (Eppendorf 5415R). The soluble protein containing supernatant was retained and the concentration of protein determined using the 2D-Quant kit and following the manufacturer's protocols (Amersham Biosciences). The method incorporates the quantitative precipitation of protein, while any contaminating agents remain in solution. A standard curve was established on a series of protein dilutions (0 – 50 µg) to which various volumes of the protein-containing supernatant were compared. Precipitant (500 µl) was added to each of the standard curve and unknown samples. These were mixed by vortexing, incubated at room temperature for 3 minutes, 500 µl of co-precipitant was added and again mixed by vortexing. The samples were centrifuged at 16100g for 15 minutes (4°C) and the supernatant aspirated and discarded. The precipitate was centrifuged for a further 3 minutes at 16100g and any remaining supernatant removed and discarded. Copper solution (100 µl), followed by 400 µl of water was added to the pellet and vortexed to resuspend. Working solution was prepared according to manufacturer's instructions, prior to starting the quantification and 1 ml was added to the first tube and immediately mixed by inversion. Each of the subsequent tubes had working solution added in this manner. The samples were incubated at room temperature for 20 minutes, whereafter 300 µl of each was transferred (in triplicate) to a multiwell plate for scanning at 492 nm (Multiskan Ascent V1.24 scanner).

3.2.3 Isoelectric focussing (IEF)

A semi-quantitative two-dimensional electrophoresis protocol that had been optimised for *P. falciparum* was followed [154]. Soluble protein (400 µg in rehydration buffer) was placed in ceramic IPG strip holders, 18 cm IPG strips (Immobiline™ DryStrip pH 3-10, 18 cm, GE Healthcare) added, covered with mineral oil and placed on the Ettan IPGphor II (Amersham Biosciences) for active rehydration and first dimension IEF under the conditions set out in Table 3.1.

Table 3.1. IEF profile employed for 18 cm IPG strips.

Cycle	Step	Voltage (V)	Time or Vhrs
1	Step 'n hold	30	10 hr
2	Gradient	200	10 min
3	Step 'n hold	200	20 min
4	Gradient	500	20 min
5	Step 'n hold	500	20 min
6	Gradient	2000	20 min
7	Step 'n hold	2000	45 min
8	Gradient	8000	100 min
9	Step 'n hold	8000	to 24000 Vhrs

3.2.4 Second dimension sodium dodecyl sulphate polyacrylamide gel electrophoresis (SDS-PAGE)

Following first dimension IEF, the oil was rinsed off the strips with water. The strips were first equilibrated in equilibration buffer A (50 mM Tris HCl pH 6.8, 6 M urea, 30% (v/v) glycerol, 2% SDS and 2% (w/v) DTT) for 10 minutes with agitation. This was followed by 10 minutes in equilibration buffer B (50 mM Tris HCl pH 6.8, 6 M urea, 30% (v/v) glycerol, 2% SDS and 2.7% (w/v) iodoacetamide), where the iodoacetamide alkylates any thiol groups present to prevent their reoxidation during electrophoresis. The strips were lastly equilibrated in 1x SDS running buffer (25 mM Tris, 192 mM Glycine, 0.1% SDS) for 10 minutes. The strips were subsequently laid on top of 10% acrylamide gels (16 cm wide x 16 cm long x 1mm thick), sealed in place with 1% agarose and electrophoresed at a limit of 500 V and 80 mA (Hoefer™ SE 600 vertical gel electrophoresis system) until the bromophenol blue (included in the equilibration buffers at 0.0025% w/v) reached the bottom of the gel (approximately 3½ hours).

The gels were removed and placed in glass bowls (2 gels per bowl) containing fixing solution (40% ethanol, 10% acetic acid) for a minimum of 16 hours. The gels were stained by addition of 1x Flamingo™ fluorescent gel stain (Bio-Rad) and incubated at room temperature overnight, with agitation. The Flamingo™ stain binds to denatured protein. It is MS compatible, allows quantitation over a wide dynamic range and is very sensitive (0.25 - 0.5 ng of protein). Once bound to protein it has a fluorescence excitation maximum of 512 nm and a fluorescence emission maximum of 535nm [254]. The gels were washed with 0.1% (v/v) Tween 20 for 20 minutes, followed by water for 5 minutes and subsequently a final rinse with water. The gels were scanned on the Versadoc 3000 (Bio-Rad) using PDQuest 7.1.1 (Bio-Rad).

3.2.5 Data analysis and protein identification

Differential protein expression was determined using PDQuest 7.1.1. Gels were cropped to equal sizes, spot-finding performed; and both automated and manual spot-matching executed.

Normalisation using the total density in the image was carried out, as some saturated spots were present, where the raw quantity of each spot was divided by the total intensity value of all the pixels in the image. Qualitative (uniquely present in a specific sample) and quantitative differentially expressed spots were identified by the program and manually checked for validity. Appropriate spots were excised from the gels (between 2 and 3 spots were combined) and sent for identification using mass spectrometry at the Centre for Proteomic & Genomic Research (CPGR) in Cape Town, South Africa (the protocol used by CPGR is included in Supplementary Material S7).

Additionally, several differentially regulated spots were analysed at the Council for Scientific and Industrial Research (CSIR, South Africa). The excised, dried gel spots were washed with 200 μ l of water and incubated at room temperature for 10 minutes with occasional vortexing. The water was aspirated and the wash step was repeated, followed by the addition of 200 μ l of 50% acetonitrile with incubation at room temperature for 10 minutes, with occasional vortexing. The acetonitrile was removed and replaced with 200 μ l of 50 mM ammonium bicarbonate. The samples were incubated at room temperature for 10 minutes with occasional vortexing, after which the ammonium bicarbonate was aspirated. The 50% acetonitrile and 50 mM ammonium bicarbonate steps were repeated and 100 μ l of 100% acetonitrile was added to the gel fragments that were then incubated until they turned white. The 100% acetonitrile was removed and replaced with 200 μ l of 50 mM ammonium bicarbonate, incubated at room temperature for 10 minutes, then aspirated, whereafter 200 μ l of 50% acetonitrile was added and incubated at room temperature for 20 minutes. The acetonitrile was removed and the samples dried *in vacuo* (Bachofen vacuum concentrator) for approximately one hour.

Trypsin (10 ng / μ l in trypsin resuspension buffer, Promega) was added to the prepared gel fragments and digestion proceeded at 37°C, overnight. Acetonitrile (15 μ l of 70%) was added and incubated at room temperature for 30 minutes. The peptide containing supernatant was aspirated and transferred to a clean microfuge tube. A further 15 μ l of 70% acetonitrile was added to the gel fragment, with incubation at room temperature for 30 minutes. The supernatant was aspirated and added to that obtained initially. The peptides were dried *in vacuo*. The peptides were dissolved in 10% acetonitrile, 0.1% formic acid and mixed with saturated α -cyano-4-hydroxycinnamic acid prior to spotting onto the MALDI sample plate. The samples were run using a QSTAR® Elite (Q-TOF) mass spectrometer (Applied Biosystems) with a MALDI source. Based on sample concentration and whether single MS or MS/MS was performed, the intensity of the laser pulses (generated using a Nitrogen laser) was between 15 and 25 μ J. Single MS spectra were acquired for 15-30 seconds and the 50 highest peaks from the MS spectra were automatically selected for MS/MS acquisition.

Tandem spectra were acquired for between 4 and 8 minutes, depending on sample concentration. The cooling gas in Q0 and the collision gas in Q2 was argon. A nine-peptide mixture covering the scan range of 500 – 3500 Da was used to optimise the collision energy, which was then automatically set during MS/MS experiments using the Information Dependent Acquisition (IDA) function of the Analyst QS 2.0 software. A two point external calibration using the peptides Bradykinin 1-7 and Somatostatin 28 ($[M+H]^+ = 757.3992$ Da and 3147.4710 Da, respectively) was conducted in TOF-MS mode. The obtained data was submitted to MASCOT (www.matrixscience.com) for analysis and identification.

3.3 RESULTS

The transfer of information from the transcript to the protein level, along with any regulation of translational activity, is obviously of great interest. A smaller, focused proteomics experiment, incorporating only one time-point, was thus performed to investigate the effect of ODC inhibition at protein level.

As expected, DFMO-treatment of the *P. falciparum* culture resulted in similar morphologic phenomena as observed during the transcriptomics experiments (results not shown). The parasite cultures were processed for proteomics and the total protein concentration in the treated parasite sample was determined to be 2.55 mg/ml, while the total protein concentration in the untreated parasite sample was 3.53 mg/ml. This disparity between the amount of total protein isolated from treated and untreated parasites was also observed in the transcriptomics study, where less RNA was obtained from treated samples when compared with the untreated samples (Chapter 2).

The samples were subjected to the various steps of 2D electrophoresis and the gels were visualised by means of Flamingo™ Fluorescent Gel Stain. The four replicate gels of each of the treated and untreated parasite samples are given in Figure 3.1 (a) and (b). PDQuest 7.1.1 analysis allows direct comparison of several spots of interest on all the replicate 2D-gels. The data from all the replicate gels (quadruplicates of treated and untreated, respectively) is used to generate a master image containing all the spots. Each spot can then be analysed, in order to determine whether it has been affected by treatment or not. Figure 3.1 shows a simplistic representation of the analysis process.

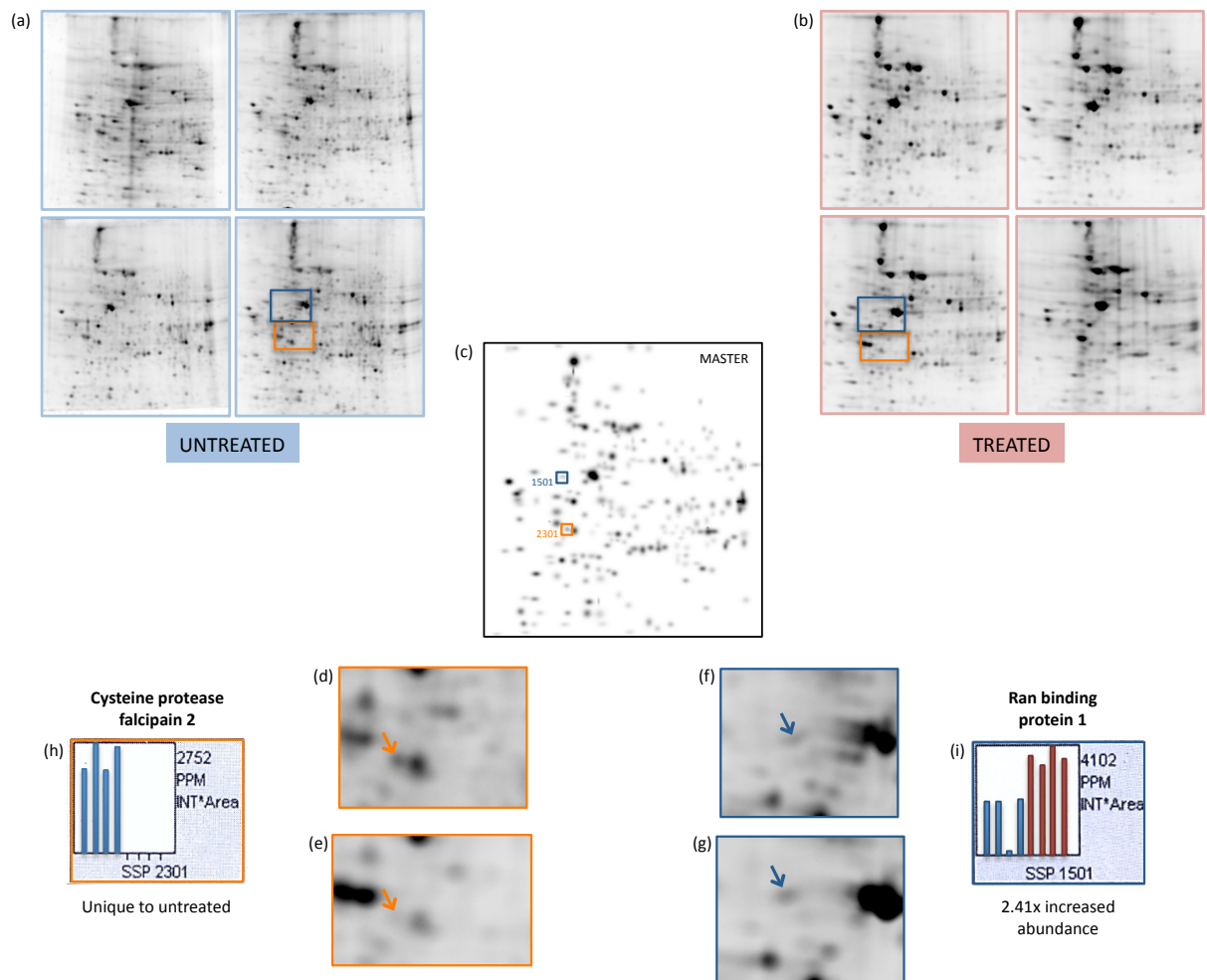


Figure 3.1. Simplistic overview of the PDQuest analysis process. (Replicate (quadruplicate) (a) untreated and (b) treated gels. (c) Master image containing all spots, generated from all eight gels. Two spots (1501 – blue box and 2301 – orange box) are highlighted to demonstrate the evaluation process. (d) Enlarged inset of untreated gel for spot 2301 (arrow) and (e) an area of the treated gel indicating the absence of spot 2301 (arrow). (f) Enlarged inset of an area of the untreated gel for spot 1501 (arrow) and (g) of treated gel indicating the increase in spot 1501 (arrow). (h) PDQuest results for spot 2301 showing the spot intensity for the untreated protein sample (blue bars) and absence of any bars for the treated protein sample. (i) PDQuest results for spot 1501 showing the spot intensity for the untreated (blue bars) and the treated (red bars) protein samples. The bars represent the normalised intensity for the spot of interest in each of the 8 gels.

The PDQuest analysis was initially performed and a master gel containing 390 spots generated. The analysis was repeated to reduce the effect of spot saturation (a gel set subjected to less exposure during scanning was used) and a second master gel containing 237 spots was generated (Table 3.2). Numerous spots were common to both master gels.

Table 3.2. Statistics of spot count and matching for initial and saturated analyses of gels using PDQuest.

	Initial	Saturated
Master image spot count	390	237
Average match rate ^a per gel	97.1% ± 2.2	96.4% ± 3.1
Average number of spots per gel	213	144

^a match rate is the average of all 8 gels, with the standard deviation.

Spots with differing intensity (greater than 2-fold regulated, or unique to a sample) between the treated and the untreated parasites were identified (Figure 3.2) using PDQuest.

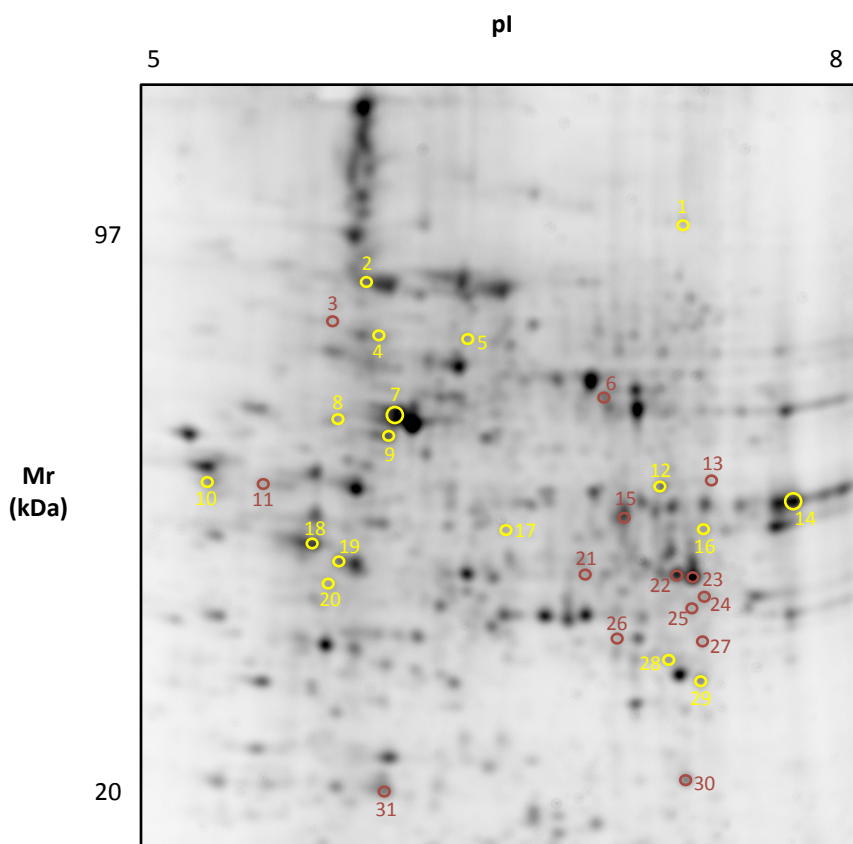


Figure 3.2. Spots (red and yellow) identified as differentially regulated. The yellow highlighted spots were identified with mass spectrometry (Table 3.5).

The master gels were used as a guide for excision of the spots of interest, which were subsequently identified by mass spectrometry at either the CPGR (www.cpgr.org.za), or the CSIR (www.csir.co.za). The results obtained are given in Table 3.3.

Table 3.3. Proteins identified as differentially expressed in the *P. falciparum* parasite following DFMO-induced inhibition of ODC.

Spot number	Accession number	PlasmoDB ID	Name	Mascot Score	Protein Score CI% ^a	Peptide count	% sequence coverage	Molecular weight (kDa)	pI
Proteins with decreased abundance									
7 ^{1,2}	S12628	PFL2215w	Actin I	185	100.00	19	53	42	5.00
9 ¹	Q8IIF6_PLAF7	PF11_0218	Conserved <i>Plasmodium</i> protein, unknown function	48	81.72	22	16	185	4.74
10 ¹	Q8IM16_PLAF7	PF14_0075	Plasmeprin IV	61	99.084	11	34	51	5.19
12 ¹	Q703U6_PLAFA	PF11_0313	60S ribosomal protein P0	86	100.00	12	53	35	6.70
14 ¹	Q8IKK7_PLAF7	PF14_0598	Glyceraldehyde-3-phosphate dehydrogenase	133	100	15	66	36.636	7.77
16 ¹	Q8I2F2_PLAF7	PF11780w	<i>Plasmodium</i> exported protein (PHISTc), unknown function	52	92.888	14	27	46	10.37
17 ¹	AAN35353	PF10_0155	Enolase	49	87.35	10	30	49	6.54
19 ¹	Q9NBD4_PLAFA	PF11_0165	Falcpain-2A	78	99.98	13	38	56	7.49
28 ¹	Q9U526_PLAFA	PF08_0071	Fe-superoxide dismutase	64	99.59	8	52	23	6.79
29 ¹	Q6LEZ9_PLAF7	PF11335c	4-methyl-5(B-hydroxyethyl)-thiazol monophosphate biosynthesis enzyme	155	100.00	15	89	20	7.46
Proteins with increased abundance									
1 ¹	Q8IKW5_PLAF7	PF14_0486	Elongation factor 2	148	100.00	26	37	93.524	6.78
5 ²	O97247_PLAF7	PFC0285c	T-complex protein beta subunit, putative	459	NA	11	27	59	5.43
6 ¹	Q8I2X4_PLAF7	PFI0875w	Heat shock protein 70 (HSP70) homologue	168	100.00	24	44	72	4.93
8 ²	Q76NN6_PLAF7	PFD0950w	Ran binding protein 1, putative	101	NA	2	9	33	4.63
18 ^{1,2}	Q8IB17_PLAF7	MAL8P1.69	14-3-3 protein, putative	126	100.00	14	56	30	4.56
20 ¹	Q8I9F4_PLAFA	PFI0930c	Nucleosome assembly protein	48	82.94	8	31	32	3.95
23 ^{1,2}	Q8I2X4_PLAF7	PFI0875w	Heat shock protein 70 (HSP70) homologue	91	100.00	16	30	72	4.93

^a The protein score CI% refers to the confidence interval of the Mascot identification - above 95% is considered a positive identification, while between 80 and 90% requires further evaluation.

¹ Mass spectroscopy performed at CPGR.

² Mass spectroscopy performed at CSIR.

Table 3.4 presents some of the characteristics of the differentially expressed proteins. The most significant are the proteins that are unique to a sample. In this instance, only the untreated samples have proteins unique to them, of which superoxide dismutase is noteworthy, as the link between redox metabolism and the polyamines has been established [219]. The remaining unique proteins include enolase, falcpain 2, a 60S ribosomal protein, 4-methyl-5(B-hydroxyethyl)-thiazol monophosphate biosynthesis enzyme (involved in thiamine biosynthesis), an exported protein and a hypothetical protein. Within the proteins that show an increase in abundance, the most significantly changed (4.3x) is elongation factor 2.

Table 3.4 Characteristics of the differentially expressed proteins obtained from PlasmoDB (www.plasmodb.org). The minimum and maximum expression time for the gene transcripts are given. The presence or absence of the proteins in the proteome of AdoMetDC-inhibited (T1: 16 hours post infection (hpi) and T2: 20 hpi) [2] and spermidine synthase inhibited (t1: 18 hpi; t3: 30 hpi) [3] parasites is also shown. NA = not available.

Spot number	PlasmoDB ID	Name	Regulation	GO: molecular function	GO: biological process	GO: cellular component	Transcript: minimum expression time (hpi)	Transcript: maximum expression time (hpi)	Transcript: maximum fold-induction	AdoMetDC inhibition	Spermidine synthase
<i>Proteins with decreased abundance</i>											
7	PFL2215w	Actin I	3.33	structural constituent of cytoskeleton, protein binding	cytoskeleton organization	actin filament	15	39	42.43	Down (T2)	-
9	PF11_0218	Conserved <i>Plasmodium</i> protein, unknown function	Unique to untreated	none	none	apicoplast	19	38	2.71	-	-
10	PF14_0075	Plasmeprin IV	3.7	aspartic-type endopeptidase activity	hemoglobin catabolic process	membrane, food vacuole	36	47	7.04	-	-
12	PF11_0313	60S ribosomal protein P0	Unique to untreated	structural constituent of ribosome	translational elongation, translation, ribosome biogenesis	mitochondrion, cytosolic large ribosomal subunit	42	16	5.05	-	-
14	PF14_0598	Glyceraldehyde-3-phosphate dehydrogenase	2.5	glyceraldehyde-3-phosphate dehydrogenase (phosphorylating) activity, NAD or NADH binding	glycolysis, gluconeogenesis	mitochondrion	42	27	5.96	Down (T1)	Down (t1, t3)
16	PFI1780w	<i>Plasmodium</i> exported protein (PHISTc), unknown function	Unique to untreated	none	none	none	37	13	10.78	-	-
17	PF10_0155	Enolase	Unique to untreated	phosphopyruvate hydratase activity	glycolysis, gluconeogenesis	phosphopyruvate hydratase complex	38	16	5.35	Down (T1)	Down (t1)
19	PF11_0165	Falcpain-2A	Unique to untreated	cysteine-type endopeptidase activity	proteolysis	membrane, food vacuole	36	19	7.96	Down (T2)	-
28	PF08_0071	Fe-superoxide dismutase	Unique to untreated	superoxide dismutase activity, metal ion binding	response to oxidative stress, superoxide metabolic process	none	1	28	2.04	-	-
29	PFF1335c	4-methyl-5(B-hydroxyethyl)-thiazol monophosphate biosynthesis enzyme	Unique to untreated	none	thiamin biosynthetic process	none	41	19	5.00	-	-
<i>Proteins with increased abundance</i>											
1	PF14_0486	Elongation factor 2	4.3	translation elongation factor activity, GTP binding, GTPase activity	translational elongation	none	46	17	3.69	Up (T2)	-
5	PFC0285c	T-complex protein beta subunit, putative	2.93	ATP binding, unfolded protein binding	protein folding	chaperonin-containing T-complex	36	21	4.34	-	-
6 / 23	PFI0875w	Heat shock protein 70 (HSP70) homologue	3.51	ATP binding	none	none	41	31	4.64	-	Down (t3)
8	PFD0950w	Ran binding protein 1, putative	2.41	GTPase activity, GTP binding	DNA replication, intracellular transport	none	45	1	2.30	-	Down (t3)
18	MAL8P1.69	14-3-3 protein, putative	3.51	protein domain specific binding	none	none	40	31	3.22	-	-
20	PFI0930c	Nucleosome assembly protein	2.42	none	nucleosome assembly	nucleus	NA	NA	NA	-	-

When the proteins identified as differentially expressed upon inhibition of ODC are compared with those from AdoMetDC inhibition, some proteins are common to both groups. More proteins of decreased abundance than of increased abundance are present, but the ODC-inhibited proteome study was not exhaustive, so additional proteins that are common to both groups may yet be identified. Within the proteins of decreased abundance, proteins that are common to both groups are mostly involved in cell metabolism and structure (actin, glyceraldehyde-3-phosphate dehydrogenase, enolase and falcipain 2). Elongation factor 2 is of increased abundance and present in both groups.

Chapter 2 highlighted a link between polyamine metabolism and redox metabolism that had been identified by Sturm *et al.*, in which several enzymes involved in polyamine biosynthesis were captured in a yeast two-hybrid experiment using the redox associated proteins thioredoxin, glutaredoxin and plasmoredoxin as bait [219]. Table 3.5 highlights the commonalities between proteins or transcripts affected by inhibition of ODC, in comparison with the identified binding partners of the thioredoxin superfamily [219]. Artemether and lumefantrine [162] were included in the comparison to determine if the similarities may be polyamine associated, or if they may be common to drug perturbed *P. falciparum* parasites.

Of the 32 proteins identified by Sturm *et al.*, six (18.75%) were present in the SSH-cDNA microarray data, seven (22%) were present in the oligo microarray data (this would be 25% if the saturated OAT was included) and four (12.5%) were present in the proteomic data. Combined, 50% of the proteins identified as part of the redox system were also affected by inhibition of ODC, on either transcript or protein level. Of the CoArtem drugs, eight (25%) of the artemether and five (16%) of the lumefantrine proteins are present in the thioredoxin superfamily. The DFMO transcriptome has the greatest number of proteins in common, followed by the artemether proteome. The DFMO proteome has the least in common, but it should be remembered that the DFMO proteome study was not exhaustive. Of the drug perturbation proteins present in the anti-oxidative stress category (DFMO transcriptome: 33%; artemether proteome: 33%), all are of decreased protein abundance, while all those in the transcription/translation and protein-folding categories (DFMO transcriptome: 22%; DFMO proteome: 11%; artemether proteome: 33%; lumefantrine proteome: 22%) are of increased abundance. Carbohydrate and AdoMet metabolism also have many proteins in common between the thioredoxin superfamily and the drug-perturbation studies, most of which are of decreased abundance, except for the lumefantrine proteins and OAT in the DFMO transcriptome, which are of increased abundance (DFMO transcriptome: 57%; DFMO proteome: 14%; artemether proteome: 43%; lumefantrine proteome: 29%).

Table 3.5. Proteins identified as binding to either thioredoxin (Trx), plasmoredoxin (Plrx) or glutaredoxin (Grx) [219]. Those common to the DFMO transcriptomic (as identified by SSH cDNA microarray and oligo microarray) and proteomic profile, as well as those identified in the artemether and lumefantrine proteomic profiling [162] are identified (along with the direction of regulation).

Bait	PlasmoDB ID	Gene annotation	DFMO transcriptome (cDNA/Oligo)	DFMO proteome	Artemether proteome (Makanga et al.)	Lumefantrine proteome (Makanga et al.)
Anti-Oxidative Stress System						
Trx	PF14_0368	2-Cys peroxiredoxin (2-Cys-Prx, cytosolic)			Down	
Trx	PF08_0131	1-Cys peroxiredoxin (1-Cys-Prx, cytosolic)	Down/Down			
Trx	Grx	PFC0166w	Plasmoredoxin (Thioredoxin-like redox-active protein)			
Transcription/Translation						
Trx	PF13_0042	Fork head domain protein, putative				
Grx	Plrx	PF14_0486	Elongation factor 2	Up		
Grx	Plrx	PFC0295c	40S ribosomal protein S12		Up	
Grx	Plrx	PFD1055w	Ribosomal protein S19s, putative			
Protein Folding						
Trx	Grx	Plrx	PF10875w		Up	Up
Trx	Grx	Plrx	PF08_0054	Heat shock 70 kDa protein	Up	
Trx	Grx	Plrx	PF07_0029	Heat shock protein 86	Up	Up
	Plrx	PF11_0258	Co-chaperone GrpE, putative			
	Plrx	MAL8P1.17	Disulfide isomerase, putative			
Carbohydrate Metabolism						
Trx	Grx	Plrx	PFF1155w	Hexokinase		
Trx	Grx	Plrx	PFF1300w	Pyruvate kinase, putative	Down	
Grx	Plrx	PF14_0598	Glyceraldehyde-3-phosphate dehydrogenase		Down	Up
Grx	Plrx	PF13_0141	L-lactate dehydrogenase	Down		
AdoMet Metabolism						
Trx	Grx	Plrx	PFF0435w	Ornithine aminotransferase	Up/Saturated	Up
Trx	Grx	Plrx	PF11090w	S-adenosylmethionine synthetase	Down	
Trx	Grx	Plrx	PFE1050w	S-adenosyl-L-homocysteine hydrolase	Down	
Lipid Metabolism						
Grx	MAL13P1.214	Phosphoethanolamine N-methyltransferase, putative				
Plrx	PFB0385w	Acyl carrier protein, putative	Down			
Hemoglobin Catabolism						
Trx	Plrx	PF14_0078	HAP protein/Plasmepsin III	Up	Up	Up
DNA Synthesis and Repair						
Plrx	PF0715c	Endonuclease iii homologue, putative				
Plrx	PF14_0053	Ribonucleotide reductase small subunit (R2)	Down			
Signal Transduction						
Trx	Grx	Plrx	MAL8P1.69	14-3-3 protein homologue, putative	Up	
	Plrx	MAL13P1.309	14-3-3 protein, putative			
Trx		MAL13P1.241	GTPase, putative			
	Grx	PF08_0019	Guanine nucleotide-binding protein, putative/receptor for activated C kinase homolog, PFRACK	Up		
	Plrx	MAL7P1.122	Conserved GTP-binding protein, putative			
Others						
Trx	PF14_0036	Acid phosphatase, putative				
	Plrx	PF10_0065	Hypothetical protein			
	Plrx	PF14_0190	Hypothetical protein			

A protein interaction network was compiled using yeast-two-hybrid (Y2H) data [255]. This data in PlasmoDB, was used to obtain the proteins identified as either bait or prey (i.e. interacting proteins) with the proteins that were differentially expressed upon DFMO treatment (Table 3.6).

Of the proteins showing differential expression upon DFMO treatment, nucleosome assembly protein (PF10930c) has the greatest number of binding partners with 28, followed by 14-3-3 protein (MAL8P1.69) with 20. Plasmepsin IV (PF14_0075), Fe-superoxide dismutase (PF08_0071) and 4-methyl-5(B-hydroxyethyl)-thiazol monophosphate biosynthesis enzyme (PFF1335c) have no proteins interacting with them in the interaction network Y2H study. AdoMetDC-ODC has 2 (PF10_0211 and MAL13P1.202), but also interacts with itself.

Table 3.6. Number of interacting proteins [255] found for the proteins showing differential expression upon DFMO treatment. The upper portion of the table contains proteins that showed decreased abundance upon treatment, while the lower portion shows those that showed increased abundance.

PlasmoDB ID	Name	Number of interacting proteins
PF08_0071	Fe-superoxide dismutase	0
PF10_0155	Enolase	9
PF11_0165	Falcipain-2A	8
PF11_0218	Conserved <i>Plasmodium</i> protein, unknown function	6
PF11_0313	60S ribosomal protein P0	4
PFF1335c	4-methyl-5(B-hydroxyethyl)-thiazol monophosphate biosynthesis enzyme	0
PFI1780w	<i>Plasmodium</i> exported protein (PHISTc), unknown function	15
PF14_0075	Plasmepsin IV	0
PFL2215w	Actin I	6
PF14_0598	Glyceraldehyde-3-phosphate dehydrogenase	11
PF14_0486	Elongation factor 2	2
MAL8P1.69	14-3-3 protein, putative	20
PFI0875w	Heat shock protein 70 (HSP70) homologue	17
PFC0285c	T-complex protein beta subunit, putative	1
PFI0930c	Nucleosome assembly protein	28
PFD0950w	Ran binding protein 1, putative	3

All the various interacting proteins were compared to determine if any of them were present for more than one protein from the DFMO treated proteome and a map of the interactions is shown in Figure 3.3. Only proteins with more than one interacting partner are shown in the map and the greatest number of interacting partners for any of the proteins is four. Each of PF14_0598 (glyceraldehyde-3-phosphate dehydrogenase), MAL8P1.69 (14-3-3 protein), PFI0875w (HSP 70 homologue) and PFI1780w (PHISTc) has four interactions with other partners. Of these, only PF14_0598 has an interaction with another protein from the DFMO treated proteome (PF10_0155 - enolase) which then also interacts with another DFMO treatment proteome protein PFI0930c (nucleosome assembly protein).

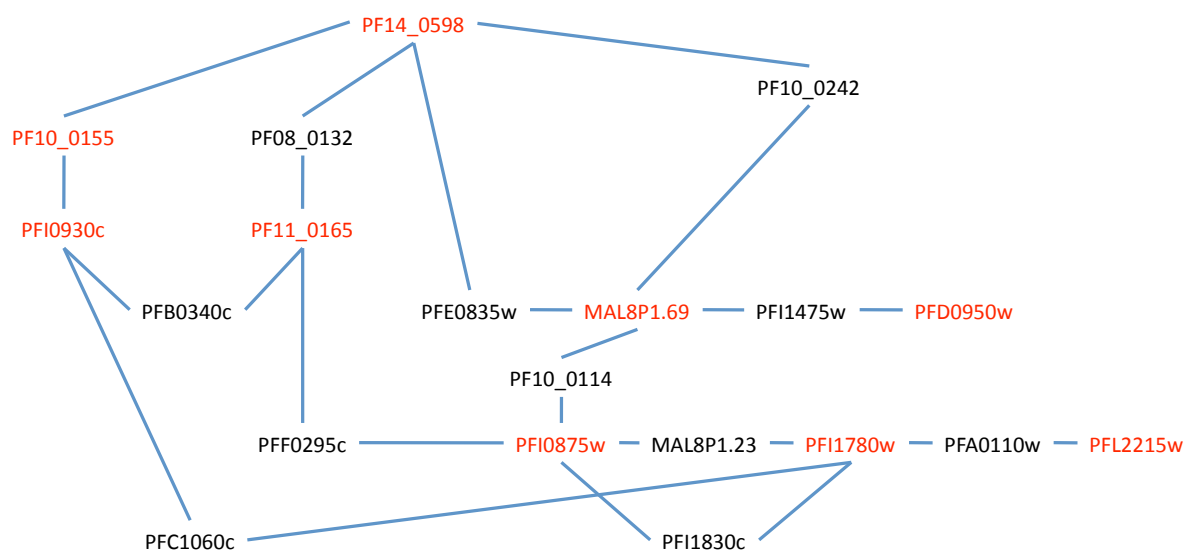


Figure 3.3. Interactions present between the proteins differentially expressed upon DFMO treatment (red) and their binding partners. Only proteins and binding partners involved in more than one interaction are shown.

3.4 DISCUSSION

In order to further investigate the effect of ODC-inhibition on the *P. falciparum* parasite, the effect of DFMO-treatment on the parasite proteome was investigated using 2D electrophoresis. Of the 31 spots identified as being differentially expressed, 17 were annotated of which two are hypothetical proteins. No additional information on PF11_0218 can be gleaned, while PlasmoDB version 6.1 (September 2009, www.plasmodb.org) annotates PFI1780w as an exported protein and part of the PHIST (*Plasmodium* helical interspersed subtelomeric) family, which was identified by Sargeant *et al.* [230]. The nature and function of PF11_0218 is interesting as it appears to be a true (translated) protein and is affected by ODC-inhibition. This thus warrants further investigation.

In Chapter 2 a link between polyamine metabolism and redox metabolism was highlighted [219] (Table 3.5). As seen in the transcriptomic data (Chapter 2), where the transcript for 1-cys peroxiredoxin showed decreased abundance, here the iron-superoxide dismutase protein is absent in the treated parasites. Combined, 50% of the proteins identified as part of the redox system were also affected by inhibition of ODC, compared with 25% for artemether and 16% for lumefantrine. Interestingly, a report of proteins affected by either artemisinin or chloroquine treatment [163], showed only one protein in common with those identified by Sturm *et al.* (namely PF11_0258, the co-chaperone GrpE), with only the transcript for thioredoxin (PF14_0545) affected by chloroquine [138]. In their investigation of the effect of the components of CoArtem (artemether and

lumefantrine) on the parasite proteome, Makanga *et al.* found eight (artemether) and five (lumefantrine) proteins in common with those identified by Sturm *et al.* (Table 3.5). This is not surprising, as it is well known that the mechanism of artemisinin and its related compounds is through the endoperoxide moiety, which when cleaved results in both carbon and oxygen centred radicals (though it is thought that artemisinin action is more likely to be through the alkylating activity of the carbon centred radicals) [162].

Oxidative stress results in elongation factor 2 being oxidatively modified and consequently in less active protein and therefore in reduced protein biosynthesis [219]. Inhibition of ODC results in an increase in elongation factor 2 protein (with an increase in abundance of 4.3x, this was the most extensively changed), along with increases in both transcript and protein levels of HSP70. Some heat shock proteins are redox controlled. Hsp33 is a prime example of such a redox-regulated chaperone. On a transcriptional level, it is regulated by heat shock, while on a post-translational level it is regulated via redox control. Hsp33 and several other proteins are redox regulated through cysteine centres that co-ordinate zinc [256]. Within the ATPase domain of HSP70, cysteine 20 is well conserved (amongst bacteria, fungi, plants and animals) and is suggested to be a target of redox regulation [219, 257]. Within the *P. falciparum* HSP70 proteins and homologues, there is indeed a conserved cysteine around position 27. This is also in the ATPase domain [258], though the ability of this Cys residue to co-ordinate zinc remains to be determined. Indeed, co-ordinated expression of heat shock proteins and antioxidant proteins has been demonstrated in *P. falciparum*. An increase in both of these was observed when the parasites were faced with an environment of oxidative stress [259].

Putrescine depletion within the malaria parasite also results in a decrease in two enzymes within the glycolytic pathway, namely enolase and glyceraldehyde-3-phosphate dehydrogenase. Both of these are involved in the short branch of the pathway in which glyceraldehyde-3-phosphate is converted into pyruvate. Glyceraldehyde-3-phosphate dehydrogenase also undergoes thiol/disulphide redox status changes that affect its activity. Again, in many species, cysteine residues are involved [219]. Glyceraldehyde-3-phosphate dehydrogenase is also one of the four proteins that have the greatest number of interactions (4) in the interactome map (Figure 3.3). Enolase was not identified as a thioredoxin family binding partner, but has been shown to be redox regulated in some plant species [219]. Enolase however, may also play a greater role within the parasite, depending on location. That near the merozoite surface may facilitate invasion; in the food vacuole, development or formation of the vacuole may be facilitated; while in the nucleus, enolase may very well be involved in transcription [260]. It is also the link in the only interactions between proteins of the DFMO treated

proteome (Figure 3.3). The decrease in the amount of 4-methyl-5(B-hydroxyethyl)-thiazol monophosphate biosynthesis enzyme, a key enzyme in the biosynthesis of thiamine (Vitamin B1) can also be linked to glycolysis, as thiamine-pyrophosphate is required for the enzymatic activity of pyruvate decarboxylase, pyruvate dehydrogenase, α -ketoglutarate dehydrogenase and transketolase [261].

Of the interactome proteins, three are present in the thioredoxin binding study [219], namely glyceraldehyde-3-phosphate dehydrogenase (PF14_0598), 14-3-3 protein (MAL8P1.69) and HSP 70 homologue (PFI0875w). Strangely, no proteins were found to interact with OAT in the interaction network Y2H study [255], while in the thioredoxin Y2H study, thioredoxin, glutaredoxin and peroxiredoxin were found to bind to OAT [219].

As transcriptional level changes are evident at later time-points in the parasite life-cycle (Chapter 2), proteomic investigation at additional time-points would yield useful information.

3.5 CONCLUSION

As with the transcriptome, DFMO-inhibition of ODC and the putrescine depletion had a defined impact on the parasite proteome. Taken in combination with the microarray data, a picture begins to emerge of the ODC-inhibited parasite. Redox status is impaired and compensatory responses especially with regard to transcription appear to be operational. Several proteins or transcripts for proteins involved with signalling, possibly to realise this compensatory response are also observed. Given that several anti-malarial drugs function through redox metabolism, this link between the polyamine pathway and redox metabolism as highlighted by Sturm *et al.* and supported by these experiments warrants further investigation.

CHAPTER 4

The relationship between ornithine and polyamine metabolism

4.1 INTRODUCTION

Metabolic regulation is a multi-faceted process and various levels of regulation exist in order to maintain homeostasis within a system. These include transcriptional and post-transcriptional regulation of the transcript, translational and post-translational regulation of the protein and regulation of enzyme activity. Polyamines are essential for normal cell growth and development and within other organisms their levels are regulated by biosynthesis, degradation and transport [262]. Interestingly, there is usually also tight control of metabolites closely related to polyamines, including the polyamine precursor, ornithine. Ornithine is produced in the parasite through the action of arginase and ornithine aminotransferase (OAT, EC 2.6.1.13, L-ornithine:2-oxo-acid aminotransferase), which catalyses the reversible production of glutamate-5-semialdehyde from ornithine (Figure 4.1) and as such plays a role in the homeostasis of ornithine.

Transcriptional, translational and post-translational regulation of mammalian OAT by a variety of stimuli has been identified [263-266]. Interestingly, OAT activity can also be regulated by various metabolites. Of particular interest, amines (certain polyamines and amino acids) have been found to inhibit OAT activity in some mammals [266], bacteria [265] and plants [267].

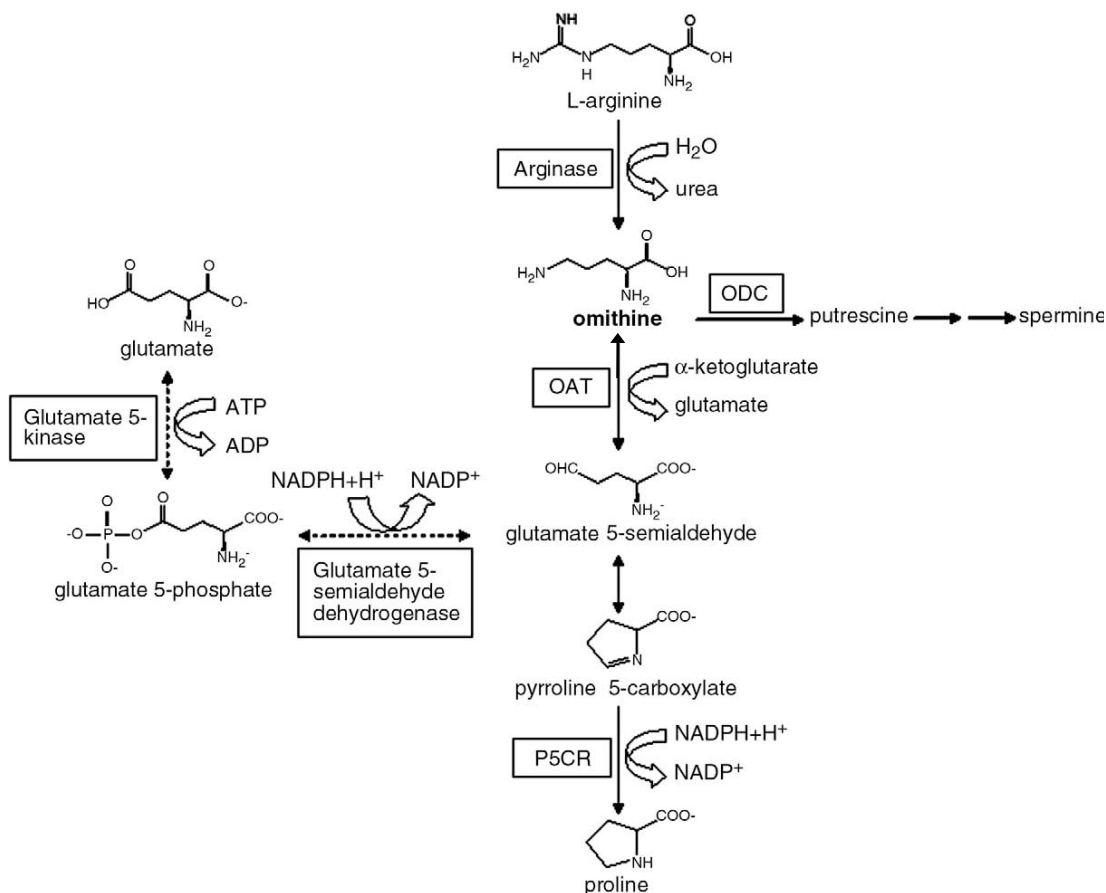


Figure 4.1. The synthesis and metabolism of ornithine. P5CR: pyrroline-5-carboxylate reductase; P5CS: pyrroline-5-carboxylate synthase. The dashed arrows indicate reactions that are yet to be demonstrated in *P. falciparum*. Modified from [268].

P. falciparum OAT (PFF0435w) was first characterised by Gafan *et al.* in 2001, where they cloned, sequenced, expressed and investigated various aspects of the enzyme's specificity and kinetics [96]. The three-dimensional structure of PfOAT has been elucidated and the overall structure is homodimeric and is similar to that of human OAT [268]. The physical characteristics of PfOAT include a molecular weight of 46056 Da and a pI of 6.88 (www.plasmodb.org). According to Gafan *et al.*, the apparent K_m (ornithine) of the enzyme (in the presence of 10 mM α-ketoglutarate) is 3.95 ± 1.04 mM, while the apparent V_{max} is 56.12 ± 7.43 nmol/min/mg [96].

Very few studies have investigated the relationship between ornithine and the polyamines within the *P. falciparum* parasite. However, in this study, a very clear and specific effect was seen after DFMO-treatment of *P. falciparum* parasites *in vitro*, where the transcript for OAT showed increased abundance upon putrescine-depletion in this parasite. This observation was also seen for perturbation of *P. falciparum* parasites with inhibitors affecting putrescine biosynthesis and this increase in OAT transcript (and protein) abundance was interpreted as a direct and thus compensatory response to putrescine depletion [1, 188, 189]. In these cases, ODC-inhibition with

DFMO (resulting in putrescine depletion) did not result in the expected increase in ornithine metabolite levels, rather the increase in abundance of OAT transcript/protein was shown to homeostatically control ornithine levels in the parasite [205]. An increase in OAT was not observed upon AdoMetDC- or spermidine synthase inhibition [2, 3], which deplete spermidine, but not putrescine, within the parasite. It was also not observed in many other perturbations unrelated to the polyamine pathway (parasite culture subjected to febrile temperature, artesunate, chloroquine, and the lethal anti-folate WR99210 [138, 139, 142, 144]).

As transcriptional regulation of OAT within *P. falciparum* parasites has been identified and confirmed in response to putrescine-depletion, the possibility of additional modes of regulation has been raised. Here, the relationship between polyamine metabolism and ornithine production in *P. falciparum* parasites was investigated on two separate levels, by particularly focussing on investigations of OAT. Firstly, the ability of the polyamines to act as effectors on the activity of OAT was determined. Additionally, we aimed to investigate the possibility of transcriptional level changes in OAT transcripts (and other enzymes in the polyamine pathway) upon exogenous addition of ornithine. Within the DFMO-treatment experiment, ODC is inhibited, which without any homeostatic control would theoretically result in an increase in ornithine levels. In the current experiment, exogenous ornithine was added to culture, thus mimicking part of the consequences of DFMO inhibition, but in the presence of functional ODC and thus sufficient putrescine and other polyamines. The difference between the two experiments is thus that DFMO results in a depletion of putrescine and concomitant reduction in spermidine. This then has an effect of a variety of processes within the cell. The supplementation experiment however should result in a cell containing all the polyamines required. If some measure of feedback regulation is present, it is expected that the OAT and/or ODC would increase to remove some of the excess ornithine.

4.2 MATERIALS AND METHODS

4.2.1 Biochemical investigation of the effect of polyamines on the activity of *P. falciparum* ornithine aminotransferase

4.2.1.1 Cloning of OAT into pGEM T-Easy

OAT was initially cloned using 3'-RACE (Rapid Amplification of cDNA Ends [269]). The sequence available in Genbank (accession number L15426) at the time of primer design (April 1999) was used. The forward primer (OATF1) was positioned over the start codon, while an anchored poly-T primer

was used as the reverse primer. The suitability of the primer was evaluated using OLIGO 4.1. The sequences and information of all the primers used are given in Table 4.1.

Table 4.1. Primers used for the cloning, sub-cloning and sequencing of OAT.

Primer name	Sequence (5' - 3')	Primer length	%GC	T _m ¹	3' ΔG (kcal/mol)	Most stable dimer (kcal/mol)
Anchor-poly-T ²	GCT ATC ATT ACC ACA ACA CTC T ₁₈ VN	41	21.95 - 26.83 ^a	36.8 - 40.9 ^b	-7.6	NA
OATf1	GTA AAA ATG GAT TTC GTT AAA G	22	27.27	50.94	-6.4	-5.3
Anchor	GCT ATC ATT ACC ACA ACA CTC	21	42.85	55.92	-6.4	-5.3
OATr1	ATG GAG CAC CTA ATT TAT CAG	21	38.1	53.97	-6.6	NA
OATEXf1	CTC GAG GAT TTC GTT AAA GAA TTA AAA AG	29	31.03	59.61	-7.3	-10
OATEXr1	GCT CAG CCT CAG TTA TAA <u>GTT</u> GTC ATC	27	44.44	63.45	-6.6	-10

¹: $T_m = 69.3 + (0.41 \times \%GC) - \frac{650}{L}$ where L is the length of the primer

²: The Anchor poly T primer has a degeneracy of 12

^a: minimum and maximum percentage GC respectively

^b: minimum and maximum T_m respectively (calculated for T₁₈VN only as anchor portion does not anneal)

Bold: recognition sequence of the appropriate restriction enzymes (OATEXf1: *Xho*1 and OATEXr1: *Cel*II) required for directional cloning into the pET15b expression vector.

Underlined: silent mutations to reduce primer pair compatibility

NA: not applicable.

P. falciparum RNA of good quality (as evaluated electrophoretically) was used for the synthesis of cDNA using the Anchor-poly-T primer. The RNA was isolated from *P. falciparum* parasite culture that was primarily in the ring stage. The erythrocytes were pelleted from the culture medium by centrifugation at 3000g for 10 minutes (Hermle Z320). The erythrocytes were incubated in 0.01% saponin at room temperature for 5 minutes and the released parasites pelleted by centrifugation at 3000g for 15 minutes (Hermle Z320). The parasite pellet was resuspended in 1x PBS, transferred to microfuge tubes and the parasites subsequently washed three times with 1 ml of 1x PBS. The washed parasite pellet was lysed by the addition of 2 ml of Tri-Reagent (Molecular Research Centre), followed by extensive homogenisation (Wheaton homogeniser). The homogenate was incubated at room temperature for 5 minutes, followed by the addition of 400 µl of chloroform. The mixture was vortexed thoroughly and incubated at room temperature for 10 minutes. After centrifugation at 11500g for 15 minutes (4°C, Sorvall RMC-14), the RNA containing upper aqueous phase was transferred to a clean microfuge tube and the RNA precipitated by the addition of 1 ml of isopropanol per 2 ml of Tri-Reagent used. Following incubation at room temperature for 10 minutes, the RNA was pelleted by centrifugation at 9400g for 10 minutes. The resulting RNA pellet was washed with 75% ethanol (1 ml per 1 ml of Tri-Reagent used). The pellets were allowed to air-dry and were resuspended in 80 µl of FORMAZol™ (Molecular Research Centre). The procedure was repeated with a mainly trophozoite containing culture and the RNA from the two isolations pooled to obtain a mixture of RNA from the parasite life-cycle.

PCR reactions of 50 µl each containing 25 ng of cDNA, 1x ExTaq PCR buffer (TaKaRa), 2 mM MgCl₂, 0.2 mM (each) dNTPS (TaKaRa), 10 pmol OATf1, 10 pmol anchor and 2.5 U of ExTaq DNA polymerase

(TaKaRa) were set up. The cycling conditions on the thermal cycler (Perkin Elmer, PE2400) consisted of 94°C for 3 minutes, followed by 2 minutes at 80°C (enzyme was added during hot start). The samples were then subjected to 28 cycles of 94°C for 30 seconds, 50°C for 30 seconds and 72°C for 2 minutes, followed by a final extension of 72°C for 7 minutes.

A volume (25 µl) was removed for conventional agarose electrophoresis and the remaining samples pooled. Glycerol (to a final concentration of 5% (v/v)) was added and the samples electrophoresed using a 1.5% agarose/TAE gel containing 10 µg/ml crystal violet. The electrophoresis buffer was also 1x TAE with 10 µg/ml crystal violet. The bands were excised and purified using silica [270]. Excess 6 M NaI (700 µl) was added to the gel slices and heated at 55°C for 10 minutes to melt the gel. Silica (20 µl) was then added and the tubes incubated at room temperature for 20 minutes with continual end-over-end mixing. This was followed by 15 minutes on ice, with occasional mixing. The silica was pelleted by centrifugation in a benchtop microfuge for 45 seconds, washed twice with 500 µl of wash buffer (10 mM Tris pH 7.5, 50 mM NaCl, 2.5 mM EDTA, 50% ethanol). The DNA was eluted by the addition of 30 µl of H₂O and incubation at 55°C for 5 minutes, followed by pelleting of the silica. The eluate was aspirated, the concentration determined spectrophotometrically and stored at -20°C until needed for ligation.

The purified OAT amplicon was ligated into pGEM® T-Easy using the pGEM® T-Easy kit (Promega) and following the manufacturer's instructions. Amplicon DNA (90 ng) was ligated to 50 ng of vector using 3 Weiss units of T4 DNA ligase in 1x ligation buffer. The reaction was incubated at 4°C for 16 hours and the enzyme inactivated at 70°C for 15 minutes. Five microlitres of the ligation mixture was subsequently transformed into 100 µl of competent SURE *E.coli*. The transformation proceeded with 30 minutes on ice, followed by 45 seconds at 42°C, then 2 minutes on ice. LB-Broth (900 µl containing 20 mM glucose) was added and the tubes incubated at 30°C, with vigorous shaking for 1 hour. Transformation mixture (100 µl) was plated onto LB-agar plates containing 100 µg/ml ampicillin and with 32 µl of 20 mg/ml X-gal and 4 µl of 200 mg/ml IPTG spread on the surface to enable blue-white selection. The plates were subsequently incubated at 30°C overnight. Six white potentially recombinant colonies were inoculated into 5 ml of LB-broth containing 50 µg/ml ampicillin and incubated at 30°C overnight with vigorous shaking.

Plasmid DNA was isolated from the bacterial cultures using the conventional mini-prep method [193]. The culture (4ml) was pelleted by centrifugation at 3000g for 10 minutes (Hermle Z252M). The supernatant was discarded and the cell pellet resuspended in 200 µl of Solution 1 (50 mM glucose, 25 mM Tris-HCl, 10 mM EDTA). Solution 2 (200 µl of 0.2M NaOH, 1% (w/v) SDS) was added, mixed

with end-over-end rotation and incubated on ice for 5 minutes, followed by the addition of 200 μ l of Solution 3 (3M potassium-acetate, pH 5.4) and incubation on ice for 10 minutes. The samples were centrifuged at 16100g (Sorvall RMC 14) for 15 minutes and the supernatants transferred to clean microfuge tubes. Biophenol (600 μ l, pH 7.8-8.2, ICN) was added and the tubes vortexed for 1 minute, followed by centrifugation for 2 minutes (16100g, Sorvall RMC14). The aqueous (upper) phases were aspirated and transferred to clean tubes. Chloroform:isoamylalcohol (600 μ l, 24:1) was added, followed by a brief vortex and centrifugation to define the layers. The aqueous phase was aspirated, transferred to clean tubes and 1 ml of ice-cold absolute ethanol added. The tubes were incubated at -70°C for 25 minutes, followed by centrifugation at maximum speed for 25 minutes (Sorvall RMC14). The supernatants were aspirated and discarded and the pellets washed with 700 μ l of 70% ice-cold ethanol. The tubes were centrifuged at maximum speed (Sorvall RMC14) for 7 minutes and the supernatants discarded. The pellets were dried *in vacuo* (Bachofer vacuum concentrator), then resuspended in 20 μ l of TE-buffer (10 mM Tris-HCl, 1 mM EDTA) containing 0.4 μ g/ μ l RNase A. Positive recombinant clones were identified by means of restriction digestion of 3 μ l of plasmid with 12 units *Eco*R1 in a 10 μ l reaction for 3 hours at 37°C. The samples were electrophoresed using 1% agarose/TAE.

In order to confirm the identity of the inserts in the recombinant clones, plasmid DNA was isolated for sequencing using the High Pure Plasmid Isolation Kit (then Boehringer Mannheim, now Roche) and following the manufacturer's instructions. The presence of inserts was confirmed with *Eco*RI digestion.

Sequencing reactions contained 210 ng of plasmid DNA, 1.6 pmol of primer (either T7, SP6 or OATr1 - as reverse internal primer starting at position 1269, designed and evaluated using OLIGO 4.1 (Table 4.1)) and ABI sequencing buffer and sequencing mix in a 20 μ l reaction. Cycling at 96°C for 10 seconds, 50°C for 5 seconds and 60°C for 4 minutes for a total of 25 cycles, preceded precipitation of the amplified products. Water (16 μ l) and 64 μ l of absolute (ice-cold) ethanol were added to the 20 μ l reaction mix. The tubes were briefly vortexed and incubated at room temperature for 15 minutes. This was followed by centrifugation at maximum speed (Sorvall RMC 14) for 15 minutes (at room temperature). The supernatants were carefully aspirated and the pellets washed with 100 μ l of 70% ethanol. The tubes were centrifuged for 10 minutes, the supernatants aspirated and the pellets dried *in vacuo* for 10 minutes. The sequencing gels were run by the sequencing facility of the University of Pretoria, following their optimised protocols.

4.2.1.2 Cloning of OAT into pET15b

Forward and reverse expression primers were designed using the OAT sequence. The primer sequences are given in Table 4.1. The 5'-end of each primer included the recognition sequence of the respective primers for directional cloning (*Xho*I in the case of OATEXf1 and *Ce*III for OATEXr1). It was also necessary to incorporate two silent mutations into the OATEXr1 sequence to prevent excessive primer pair complementarity.

The PfoAT insert was sub-cloned into the expression vector pET15b using the following strategy. First the appropriate restriction digestion sites were incorporated into the sequence by PCR amplification using the expression primers (OATEXf1 and OATEXr1) with plasmid DNA from a positive recombinant clone as template. This was then ligated into pGEM T-Easy and transformed into ultracompetent XL-2 Blue *E. coli* (Stratagene). Positive recombinant clones were identified using colony PCR and plasmid DNA was isolated from the positive clones using the High Pure Plasmid Purification Kit (Roche). The identity of the insert was confirmed by sequencing and the plasmid DNA was then digested with *Xho*I and *Ce*III to generate a sticky ended fragment for directional cloning. The pET15b vector was also digested with these two restriction enzymes. The insert and vector were ligated using the buffer and T4 DNA ligase from the pGEM T-Easy kit and transformed into ultracompetent XL2 Blue *E. coli*. Positive clones were again identified by colony PCR and isolated plasmid DNA sequenced.

Sequencing reactions contained either 440 ng (OATEX-pGEM) or 700 ng (OATEX-Pet15b) of plasmid DNA, 5 pmol of primer (OATEX-pGEM: T7, SP6 and OATr1, annealed at 50°C and OATEX-pET15b: OATEXf1 and OATEXr1, annealed at 56°C), 4 µl of 5x buffer and 2 µl of ABI Big Dye Ready Reaction sequencing mix and mix in a 20 µl reaction. Cycling at 96°C for 10 seconds, 50/56°C for 5 seconds and 60°C for 4 minutes for a total of 25 cycles, preceded precipitation of the amplified products. Sodium acetate (2 µl, 3 M, pH 5.4) and 50 µl of absolute (ice-cold) ethanol were placed in a clean tube and the 20 µl reaction added to this. This was followed by centrifugation at 16100g (Eppendorf 5415R) for 30 minutes (4°C). The supernatants were carefully aspirated and the pellets washed with 175 µl of ice-cold 70% ethanol. The tubes were centrifuged for 10 minutes, the supernatants aspirated and the pellets dried *in vacuo* for 10 minutes. The sequencing gels were run by the sequencing facility of the University of Pretoria.

4.2.1.3 Expression and purification of OAT

OATEX-pET15b (45ng) was transformed into chemically competent BL21 Star™ *E. coli* cells using heat shock [193]. Of the transformation mixture, 800 µl was added to 9.2 ml of LB-broth containing 50 µg/ml ampicillin and incubated at 37°C overnight, with vigorous shaking. Overnight culture (1 ml) was

inoculated into 198 ml of LB-broth containing 50 µg/ml ampicillin and incubated at 37°C for 3.5 hours (until the optical density at 600 nm was 0.4). Heterologous protein expression was induced by the addition of IPTG (final concentration of 100 µM). The culture was subsequently incubated at 30°C for a further 3.5 hours. The culture was centrifuged at 3000rpm (Beckman J6) for 10 minutes to pellet the cells.

Induced bacterial pellet (~1 ml) was lysed by the addition of 3 ml of Bugbuster reagent (Merck) and 4 µl of DNase 1 (Fermentas). Uninduced pellet was lysed with 1 ml of Bugbuster, with the addition of 1.8 µl of DNase 1. The tubes were rotated at 4°C overnight. Soluble protein was obtained by centrifugation of the lysate at 16000g (Eppendorf 5415R) for 30 minutes (at 4°C). The supernatant (containing soluble protein) was transferred to clean tubes and the insoluble protein pellet was retained for electrophoretic evaluation.

His-Select Nickel Affinity Resin was used for the immobilised metal affinity chromatographic purification of OAT. Beads (1 ml - capable of binding approximately 15 mg of protein) were washed with 2 column volumes of water, followed by 3 column volumes of equilibration buffer (50 mM sodium-phosphate pH 8, 0.3 M NaCl, 20 mM imidazole). The soluble protein fraction (~4 ml) was loaded and subsequently washed twice with 10 column volumes of equilibration buffer. The inclusion of 20 mM imidazole in the wash buffer used during IMAC was included to remove contaminants. The purified protein was eluted with 8 ml of elution buffer (50 mM sodium-phosphate pH 8, 0.3 M NaCl, 250 mM imidazole) and collected in four fractions of 2 ml each. Fraction 1 was subsequently dialysed overnight at 4°C against a buffer of 10 mM HEPES, 1 mM DTT and 1 mM EDTA, using Snakeskin dialysis tubing with a molecular weight cut-off of 10000 Da (Pierce). The concentration of dialysed OAT was determined using Bradford Reagent (Bio-Rad). A standard curve containing BSA at concentrations of between 1.25 and 15 µg/ml was prepared and the concentration of the dialysed protein, as well as fraction 2 of the eluted protein (each with a corresponding blank of the appropriate buffer) was determined. The homogeneity of the fractions was evaluated by SDS-PAGE using 12.5% acrylamide-methylene-(bis)-acrylamide gels (0.375 M Tris-HCl pH 8.8; 0.1% SDS; 0.05% ammonium persulphate; 0.5% *N,N,N',N'*-tetramethylethylenediamine (TEMED)), with a 4% acrylamide-methylene-(bis)-acrylamide stacking gel (0.125 M Tris-HCl pH 6.8; 0.1% SDS; 0.05% ammonium persulphate; 0.5% TEMED) stained with silver or colloidal Coomassie. The gels (10 cm x 8 cm x 1 mm) were electrophoresed using a Minigel G-41 (Biometra) at 60 V for the stacking and 80 V for the separating gels, in a running buffer of 0.25 M Tris; 0.1% SDS; 192 mM glycine, pH 8.3. For silver staining, the gels were fixed with 50% methanol:10% acetic acid:40% water for one hour, whereafter they were washed with 50% ethanol: 50% water for half an hour. The ethanol wash was repeated,

the gel then sensitised for 2 minutes in 0.02% (w/v) sodium thiosulphate, washed twice with water and incubated in 0.2% (w/v) silver nitrate solution for 20 minutes. After three water washes the gel was developed using a solution of 6% (w/v) sodium carbonate, 0.5% (w/v) sodium thiosulphate and 0.05% (v/v) formaldehyde and staining was stopped with the fix solution. For colloidal Coomassie staining, the gels were incubated overnight in Colloidal Coomassie Brilliant Blue G250 stock solution (2% (v/v) phosphoric acid, 10% (w/v) ammoniumsulfate, and 0.1% (v/v) Coomassie Brilliant Blue G250) diluted (4:1) with methanol, followed by a quick wash with 25% methanol:10% acetic acid. Destaining was in 25% methanol for 3 – 4 hours.

4.2.1.4 OAT activity assay

The assay for OAT was based on various aspects of a modified method described by Gafan *et al.* [96] for their characterisation of *P. falciparum* OAT and the original assay developed by Kim *et al.* [271]. The assay reaction contained 250 μ l of 2x phosphate buffer (200 mM sodium-phosphate pH 7.4), 10 mM α -ketoglutarate, 0.05 mM pyridoxal-5-phosphate, an appropriate volume of OAT (~15 μ l of the dialysed enzyme) and 15 mM ornithine in a final reaction volume of 500 μ l. All the reaction components except the substrate were equilibrated at 37°C for 2 minutes (AccuBlock™ Digital Dry Bath, Labnet International Inc) after which the reaction was initiated by the addition of ornithine and incubated for a further 20 minutes at 37°C. Subsequently, 75 μ l of 3 M HCl and 50 μ l of 2% ninhydrin were added and the reactions incubated at 100°C for 5 minutes. The reactions were cooled to room temperature and centrifuged at 14100g (Eppendorf MiniSpin plus) for 10 minutes to pellet the formed pigment which was solubilised in 250 μ l of absolute ethanol and again pelleted at 14100g (Eppendorf MiniSpin plus) for 5 minutes. The absorbance of the supernatant was measured at 510 nm (Shimadzu spectrophotometer). The amount of pigment present was calculated using a millimolar extinction coefficient of 16.5 [271] and the Beer-Lambert Law.

The pH of the assay is affected by the constituents, particularly the α -ketoglutarate. The α -ketoglutarate was thus prepared as a stock of 200 mM in 0.36 M NaOH (the pH of this solution is approximately 5.1). Of this, 25 μ l was added to the reaction for a final concentration of 10 mM and thus did not affect the pH significantly. It was also confirmed that the progress of the reaction did not result in a change in pH. The amount of OAT to add was determined by assaying with varying concentrations of enzyme (typically 5, 10, 15, 20 and 25 μ l of enzyme were added).

For the polyamine inhibition studies, 10 mM of putrescine, spermine, spermidine, cadaverine and ornithine (as an additional control), respectively were added to the reactions. The study employed three replicates, and each was performed in triplicate. The effect of ornithine concentration on OAT

activity was also determined by varying the ornithine concentration (15 mM, 30 mM and 45 mM ornithine were tested).

4.2.2 Effect of exogenously supplemented ornithine on the polyamine pathway related transcripts in *P. falciparum*

4.2.2.1 P. falciparum culture and treatment

Continuous 3D7 *P. falciparum* culture was maintained *in vitro* as described in Section 3.2.1.1. Any culture used for experiments was synchronised a minimum of three times [192].

4.2.2.2 Malstat

The Malstat assay [272] is based on the activity of lactate dehydrogenase (pLDH; in *Plasmodium* the enzyme is distinct from the human homologue) giving an indication of parasite viability. In the presence of pLDH and the coenzyme APAD (3-acetylpyridine adenine dinucleotide) L-lactate is produced from pyruvate. This results in the formation of reduced APAD, which then reduces nitroblue tetrazolium (NBT). This blue formazan (reduced NBT) product can then be measured spectrophotometrically [273].

Serial two-fold dilutions of ornithine were prepared in complete culture medium from 500 mM to 7.813 mM and also included the ten-fold dilution 0.7813 mM. A 96-well culture plate was used for the experiment and included each of the dilutions (50 µl), while 50 µl of complete culture medium was placed in the control wells. To each well, 50 µl of either ring stage parasite culture (1% parasitaemia, 10% haematocrit), washed erythrocytes (10% haematocrit) or complete culture medium was added. Due to the dilution the final haematocrits were 5%. Each sample was tested in triplicate. The plate was incubated at 37°C in a gas chamber (5% O₂, 5% CO₂ and 95% N₂) for 48 hours.

Subsequently, 100 µl of Malstat™ reagent (0.2% (v/v) Triton-X 100 was added to 0.1 M Tris-HCl pH 9.1, followed by the addition of 2.1% (w/v) lithium-lactate, and 0.022% (w/v) APAD) was added to the wells of a clean 96-well ELISA plate. The culture and control samples from above were resuspended by pipetting and 6 µl from each well transferred to the Malstat™ reagent-containing plate. To this, 25 µl of freshly prepared NBT/PES (phenazine ethosulphate) solution (a 240 µM PES (Sigma) solution was prepared with NBT (Sigma) added to a final concentration of 2 mM and kept in the dark) was added to each well. The plate was incubated in the dark for 30 minutes, 30 µl of 10% acetic acid added and the intensity of the developed colour read at 650 nm on the Multiskan Ascent V1.24

scanner (Thermo Labsystems). The replicates were averaged and the background (uninfected erythrocytes) subtracted. A dose response curve was plotted using SigmaPlot 2004 for Windows, version 9 (Systat Software Inc).

4.2.2.3 Treatment and harvesting of parasites for real-time PCR analyses

Ornithine (50 mM) was prepared in complete culture medium. Early ring stage *P. falciparum* parasites (~2 hours post-invasion) at a parasitaemia of ~7% was used. The culture was pelleted by centrifugation at 1500g for 5 minutes (Hermle Z320) and resuspended in the original volume of medium (either ornithine-treated or untreated). This resuspended culture (2 ml) was placed into a well of a 12-well sterile culture plate (in triplicate). The plate was placed in a gas chamber (see Section 4.2.2.2) and incubated at 37°C for 24 hours. Following this, the cells were pelleted by centrifugation at 6000g (Hermle Z252M) for 5 minutes. The supernatant was aspirated and the cells washed with 2 ml of 1x PBS. The cells were again pelleted by centrifugation (6000g, 5 minutes), the supernatant aspirated and the pellets frozen at -70°C.

4.2.2.4 RNA isolation and cDNA synthesis

RNA was isolated from the pelleted cells using the protocol described in Chapter 2 (Section 2.2.1.4). Some modifications to the volumes used were made due to the smaller sample size: 600 µl of Buffer RLT was added to the sample, mixed and transferred to one QIA-Shredder column. Following centrifugation and transfer to a clean tube, 600 µl of TRI-Reagent was added, split into two fractions and incubated. Subsequently 300 µl of chloroform was added to each, incubated and centrifuged. Ethanol (500 µl of 70%) was added to the aqueous layer obtained and this was loaded onto one RNeasy column. The RNA was eluted into 30 µl of water.

cDNA was synthesised from ~500 ng RNA with 12 pmol of poly-T primer (T₂₃VN) and 24 pmol of random nonamer in 20 µl final volume. The reactions were incubated at 70°C for 5 minutes, followed by 5 minutes on ice. The remainder of the reaction components were subsequently added as a mastermix with final concentrations of 1x ImProm-II™ reaction buffer (Promega), 3 mM MgCl₂, 0.5 mM dNTP mix, ImProm-II™ Reverse transcriptase (2 µl per 40 µl reaction) and water to a final reaction volume of 40 µl. The reactions were incubated at 25°C for 5 minutes, followed by 42°C for 1 hour. The enzyme was then inactivated by 70°C for 15 minutes. All the incubation steps were performed in a thermal cycler (Applied Biosystems). Any remaining RNA was hydrolysed by the addition of 8 µl of 0.5 M EDTA and 8 µl of 1 M NaOH with incubation at 65°C for 10 minutes.

The cDNA was then purified using the QIA-Quick PCR Purification Kit (QIAGEN). Five volumes of Buffer PBI were added to the cDNA sample. This contains a pH indicator and since the NaOH concentration was high, the pH was too alkaline for binding and was lowered by the addition of 10 μ l of 3 M Na-acetate (pH 5). The sample was loaded onto the column centrifuged for 1 minute at 14100g (Eppendorf MiniSpin Plus). Buffer PB (750 μ l) was added and the samples centrifuged at 14100g for 1 minute. The flow-through was discarded, the column centrifuged for a further 1 minute and then transferred to a clean microfuge tube. The purified cDNA was eluted by the addition of 30 μ l of water, incubation at room temperature for 2 minutes and centrifugation at 14100g for 1 minute. The concentration was determined using the Gene Quant.

4.2.2.5 Semi-quantitative real-time PCR

The primers that were designed for the real-time PCR validation of the SSH-microarray were employed for these experiments, along with several primer sets designed by Tharina van Brummelen (TvB) [205] and a primer set for spermidine synthase designed by John Becker (JB) [3] (Table 4.2).

Table 4.2. Information for primer sets employed for real-time PCR.

Primer name	Position	Primer sequence (5' - 3')	Product length (bp)	Primer length (bp)	Most stable dimer (kcal/mol)	ΔG 3' (kcal/mol)	%GC	T _m ¹	Design
OATf	495	CAA CTT TGG TCC ATT CGT ACC	165	21	-5	-6.7	47.6	58	KC
OATr	637	GCT ACA CCT GGG AAA TAA CTA TC		23		-5.7	43.5	59	
LDHf	205	GAT TTG GCT GGA GCA GAT GTA	169	21	-4.7	-5.7	47.6	58	KC
LDHr	348	CAA CAA TAA TAA AAG CAT TTG GAC AA		26		-6.7	26.9	55	
SAMDC/ODCf	694	AAT CAA TTC CAT GAC GCT TAT CTG	165	24	-5.3	-6.6	37.5	58	KC
SAMDC/ODCr	835	ACA ATT CAC CAT TCC TGT ATC TTC		24		-6.7	37.5	58	
LDCf	2778	AGA GGG ATA TGG ATT GGT AGA	161	21	-5.7	-5.5	42.9	56	TvB
LDCr	2916	TTC TCT TCA TGT ATG ATA CAG TA		23		-5.8	30.4	54	
ARGf	69	CGT TTC CAT TAT TGG TTC TC	164	20	-5	-6.7	40.0	53	TvB
ARGr	208	GTT TCA TTT CAT TAT CCC CAT TAT C		25		-6	32.0	56	
MATf	273	TTT AGA TTA CAA AAC GGC AGA GAT AA	160	26	-5.3	-6	30.8	57	TvB
MATr	407	AGG CAT ATA ATT CTC AGT TTC ATC AG		26		-6.6	34.6	58	
SPDf	650	ACA ACG CCC TAA AGC CTA AC	70	20	-10	-5.8	50	57	JB
SPDr	718	ATT GTT CCC ACG TGT ATC CAG		21		-8.2	47.6	58	

¹ calculated annealing temperature ($T_m = 69.3 + (0.41 \times \%GC) - (650/L)$, where L is the primer length) [201].

A standard curve for lactate dehydrogenase (LDH) was produced using cDNA from an untreated sample. A dilution series of the cDNA was prepared (4.3 ng, 0.43 ng, 0.215 ng, 0.086 ng and 0.043 ng) and 2.5 μ l used per reaction. Five pmol of each primer (in this case, LDHf and LDHr) was used, along with the KAPA™ SYBR® FAST qPCR kit (Mastermix (2x) LightCycler® 480) from KAPA Biosystems. Duplicate 10 μ l reactions were set up for each of the cDNA dilutions, along with a negative control. The cycling conditions on the LightCycler 480 (Roche) are given in Table 4.3.

Table 4.3. Cycling conditions for amplification using the LightCycler 480.

Name	Analysis mode	Cycles	Target temperature	Hold time	Acquisition mode	Ramp rate (°C/s)
Pre-incubation	None	1	95°C	10 min	None	4.8
Amplification	Quantification	40	95°C	10 sec	None	4.8
			55°C	5 sec	None	2.5
			72°C	7 sec	Single	4.8
Melting curves	Melting curves	1	95°C	5 sec	None	4.8
			65°C	5 sec	None	2.5
			95°C		Continuous (5 per °C)	0.11
Cooling	None	1	40°C	30 sec	None	2.5

Real-time PCR was performed on the ornithine-supplemented samples, relative to the unsupplemented samples using the primers indicated in Table 4.1. In each case 5 pmol of the appropriate primer was used, with 1.625 ng of template cDNA and the KAPA™ SYBR® FAST qPCR kit. Cycling on the LightCycler 480 was as in Table 4.3. The ratio of supplemented sample over unsupplemented was normalised against LDH.

4.3 RESULTS

4.3.1 Biochemical investigation of the effect of polyamines on the activity of *P. falciparum* ornithine aminotransferase

4.3.1.1 Cloning of PfOAT

P. falciparum OAT was amplified from parasite RNA using 3'-RACE. Figure 4.2 (a) shows the single band expected at ~1300 bp. Purified product was cloned into pGEM T-Easy and positive clones containing inserts of the correct size obtained, the identity of which was confirmed by nucleotide sequencing as being OAT from *P. falciparum* parasites. PfOAT was subsequently sub-cloned into pET15b for expression by re-amplification of the full-length amplicon with cloning ends (Figure 4.2 (b)). Amplicons (PfOATEX) were again cloned into pGEM T-Easy to facilitate sub-cloning into pET15b and transformants containing positive inserts were identified by a colony screening PCR. Both pET15b plasmid and plasmid from a positive OAT clone were isolated and digested with the restriction enzymes *Xho*I and *Bsp*I (*Cel*II) to obtain sticky ended products (Figure 4.2 (c)). The bands were excised from the gel, purified and ligated.

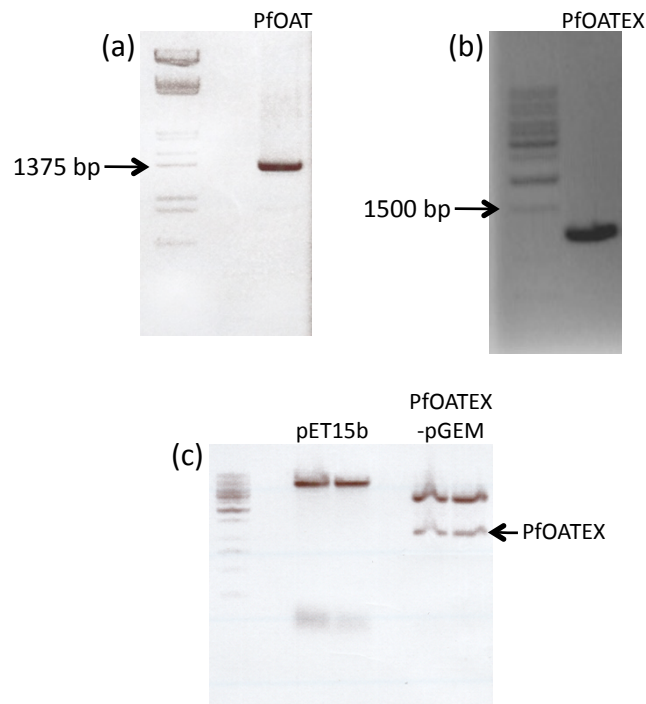


Figure 4.2. Cloning of PfoAT for heterologous protein expression in *E.coli*. (a) Amplicon obtained from PCR using OATf1 and Anchor primers for cloning of PfoAT into pGEM T-Easy (1.5% agarose). (b) Amplicon obtained from PCR using expression primers (OATEXf1, OATEXr1) for sub-cloning of PfoATEX into pGEM T-Easy (1.5% agarose). (c) Sticky ended products obtained after *Xho*1 and *Bsp*1 (*Cel*II) digestion for sub-cloning of PfoATEX into pET15b (1% agarose).

Colony PCR screening of the transformants was again used to identify positive clones. The inserts of the positive clones obtained were sequenced to confirm the correct sequence and orientation of the reading frame.

4.3.1.2. Expression of PfoAT

OATEX-pET15b was transformed into BL 21 Star™ *E. coli* and induced with IPTG to allow heterologous protein expression. SDS-PAGE (Figure 4.3) revealed that induced cells have an increase in the amount of protein present at around 45 kDa. This additional protein also appears to be distributed between the soluble and insoluble protein fractions. PfoAT has a molecular mass of 46 kDa. No leaky expression of OAT is visible in the uninduced sample.

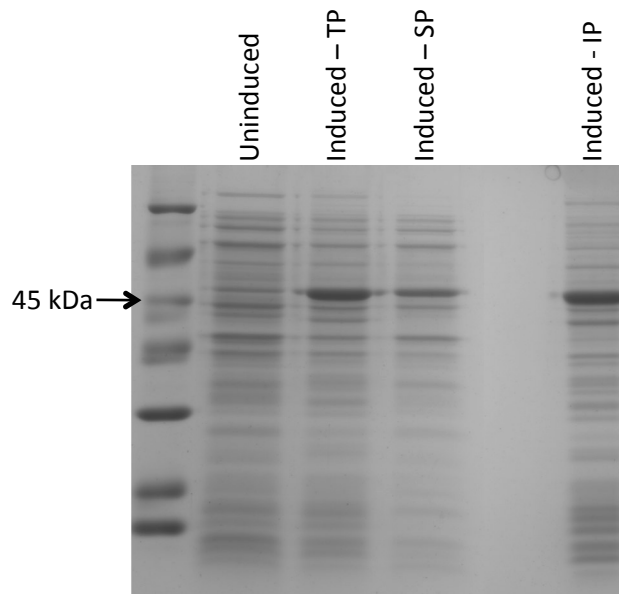


Figure 4.3. Protein expression in PfoAT-PET15b transformed IPTG induced and uninduced BL 21 Star™ *E. coli* cells. The total protein (TP) from the induced cells was separated into soluble (SP) and insoluble (IP) protein fractions. 12.5% SDS-PAGE gel stained with colloidal Coomassie.

The soluble protein fraction was used for further purification with IMAC (His-tag). SDS-PAGE of the eluted fractions indicated that the ~45kDa protein was significantly more homogenous, as no contaminating proteins are visible on the silver stained gel (Figure 4.4). Eluted fractions 1 through 4 all contain protein, although much of it is in fractions 1 and 2. Mass spectroscopy confirmed that the protein present is *P. falciparum* OAT (Mascot score: 17660).

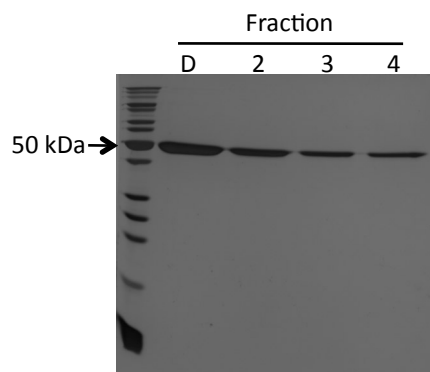


Figure 4.4. Typical silver stained, 12.5% SDS-PAGE gel of IMAC-purified PfoAT. The gel was loaded with marker and dialysed OAT fractions 1 (D), 2, 3 and 4.

4.3.1.3 Assay of PfoAT in the presence of polyamines

Gafan *et al.* determined that the K_m of PfoAT is 3.95 ± 1.04 mM [96] and they used 50 mM ornithine in their assay as opposed to the 30 mM used by Kim for the mouse OAT (K_m is 2.9 mM) [271, 274]. However, at equimolar (50 mM) concentrations of substrate (ornithine) and spermine, a precipitate was observed. This was also true at a concentration of 25 mM each, whereas 10 mM showed no

apparent precipitate formation. A combination of 10 mM polyamine and excess (15 mM) ornithine was subsequently used.

The linear progression of product formation with increasing enzyme concentration is evident in Figure 4.5 ($R^2 = 0.98$).

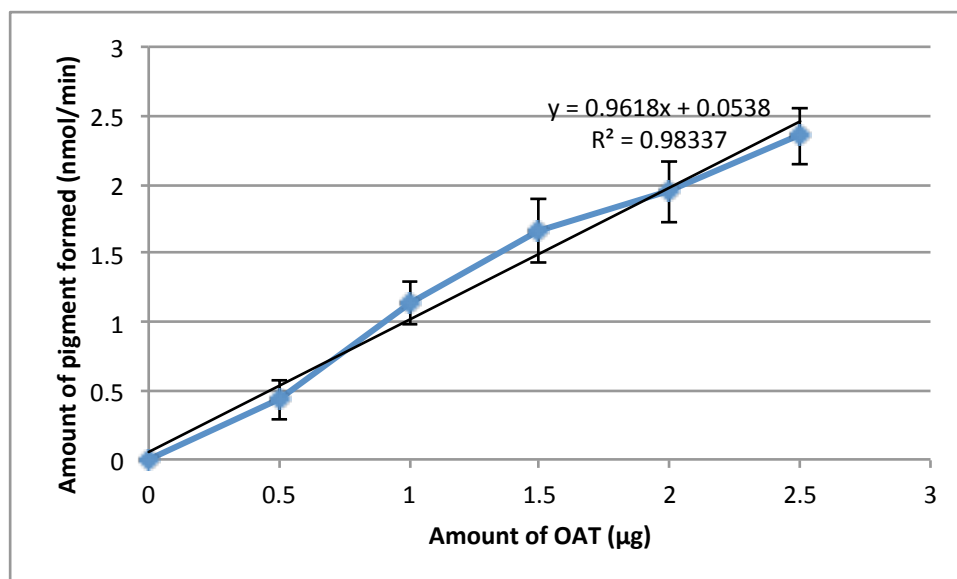


Figure 4.5. Relationship between OAT concentration and enzyme activity, as determined by the amount of pigment formed per minute. Data are representative of three biologically independent experiments each performed in triplicate \pm standard deviation.

The specific activities obtained for the three protein isolations used for this experiment were 967, 968 and 1082 nmol/min/mg protein respectively.

Subsequently, the effect of the presence of several polyamines (putrescine, spermine, spermidine, cadaverine) and additional ornithine (substrate) on the activity of PfOAT was determined in order to elucidate if any change in activity is observed that can be attributed to regulation (Figure 4.6).

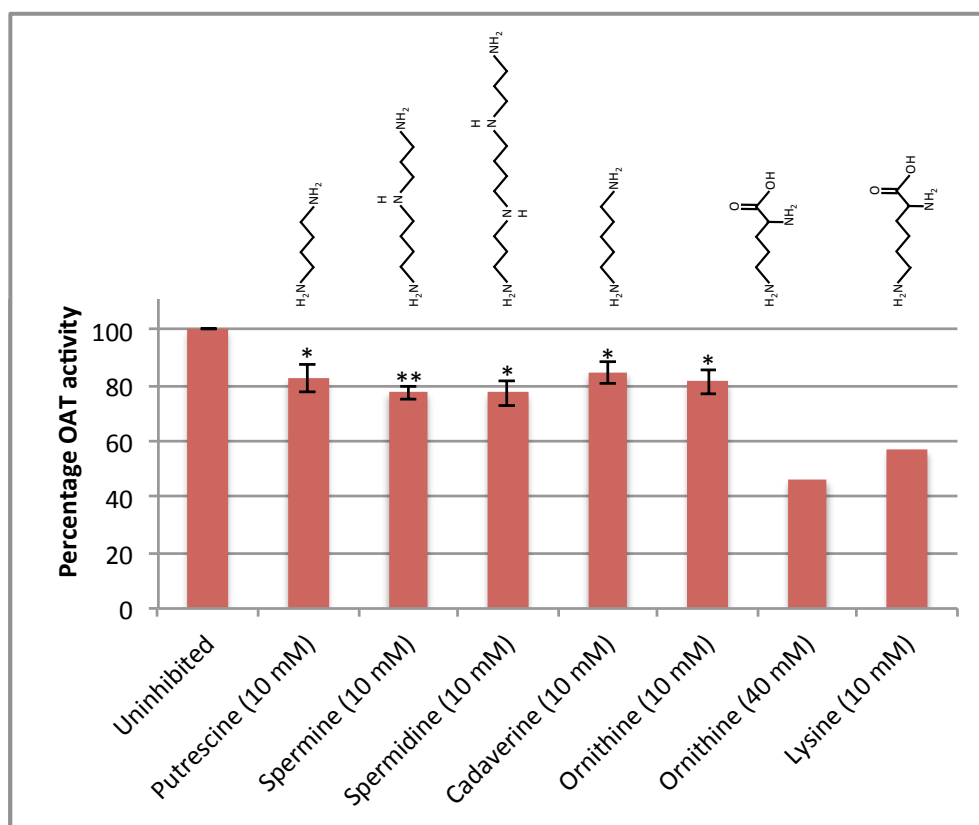


Figure 4.6. The effect of polyamines (putrescine, spermine, spermidine, cadaverine), ornithine and lysine on the activity of PfOAT in the presence of 15 mM ornithine and 10 mM α -ketoglutarate. Data represent three biologically independent experiments (except ornithine (40 mM) and lysine, $n=1$), each performed in triplicate \pm standard error deviation. * $P<0.05$ and ** $P<0.01$ for a two-tailed t -test, $n=3$, using the arcsine of the percentage remaining OAT activity.

When the addition of exogenous polyamines is compared with the untreated control, the presence of the polyamines significantly ($P<0.05$, two-tailed t -test, $n=3$, using the arcsine of the percentage remaining OAT activity) decrease OAT activity to approximately 80% of the uninhibited activity. However, it does appear as if this effect is non-specific, as all the added compounds were able to reduce OAT activity. The addition of lysine also appears to have an inhibitory effect as only 56% of the enzyme activity remains. Treatment with ornithine (substrate) resulted in a concentration-dependent decrease in OAT activity, with only $46.3 \pm 1.7\%$ of the activity remaining at high ornithine concentrations.

4.3.2 Effect of exogenously supplemented ornithine on the polyamine pathway related transcripts in *P. falciparum* parasites

The transcriptomic profiling presented in Chapter 2 revealed that DFMO-induced ODC inhibition affected several transcripts of proteins closely related to polyamine metabolism in the parasite. This also highlighted that the parasite compensated for increased ornithine concentration (due to lack of

further ornithine processing into putrescine by the inhibited ODC) by increasing the number of OAT transcripts present, thereby resulting in homeostatic control of ornithine levels.

To metabolically mimic increased levels of ornithine that may be present in ODC-inhibited parasites, exogenous ornithine was added to *in vitro* cultivated *P. falciparum* parasites. To obtain an indication of the concentration of ornithine to be used in the experiment, the IC_{50} of ornithine for *in vitro* *P. falciparum* culture was determined. The parasites showed a dose-dependent response to the addition of the exogenous ornithine, with the IC_{50} of ornithine calculated as 67.20 ± 1.06 mM (Figure 4.7).

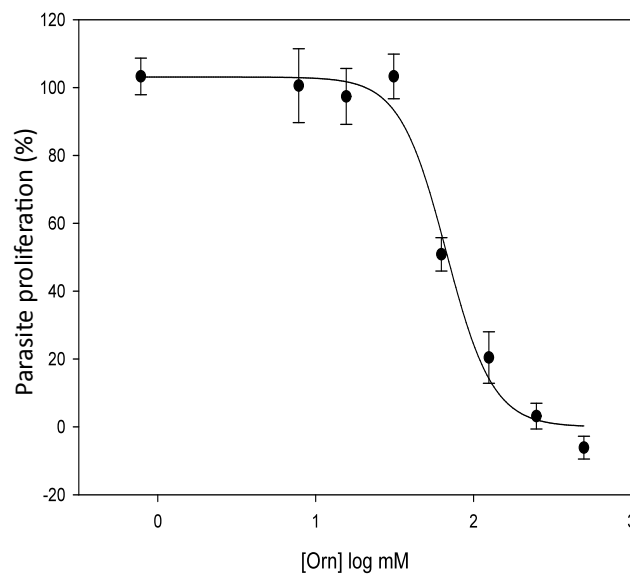


Figure 4.7. Dose-response curve of ornithine supplemented *P. falciparum* parasites *in vitro*. Ring stage parasites were supplemented with various concentrations of ornithine and the Malstat assay was performed after 24 hours. A percentage response to the treatment was calculated by dividing supplemented by unsupplemented response and multiplying by 100. The error bars represent the standard error of the mean.

In vitro parasite cultures were thus treated with exogenous ornithine at 50, 125 and 250 mM. RNA was isolated, converted to cDNA and used for semi-quantitative real-time PCR monitoring of selected transcripts. Figure 4.8 presents the results of treatment of *P. falciparum* with 50 mM exogenous ornithine on the levels of selected transcripts related to the polyamine biosynthetic pathway, normalised to LDH (average fold change of LDH prior to normalisation was 0.98, while that of an RNA spike included in one of the replicates to confirm normalisation was 0.994).

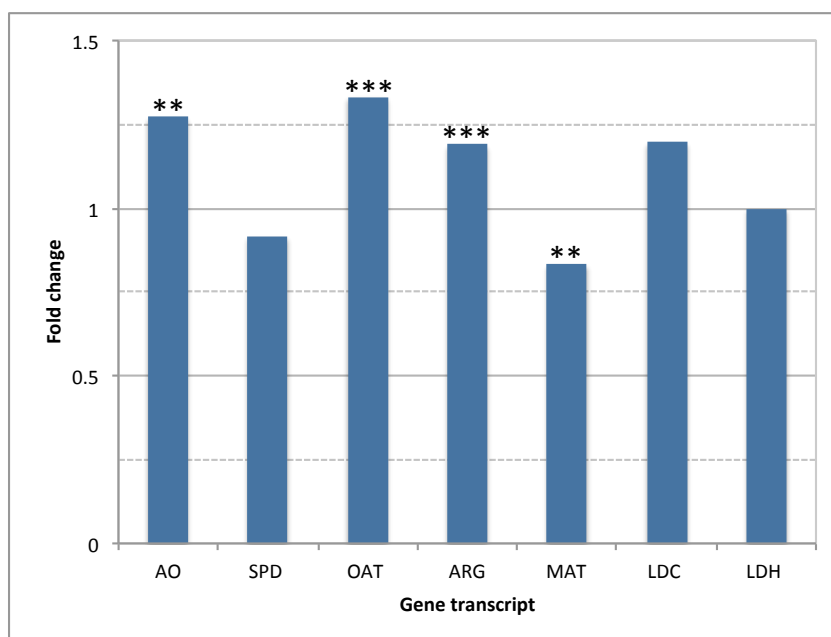


Figure 4.8. Effect of 50 mM ornithine on the various transcripts in the polyamine pathway, normalised to LDH. AO: AdoMetDC-ODC; SPD: spermidine synthase; OAT: ornithine aminotransferase; ARG: arginase; MAT: S-adenosylmethionine transferase; LDC: lysine decarboxylase and LDH: lactate dehydrogenase. The *P*-value was calculated using a paired *t*-test, as calculated using the raw data (normalised to the average value for LDH) and comparing treated with untreated values for each gene, respectively. ** $P < 0.01$ and *** $P < 0.001$. Data indicate the fold change difference between ornithine supplemented and unsupplemented parasites and are representative of three experiments, performed in triplicate.

A statistically significant increase of 1.33-fold ($P = 0.0007$, $n = 3$) in OAT transcripts was observed when the parasites were supplemented with 50 mM exogenous ornithine. Additionally, a significant increase in the transcripts for AdoMetDC-ODC and arginase and a decrease in MAT was also evident. At 50 mM, the concentration of ornithine added exogenously is slightly below the IC_{50} value calculated for ornithine (0.74x) and the results should thus give an indication of the situation in the parasites upon addition of the exogenous ornithine, without too much confounding of the observations by a death or stress response. However, parasites treated with exogenous ornithine at concentrations of 125 mM and 250 mM showed general stress responses, as observed from the decrease in abundance of household gene transcripts like LDH and cyclophilin (Figure 4.9).

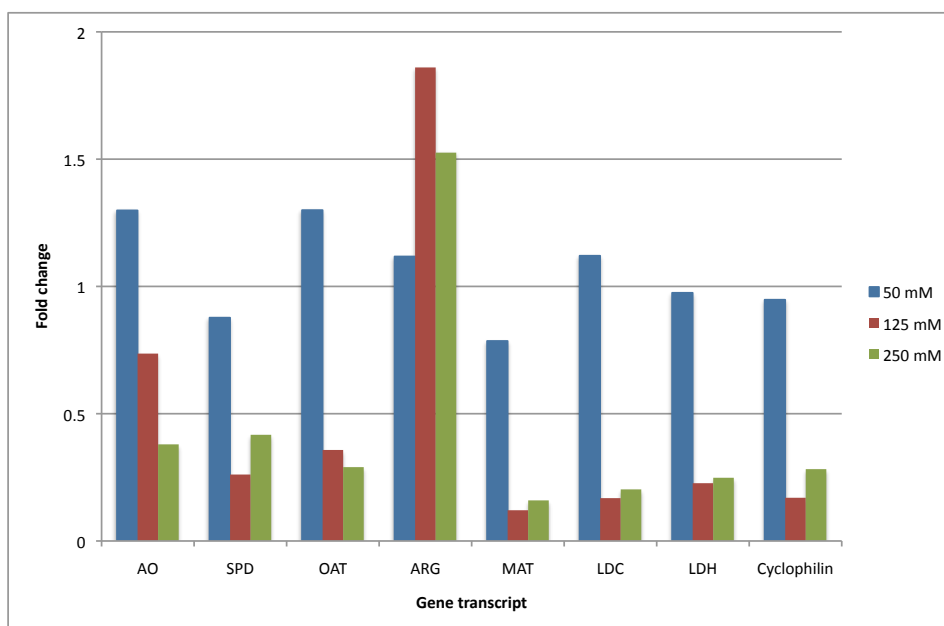


Figure 4.9. Fold change of various transcripts within the polyamine pathway upon addition of varying concentrations (50 mM, 150 mM or 250 mM) of ornithine. This data is not normalised as at the two higher concentrations of added reagent, the house-keeping genes are adversely affected. Data indicate the fold change difference between ornithine supplemented and unsupplemented parasites and are representative of three experiments, performed in triplicate.

From Figure 4.9, it is also apparent that with increasing concentrations of ornithine, the number of transcripts for arginase increases, while all the other transcripts (including the household genes) are negatively affected and show a marked decrease in transcript abundance. This observation of increased arginase transcripts is not limited to ornithine supplementation, but was also observed with exogenous supplementation of lysine (although the values only increase dramatically at 250 mM (2.29x) compared with 1.13x at 125 mM - results not shown) and in other studies upon supplementation with methionine (1.99x at 100mM) [2].

4.4 DISCUSSION

4.4.1 Biochemical investigation of the effect of polyamines on ornithine aminotransferase

Regulation of OAT within mammalian species has been well characterised, as OAT deficiency (autosomal and recessively inherited) leads to an intra-ocular rise in ornithine concentrations, which over a period of several decades leads to gyrate atrophy of the choroid and retina [275]. Within two human retinoblastoma lines that synthesise OAT at different rates, both had equivalent amounts of mRNA, yet different protein concentrations and activities. Differences in concentration of translation initiation factor eIF-4E were found, implying that cellular levels of eIF-4E were capable of modulating OAT translation through post-transcriptional regulation mechanisms [276]. OAT activity can also be

regulated by various metabolites. Although putrescine (8%) showed no effect on rat brain, inhibition of OAT activity was observed upon addition of amongst others, L-valine (41% inhibition), and the polyamines spermine (56%) and spermidine (48%) [266]. Organ/tissue specificity also plays a role. In the liver, there is a transcriptional and translational increase induced by glucagon, cAMP or a protein-rich diet, which can be repressed by glucose. In the kidney, glucagon and protein play no role, but oestrogen and thyroid hormone result in an increase in transcription of OAT [276]. OAT from *Bacillus sphaericus* was found to be inducibly formed by the addition of L-arginine and L-ornithine to the medium, while inhibition of enzyme activity through the addition of L-lysine (35% inhibition), L-arginine (28%), L-valine (35%), cadaverine (57%) or putrescine (63%) occurs [265]. The pea plant (*Pisum sativum*) also shows a weak inhibitory effect of putrescine (K_i : 90 mM), spermidine (K_i : 25 mM), spermine (K_i : 17 mM) and several other di- and polyamines upon OAT activity [267].

The ability of different metabolites, including ornithine, to affect the activity of PfOAT was investigated here. Although the addition of polyamines or ornithine results in approximately a 20% decrease in OAT activity (statistically significant), this reduction appears to be non-specific, as all the added compounds produce a similar result, irrespective of size. The presence of charged compounds creating a non-specific inhibition could be one explanation, though spatial configuration may also play a role as is shown by increased inhibition by lysine (56% residual activity) compared with ornithine (~80% residual activity). Inhibition of OAT by amino acids is not unknown. Rat brain OAT is inhibited by valine, leucine and isoleucine [266] and *B. sphaericus*, by lysine, arginine and valine [265]. Of these lysine and arginine are positively charged at physiological pH (like the polyamines), though leucine, isoleucine and valine are all non-polar. An alignment (Supplementary Material S8, Figure S8.1) of the protein sequence of human and *P. falciparum* OAT, with the three proteins capable of being inhibited by amines (*B. sphaericus*, *P. sativum*, *R. norvegicus*) shows a large degree of conservation between all five species. A substrate binding loop in PfOAT contains two cysteine residues that are conserved in *Plasmodium* species, but do not occur in other species. These residues mediate binding of thioredoxin to PfOAT and this facilitates a modulation of PfOAT activity, where thioredoxin stimulates PfOAT activity *in vitro* 10-fold [268]. This, along with other differences may be the reason for non-specific inhibition exerted by the polyamines on PfOAT. Docking studies to elucidate the potential of polyamines and other (charged) amino acids to interact with PfOAT would be a feasible next step.

4.4.2 Effect of exogenously supplemented ornithine on the polyamine pathway of *P. falciparum* parasites

To confirm that the increase in OAT transcripts observed upon DFMO-treatment (Chapter 2 and [1]) is indeed a drug specific response and to determine the effect of increased ornithine on the enzymes of the polyamine pathway in the presence of functional ODC, exogenous ornithine was added to *P. falciparum* parasite culture. Table 4.4 highlights the results obtained upon ornithine supplementation and compares them with those observed upon ODC-inhibition.

Table 4.4. Comparison of differences observed in polyamine related transcripts upon ODC inhibition (T1: 23 hpi; T2: 31 hpi) and ornithine supplementation (26 hpi).

	ODC-inhibition		Ornithine supplementation
	T1	T2	
AdoMetDC/ODC	↓	↓	↑
Spermidine synthase	~	~	~
OAT	↑↑↑	↑↑	↑
Arginase	~	~	↑
S-adenosylmethionine transferase	↓↓↓	↓↓↓	↓
Lysine decarboxylase	↑↑	↑	~
Lactate dehydrogenase	↓	↓	~
Cyclophilin	~	~	~

An increase in both AdoMetDC-ODC and OAT transcript levels was observed upon ornithine supplementation (Table 4.4), indicating at least a transcriptional level of regulation for these enzymes. A significant difference between the ODC inhibition and ornithine supplementation experiments is that with inhibition AdoMetDC-ODC transcript levels tends to decrease (see Chapter 2 and [1]), whilst with ornithine supplementation, AdoMetDC-ODC transcript levels start increasing. As it would be expected that the parasite would attempt to replace the deficit of AdoMetDC-ODC upon inhibition, this seems somewhat contradictory. This may potentially be explained by the role of the polyamines within the cell, and that AdoMetDC-ODC expression is somehow affected by the polyamines, as when sufficient polyamines are present, the cell compensates for increased ornithine by producing increased AdoMetDC-ODC and OAT. However, AdoMetDC-ODC is the rate-limiting enzyme of the polyamine pathway so alternative methods of regulation of ODC should also not be excluded. The bifunctional nature of AdoMetDC-ODC also provides some regulatory effects on the individual enzyme activities [85, 86]. Of the two enzymes catabolising ornithine, it appears that ODC is the most specific (K_m : 41 μ M), but that OAT is the faster enzyme, as OAT (K_m : 1.6 mM) has a k_{cat} of 9.76 s^{-1} [268], compared with ODC, which has a k_{cat} of approximately 0.05 s^{-1} [86]. The k_{cat}/K_m is a

measure of the catalytic efficiency of an enzyme, as it relates turnover with substrate specificity [277]. OAT has a value of $6.1 \text{ s}^{-1}\text{mM}^{-1}$, compared with ODC at $1.2 \text{ s}^{-1}\text{mM}^{-1}$ and is thus more efficient. It has also been calculated that OAT is approximately 1% of the protein of the parasite cytosol (unlike many OATs, PfOAT has no mitochondrial targeting sequence) [268]. Substrate availability however, also plays a role and the intracellular concentration of ornithine is calculated to be $28.5 \mu\text{M}$ [85], below the K_m of ODC and well below that of OAT. It thus seems likely that the scenario in malaria is that ornithine will primarily be used for the production of polyamines by the more specific ODC, unless ornithine concentration starts increasing (as is likely the case with DFMO-treatment). At this point the more efficient OAT has sufficient capacity to rapidly remove it from the system. Excretion of ornithine to the extracellular environment also occurs [278]. The effect of co-inhibition of OAT (with 5-fluoromethylornithine - a specific and irreversible inhibitor of OAT) and ODC would thus prove useful in determining what other effects ornithine accumulation would have within the parasite. Co-inhibition of OAT with canaline and of ODC with DFMO has been performed and proved to act synergistically. However, as canaline is not OAT specific and also inhibits aspartate aminotransferases (involved in methionine regeneration) and diverse PLP-dependent enzymes, this is not a true indication of the consequences of co-inhibition of OAT and ODC [279]. In mice, the concomitant addition of 5-fluoromethylornithine and DFMO in their drinking water resulted in blood ornithine concentrations that were a factor of 2-3 higher than in those receiving only 5-fluoromethylornithine [275].

A decrease in the abundance of MAT transcripts is noted. It was speculated that decarboxylated AdoMet is the limiting factor in spermidine production [85] and it has been shown that AdoMetDC activity is modulated by the hinge ODC region of the bifunctional protein, thus ensuring that metabolically important AdoMet is not pre-emptively removed from the system [86]. Within *Leishmania*, MAT levels are capable of being post-translationally regulated by 26S proteasomal degradation and AdoMet concentration is thus maintained in a MAT over-expressing *Leishmania* culture [280]. This may therefore indicate another regulatory point to ensure that even though excess putrescine may be available (through ODC action) for spermidine synthesis, the reaction does not proceed, as there is a shortage of dcAdoMet (Figure 4.2). This may provide time for the regulation and maintenance of ornithine levels to occur. This is substantiated by the fact that no change was observed in spermidine synthase transcript levels, indicating the disruption in ornithine homeostasis had been satisfactorily dealt with.

In theory, arginase transcript abundance would decrease in order to prevent any additional ornithine formation (Figure 4.2). Although feedback regulation of arginase is possible, the K_i of ornithine for

arginase is 19 mM, while the physiological ornithine concentration within the parasite is 28.5 μ M [78, 85]. It should also be noted that the intracellular ornithine concentration in ornithine-supplemented parasites remains unknown and should be determined in future work on this topic. Upon ornithine supplementation, arginase transcript abundance started showing an inexplicable tendency to increase, contrary to what was expected. In a metabolomic study of the parasite, Olszewski *et al.* observed that much of the arginine obtained from haemoglobin digestion is converted to ornithine (through the action of the parasites arginase) and that this is then exported and thus it does not accumulate within the parasite. Various reasons for this are proposed, one being that a reduction in plasma arginine concentrations modulates the effect of host nitric oxide synthase, thus protecting gametocytes from nitric oxide mediated inactivation and increasing infectivity [278]. It is thus possible that under the stress condition induced by increasing the concentration of ornithine (which proved to be toxic to *E. coli* at high concentrations [281]), the parasite employs one of its inherent 'defense mechanisms'.

4.5 CONCLUSION

The aim of the work presented in this chapter was to provide supplementary information on the effect of ornithine accumulation and whether the polyamines fulfil a regulatory role upon OAT activity within the *P. falciparum* parasite. An increase in the ornithine concentration without the decrease in putrescine concentration also results in an increase in OAT transcripts observed upon ODC-inhibition. An increase in AdoMetDC-ODC and an inexplicable increase in arginase were also observed. The increase in arginase transcripts was observed in several other perturbations (excess lysine, methionine and several others) and is possibly indicative of a stress response within the parasite.

Upon the addition of exogenous polyamines to PfoAT, inhibition of activity occurs though it appears that this is non-specific and thus not of a regulatory nature. This observation does require further investigation though to clarify the role of the presence of charged molecules on the activity of the enzyme. Tighter control over the timing of the assays post enzyme purification is also recommended. As mentioned previously, Sturm *et al.* demonstrated redox regulation of OAT activity [219]. This indicates that there is a level of post-translational regulation present, but may be under the control of alternative metabolites or pathways, especially as they postulate that there is an interrelationship between the methyl transfer reactions and polyamine biosynthesis (via AdoMet). This unfortunately only adds to the complexity of regulation within the polyamine pathway and confounds elucidation.

CHAPTER 5

Concluding discussion

Malaria – a disease afflicting millions of people and prevalent in developing countries that can ill afford the cost of prevention, treatment and the effect of sick workers on their economy. Prevention of malaria includes chemoprophylaxis, the use of insecticide treated bed nets and spraying of residences with insecticides. Unfortunately many of the drugs in current use against the malaria parasite are failing and a completely effective vaccine is not yet in sight. The search for new drugs and their targets is thus of primary importance in the campaign against malaria and is the subject of much research throughout the world.

Of the various metabolic pathways in the malaria parasite, the enzymes of the polyamine biosynthetic pathway are attractive chemotherapeutic drug targets, as the ubiquitous polycationic polyamines are essential for many growth and development processes. AdoMetDC-ODC is the rate-limiting enzyme of the polyamine pathway and its unique bifunctional nature, differentiating it from the human ODC, makes it a particularly attractive target. The primary objective of this study was to investigate the functional consequences of inhibition of the ODC subunit (induced by DFMO-treatment) of the bifunctional enzyme on *P. falciparum* parasites, in order to contribute to the chemical validation of bifunctional AdoMetDC-ODC as a therapeutic drug target in malaria parasites. DFMO is used for the treatment of African sleeping sickness, showed some potential in the treatment of cancer and is a known inhibitor of *P. falciparum* ODC and life-cycle progression, through the depletion of putrescine and spermidine [63].

In this study the functional consequences of inhibition of ODC by DFMO were evident globally as differential expression, of both the transcriptome and proteome, in the *P. falciparum* parasite. Particularly, differentially regulated transcripts and proteins pertaining to the polyamine and redox pathways were observed (Figure 5.1). This reveals potential, novel homeostatic control mechanisms related to polyamine metabolism in the parasite and additionally confirms evidence of the important link between polyamines and redox homeostasis in the parasite [219], as the two major novel descriptors arising from this study.

The regulation of polyamine biosynthesis is a complex interplay of biosynthesis, interconversion and transport [54, 67]; in *P. falciparum* however, this process is much more simplistically regulated [85].

In this work, a clear link between polyamine and ornithine metabolism was established, as inhibition of ODC leads to a highly specific increase in OAT expression within the parasite. Moreover, exogenous addition of ornithine to the parasite culture confirms this. This increase in OAT transcripts was also observed upon co-inhibition of ODC-AdoMetDC with DFMO and MDL73811 [1], but was not seen upon inhibition of only AdoMetDC (S Smit, personal communication) or spermidine synthase [3]. This suggests that any accumulation of ornithine, which should be toxic to the parasite, has been satisfactorily dealt with by the increased abundance of transcripts coding for OAT, which is capable of catabolising ornithine. The metabolic consequence of increased OAT abundance is thus evident as homeostatic maintenance of ornithine levels. Indeed, this is also confirmed by metabolic analysis of DFMO/MDL73811 treated parasites, where ornithine concentration remains unchanged [1]. These responses have not been described for any other organism beyond *P. falciparum* and may indicate a unique ability of this parasite to control the available levels of ornithine as precursor for polyamine biosynthesis, in lieu of other regulatory systems (like antizyme) controlling polyamine metabolism. This does however imply that the parasite may rely more heavily on AdoMetDC-ODC as metabolic control point in this pathway compared to other organisms. This may have implications for the design of specific inhibitory compounds affecting polyamine biosynthesis in malaria parasites. However, with spermidine present at the highest levels in the parasite [63], the importance of spermidine synthase should not be disregarded.

For a long time, the major functions ascribed to the polyamines have been their involvement in cellular growth and replication processes. Polyamines are capable of amongst others, binding and therefore stabilising DNA, RNA and the phospholipids of biomembranes [54]. The consequence of the depletion in putrescine in this study is shown by the changes in abundance of transcripts associated primarily with protein modification and signal transduction, DNA metabolism, primary metabolism and the cell cycle. Beyond these functions, recently, a connection has been established between the polyamines and the maintenance of redox potential in the parasites [219, 268]. This study confirms this and indicates that possibly the major functional consequence of putrescine depletion is not just macromolecular destabilisation, but a redox imbalance, which contributes to the growth arrest phenotype. Particularly interesting is the significant decrease in abundance of transcripts for thioredoxin, thioredoxin reductase and 1-cys peroxiredoxin (Figure 5.1). Again, these observations are polyamine specific, as confirmed by inhibitions of the polyamine biosynthetic enzymes [1-3], indicating that the reduction in redox associated transcripts is a result of polyamine depletion. Of the redox-associated transcripts affected by polyamine depletion, 1-cys peroxiredoxin is the only transcript common to all inhibitions of the polyamine biosynthetic enzymes, indicating a strong association between this transcript and polyamine depletion.

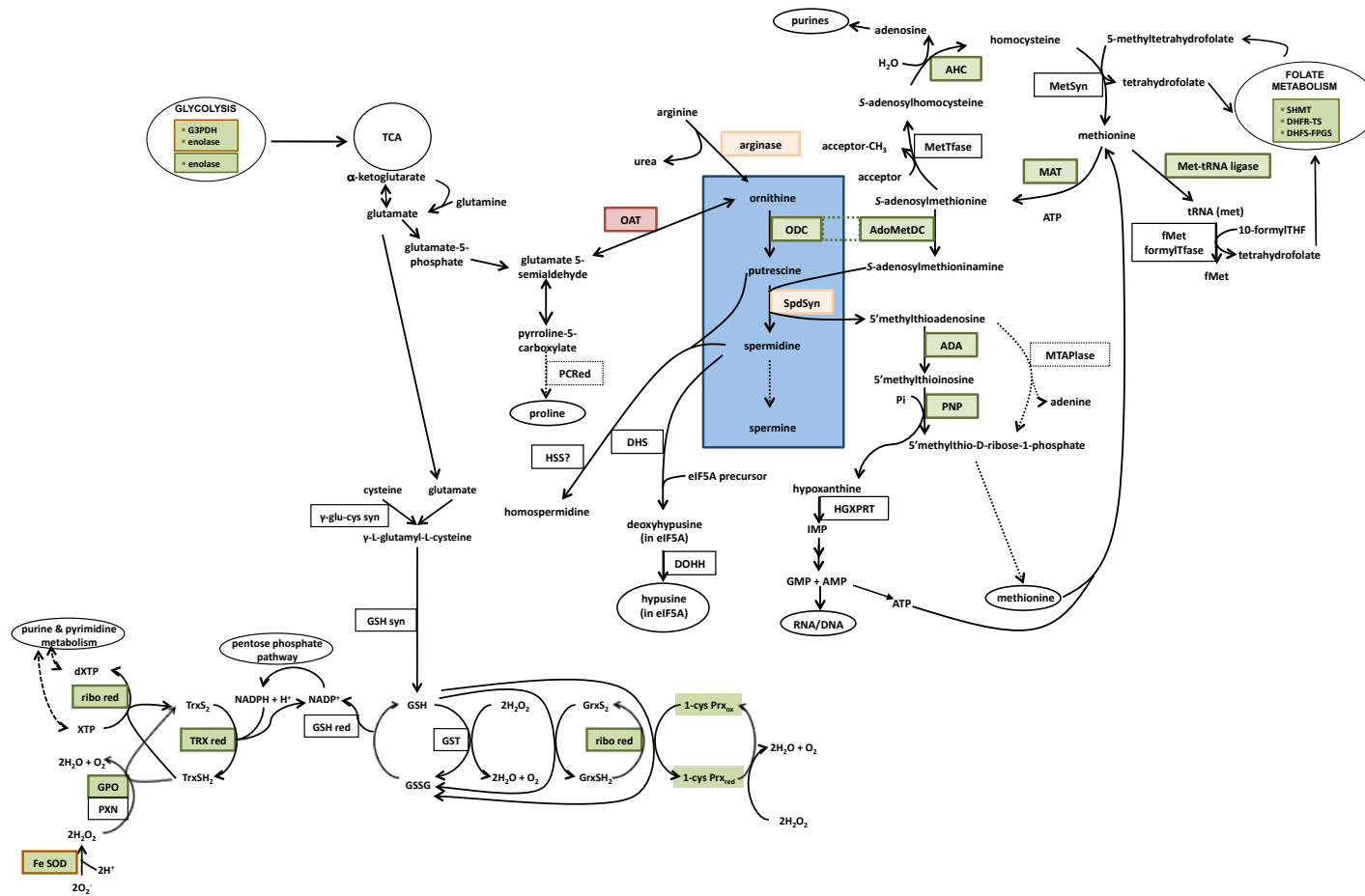


Figure 5.1. Overview of the polyamine and redox pathways indicating those enzymes (framed) and proteins affected by ODC inhibition. Green = decreased abundance, red = increased abundance, apricot = no change. Orange box framing = protein was affected. Dashed arrows indicate reactions that have not been demonstrated in *P. falciparum*. ODC: ornithine decarboxylase; AdoMetDC: S-adenosylmethionine decarboxylase; OAT: ornithine aminotransferase; SpdSyn: spermidine synthase; ADA: adenosine deaminase; PNP: purine nucleoside phosphorylase; MTAPase: methylthioadenosine phosphorylase; HGXPRT: hypoxanthine phosphoribosyltransferase; DOHH: deoxyhypusine hydrolase; DHS: deoxyhypusine synthase; HSS: homospermidine synthase; PCRed: pyrroline carboxylate reductase; AHC: adenosylhomocysteinase; MetSyn: methionine synthase; MAT: S-adenosylmethionine synthetase; MetTfase: methionine transferase; 1-cys prx: 1-cys peroxiredoxin; ribo red: ribonucleotide reductase; THF: tetrahydrofolate; TRX red: thioredoxin reductase; GPO: glutathione peroxidase; PXN: peroxiredoxin; FeSOD: iron superoxide dismutase; Trx: thioredoxin; γ -glu-cys syn: γ -glu-cys synthase; GSH syn: glutathione synthase; GSH red: glutathione reductase; GSH: glutathione; GSSG: reduced glutathione; GST: glutathione S-transferase; Grx: glutaredoxin; fMet formylTfase: methionyl-tRNA formyltransferase; TCA: tricarboxylic acid cycle; SHMT: serine hydroxymethyltransferase; G3PDH: glyceraldehyde-3-phosphate dehydrogenase; DHFR-TS: dihydrofolate reductase-thymidylate synthase; DHFS-FPGS: dihydrofolate synthase-folylpolyglutamate synthase.

Related to changes in redox status of the parasite upon polyamine perturbation is that additional transcripts shown in this study to be affected by ODC-inhibition, have been linked to redox potential in cells. OAT activity in *P. falciparum* parasites has been shown to be stimulated by thioredoxin [219, 268]. Additionally, LDC produces cadaverine, which is capable of scavenging superoxide radicals [243]. Moreover, a recent publication investigated S-glutathionylation of parasite proteins and proposed that this post-translational modification of thiol groups with glutathione can function as a redox switch, capable of mediating redox regulation and signal transduction in cells [282]. S-glutathionylation can, in response to oxidative stress, induce functional changes in the target proteins thereby, in the majority of cases, inhibiting them. However, some proteins are actually activated by S-glutathionylation. As a result, this post-translational modification can manifest as an antioxidant defence mechanism in cells, as it protects cysteine residues from irreversible overoxidation, which would result in loss of protein function [283]. All of the proteins identified in the proteome of ODC-inhibited *P. falciparum* parasites, with the exception of the β -subunit of the T-complex protein (PFC0285c) and 105 of the transcripts affected by DFMO-treatment are capable of being S-glutathionylated. Interestingly, transcripts identified as being involved in polyamine metabolism (adenosine deaminase (PF10_0289), AdoMetDC-ODC (PF10_0322), S-adenosylhomocysteine hydrolase (PFE1050w), OAT (PFF0435w), MAT (PF11090w) and uridine phosphorylase (PFE0660c)) are all predicted to be S-glutathionylated. The link between redox homeostasis and the polyamine pathway should also be explored in greater detail, particularly as some of the current anti-malarials actually exert their action through oxidative mediated processes (e.g. the mechanism of action of artemisinin and its related compounds occurs through cleavage of the endoperoxide moiety resulting in carbon and oxygen centred radicals) [162].

To conclude, the results of this study show that inhibition of ODC has definite effects on both the transcriptome and the proteome of *P. falciparum* parasites. Numerous metabolic processes affected by inhibition and potentially contributing to the resulting cytostasis were identified. The increase in abundance of a transcript compensating for perturbation of ornithine concentration due to ODC-inhibition was established. Additionally, a previously proposed connection between redox homeostasis and the polyamines was confirmed, indicating that putrescine depletion creates an environment with decreased potential for coping with oxidative stress. Future studies should focus on the possibility of therapy utilising inhibitors of AdoMetDC-ODC, in combination with either, spermidine synthase or one of the components of the redox system. This would have a tremendously negative effect on the parasite through concomitant depletion of the crucial polyamines, coupled with increased oxidative stress.

Though functional genomics alone cannot validate a drug target, the application thereof to the process is invaluable, as the compensatory, synergistic and antagonistic pathways and/or transcripts become apparent. The identification of changes to proteins of unknown function (the hypothetical proteins) is also important, as these are inherently attractive targets due to their lack of human homologues. Within the scope of enzyme bifunctionality the prospects are even more advantageous, as comparisons of inhibition of the various enzyme activities enables the allocation of specific consequences to a particular activity. This may facilitate the identification of future drug targets.

REFERENCES

1. van Brummelen, A., *et al.* (2009). Co-inhibition of *Plasmodium falciparum* S-adenosylmethionine decarboxylase/ornithine decarboxylase reveals perturbation-specific compensatory mechanisms by transcriptome, proteome and metabolome analyses. *J. Biol. Chem.*, **284**(7): 4635-4646.
2. Smit, S. (2011). Functional consequences of the inhibition of Malaria S-adenosylmethionine decarboxylase as a key regulator of polyamine and methionine metabolism. PhD thesis, in Department of Biochemistry, University of Pretoria, Pretoria
3. Becker, J., *et al.* (2010). *Plasmodium falciparum* spermidine synthase inhibition results in unique perturbation-specific effects observed on transcript, protein and metabolite levels. *BMC Genomics*, **11**: 235.
4. Fornaciari, G., *et al.* (2010). Malaria was “the killer” of Francesco I de’ Medici (1531-1587). *Am. J. Med.*, **123**(6): 568-569.
5. Sherman, I., (editor). (1998). Malaria. Parasite biology, pathogenesis and protection. American Society for Microbiology Press.
6. Reiter, P. (2000). From Shakespeare to Defoe: Malaria in England in the Little Ice Age. *Emerg. Infect. Dis.*, **6**(1): 1-11.
7. Hagan, P. and Chauhan, V. (1997). Ronald Ross and the problem of malaria. *Parasitol. Today*, **13**(8): 290-295.
8. Gardiner, D.; McCarthy, J.; and Trenholme, K. (2005). Malaria in the post-genomics era: light at the end of the tunnel or just another train. *Postgrad. Med. J.*, **81**: 505-509.
9. Wirth, D. (2002). The parasite genome: Biological revelations. *Nature*, **419**: 495-496.
10. Thompson, J.; Janse, C.J.; and Waters, A.P. (2001). Comparative genomics in *Plasmodium*: a tool for the identification of genes and functional analysis. *Mol. Biochem. Parasitol.*, **118**(2): 147-154.
11. James, A.A. (2002). Engineering mosquito resistance to malaria parasites: the avian malaria model. *Insect Biochem. Mol. Biol.*, **32**(10): 1317-1323.
12. Fricke, J.M.; Vardo-Zalik, A.M.; and Schall, J.J. (2010). Geographic genetic differentiation of a malaria parasite, *Plasmodium mexicanum*, and its lizard host, *Sceloporus occidentalis*. *J. Parasitol.*, **96**(2): 308-313.
13. Greenwood, B., *et al.* (2005). Malaria. *Lancet*, **365**: 1487-1498.
14. Pain, A., *et al.* (2008). The genome of the simian and human malaria parasite *Plasmodium knowlesi*. *Nature*, **455**(7214): 799-803.
15. Cox-Singh, J., *et al.* (2008). *Plasmodium knowlesi* malaria in humans is widely distributed and potentially life threatening. *Clin. Infect. Dis.*, **46**(2): 165-171.
16. White, N. (2008). *Plasmodium knowlesi*: The fifth human malaria parasite. *Clin. Infect. Dis.*, **46**: 172-173.
17. World Health Organization, (2010). World Malaria Report 2010. World Health Organization: Geneva, Switzerland.
18. World Health Organization, (2009). World Malaria Report 2009. Geneva. p. 1-163.
19. Lagerberg, R.E. (2008). Malaria in pregnancy: a literature review. *J. Midwifery Women's Health*, **53**(3): 209-215.
20. Heddini, A. (2002). Malaria pathogenesis: a jigsaw with an increasing number of pieces. *Int. J. Parasitol.*, **32**(13): 1587-1598.
21. Mackintosh, C.L.; Beeson, J.G.; and Marsh, K. (2004). Clinical features and pathogenesis of severe malaria. *Trends Parasitol.*, **20**(12): 597-603.
22. United Against Malaria, (2010). Building the winning team to beat malaria.
23. United Nations, (2010). The Millenium Development Goals report. New York.
24. Malaria Consortium, (2009). Malaria and the G8: leading or lagging? : Brussels.
25. Greenwood, B. and Targett, G. (2009). Do we still need a malaria vaccine? *Parasite Immunol.*, **31**: 582-586.
26. Herren, H. and Mbogo, C. (2010). The role of DDT in malaria control. *Environ. Health Perspect.*, **118**(7): A282-A283.
27. Roberts, D. and Tren, R. (2010). DDT in malaria control: Roberts and Tren respond. *Environ. Health Perspect.*, **118**(7): A283.

28. Greenwood, B. (2008). Control to elimination: implications for malaria research. *Trends Parasitol.*, **24**(10): 449-454.
29. Newman, R. (2010). Malaria control beyond 2010. *BMJ*, **340**: c2714.
30. Hargreaves, K., *et al.* (2000). *Anopheles funestus* resistant to pyrethroid insecticides in South Africa. *Med. Vet. Entomol.*, **14**(2): 181-189.
31. Mouatcho, J., *et al.* (2007). Indoor collections of the *Anopheles funestus* group (Diptera: Culicidae) in sprayed houses in northern KwaZulu-Natal, South Africa. *Malaria J.*, **6**(30): doi:10.1186/1475-2875-6-30.
32. Wang, R.; Smith, J.; and Kappe, S. (2009). Advances and challenges in malaria vaccine development. *Expert Rev. Mol. Med.*, **11**: e39.
33. Kappe, S., *et al.* (2010). That was then but this is now: Malaria research in the time of an eradication agenda. *Science*, **328**: 862-866.
34. Casares, S.; Brumeanu, T.; and Richie, T. (2010). The RTS,S malaria vaccine. *Vaccine*, **28**(31): 4880-4894.
35. Agnandji, S., *et al.* (2011). First Results of Phase 3 Trial of RTS,S/AS01 Malaria Vaccine in African Children. *New Engl. J. Med.*, **365**(20): 1863-1875.
36. RTS,S Clinical Trials Partnership, *et al.* (2012). A Phase 3 Trial of RTS,S/AS01 Malaria Vaccine in African Infants. *New Engl. J. Med.*, **367**(24): 2284-2295.
37. Butler, D. (2002). What difference does a genome make? *Nature*, **419**: 426-428.
38. Chauhan, P. and Srivastava, S. (2001). Present trends and future strategy in chemotherapy of malaria. *Curr. Med. Chem.*, **8**: 1535-1542.
39. Craft, J.C. (2008). Challenges facing drug development for malaria. *Curr. Opin. Microbiol.*, **11**(5): 428-433.
40. Hyde, J.E. (2007). Drug-resistant malaria – an insight. *FEBS J.*, **274**(18): 4688-4698.
41. Hyde, J. (2005). Drug-resistant malaria. *Trends Parasitol.*, **21**(11): 494-498.
42. Duffy, P. and Sibley, C. (2005). Are we losing artemisinin combination therapy already? *Lancet*, **366**: 1908-1909.
43. World Health Organization, (2010). Guidelines for the treatment of malaria - Second edition.). World Health Organization: Geneva.
44. Jambou, R., *et al.* (2005). Resistance of *Plasmodium falciparum* field isolates to in-vitro artemether and point mutations of the SERCA-type PfATPase6. *Lancet*, **366**: 1960-1963.
45. Schlitzer, M. (2008). Antimalarial drugs – what is in use and what is in the pipeline. *Arch. Pharm.*, **341**(3): 149-163.
46. Dharia, N., *et al.* (2010). Genome scanning of Amazonian *Plasmodium falciparum* shows subtelomeric instability and clindamycin-resistant parasites. *Genome Res.*, **20**(11): 1534-1544.
47. Medicines for Malaria Venture, (2009). Annual Report. Geneva.
48. Yeh, I., *et al.* (2004). Computational analysis of *Plasmodium falciparum* metabolism: organizing genomic information to facilitate drug discovery. *Genome Res.*, **14**: 917-924.
49. Yeh, I. and Altman, R. (2006). Drug targets for *Plasmodium falciparum*: a post-genomic review/survey. *Mini-Rev. Med. Chem.*, **6**: 177-202.
50. Toomey, D., *et al.* (2009). Genomes2Drugs: Identifies target proteins and lead drugs from proteome data. *PLoS ONE*, **4**(7): e6195.
51. Fatumo, S., *et al.* (2009). Estimating novel potential drug targets of *Plasmodium falciparum* by analysing the metabolic network of knock-out strains *in silico*. *Infect., Genet. Evol.*, **9**(3): 351-358.
52. Gamo, F., *et al.* (2010). Thousands of chemical starting points for antimalarial lead identification. *Nature*, **465**(7296): 305-310.
53. Kusano, T., *et al.* (2008). Polyamines: essential factors for growth and survival *Planta*, **228**(3): 367-381.
54. Wallace, H.; Fraser, A.; and Hughes, A. (2003). A perspective of polyamine metabolism. *Biochem. J.*, **376**: 1-14.
55. Shah, P. and Swiatlo, E. (2008). A multifaceted role for polyamines in bacterial pathogens. *Mol. Microbiol.*, **68**(1): 4-16.
56. Seiler, N. and Raul, F. (2005). Polyamines and apoptosis. *J. Cell. Mol. Med.*, **9**(3): 623-642.
57. Pignatti, C., *et al.* (2004). Signal transduction pathways linking polyamines to apoptosis. *Amino Acids*, **27**: 359-365.
58. Al-Olayan, E.; Williams, G.; and Hilary Hurd, H. (2002). Apoptosis in the malaria protozoan, *Plasmodium berghei*: a possible mechanism for limiting intensity of infection in the mosquito. *Int. J. Parasitol.*, **32**: 1133-1143.

59. Deponte, M. and Becker, K. (2004). *Plasmodium falciparum* – do killers commit suicide? Trends Parasitol., **20**(4): 165-169.
60. Soulet, D., *et al.* (2002). Role of endocytosis in the internalization of spermidine - C₂-BODIPY, a highly fluorescent probe of polyamine transport. Biochem. J., **367**: 347-357.
61. Muller, S.; Coombs, G.; and Walter, R. (2001). Targeting polyamines of parasitic protozoa in chemotherapy. Trends Parasitol., **17**(5): 242-248.
62. Metcalf, B., *et al.* (1978). Catalytic irreversible inhibition of mammalian ornithine decarboxylase (EC4.1.1.17) by substrate and product analogues. J. Am. Chem. Soc., **100**: 2551-2553.
63. Assaraf, Y., *et al.* (1987a). Effect of polyamine depletion on macromolecular synthesis of the malarial parasite, *Plasmodium falciparum*, cultures in human erythrocytes. Biochem. J., **242**: 221-226.
64. Wallace, H. and Fraser, A. (2004). Inhibitors of polyamine metabolism. Amino Acids, **26**: 353-365.
65. Poulin, R., *et al.* (1992). Mechanism of the irreversible inactivation of mouse ornithine decarboxylase by alpha-difluoromethylornithine. J. Biol. Chem., **267**(1): 150-158.
66. Qu, N., *et al.* (2003). Inhibition of human ornithine decarboxylase activity by enantiomers of difluoromethylornithine. Biochem. J., **375**: 465-470.
67. Pegg, A. (2006). Regulation of ornithine decarboxylase. J. Biol. Chem., **281**(21): 14529-14532.
68. Shantz, L. and Pegg, A. (1999). Translational regulation of ornithine decarboxylase and other enzymes of the polyamine pathway. Int. J. Biochem. Cell Biol., **31**: 107-122.
69. Holm, I., *et al.* (1989). Feedback control of ornithine decarboxylase expression by polyamines. Biochem. J., **258**: 343-350.
70. Autelli, R., *et al.* (1990). Feedback regulation of ornithine decarboxylase expression. FEBS Lett., **260**(1): 39-41.
71. Assaraf, Y., *et al.* (1984). Polyamine levels and the activity of their biosynthetic enzymes in human erythrocytes infected with the malarial parasite, *Plasmodium falciparum*. Biochem. J., **222**: 815-819.
72. Assaraf, Y., *et al.* (1986). *Plasmodium falciparum*: Synchronisation of cultures with DL-alpha-difluoromethylornithine, an inhibitor of polyamine biosynthesis. Exp. Parasitol., **61**: 229-235.
73. Assaraf, Y., *et al.* (1987b). Cytostatic effect of DL-alpha-difluoromethylornithine against *Plasmodium falciparum* and its reversal by diamines and spermidine. Parasitol. Res., **73**: 313-318.
74. Das Gupta, R., *et al.* (2005). 3-aminooxy-1-aminopropane and derivatives have an antiproliferative effect on cultured *Plasmodium falciparum* by decreasing intracellular polyamine concentrations. Antimicrob. Agents Chemother., **49**(7): 2857-2864.
75. Müller, S., *et al.* (2000). In the human malaria parasite *Plasmodium falciparum*, polyamines are synthesized by a bifunctional ornithine decarboxylase, S-adenosylmethionine decarboxylase. J. Biol. Chem., **275**(11): 8097-8102.
76. Bitonti, A.J., *et al.* (1989). Bis(benzyl)polyamine analogs inhibit the growth of chloroquine-resistant human malaria parasites (*Plasmodium falciparum*) *in vitro* and in combination with α -difluoromethylornithine cure murine malaria. Proc. Natl. Acad. Sci. U.S.A., **86**: 651-655.
77. Bitonti, A.; Bush, T.; and McCann, P. (1989). Regulation of polyamine biosynthesis in rat hepatoma (HTC) cells by a bisbenzyl polyamine analogue. Biochem. J., **257**: 769-774.
78. Müller, I.; Walter, R.; and Wrenger, C. (2005). Structural metal dependency of the arginase from the human malaria parasite *Plasmodium falciparum*. Biol. Chem., **386**: 117-126.
79. Müller, I., *et al.* (2008). Assessing the polyamine metabolism of *Plasmodium falciparum* as chemotherapeutic target Mol. Biochem. Parasitol., **160**: 1-7.
80. Burger, P., *et al.* (2007). Structural and mechanistic insights into the action of *Plasmodium falciparum* spermidine synthase Bioorg. Med. Chem., **15**(4): 1628-1637.
81. Haider, N. (2005). The spermidine synthase of the malaria parasite *Plasmodium falciparum*: molecular and biochemical characterisation of the polyamine synthesis enzyme. Mol. Biochem. Parasitol., **142**: 224-236.
82. Birkholtz, L., *et al.* (2011). Polyamine homeostasis as a drug target in pathogenic protozoa: peculiarities and possibilities. Biochem. J., **438**: doi:10.1042/BJ20110362
83. Dowling, D., *et al.* (2010). Crystal structure of arginase from *Plasmodium falciparum* and implications for L-arginine depletion in malarial infection. Biochemistry, **49**: 5600-5608.
84. Williams, M.; Louw, A.; and Birkholtz, L.-M. (2007). Deletion mutagenesis of large areas in *Plasmodium falciparum* genes: a comparative study. Malaria J., **6**(64): doi:10.1186/1475-2875-6-64.
85. Wrenger, C., *et al.* (2001). The *Plasmodium falciparum* bifunctional ornithine decarboxylase, S-adenosyl-L-methionine decarboxylase, enables a well balanced polyamine synthesis without domain-domain interaction. J. Biol. Chem., **276**(32): 29651-29656.

86. Williams, M., *et al.* (2011). Biochemical characterisation and novel classification of monofunctional S-adenosylmethionine decarboxylase of *Plasmodium falciparum*. *Mol. Biochem. Parasitol.*, **180**(1): 17-26.
87. Birkholtz, L.-M., *et al.* (2004). Parasite-specific inserts in the bifunctional S-adenosylmethionine decarboxylase/ornithine decarboxylase of *Plasmodium falciparum* modulate catalytic activities and domain interactions. *Biochem. J.*, **377**: 439-448.
88. Krause, T., *et al.* (2000). The ornithine decarboxylase domain of the bifunctional ornithine decarboxylase/S-adenosylmethionine decarboxylase of *Plasmodium falciparum* : recombinant expression and catalytic properties of two different constructs. *Biochem. J.*, **352**: 287-292.
89. Wells, G., *et al.* (2005). Novel properties of malarial S-adenosylmethionine decarboxylase as revealed by structural modelling. *J. Mol. Graphics Model.*, **24**: 307-318.
90. Birkholtz, L., *et al.* (2003). Comparative properties of a three-dimensional model of *Plasmodium falciparum* ornithine decarboxylase. *Proteins*, **50**: 464-473.
91. Dufe, V.T., *et al.* (2007). Crystal structure of *Plasmodium falciparum* spermidine synthase in complex with the substrate decarboxylated S-adenosylmethionine and the potent inhibitors 4MCHA and AdoDATO. *J. Mol. Biol.*, **373**(1): 167-177.
92. Kaiser, A., *et al.* (2001). Effects of drugs inhibiting spermidine biosynthesis and metabolism of the *in vitro* development of *Plasmodium falciparum*. *Parasitol. Res.*, **87**: 963-972.
93. Kaiser, A., *et al.* (2003). Targeting enzymes involved in spermidine metabolism of parasitic protozoa - a possible new strategy for anti-parasitic treatment. *Parasitol. Res.*, **91**: 508-516.
94. Kaiser, A., *et al.* (2006). Inhibition of hypusine biosynthesis in *Plasmodium*: a possible, new strategy in prevention and therapy of malaria. *Mini-Rev. Med. Chem.*, **6**: 1231-1241.
95. Kaiser, A., *et al.* (2007). Modification of eukaryotic initiation factor 5A from *Plasmodium vivax* by a truncated deoxyhypusine synthase from *Plasmodium falciparum*: An enzyme with dual enzymatic properties. *Bioorg. Med. Chem.*, **15**(18): 6200-6207.
96. Gafan, C., *et al.* (2001). Characterization of the ornithine aminotransferase from *Plasmodium falciparum*. *Mol. Biochem. Parasitol.*, **118**: 1-10.
97. Gardner, M., *et al.* (2002). Genome sequence of the human malaria parasite *Plasmodium falciparum*. *Nature*, **419**: 498-511.
98. Coppel, R. and Black, C. (2005). Parasite genomes. *Int. J. Parasitol.*, **35**: 465-479.
99. Carucci, D. (2002). Technologies for the study of gene and protein expression in *Plasmodium*. *Philos. Trans. R. Soc. Lond. B Biol. Sci.*, **357**: 13-16.
100. Duraisingh, M., *et al.* (2006). *Plasmodium* research in the post-genomic era. *Trends Parasitol.*, **22**(1): 1-4.
101. Bahl, A., *et al.* (2003). PlasmoDB: the *Plasmodium* genome resource. A database integrating experimental and computational data. *Nucleic Acids Res*, **31**(1): 212 - 215.
102. Fraunholz, M. and Roos, D. (2003). PlasmoDB: exploring genomics and post-genomics data of the malaria parasite, *Plasmodium falciparum*. *Redox Rep.*, **8**(5): 317-320.
103. Stoeckert Jr, C., *et al.* (2006). PlasmoDB v5: new looks, new genomes. *Trends Parasitol.*, **22**(12): 543-546.
104. Aurrecochea, C., *et al.* (2009). PlasmoDB: a functional genomic database for malaria parasites. *Nucleic Acids Res.*, **37**(Database issue): D539-43.
105. Oliver, D.; Nikolau, B.; and Wurtele, E. (2002). Functional genomics: high-throughput mRNA, protein and metabolite analyses. *Metab. Eng.*, **4**: 98-106.
106. Fraunholz, M. (2005). Systems biology in malaria research. *Trends Parasitol.*, **21**(9): 393-395.
107. Fairlamb, A. Target discovery and validation with special reference to trypanothione. In *Drugs against parasitic diseases.*
108. Jackson, L. and Phillips, M. (2002). Target validation for drug discovery in parasitic organisms. *Curr. Top. Med. Chem.*, **2**: 425-438.
109. Birkholtz, L., *et al.* (2008). Exploring functional genomics for drug target and therapeutics discovery in *Plasmodia*. *Acta Trop.*, **105**: 113-123.
110. Llinás, M.; Deitsch, K.W.; and Voss, T.S. (2008). *Plasmodium* gene regulation: far more to factor in. *Trends Parasitol.*, **24**(12): 551-556.
111. Horrocks, P., *et al.* (2009). Control of gene expression in *Plasmodium falciparum* - Ten years on. *Mol. Biochem. Parasitol.*, **164**(1): 9-25.

112. DeChering, K., *et al.* (1999). Isolation and functional characterization of two distinct sexual-stage-specific promoters of the human malaria parasite *Plasmodium falciparum* Mol. Cell. Biol., **19**(2): 967-978.
113. Functional Genomics Workshop Group (2007). Mechanisms of Gene Regulation in *Plasmodium*. Am. J. Trop. Med. Hyg., **77**(2): 201-208.
114. Sims, J.S., *et al.* (2009). Patterns of gene-specific and total transcriptional activity during the *Plasmodium falciparum* intraerythrocytic developmental cycle. Eukaryot. Cell, **8**(3): 327-338.
115. Raabe, C.A., *et al.* (2010). A global view of the nonprotein-coding transcriptome in *Plasmodium falciparum*. Nucleic Acids Res., **38**(2): 608-617.
116. De Silva, E.K., *et al.* (2008). Specific DNA-binding by apicomplexan AP2 transcription factors. Proc. Natl. Acad. Sci. U S A, **105**(24): 8393-8398.
117. Yuda, M., *et al.* (2009). Identification of a transcription factor in the mosquito-invasive stage of malaria parasites. Mol. Microbiol., **71**(6): 1402-1414.
118. Flueck, C., *et al.* (2010). A major role for the *Plasmodium falciparum* ApiAP2 protein PfSIP2 in chromosome end biology. PLoS Pathog, **6**(2): e1000784.
119. Painter, H.J.; Campbell, T.L.; and Llinás, M. (2011). The apicomplexan AP2 family: integral factors regulating *Plasmodium* development. Mol. Biochem. Parasitol., **176**(1): 1-7.
120. Lindner, S.E., *et al.* (2010). Structural determinants of DNA binding by a *P. falciparum* ApiAP2 transcriptional regulator. J. Mol. Biol., **395**(3): 558-567.
121. Campbell, T.L., *et al.* (2010). Identification and genome-wide prediction of DNA binding specificities for the ApiAP2 family of regulators from the malaria parasite. PLoS Path., **6**(10): e1001165.
122. Hernandez-Rivas, R., *et al.* (1997). Expressed *var* genes are found in *Plasmodium falciparum* subtelomeric regions. Mol. Cell. Biol., **17**(2): 604-611.
123. del Portillo, H., *et al.* (2001). A superfamily of variant genes encoded in the subtelomeric region of *Plasmodium vivax*. Nature, **410**: 839-842.
124. Florens, L., *et al.* (2002). A proteomic view of the *Plasmodium falciparum* life cycle. Nature, **419**: 520-526.
125. Bozdech, Z. and Ginsburg, H. (2005). Data mining of the transcriptome of *Plasmodium falciparum*: the pentose phosphate pathway and ancillary processes. Malaria J., **4**:17(doi:10.1186/1475-2875-1184-1117).
126. Le Roch, K., *et al.* (2003). Discovery of gene function by expression profiling of the malaria parasite life cycle. Science, **301**: 1503-1508.
127. Bozdech, Z., *et al.* (2003). The transcriptome of the intraerythrocytic developmental cycle of *Plasmodium falciparum*. PLoS Biol., **1**(1): 085-099.
128. Shock, J.; Fischer, K.; and DeRisi, J. (2007). Whole genome analysis of mRNA decay in *Plasmodium falciparum* reveals a global lengthening of mRNA half-life during the intraerythrocytic development cycle Genome Biol., **8**:R134: doi:10.1186/gb-2007-8-7-r134.
129. Llinás, M., *et al.* (2006). Comparative whole genome transcriptome analysis of three *Plasmodium falciparum* strains. Nucleic Acids Res., **34**(4): 1166-1173.
130. Hall, N., *et al.* (2005). A comprehensive survey of the *Plasmodium* life cycle by genomic, transcriptomic, and proteomic analyses. Science, **307**(5706): 82-86.
131. Silvestrini, F., *et al.* (2005). Genome-wide identification of genes upregulated at the onset of gametocytogenesis in *Plasmodium falciparum*. Mol. Biochem. Parasitol., **143**: 100-110.
132. Lovegrove, F., *et al.* (2007). Simultaneous host and parasite expression profiling identifies tissue-specific transcriptional programs associated with susceptibility or resistance to experimental cerebral malaria. BMC Genomics, **7**:295(doi:10.1186/1471-2164-7-295).
133. Siau, A., *et al.* (2007). Whole-transcriptome analysis of *Plasmodium falciparum* field isolates: identification of new pathogenicity factors. J. Infect. Dis., **196**: 1603-1612.
134. Stubbs, J., *et al.* (2005). Molecular mechanism for switching of *P. falciparum* invasion pathways into human erythrocytes. Science, **309**(5739): 1384-1387.
135. Shi, Q., *et al.* (2005). Alteration in host cell tropism limits the efficacy of immunization with a surface protein of malaria merozoites. Infect. Immun., **73**(10): 6363-6371.
136. Daily, J., *et al.* (2004). *In vivo* transcriptional profiling of *Plasmodium falciparum*. Malaria J., **3**:30(doi: 10.1186/1475-2875-1183-1130).
137. Daily, J., *et al.* (2005). *In vivo* transcriptome of *Plasmodium falciparum* reveals overexpression of transcripts that encode surface proteins. J. Infect. Dis., **191**: 1196-1203.

138. Gunasekera, A., *et al.* (2007). *Plasmodium falciparum*: Genome wide perturbations in transcript profiles among mixed stage cultures after chloroquine treatment. *Exp. Parasitol.*, **117**(1): 87-92.
139. Ganesan, K., *et al.* (2008). A genetically hard-wired metabolic transcriptome in *Plasmodium falciparum* fails to mount protective responses to lethal antifolates. *PLoS Path.*, **4**(11): e1000214. doi:10.1371/journal.ppat.1000214.
140. Dahl, E., *et al.* (2006). Tetracyclines specifically target the apicoplast of the malaria parasite *Plasmodium falciparum*. *Antimicrob. Agents Chemother.*, **50**(9): 3124-3131.
141. Le Roch, K., *et al.* (2008). A systematic approach to understand the mechanism of action of the bisthiazolium compound T4 on the human malaria parasite, *Plasmodium falciparum*. *BMC Genomics*, **9**: 513. doi:10.1186/1471-2164-9-513.
142. Natalang, O., *et al.* (2008). Dynamic RNA profiling in *Plasmodium falciparum* synchronized blood stages exposed to lethal doses of artesunate. *BMC Genomics*, **9**(1): 388.
143. Siau, A., *et al.* (2008). Temperature shift and host cell contact up-regulate sporozoite expression of *Plasmodium falciparum* genes involved in hepatocyte infection. *PLoS Path.*, **4**(8): e1000121. doi:10.1371/journal.ppat.1000121.
144. Oakley, M., *et al.* (2007). Molecular factors and biochemical pathways induced by febrile temperature in intraerythrocytic *Plasmodium falciparum* parasites. *Infect. Immun.*, **75**(4): 2012-2025.
145. Tamez, P., *et al.* (2008). An erythrocyte vesicle protein exported by the malaria parasite promotes tubovesicular lipid import from the host cell surface. *PLoS Path.*, **4**(8): e1000118. doi:10.1371/journal.ppat.1000118.
146. Flueck, C., *et al.* (2009). *Plasmodium falciparum* heterochromatin protein 1 marks genomic loci linked to phenotypic variation of exported virulence factors. *PLoS Pathog*, **5**(9): e1000569.
147. Volz, J., *et al.* (2010). Potential epigenetic regulatory proteins localise to distinct nuclear sub-compartments in *Plasmodium falciparum*. *Int. J. Parasitol.*, **40**(1): 109-121.
148. Chaal, B.K., *et al.* (2010). Histone deacetylases play a major role in the transcriptional regulation of the *Plasmodium falciparum* life cycle. *PLoS Pathog*, **6**(1): e1000737.
149. Cui, L., *et al.* (2008). Histone acetyltransferase inhibitor anacardic acid causes changes in global gene expression during *in vitro Plasmodium falciparum* development. *Eukaryot. Cell*, **7**(7): 1200-1210.
150. Dharia, N., *et al.* (2009). Use of high-density tiling microarrays to identify mutations globally and elucidate mechanisms of drug resistance in *Plasmodium falciparum*. *Genome Biol.*, **10**(2):R21.
151. Istvan, E.S., *et al.* (2011). Validation of isoleucine utilization targets in *Plasmodium falciparum*. *Proc. Natl. Acad. Sci. U S A*, **108**(4): 1627-1632.
152. Hu, G., *et al.* (2010). Transcriptional profiling of growth perturbations of the human malaria parasite *Plasmodium falciparum*. *Nat Biotech*, **28**(1): 91-98.
153. Hegde, P.; White, I.; and Debouck, C. (2003). Interplay of transcriptomics and proteomics. *Curr. Opin. Biotechnol.*, **14**: 647-651.
154. Smit, S., *et al.* (2010). Proteomic profiling of *Plasmodium falciparum* through improved, semiquantitative two-dimensional gel electrophoresis. *J. Proteome Res.*, **9**(5): 2170-2181.
155. Lasonder, E., *et al.* (2002). Analysis of the *Plasmodium falciparum* proteome by high-accuracy mass spectrometry. *Nature*, **419**: 537-541.
156. Nirmalan, N.; Sims, P.; and Hyde, J. (2004). Quantitative proteomics of the human malaria parasite *Plasmodium falciparum* and its application to studies of development and inhibition. *Mol. Microbiol.*, **52**(4): 1187-1199.
157. Foth, B.J., *et al.* (2011). Quantitative time-course profiling of parasite and host cell proteins in the human malaria parasite *Plasmodium falciparum*. *Mol. Cell. Proteomics*.
158. Vincensini, L., *et al.* (2005). Proteomic analysis identifies novel proteins of the Maurer's clefts, a secretory compartment delivering *Plasmodium falciparum* proteins to the surface of its host cell. *Mol. Cell. Proteomics*, **4**(4): 582-593.
159. Sam-Yellowe, T.Y., *et al.* (2004). Proteome analysis of rhoptry-enriched fractions isolated from *Plasmodium* merozoites. *J. Proteome Res.*, **3**(5): 995-1001.
160. Nyalwidhe, J. and Lingelbach, K. (2006). Proteases and chaperones are the most abundant proteins in the parasitophorous vacuole of *Plasmodium falciparum*-infected erythrocytes. *Proteomics*, **6**(5): 1563-1573.
161. Khan, S., *et al.* (2005). Proteome analysis of separated male and female gametocytes reveals novel sex-specific *Plasmodium* biology. *Cell*, **121**: 675-687.
162. Makanga, M., *et al.* (2005). Towards a proteomic definition of CoArtem action in *Plasmodium falciparum* malaria. *Proteomics*, **5**: 1-9.

163. Prieto, J., *et al.* (2008). Large-scale differential proteome analysis in *Plasmodium falciparum* under drug treatment. *PLoS ONE*, **3** (12): e4098.
164. Briolant, S., *et al.* (2010). *Plasmodium falciparum* proteome changes in response to doxycycline treatment. *Malaria J.*, **9**(1): 141.
165. Aly, N., *et al.* (2007). Proteome analysis of new antimalarial endoperoxide against *Plasmodium falciparum*. *Parasitol. Res.*, **100**(5): 1119-1124.
166. Radfar, A.; Diez, A.; and Bautista, J. (2008). Chloroquine mediates specific proteome oxidative damage across the erythrocytic cycle of resistant *Plasmodium falciparum*. *Free Radic. Biol. Med.*, **44**: 2034-2042.
167. Kozyan, D. and Kirschbaum, B. (1999). Comparative gene expression analysis. *Tibtech*, **17**: 73-78.
168. Desai, S., *et al.* (2000). Identification of differentially expressed genes by suppression subtractive hybridisation. In *Functional Genomics: A Practical Approach*. Hunt, S.P. and Livesey, R.J.(editors). Oxford University Press; Oxford. p. 81-112.
169. Patankar, S., *et al.* (2001). Serial analysis of gene expression in *Plasmodium falciparum* reveals the global expression profile of erythrocytic stages and the presence of anti-sense transcripts in the malarial parasite. *Mol. Biol. Cell*, **12**: 3114-3125.
170. Clontech Laboratories Inc (2008). PCR-Select™ cDNA Subtraction Kit User Manual. Protocol No. PT1117-1, Version No. PR892607.
171. Padmanabhan, P. and Sahi, S.V. (2011). Suppression subtractive hybridization reveals differential gene expression in sunflower grown in high P. *Plant Physiol. Biochem.*, **49**(6): 584-591.
172. Krishnaraj, T., *et al.* (2011). Identification of differentially expressed genes in dormant (banjhi) bud of tea (*Camellia sinensis* (L.) O. Kuntze) using subtractive hybridization approach. *Plant Physiol. Biochem.*, **49**(6): 565-571.
173. Lott, S., *et al.* (2009). DEAR1 is a dominant regulator of acinar morphogenesis and an independent predictor of local recurrence-free survival in early-onset breast cancer. *PLoS Medicine*, **6**(5): e1000068.
174. Zheng, G., *et al.* (2009). Development of *Faecalibacterium* 16S rRNA gene marker for identification of human faeces. *J. Appl. Microbiol.*, **106**: 634-641.
175. Dessens, J.T., *et al.* (2000). Identification of differentially regulated genes of *Plasmodium falciparum* by suppression subtractive hybridisation. *Parasitol. Today*, **16**(8): 354-356.
176. Ghosh, A., *et al.* (2003). Molecular strategies to study *Plasmodium*-mosquito interactions. *Trends Parasitol.*, **19**(2): 94-101.
177. Spielmann, T. and Beck, H. (2000). Analysis of stage-specific transcription in *Plasmodium falciparum* reveals a set of genes exclusively transcribed in ring stage parasites. *Mol. Biochem. Parasitol.*, **111**: 453-458.
178. Florent, I.; Charneau, S.; and Grellier, P. (2004). *Plasmodium falciparum* genes differentially expressed during merozoite morphogenesis. *Mol. Biochem. Parasitol.*, **135**: 143-148.
179. Kaiser, K., *et al.* (2004). Differential transcriptome profiling identifies *Plasmodium* genes encoding pre-erythrocytic stage-specific proteins. *Mol. Microbiol.*, **51**(5): 1221-1232.
180. Matuschewski, K., *et al.* (2002). Infectivity-associated changes in the transcriptional repertoire of the malaria parasite sporozoite stage. *J. Biol. Chem.*, **277**(44): 41948-41953.
181. Raibaud, A., *et al.* (2006). Differential gene expression in the ookinete stage of the malaria parasite *Plasmodium berghei*. *Mol. Biochem. Parasitol.*, **150**: 107-113.
182. Florent, I., *et al.* (2009). A *Plasmodium falciparum* FcB1-schizont-EST collection providing clues to schizont specific gene structure and polymorphism. *BMC Genomics*, **10**(235): doi:10.1186/1471-2164-10-235.
183. Hardiman, G. (2004). Microarray platforms - comparisons and contrasts. *Pharmacogenomics*, **5**(5): 487-502.
184. Naidoo, S.; Denby, K.; and Berger, D. (2005). Microarray experiments: considerations for experimental design. *S. Afr. J. Sci.*, **101**: 347-354.
185. Russell, S.; Meadows, L.; and Russell, R. (2009). The basics of experimental design. In *Microarray technology in practice*. Academic Press; Oxford.
186. Simon, R. and Dobbin, K. (2003). Experimental design of DNA microarray experiments. *BioTechniques*, **34**: S16-S21.
187. Churchill, G. (2002). Fundamentals of experimental design for cDNA microarrays. *Nat. Genet.*, **32**(Supplement): 490-495.
188. Dhoogra, M. (2006). Gene expression profiling of polyamine-depleted *Plasmodium falciparum*. MSc thesis, in Department of Biochemistry, University of Pretoria, Pretoria, South Africa

189. Clark, K., *et al.* (2008). Transcriptional responses of *Plasmodium falciparum* to a difluoromethylornithine-induced polyamine depletion. *Biol. Chem.*, **389**: 111-125.
190. Trager, W. and Jensen, J.B. (1976). Human malaria parasites in continuous culture. *Science*, **193**: 673-675.
191. Schuster, F. (2002). Cultivation of *Plasmodium* spp. *Clin. Microbiol. Rev.*, **15**(3): 355-364.
192. Lambros, C. and Vanderberg, J. (1979). Synchronization of *Plasmodium falciparum* erythrocytic stages in culture. *J. Parasitol.*, **65**(3): 418-420.
193. Sambrook, J.; Fritsch, E.; and Maniatis, T. (1989). *Molecular Cloning: A Laboratory Manual*. Second Edition. Cold Spring Harbor Laboratory Press; New York.
194. Smyth, G. (2005). Limma: linear models for microarray data. In *Bioinformatics and Computational Biology Solutions using R and Bioconductor*. Gentleman, R., *et al.*(editors). Springer; New York. p. 397-420.
195. Wettenhall, J.M. and Smyth, G.K. (2004). limmaGUI: A graphical user interface for linear modeling of microarray data. *Bioinformatics*, **20**(18): 3705-3706.
196. R Development Core Team (2008). *R: A language and environment for statistical computing.*: R Foundation for Statistical Computing; Vienna, Austria.
197. Benjamini, Y. and Hochberg, Y. (1995). Controlling the false discovery rate : a practical and powerful approach to multiple testing. *J. R. Stat. Soc. B*, **57**(1): 289-300.
198. Law, P., *et al.* (2008). MADIBA: A web server toolkit for biological interpretation of *Plasmodium* and plant gene clusters. *BMC Genomics*, **9**(105 doi:10.1186/1471-2164-9-105).
199. Saeed, A., *et al.* (2003). TM4: a free, open-source system for microarray data management and analysis. *BioTechniques*, **34**(2): 374-378.
200. Hall, T. (1999). BioEdit: a user-friendly biological sequence alignment editor and analysis program for Windows 95/98/NT. *Nucleic Acids Symp. Ser.*, **41**: 95-98.
201. Rychlik, W. (1993). Selection of primers for polymerase chain reaction. In *Methods in Molecular Biology, PCR Protocols: Current Methods and Applications*. White, B.(editor). Humana Press Inc; Totowa. p. 31-40.
202. Amersham Technologies, *Amersham Microarray Handbook*.
203. Gentleman, R., *et al.* (2004). Bioconductor: open software development for computational biology and bioinformatics. *Genome Biol.*, **5**: R80.
204. Yang, Y.; Paquet, A.; and Dudoit, S. (2007). Exploratory analysis for two-color spotted microarray data. R package version 1.20.0. <http://www.maths.usyd.edu.au/u/jeany/>.
205. van Brummelen, A. (2008). Functional genomics analysis of the effects of co-inhibition of the malarial S-adenosylmethionine decarboxylase/ornithine decarboxylase. PhD thesis, in Department of Biochemistry, University of Pretoria, Pretoria, South Africa
206. Ward, P., *et al.* (2004). Protein kinases of the human malaria parasite *Plasmodium falciparum*: the kinome of a divergent eukaryote. *BMC Genomics*, **5**:79.
207. Madeira, L., *et al.* (2003). Human malaria parasites display a receptor for activated C kinase ortholog. *Biochem. Biophys. Res. Comm.*, **306**: 995-1001.
208. Cowman, A.F. and Crabb, B.S. (2006). Invasion of red blood cells by malaria parasites. *Cell*, **124**: 755-766.
209. Young, J.A. and Winzeler, E.A. (2005). Using expression information to discover new drug and vaccine targets in the malaria parasite *Plasmodium falciparum*. *Pharmacogenomics*, **6**: 1-26.
210. DePristo, M.A.; Zilversmit, M.M.; and Hartl, D.L. (2006). On the abundance, amino acid composition, and evolutionary dynamics of low-complexity regions in proteins. *Gene*, **378**: 19-30.
211. Martin, R.E., *et al.* (2005). The 'permeome' of the malaria parasite: an overview of the membrane transport proteins of *Plasmodium falciparum*. *Genome Biol.*, **6**:R26.
212. Lanzer, M., *et al.* (2006). Maurer's clefts: A novel multi-functional organelle in the cytoplasm of *Plasmodium falciparum*-infected erythrocytes. *Int. J. Parasitol.*, **36**: 23-36.
213. Ting, L., *et al.* (2005). Targeting a Novel *Plasmodium falciparum* Purine Recycling Pathway with Specific Immucillins. *J. Biol. Chem.*, **280**: 9547-9554.
214. Russell, S.; Meadows, L.; and Russell, R. (2009). Data preprocessing. In *Microarray technology in practice.*. Academic Press; Oxford.
215. Quackenbush, J. (2002). Microarray data normalization and transformation. *Nat. Genet.*, **32 (Suppl)**: 496-501.
216. Yang, Y. and Thorne, N. (2003). Normalization for two-color cDNA microarray data. *Science and Statistics: A Festschrift for Terry Speed, IMS Lecture Notes - Monograph Series*, **40**: 403 - 418.

217. Smyth, G., *et al.*, (2008). limma: Linear Models for Microarray Data User's Guide
218. Russell, S.; Meadows, L.; and Russell, R. (2009). Clustering and classification. In *Microarray technology in practice.* Academic Press; Oxford.
219. Sturm, N., *et al.* (2009). Identification of proteins targeted by the thioredoxin superfamily in *Plasmodium falciparum*. *PLoS Path.*, **5**(4): e1000383.
220. Müller, I.; Hyde, J.; and Wrenger, C. (2009). Vitamin B6 metabolism in *Plasmodium falciparum* as a source of drug targets. *Trends Parasitol.*, **26**(1): 35-43.
221. Diatchenko, L., *et al.* (1996). Suppression subtractive hybridisation: A method for generating differentially regulated or tissue-specific cDNA probes and libraries. *Proc. Natl. Acad. Sci. U S A*, **93**: 6025-6030.
222. Birkholtz, L., *et al.* (2006). Integration and mining of malaria molecular, functional and pharmacological data: how far are we from a chemogenomic knowledge space? *Malaria J.*, **5**: 110.
223. Datu, B., *et al.* (2008). Transcriptional changes in the hookworm, *Ancylostoma caninum*, during the transition from a free-living to a parasitic larva. *PLoS Negl. Trop. Dis.*, **2**(1): e130.
224. Geng, Y., *et al.* (2009). Differentially expressed genes between female and male adult *Anopheles anthropophagus*. *Parasitol. Res.*, DOI 10.1007/s00436-009-1470-5.
225. Hoppe, H.; Verschoor, J.; and Louw, A. (1991). *Plasmodium falciparum*: A comparison of synchronisation methods for *in vitro* cultures. *Exp. Parasitol.*, **72**: 464-467.
226. Loikkannen, I. (2005). Polyamine homeostasis: cellular responses to perturbation of polyamine biosynthetic enzymes. PhD thesis, in University of Oulu, Oulu, Finland
227. Gunasekera, A.M., *et al.* (2003). Drug-induced alterations in gene expression of the asexual blood forms of *Plasmodium falciparum*. *Mol. Microbiol.*, **50**: 1229-1239.
228. Yoshida, M., *et al.* (2004). A unifying model for the role of polyamines in bacterial cell growth, the polyamine modulon. *J. Biol. Chem.*, **44**: 46008-46013.
229. Kikuchi, Y., *et al.* (1997). Characterization of a second lysine decarboxylase isolated from *Escherichia coli* J. *Bacteriol.*, **179**(14): 4486-4492.
230. Sargeant, T., *et al.* (2006). Lineage-specific expansion of proteins exported to erythrocytes in malaria parasites. *Genome Biology*, **7**(R12(doi:10.1186/gb-2006-7-2-r12)).
231. Young, J., *et al.* (2005). The *Plasmodium falciparum* sexual development transcriptome: A microarray analysis using ontology-based pattern identification *Mol. Biochem. Parasitol.*, **143**: 67-79.
232. Quesada-Soriano, I., *et al.* (2010). Kinetic properties and specificity of trimeric *Plasmodium falciparum* and human dUTPases. *Biochimie*, **92**: 178-186.
233. Kilbey, B., *et al.* (1993). Molecular characterisation and stage-specific expression of proliferating cell nuclear antigen (PCNA) from the malarial parasite, *Plasmodium falciparum*. *Nucleic Acids Res.*, **21**(2): 239-243.
234. Müller, S. (2004). Redox and antioxidant systems of the malaria parasite *Plasmodium falciparum* *Mol. Microbiol.*, **53**(5): 1291-1305.
235. Jaeger, T. and Flohé, L. (2006). The thiol-based redox networks of pathogens: Unexploited targets in the search for new drugs *BioFactors*, **27**: 109-120.
236. Kawazu, S., *et al.* (2005). Roles of 1-cys peroxiredoxin in haem detoxification in the human malaria parasite *Plasmodium falciparum*. *FEBS J.*, **272**: 1784-1791.
237. Buchholz, K., *et al.* (2008). Depletion of *Plasmodium berghei* plasmoredoxin reveals a non-essential role for life cycle progression of the malaria parasite. *PLoS ONE*, **3**(6): e2474.
238. Koncarevic, S., *et al.* (2009). The malarial parasite *Plasmodium falciparum* imports the human protein peroxiredoxin 2 for peroxide detoxification *Proc. Natl. Acad. Sci. U S A*, **106**(32): 13323-13328.
239. Becker, K., *et al.* (2004). Oxidative stress in malaria parasite-infected erythrocytes: host – parasite interactions *Int. J. Parasitol.*, **34**: 163-189.
240. Childs, A.C.; Metha, D.J.; and Gerner, E.W. (2003). Polyamine-dependent gene expression. *Cell. Mol. Life Sci.*, **60**: 1394-1406.
241. Krauth-Siegel, R.L. and Comini, M.A. (2008). Redox control in trypanosomatids, parasitic protozoa with trypanothione-based thiol metabolism. *Biochim. Biophys. Acta*, **1780**(11): 1236-1248.
242. Kim, J.; Choi, S.; and Lee, J. (2006). Lysine decarboxylase expression by *Vibrio vulnificus* is induced by SoxR in response to superoxide stress. *J. Bacteriol.*, **188**(24): 8586-8592.
243. Kang, I., *et al.* (2007). Cadaverine protects *Vibrio vulnificus* from superoxide stress. *J. Microbiol. Biotechnol.*, **17**(1): 176-179.
244. Chattopadhyay, M.; Tabor, C.; and Tabor, H. (2003). Polyamines protect *Escherichia coli* cells from the toxic effect of oxygen. *Proc. Natl. Acad. Sci. U S A*, **100**(5): 2261-2265.

245. Ha, H., *et al.* (1998). Structural specificity of polyamines and polyamine analogues in the protection of DNA from strand breaks induced by reactive oxygen species. *Biochem. Biophys. Res. Commun.*, **244**: 298-303.
246. Müller, I., *et al.* (2009). Poisoning pyridoxal 5-phosphate-dependent enzymes: A new strategy to target the malaria parasite *Plasmodium falciparum*. *PLoS ONE*, **4**(2): e4406, doi:10.1371/journal.pone.0004406
247. Wrenger, C., *et al.* (2005). Analysis of the vitamin B6 biosynthesis pathway in the human malaria parasite *Plasmodium falciparum*. *J. Biol. Chem.*, **280**: 5242-5248.
248. Cox, B.; Kislinger, T.; and Emili, A. (2005). Integrating gene and protein expression data: pattern analysis and profile mining. *Methods*, **35**: 303-314.
249. Barrett, J.; Brophy, P.; and Hamilton, J. (2005). Analysing proteomic data. *Int. J. Parasitol.*, **35**: 543-553.
250. Kavallaris, M. and Marshall, G. (2005). Proteomics and disease: opportunities and challenges. *Med. J. Aust.*, **182**(11): 575-579.
251. Johnson, J., *et al.* (2004). Proteomics in malaria. *J. Proteome Res.*, **3**: 296-306.
252. Evans, C., *et al.* (2012). An insight into iTRAQ: where do we stand now? *Anal Bioanal Chem*, doi: **10.1007/s00216-012-5918-6**.
253. Foth, B., *et al.* (2008). Quantitative protein expression profiling reveals extensive post-transcriptional regulation and post-translational modifications in schizont-stage malaria parasites *Genome Biol.*, **9**: R177.
254. Bio Rad, Flamingo™ Fluorescent Gel Stain - Instruction Manual
255. LaCount, D.J., *et al.* (2005). A protein interaction network of the malaria parasite *Plasmodium falciparum*. *Nature*, **438**(3): 103-107.
256. Graf, P. and Jakob, U. (2002). Redox-regulated molecular chaperones. *Cell. Mol. Life Sci.*, **59**: 1624-1631.
257. Vignols, F., *et al.* (2003). Redox Control of Hsp70-Co-chaperone Interaction Revealed by Expression of a Thioredoxin-like Arabidopsis Protein. *J. Biol. Chem.*, **278**(7): 4516-4523.
258. Shonhai, A.; Boshoff, A.; and Blatch, G.L. (2007). The structural and functional diversity of Hsp70 proteins from *Plasmodium falciparum*. *Protein Sci.*, **16**(9): 1803-1818.
259. Akide-Ndunge, O., *et al.* (2009). Co-ordinated stage-dependent enhancement of *Plasmodium falciparum* antioxidant enzymes and heat shock protein expression in parasites growing in oxidatively stressed or G6PD-deficient red blood cells. *Malaria J.*, **8**(113).
260. Pal Bhowmick, I., *et al.* (2009). *Plasmodium falciparum* enolase: stage-specific expression and sub-cellular localization. *Malaria J.*, **8**(179).
261. Wrenger, C., *et al.* (2006). Vitamin B1 de novo synthesis in the human malaria parasite *Plasmodium falciparum* depends on external provision of 4-amino-5-hydroxymethyl-2-methylpyrimidine *Biol. Chem.*, **387**: 41-51.
262. Igarashi, K. and Kashiwagi, K. (2010). Modulation of cellular function by polyamines *Int J Biochem Cell Biol*, **42**(1): 39-51.
263. Merrill, M.J.; Mueckler, M.M.; and Pitot, H.C. (1985). Levels of ornithine aminotransferase messenger RNA under conditions of cyclic AMP induction in cultured hepatocytes. *J. Biol. Chem.*, **260**(20): 11248-11251.
264. Shull, J., *et al.* (1995). Cell-type specific interactions between retinoic acid and thyroid hormone in the regulation of expression of the gene encoding ornithine aminotransferase. *Endocrinology*, **136**(5): 2120-2126.
265. Yasuda, M., *et al.* (1981). Properties of crystalline L-ornithine: α -keto-glutarate δ -aminotransferase from *Bacillus sphaericus*. *J. Bacteriol.*, **148**(1): 43-50.
266. Deshmukh, D.R. and Srivastava, S. (1984). Purification and properties of ornithine aminotransferase from rat brain. *Experientia*, **40**: 357-359.
267. Stránská, J., *et al.* (2010). Biochemical characterization of pea ornithine- δ -aminotransferase: Substrate specificity and inhibition by di- and polyamines. *Biochimie*, **92**(8): 940-948.
268. Jortzik, E., *et al.* (2010). Redox regulation of *Plasmodium falciparum* ornithine [δ]-aminotransferase. *J. Mol. Biol.*, **402**(2): 445-459.
269. Frohman, M. (1993). Rapid amplification of complementary DNA ends for generation of full-length complementary DNAs: Thermal RACE. *Methods Enzymol.*, **218**: 340-356.
270. Boyle, J. and Lew, A. (1995). An inexpensive alternative to glassmilk for DNA purification. *Trends Genet.*, **11**: 8.

271. Kim, H.-R., *et al.* (1994). Assay of ornithine aminotransferase with ninhydrin. *Anal. Biochem.*, **223**: 205-207.
272. Makler, M., *et al.* (1993). Parasite lactate dehydrogenase as an assay for *Plasmodium falciparum* drug sensitivity. *Am. J. Trop. Med. Hyg.*, **48**: 739-741.
273. Noedl, H.; Wongsrichanalai, C.; and Wernsdorfer, W.H. (2003). Malaria drug-sensitivity testing: new assays, new perspectives. *Trends Parasitol.*, **19**(4): 175-181.
274. Lim, S., *et al.* (1998). A variant of ornithine aminotransferase from mouse small intestine. *Exp. Mol. Med.*, **30**(3): 131-135.
275. Seiler, N. (2000). Ornithine aminotransferase, a potential target for the treatment of hyperammonemias. *Curr. Drug Targets*, **1**: 119-153.
276. Fagan, R.J., *et al.* (1991). Translational Control of Ornithine Aminotransferase - Modulation by initiation factor eIF-4E. *J. Biol. Chem.*, **266**(25): 16518-16523.
277. Voet, D. and Voet, J. (2004). Chapter 14: Rates of enzymatic reactions. In *Biochemistry*. John Wiley and Sons, Inc; New Jersey.
278. Olszewski, K., *et al.* (2009). Host-parasite interactions revealed by *Plasmodium falciparum* metabolomics *Cell Host Microbe*, **5**: 191-199.
279. Berger, B.J. (2000). Antimalaria activities of aminoxy compounds. *Antimicrob. Agents Chemother.*, **44**(9): 2540-2542.
280. Pérez-Pertejo, Y., *et al.* (2011). *Leishmania donovani*: proteasome-mediated down-regulation of methionine adenosyltransferase. *Parasitology*, **138**(09): 1082-1092.
281. Cataldi, A.A. and Algranati, I.D. (1989). Polyamines and regulation of ornithine biosynthesis in *Escherichia coli*. *J. Bacteriol.*, **171**(4): 1998-2002.
282. Kehr, S., *et al.* (2011). Protein S-glutathionylation in malaria parasites. *Antioxid. Redox Signal.*, **15**(11): 2855-2865.
283. Jortzik, E.; Wang, L.; and Becker, K. (2012). Thiol-based posttranslational modifications in parasites. *Antioxid. Redox Signal.*, **17**(4): 657-673.